X-300 EcoFlyer Final Report

A Feasibility Study on a Low-Emission, High-Capacity, Short-to-Medium Range Aircraft

AE3200 Design Synthesis Exercise

Group 29

Delft University of Technology

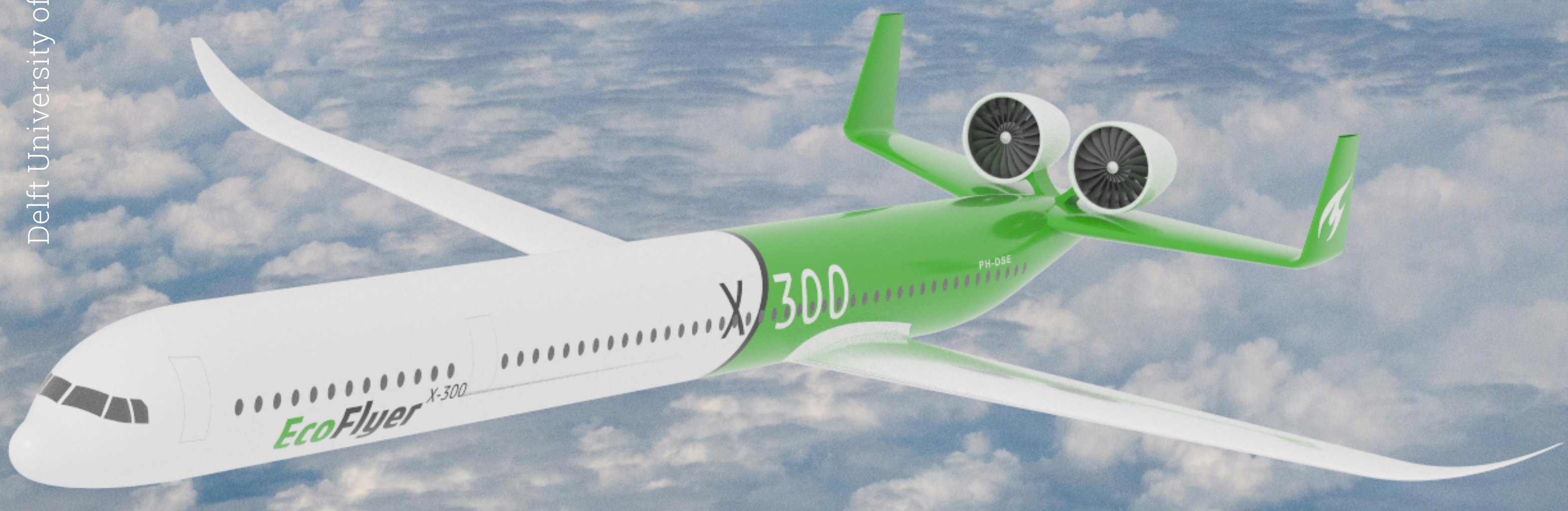

(This page is intentionally left blank)

X-300 EcoFlyer Final Report

A Feasibility Study on a Low-Emission, High-Capacity, Short-to-Medium Range Aircraft

by

Group 29

Student Name	*Student Number*
Jakub Bartmański	5449170
Gerben Drijfhout	5054559
Alexander Entchev	5220475
Matthew Fulton	5005698
Jay Pankajkumar Karia	5552257
Miguel Martins de Castro	5446031
Ararat Sahakyan	5514177
Bram Verweij	5017939
Jochem Wichers	5324505
Sjoerd Bootsma	5242053

Issue	*Amendment*	*Date*
V0.1	Unfinished draft (for TA)	19/06/2024
V0.2	Finished draft (for tutor)	19/06/2024
V1.0	Final version	25/06/2024

Course:	AE3200 Design Synthesis Exercise
Tutor:	F. Yin
Coaches:	S. Chellini, F. De Domenico, A. A. Simkooei
Project Duration:	22 April 2024 - 28 June 2024
Faculty:	Faculty of Aerospace Engineering

Preface

This report marks the culmination of ten weeks worth of work as part of the Design Synthesis Exercise (DSE) 2024. Ten students were part of Group 29 and contributed to the development of the proposed design from a mere project assignment to a comprehensive feasibility study. We hope our proposed design, the *X-300 EcoFlyer*, inspires confidence in the feasibility of unconventional aircraft concepts and demonstrates that they have a place in the commercial aviation industry.

As a team, we have found the DSE to be an incredibly rewarding learning experience, combining technical design and operational analyses. We would like to thank our tutor Feijia Yin and our coaches Simone Chellini, Francesca De Domenico, and Alireza Amiri Simkooei for their invaluable guidance throughout the project. We would also like to extend our gratitude to Arvind Gangoli Rao, Rebekka van der Grift, Steven Hulshoff, Joris Melkert, Merino Martinez, Calvin Rans, Paul Roling and Dick Simons who offered their advice during the project.

Group 29
Delft, June 2024

Executive Summary

Introduction

Commercial aviation is growing at an annual rate of 4%[1], posing significant environmental and operational challenges. To address these challenges, and to meet market demand for a 300-seat airliner by 2035, the technical feasibility and market viability of this high-capacity short-to-medium range aircraft, dubbed the *X-300 EcoFlyer*, is examined in this report. Its design, manufacturing plan, performance, and business case are assessed for this future aircraft that aims to deliver significant reductions in CO_2 ($-25\,\%$), NO_x ($-50\,\%$) and noise emissions ($-20\,\%$) compared to current state-of-the-art aircraft.

Stakeholder Requirements

The most important stakeholder requirements which drive the design are listed in Table 1

Table 1: Most important stakeholder requirements.

Identifier	**Requirement**
REQ-STK-01	The aircraft shall have a range of minimum $3000\,\mathrm{km}$.
REQ-STK-12	The aircraft's operational CO_2 emissions per passenger per kilometer shall be $25\,\%$ lower than those of the Airbus A320neo.
REQ-STK-13	The aircraft's operational NOx per passenger per kilometer emissions shall be $50\,\%$ lower than that of the Airbus A320neo.
REQ-STK-14	The cumulative effective perceived noise level (EPNL) of the aircraft shall be $20\,\%$ lower than that of the Airbus A320neo.
REQ-STK-16	The aircraft shall be able to accommodate an amount of 290 to 330 passengers.
REQ-STK-17	The aircraft shall be in service in 2035.

.

Concept Development

This report follows the conclusion of two previous reports [2, 3] in which requirements and constraints for the system (i.e. the aircraft) were established, and system concepts were traded off. Subsequently, two concepts were left for further consideration: a SAF propfan aircraft and a SAF turbofan aircraft. [1] Further development of these concepts considers the feasibility of implementing future technologies in these designs, including multi-fuel combustion, water-injected combustion, and shielding of engine noise.

Multi-fuel combustion is ruled out on the basis of insufficient ongoing development to meet the 2035 entry-into-service date. Water-injected combustion is considered a possibility, due to strong ongoing development in the industry[2][3], as well as its long-term value for manufacturers.

The final comparison between the two concepts identifies the SAF turbofan (with water-injected

[1] A SAF engine is able to run on $100\,\%$ SAF. However, due to probable SAF availability limitations at the entry into service by 2035, conventional jet fuel and a SAF blend of $6\,\%$ are used for CO_2 emission calculations.

[2] https://cordis.europa.eu/project/id/101102006

[3] https://www.mtu.de/technologies/clean-air-engine/water-enhanced-turbofan/

combustion) as the clear winner. The resulting preliminary design (established in a previous report [3]) forms the basis for the detailed design phase that follows. The design features a single-aisle fuselage, an H-tail, and engines mounted over the horizontal stabiliser.

Detailed System Design

Propulsion System

The propulsion system follows the concept of water-injected combustion. Water is injected into the combustion chamber, significantly lowering the emissions of NO_x. This water is recuperated from the exhaust by extracting waste heat from the core flow and condensing the water in it, increasing thermal efficiency. The developed performance model and sizing model result in the engine characteristics captured in Table 2. A notable reduction in NO_x emissions of over $90\,\%$ is achieved compared to the A320Neo LEAP-1A26 engines [4][5][6][7].

Table 2: X-300 engine performance in cruise compared to LEAP-1A26.

Parameter Description	Symbol	X-300	LEAP-1A26	Unit
Thrust-specific fuel consumption	TSFC	12.03	14.4 [4]	$\mathrm{g \cdot kN^{-1} \cdot s^{-1}}$
Emission index NO_x	EI_{NOx}	0.469	7.24 [5]	$\mathrm{g \cdot kg^{-1}}$
Overall pressure ratio	OPR	31.5	40 [6]	–
Water-to-air ratio	WAR	0.1482	0	–
Nacelle outer diameter	d_{outer}	3.02	2.54 [7]	m

Auxiliary Systems

The electrical power budget consists of systems and components that require electrical power. Due to the implementation of an electric environmental control system (ECS) and the elimination of bleed air, $380\,\mathrm{kW}$ of power has been allocated to this system, making it the largest consumer of electricity on the aircraft. The total required power is estimated at $880\,\mathrm{kW}$.

The fuel system is sized to contain the required fuel volume of $28 \times 10^3\,\mathrm{L}$, or $22.5 \times 10^3\,\mathrm{kg}$. The tank is partitioned into a centre section, inner tanks, outer tanks and surge tanks. The piping, pumps and valves are designed to supply the engines and APU with fuel, whilst providing full redundancy in case of failures.

In-wheel Electrical Taxiing System (IWETS)

To reduce local NO_x emissions and improve air quality at airports, the aircraft is outfitted with an in-wheel electrical taxiing system (IWETS). Batteries and motors power four wheels on the main landing gear such that the aircraft can taxi electrically. This saves $837\,\mathrm{kg}$ of fuel on a nominal mission profile.

Environmental Control System (ECS)

The environmental control system (ECS) is responsible for cabin pressurisation, thermal control and air supply to passengers and crew. Conventionally, bleed-air is used to achieve the required function, but this comes at the cost of reduced engine performance. Instead, the X-300 utilises an electric ECS, resulting in a $3\,\%$ reduction in fuel burn. The system draws electrical power from the engine generators. The elimination of bleed air also necessitates the implementation of electric de-icing systems, as well as electric engine starters.

[4] https://www.ainonline.com/aviation-news/air-transport/2019-08-19/aviadvigatel-mulls-higher-thrust-pd-14s-replace-ps-90a

[5] Modelled using `https://www1.grc.nasa.gov/beginners-guide-to-aeronautics/enginesimu/`

[6] https://www.cfmaeroengines.com/wp-content/uploads/2017/09/Brochure_LEAPfiches_2017.pdf

[7] https://web.archive.org/web/20181013014334/https://www.easa.europa.eu/sites/default/files/dfu/EASA%20E110%20TCDS%20Issu 1A-1C.pdf

Airframe Structure and Materials

The structural characteristics of the design were established by performing a weight estimation of the fuselage and the empennage. The analysis showed the single-aisle configuration is feasible in terms of the yielding stress and shear strength of the chosen airframe material: Al-Li 8090. Furthermore, to investigate the landing-induced bending of the fuselage, a deflection analysis has been performed, yielding a maximum average deflection of the nose with respect to the main landing gear of $1.5\,°$.

For the selection of aircraft materials, attention was paid to their recyclability. The materials range from carbon-fibre-reinforced-composites (constituting, for instance, the engine nacelles and the cabin floor) to traditional aluminium-lithium alloy (Al-Li 8090) comprising the fuselage as well as a variety of titanium-aluminium alloys (used for the landing gear or high-temperature compressor rotors).

Airframe Aerodynamics

To choose an aerofoil for the wing, a trade-off was performed between three different aerofoils optimized for low subsonic speeds, with the NACA 2412 aerofoil winning the trade-off.

A computational fluid dynamics (CFD) analysis is conducted for the NACA 2412 aerofoil to compute its aerodynamic characteristics during cruise. From these, an estimation was made for the wing as well, using semi-empirical methods.

The overall performance of the wing is acceptable (i.e. it contributes to the attainment of the requirements), although the drag coefficient curve could be optimised for higher efficiency during flight since the increase of drag coefficient with increasing lift coefficient is very large at the moment. In further development, a CFD analysis should be done for the entire wing and multiple different aerofoils along the wingspan should be considered. The maximum lift coefficient of the wing ($C_{L_{max}}$) at cruise conditions is 1.33, while the minimum drag coefficient ($C_{D_{max}}$) is 0.0085. This is deemed too low and can be attributed to the low-accuracy semi-empirical model used to obtain the wing drag polar.

Airframe Stability and Control

To assess the stability and control of the aircraft, a loading diagram was constructed in order to determine the centre of gravity range of the X-300 in all loading cases. A scissor plot containing the stability and controllability curves was also constructed in order to assess whether the aircraft is controllable and stable within the centre of gravity range. Analysing this plot suggested that the wing position and horizontal tail size established during the preliminary design did not comply with the stability and controllability constraints. This led to the wing being moved forward with respect to the fuselage and the tail size being reduced. This was in line with expectations due to the fact that an H-tail is typically more effective than a standard tail and will therefore have a smaller area.

When taking into consideration the landing gear and engine placement, the stability and control characteristics varied. The centre of gravity shifted further aft, causing it to be located behind the centre of pressure of the aircraft. This evidently caused the aircraft to be longitudinally and statically unstable. As a result, the wing position had to be pushed back relative to the fuselage. Due to the wing being relatively light compared to other systems the aircraft comprises, moving it further aft allows for the centre of pressure to move further aft than the centre of gravity, therefore enabling longitudinal static stability. In addition to this, the wing had to house the main landing gear when fully retracted, giving even greater cause to move the wing further aft.

Moving the wing further aft also resulted in a larger tail size, which was expected and even desired. A larger tail size would be needed, as a larger tail force is needed to keep the aircraft stable, due to the shorter moment arm between the centre of gravity and the tail force. The increase in tail size would also be beneficial in accommodating the WIT engines and shielding the noise emissions produced. The table below shows the final outputs of the sizing of the tail to ensure stability and controllability in all phases of flight.

Table 3: Sizing characteristics of the tail.

Parameter	Value	Unit
$X_{CG_{OEM}}$	31.39	m
$X_{CG_{front}}$	27.67	m
$X_{CG_{aft}}$	31.44	m
X_{LEMAC}	32.5	m
S_h	72.65	m^2
A_h	3	$-$
span$_h$	16.21	m
Taper ratio	0.5	$-$

Performance

Flight Performance

The flight performance analysis for the X-300 consists of calculating take-off distance, landing distance, cruise performance and a payload range diagram. The results of this can be seen in Table 4, and it can be concluded that the aircraft satisfies the performance requirements.

Table 4: X-300 Flight performance summary.

Parameter	Value
Take-off distance	$1669\,\mathrm{m}$
Landing distance	$1475\,\mathrm{m}$
Maximum cruise altitude	$9280\,\mathrm{m}$
Maximum cruise speed	$200\,\mathrm{m/s}$
Harmonic range	$3000\,\mathrm{km}$
Range at maximum fuel	$5331\,\mathrm{km}$
Ferry range	$8575\,\mathrm{km}$

Climate Impact

Without SAF CO_2 life-cycle emissions being accounted for, the X-300 reduces CO_2 emissions per Available Seat Kilometer (ASK) by $27.7\,\%$ compared to the A320Neo by performance improvements alone. Including SAF life-cycle for a $6\,\%$ SAF blend the CO_2 reduction is $31.0\,\%$ per ASK.

The NO_x emissions are significantly reduced by the WIT engines. The total landing and take-off cycle (LTO) NO_x emissions are calculated based on engine LTO NO_x emission data. The LTO emission of the WIT engine is $1940\,\mathrm{g}$. This makes the engines compliant with the future ICAO standard for 2027. The cruise emissions are calculated using the WIT engine model. The total NO_x emission per ASK for the X-300 is 0.020 g / ASK. This is an $90.5\,\%$ reduction compared to the A320Neo. All in all, both the CO_2 and NO_x reduction requirements are achieved by the design.

Noise Emissions

An assessment of the X-300's noise emissions (and specifically, cumulative EPNL) was conducted by means of a statistical analysis of existing aircraft's noise levels. Using data from the ICAO Noise Database (see Appendix A), statistical relationships were derived between EPNL and the following aircraft parameters: maximum take-off mass, maximum landing mass, wing surface area, and sea-level static thrust. These relationships were used to estimate a "baseline" EPNL; here, "baseline" means without accounting for fan/engine noise shielding. From this baseline EPNL value, a reduction ($\Delta\mathrm{EPNdB}$) was subtracted to reflect the shielding effects. This reduction was estimated based on a review of existing literature on the topic. The analysis yields a cumulative EPNL of $254.4\,\mathrm{dB}$ for the X-300, $4.2\,\mathrm{EPNdB}$ (or $25.3\,\%$) lower than the average cumulative EPNL of the A320neo.

Sensitivity Analysis

A sensitivity analysis of the aircraft model was conducted to assess if changing aircraft parameters in future design stages would affect the operating empty mass (OEM) of the X-300. For this design, the wing area, thickness-to-chord ratio, and position of the wing along the fuselage were varied.

The result of this analysis was that the OEM showed a consistent trend when the wing area and wing position were varied. However, it was noticed that the model is quite sensitive when varying the thickness-to-chord ratio where small changes would cause sudden OEM changes. Therefore it is recommended to revisit and modify the model to avert this in the future.

Final Design

The final design of the X-300 EcoFlyer is presented below, including important performance specifications as well as the internal and external configuration. The resulting final design parameters can be seen in Figure 5 while the internal configuration of the X-300 can be seen in Figure 1 and Figure 2. The internal configuration is a single-aisle, with a 3-3 seating layout. Additionally, there are 55 rows of seats to accommodate an exit limit of 330 passengers.

Table 5: Table indicating the X-300 final design and performance metrics.

Parameter	Value	Unit
Capacity	330	–
Harmonic Range	3000	km
Flight Ceiling	9280	m
Cruise Mach	0.65	–
Wingspan	47.4	m
OEM	63 926	kg
MTOM	123 448	kg
L/D	18.8	–
Engine TSFC	12	$\mathrm{g \cdot kN^{-1} s^{-1}}$

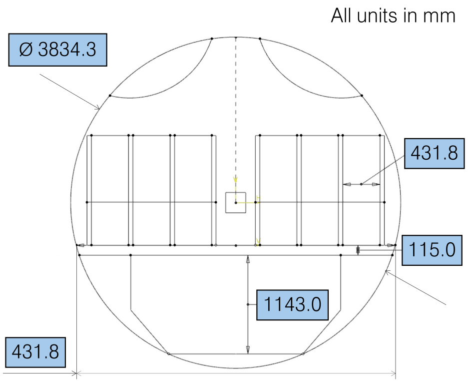

Figure 1: Figure showing the internal dimensions of cabin and cargo bay. All units in mm.

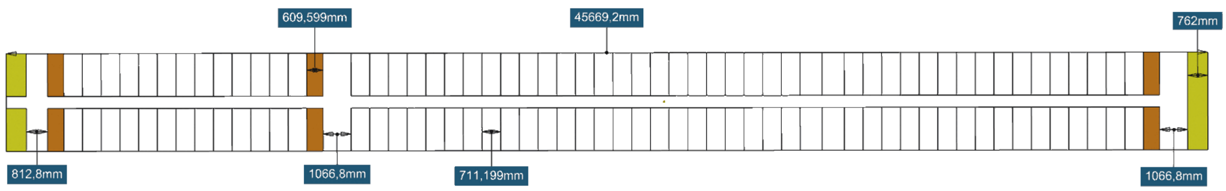

Figure 2: Internal top view of floor plan of the cabin.

Figure 3 shows the external layout of the X-300. Some unique characteristics regarding the exterior configuration of the aircraft include its slender fuselage and large WIT engines which are located on the H-tail for noise shielding purposes.

Figure 3: Rendered model of the X-300 EcoFlyer.

Manufacturing, Assembly and Integration

A general manufacturing plan is drafted to prepare for the aircraft series production to start in the year 2034. For this, it is established that, first, separate parts, such as spars and stringers are produced, followed by a sub-assembly mounting (some sub-systems are bought from external parties). At this stage, sub-systems of the aircraft, like the wingbox or the flap deployment mechanism, are constructed. Thereafter, these are assembled together into bigger systems, such as the whole wing or the cockpit section. Finally, these large systems are assembled together in the final assembly line to make the entire aircraft.

Furthermore, several non-destructive methods will be used during manufacturing for quality control, such as thermography and fluorescent penetrant.

Sustainable Development Strategy

The two major goals of the X-300 EcoFlyer are to reduce the CO_2 per ASK by $25\,\%$ compared to the A320Neo and to reduce the NO_x per ASK by $50\,\%$. As part of the CO_2 emission analysis, an assessment of future SAF adoptions is made. This assessment is centered around SAF adoption targets for the major targeted markets (those being Asia-Pacific, India, and the Middle East). An average available SAF blend of $6\,\%$ is forecasted. The catalytic hydrothermolysis jet fuel (CHJ) SAF type offers the best CO_2 reduction for its price. A $6\,\%$ CHJ SAF blend has a $4.6\,\%$ reduction in CO_2 life-cycle emissions compared to conventional jet fuel

Operations and Logistics

A reliability, availability, maintainability, and safety (RAMS) analysis was conducted for the entire aircraft. The focus was put on systems that differ from reference aircraft (A320neo). The reliability of the IWETS, ECS and WIT engine was assessed. Due to their innovative nature, there are doubts about their reliability, but increased monitoring and redundancies can be implemented to mitigate these.

For timely volume production of the X-300, the availability of required materials and systems was assessed. The availability of the advanced engine was considered a risk that is to be managed in further development. The supply chain of the most critical materials was deemed to be robust.

With respect to maintenance, the placement of the engines requires adjustments in maintenance, repair, and overhaul practices, and the IWETS should be subjected to additional line checks. To reduce overall maintenance time and cost, predictive maintenance based on advanced monitoring systems is employed in addition to the regular ABC checks. An aircraft system failure tree identifies safety critical systems that require additional considerations. To address the safety concerns, dissimilar redundant systems are implemented for parts of the WIT engine, ECS, and IWETS.

Business Case

The X-300 targets the 300 passengers, short-to-medium range aircraft market, which is forecast to grow significantly towards 2050. This market sector is also expected to be responsible for the largest share of aircraft emissions. The growth in this segment is expected to be centred in the Asia-Pacific market, where there are many high-capacity routes.

In this market, the X-300 is expected to compete with next-generation widebodies and narrowbodies (potentially powered by hydrogen) not only from established OEMs but also from the emerging manufacturers, such as Comac in China. Taking into account range, seating capacity, climate impact, direct operating cost, and market fit, the expected market share of the X-300 is $37\,\%$ in a highly competitive scenario. In a more optimistic scenario, the market share could be $54\,\%$. An overall market share of $46\,\%$ is assumed, resulting in a total of almost 1100 aircraft sold over a 30 year period.

The RAND DAPCA IV model is used to estimate that the total research, development, test, and evaluation cost is around $\$9\,\mathrm{billion}$. The total production cost per aircraft is expected to reach $\$98\,\mathrm{million}$ with a market price of $\$128\,\mathrm{million}$ to have a profit margin of $30\,\%$. At this price, it is $17\,\%$ more expensive than the A320neo, but significantly lower than available widebodies. The unit cost, taking into account the development cost as well, reaches $\$109\,\mathrm{million}$ in 2024 or €$133\,\mathrm{million}$ for 2035. Considering all costs, sales and inflation, the return on investment is expected to be $18\,\%$ with a break-even point at 360 aircraft.

Critical for operators is the direct operating cost per available seat kilometre. The X-300 achieves a $10\,\%$ saving with respect to the A320neo due to its increased fuel efficiency, despite higher maintenance costs attributable to the new engine design and implementation of additional novel systems (such as IWETS).

Technical Risk Assessment

Once the design is finalised, a technical risk assessment is conducted. Risks identified included the reliability of the engine, the performance of the IWETS and a relatively low flight ceiling.

The risks which were deemed to be critical and required mitigation strategies in the future included potential improvements in composite recycling technology by competitors and readiness of the WIT engine.

Compliance Matrix

A compliance matrix was established to check how the design, at its current stage of development, complies with stakeholder, mission, and system requirements. In this compliance matrix, the requirements already met at this stage of design were marked as complete, while those not yet satisfied were marked as such, with supplementary reasoning provided. In total, $46.7\,\%$ of the requirements have been marked as satisfied so far and only $2.5\,\%$ have failed to be met.

In Table 6, the most relevant stakeholder requirements are listed; a green circle (●) indicates that the requirement has been satisfied, and a yellow circle (●) indicates the requirement is yet to be satisfied at a later design stage.

Table 6: Compliance matrix with most important stakeholder requirements. The green and yellow circles denote requirement compliance and not *yet* satisfied requirements, respectively.

Identifier	Requirement	Compliant
REQ-STK-01	The aircraft shall have a maximum range of $3000\,\mathrm{km}$ or above	●
REQ-STK-12	The aircraft's operational CO_2 emissions per passenger per kilometer shall be $25\,\%$ lower than those of the Airbus A320neo	●
REQ-STK-13	The aircraft's operational NOx per passenger per kilometer emissions shall be $50\,\%$ lower than that of the Airbus A320neo	●
REQ-STK-14	The cumulative effective perceived noise level (EPNL) of the aircraft shall be $20\,\%$ lower than that of the Airbus A320neo	●
REQ-STK-16	The aircraft shall be able to accommodate an amount of 290 to 330 passengers	●
REQ-STK-17	The aircraft shall be in service in 2035	●

Post-DSE Development Logic

After the DSE, the development of the aircraft will continue in line with the maturity gate development cycle outlined by Airbus. The importance of establishing supplier relationships is highlighted, particularly for the development of the WIT engine. The timeline builds towards an entry-into-service in 2035, with the first flight planned for 2033.

Conclusion

In relation to the market gap and technical challenges which the X-300 is designed to address, this study has proven the following:

- The single-aisle design of the X-300 is suitable for a 300-passenger capacity and performs better on fuel consumption compared to an equivalently-sized twin-aisle alternative.
- The performance of the WIT engine shows that there is significant potential to reduce the climate effect of aviation without having to resort to alternative fuels such as hydrogen.
- Engine noise shielding proves to be an effective way of reducing an aircraft's noise emissions, independent of the engine noise itself.
- Being purpose-built for high-demand short-haul routes, the X-300 yields superior operating economics compared to the high-capacity long-range aircraft which currently operate said routes. This makes it a strong competitor for future high-demand short-haul operations.
- Despite its positive effect on CO_2 emissions, the use of a SAF-kerosene blend is hampered by operational constraints, as it relies on all airports (which a given aircraft operates from) being equipped with a SAF supply infrastructure in order to bring significant reductions in CO_2 emissions in the context of an aircraft's operational lifetime.

Steps to be taken in future development efforts of the X-300 include:

- A more comprehensive structural analysis of the fuselage cross section (using a skin and stiffener model) and the wingbox to obtain a more accurate estimate of the aircraft's mass.
- A closer examination of the horizontal stabilizer, which is currently larger than necessary because of the constraints imposed by the landing gear, wing positioning, and noise shielding.
- A more detailed appraisal of the aircraft's environmental impact, including analysis of soot emissions, contrail formation, and embodied energy of the materials used.
- Further development of the engine model to cover additional design points and operating conditions.

Contents

Preface i

Executive Summary ii

Abbreviations xiii

1 Introduction 1

2 Stakeholder Requirements 2

3 Aircraft Concept Development 3
- 3.1 Design Concept Recap . . . 3
- 3.2 Initial Trade-Off Summary . . . 5
- 3.3 Concept Development . . . 7
  - 3.3.1 Assessment of Technology Improvements . . . 7
  - 3.3.2 Propfan Concept Development . . . 8
  - 3.3.3 Turbofan Concept Development . . . 9
  - 3.3.4 Concept Selection . . . 10
- 3.4 Preliminary Design Parameters . . . 10

4 Functional Analysis 12
- 4.1 Functional Breakdown Structure . . . 12
- 4.2 Functional Flow Diagram . . . 12

5 Detailed System Design 16
- 5.1 Propulsion System . . . 16
  - 5.1.1 Engine Performance: Concept . . . 16
  - 5.1.2 Engine Performance: Model Description . . . 17
  - 5.1.3 Engine Performance: Model Matching . . . 22
  - 5.1.4 Engine Performance: Model Application . . . 24
  - 5.1.5 Engine Performance: Verification and Validation . . . 26
  - 5.1.6 Engine Sizing: Model Description . . . 28
- 5.2 Electrical System Power Budget . . . 29
- 5.3 Fuel System . . . 30
- 5.4 In-Wheel Electrical Taxiing System (IWETS) . . . 33
- 5.5 Environmental Control System (ECS) . . . 35
- 5.6 Airframe . . . 36
  - 5.6.1 Material Characteristics . . . 36
  - 5.6.2 Structural Characteristics . . . 38
  - 5.6.3 Aerodynamic Characteristics . . . 42
  - 5.6.4 Stability and Control Characteristics . . . 48

6 Performance Analysis 55
- 6.1 Flight Performance . . . 55
  - 6.1.1 Payload Range . . . 55
  - 6.1.2 Airfield Performance . . . 56
  - 6.1.3 Cruise Performance . . . 58
  - 6.1.4 Verification and Validation . . . 59

6.2 CO_2 Emissions . . . 59
6.3 NO_x Emissions . . . 60
6.3.1 LTO NO_x Emissions . . . 60
6.3.2 NO_x Cruise Emissions . . . 60
6.3.3 NO_x Emissions Results . . . 62
6.4 Noise Emissions . . . 62
6.4.1 Applicable Noise Limits . . . 62
6.4.2 Baseline Noise Level . . . 63
6.4.3 Effects of Noise-Reducing Design Modifications . . . 65
6.4.4 Final Noise Level . . . 67
6.5 Sensitivity Analysis . . . 67

7 Final Design Specification **70**
7.1 Internal Configuration . . . 70
7.2 External Configuration . . . 71

8 Manufacturing, Assembly, and Integration Plan **74**
8.1 Manufacturing, Assembly and Integration Timeline . . . 74
8.2 Inventory and Quality Control . . . 75

9 Sustainable Development Strategy **77**
9.1 X-300 Sustainability Impact . . . 77
9.2 Contrail & Cirrus Cloud Formation . . . 78
9.3 SAF Adoption Goals . . . 78
9.4 Economically Efficient SAF . . . 79
9.5 Fuel Life-Cycle Analysis . . . 80

10 Operations and Logistics **81**
10.1 RAMS Characteristics . . . 81
10.1.1 Qualitative Reliability . . . 81
10.1.2 Quantitative Reliability . . . 82
10.1.3 Availability and Maintainability . . . 83
10.1.4 Safety . . . 84
10.2 Operations and Logistic Concept Description . . . 87
10.2.1 Concept of Operations . . . 87
10.2.2 Operational and Logistic Considerations . . . 87

11 Business Case **90**
11.1 Market Analysis . . . 90
11.1.1 Target Market . . . 90
11.1.2 Stakeholders Analysis . . . 92
11.2 Product Positioning . . . 94
11.2.1 Market Size . . . 94
11.2.2 Position and Share in Future Market . . . 95
11.2.3 Expected Number of Deliveries . . . 96
11.3 Cost Analysis . . . 98
11.3.1 Cost Breakdown Structure . . . 98
11.3.2 Production and Development Cost . . . 98
11.3.3 Market Price . . . 100
11.3.4 Direct Operating Cost . . . 100
11.4 Sales Estimation . . . 102
11.5 Final Market Positioning . . . 102

12 Resource and Budget Breakdown **104**

13 Technical Risk Assessment **106**
14 Compliance Matrix **110**
15 Post-DSE Development Logic **119**
16 Conclusion **123**
Bibliography **128**
A Data for Noise Analysis **129**
B Task Division **130**

Abbreviations

Abbreviation	Definition
AC	Aircraft
AFJ	Alcohol to jet fuel
ANA	All nippon airways
ASK	Available seat kilometer
APU	Auxiliary power unit
AR	Aspect ratio
BH	Block hour
BPR	Bypass ratio
BPF	Bypass fan
CAEP	Committee on aviation environmental protection
CEA	Chemical equilibrium applications
CF	Core fan
CFD	Computational fluid dynamics
CHJ	Catalytic hydrothermolysis jet fuel
CG	Center of Gravity
CO_2	Carbon dioxide
CS	Certification specifications
DAPCA	Development and procurement costs of aircraft
DOC	Direct operating cost
DSE	Design synthesis exercise
EASA	European aviation safety agency
ECS	Environmental control system
EI	Emission index
EIS	Entry into service
EPNL	Effective perceived noise level
EU	European union
FAR	Fuel-to-air ratio
FCS	Flight control System
FL	Flight level
FT	Fischer-Tropsch
GWP	Global warming potential
HEFA	Hydroprocessed esters and fatty acids
HFS	Hydroprocessed fermented sugars
HPC	High pressure compressor
HPT	High pressure turbine
ICAO	International civil aviation organization
ID	Identifier
ISA	International standard atmosphere
LCA	Life cycle analysis
IWETS	In-wheel electrical taxiing system
LEMAC	Leading edge mean aerodynamic chord
LG	Landing gear
LH2	Liquid hydrogen

Abbreviation	Definition
LHV	Lower heating value
LP	Low-pressure
LPT	Low pressure turbine
LTO	Landing and take-off
MAC	Mean aerodynamic chord
MFP	Mass flow parameter
MG	Mission gate
MLG	Main landing gear
MLM	Maximum landing mass
MMH/FH	Maintenance man hours per fight hour
MRO	Maintenance, repair and overhaul
MRW	Maximum ramp weight
MTOM	Maximum take-off mass
MTOW	Maximum take-off weight
NACA	National advisory committee for aeronautics
NASA	National aeronautics and space administration
NLG	Nose landing gear
NO_x	Nitrous oxides
OEM	Operating empty mass
OEM	Original equipment manufacturer
OEW	Operating empty weight
OPR	Overall pressure ratio
PAX	Passengers
PCC	Pearson correlation coefficient
RAMS	Reliability, availability, maintainability and safety
RANS	Reynolds-averaged Navier Stokes
RDT&E	Research, development, test and evaluation
RE	Reynolds number
S	Wing area
SAF	Sustainable aviation fuel
SI	Système international
SLST	Sea-level static thrust
ST	Steam-turbine
SWOT	Strengths, Weaknesses, opportunities and threats
TF	Technology factor
TIT	Turbine inlet temperature
TO	Take-off
TRL	Technology readiness level
TSFC	Thrust specific fuel consumption
WAR	Water-to-air ratio
WIT	Water-injected-turbofan
WFR	Water-to-fuel ratio

1 Introduction

Demand for commercial aviation is increasing at rates of $4\,\%$ annually [1], which poses many challenges for the passenger air transport sector. The rising number of flights exacerbates the industry's detrimental effects on the environment (about $4\,\%$ of human-induced global warming is attributed to civil aviation [4]). Historically and at present, many large-capacity aircraft designed for long ranges (e.g. Boeing 747, Airbus A330, Boeing 787, Airbus A350) are operated on short-medium range, high-demand routes, especially in East Asia [5]. Because these aircraft are not optimised for the sectors they fly, they yield suboptimal fuel consumption, higher CO_2 and NO_x emissions, and unfavourable operating economics in those sectors compared to smaller purpose-built aircraft. This incompatibility between aircraft and route characteristics is only set to increase in the coming decades. From 2035 onwards, it is expected that the most sought after aircraft capacity will be 211 to 300 seats [5]. Given that there are no aircraft in production at the moment which offer this capacity, and that there is no indication of such an aircraft being announced soon, there is a clear market gap for a passenger airliner in the aforementioned seat range.

The aim of this report is to study the feasibility and viability of a short-to-medium range passenger airliner with a significantly reduced environmental impact compared to current state-of-the-art aircraft. The proposed concept, dubbed the *X-300 EcoFlyer*, must offer a capacity of approximately 300 passengers and a range of $3000\,\mathrm{km}$ while yielding $25\,\%$ lower CO_2 emissions, $50\,\%$ lower NO_x emissions, and $20\,\%$ lower noise emissions compared to an Airbus A320neo.

This report builds on the outcomes presented in two previous reports [2, 3]. To summarise the past work, the highest-level stakeholder requirements are presented in Chapter 2, and a summary of the previously conducted trade-off and preliminary design are provided in Chapter 3. The latest work begins with an update of the previously established aircraft functions (Chapter 4), followed by detailed system design (Chapter 5) and flight performance analysis (Chapter 6). The final design specification is summarised in Chapter 7. Other considerations in this feasibility study include a manufacturing plan (Chapter 8), a sustainability strategy (Chapter 9), and an operations and logistics characterisation (Chapter 10). To make the case for the viability of the X-300, a business case (Chapter 11) and a technical risk assessment (Chapter 13) are also discussed. To complete the study, a compliance matrix is presented (Chapter 14) along with guidelines for developing the project further in the future (Chapter 15). Final conclusions are given in Chapter 16.

2 Stakeholder Requirements

This chapter includes a list of the highest-level stakeholder requirements for the X-300. These were derived during the baseline design phase [2]. The coloured circle in the right-most column represents the priority of the requirement. In order of increasing priority, there are: key requirements (●), driving requirements (●), and killer requirements (●). The design that is conducted aims to meet these requirements. The compliance with these requirements, based on the final design, is elaborated on in Chapter 14.

Table 2.1: Stakeholder requirements. Key, driving, and killer requirements are depicted with yellow, red, and black circles, respectively.

Identifier	Requirement	Priority
REQ-STK-01	The aircraft shall have a maximum range of $3000\,\mathrm{km}$ or above	Red
REQ-STK-02	The aircraft shall have a maximum endurance of six hours or above	Red
REQ-STK-03	The aircraft shall cruise at a ground speed of $700\,\mathrm{km/h}$ or more	Red
REQ-STK-04	The maximum cruise flight level shall be FL290 or above	Red
REQ-STK-05	The required take-off distance shall be $2100\,\mathrm{m}$ or below	Red
REQ-STK-06	The required landing distance shall be $1500\,\mathrm{m}$ or below	Red
REQ-STK-07	The aircraft shall comply with the CS-25 regulations	Yellow
REQ-STK-08	The operational reliability of the aircraft shall be equal or higher than the A320neo	Yellow
REQ-STK-09	The aircraft shall have no required additional maintenance compared to the A320neo	Yellow
REQ-STK-10	$75\,\%$ or more of the materials used in the aircraft parts shall be recyclable/re-processable	Red
REQ-STK-11	The total environmental impact of the aircraft's life-cycle shall be less than that of the A320neo	Red
REQ-STK-12	The aircraft's operational CO_2 emissions per passenger per kilometer shall be $25\,\%$ lower than those of the Airbus A320neo	Red
REQ-STK-13	The aircraft's operational NOx per passenger per kilometer emissions shall be $50\,\%$ lower than that of the Airbus A320neo	Red
REQ-STK-14	The cumulative effective perceived noise level (EPNL) of the aircraft shall be $20\,\%$ lower than that of the Airbus A320neo	Red
REQ-STK-15	The unit cost of each aircraft shall be less than €130 million in 2024	Black
REQ-STK-16	The aircraft shall be able to accommodate an amount of 290 to 330 passengers	Red
REQ-STK-17	The aircraft shall be in service in 2035	Red

3
Aircraft Concept Development

To meet the stakeholder requirements listed in Chapter 2, aircraft concepts were conceived during the conceptual design phase, which is covered in the Midterm Rreport [3]. The trade-off of these concepts, summarised in Section 3.2, resulted in two options that were too close to call. These concepts are developed further, such that they can be weighted against each other on a set of critical metrics in Section 3.3.

3.1. Design Concept Recap

This section will provide a recap of the design process used to develop the preliminary design in the midterm report. The results of this process were used for the trade-off. Additionally, the mission profile of the aircraft can be seen in Figure 3.1.

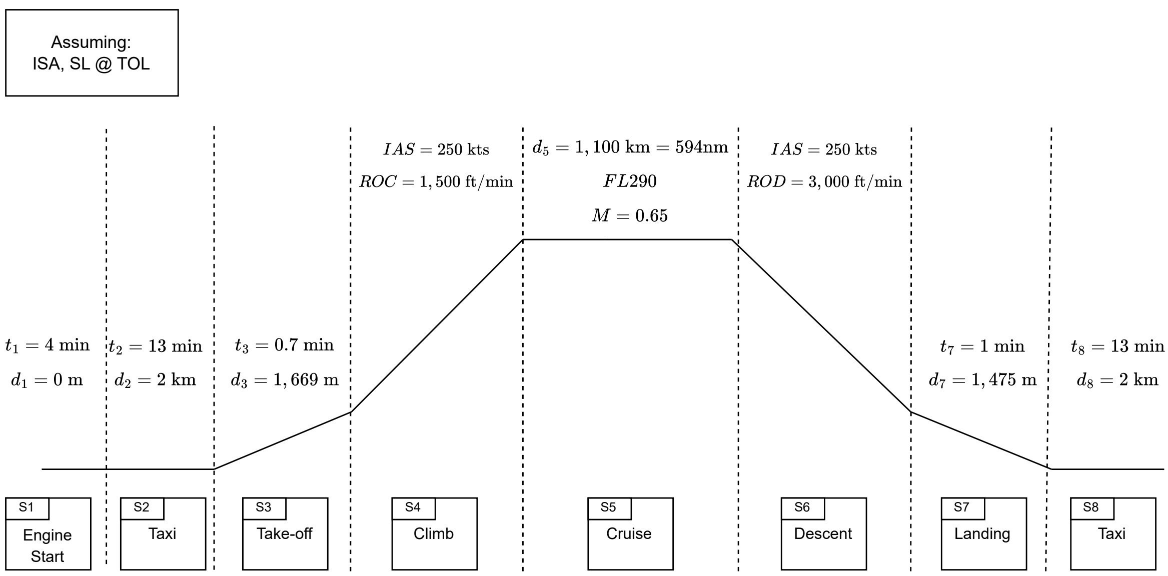

Figure 3.1: The X-300 EcoFlyer mission profile.

The basis of the Python program written for the preliminary design was on empirical Class I and Class II estimations from literature [6]. This process was divided into modules to reduce the chances of errors and to help with parallel programming. Additionally, sizing of high-lift devices and ailerons was done in the midterm phase but was not part of the weight calculations. Figure 3.2 displays a flowchart of the code iteration process.

1. **Select configuration**: All of the configurations in the trade-off were input in a file such that they could be selected easily.
2. **Gather and initialise statistical data**: For Class I estimations, statistical data relating to aircraft parameters such as weight, thrust, and take-off distance were gathered. Initial data, such as TSFC and lift-to-drag ratio, for the first iteration was also input from the literature.
3. **Perform Class I weight estimation**: This module comprised calculating the OEM, MTOM, fuel consumption, and flight endurance from statistical methods. A thrust-to-weight and wing-loading diagram was also created to estimate the required thrust and wing area.
4. **Wing planform sizing**: This module sizes the wing planform parameters. This includes wingspan, chord length, and sweep.
5. **Hydrogen tank sizing**: If the chosen configuration assumed liquid hydrogen as an energy source, then this module was run. This module calculated the tank mass and the increase in fuselage length due to the tank.
6. **Fuselage sizing**: This module calculated the fuselage dimensions, such as fuselage diameter and length. It also calculated the cargo space available for the aircraft.
7. **Empennage sizing**: This module analysed the CG excursion which determined the position of the wing, as well as the size and position of the empennage.
8. **Class II lift and drag estimation**: This module calculated the lift and drag coefficients using more detailed methods, albeit still empirical. This returned the lift and drag ratio which would affect the fuel consumption and mass in further iterations.
9. **Class II weight estimation**: In this module, the aircraft's weight was calculated at a component level (as opposed to Class I which uses the whole aircraft at once). This led to more detailed estimations.
10. **Finish iteration**: After the weight is known from Class II estimations, it is checked whether the weight is within $0.005\,\%$ of the weight calculated in the previous iteration. If it is, then the design has converged, and all the parameters are stored. If not, another iteration is performed

Verification and validation were done to ensure that the code gave valid results. Code verification included performing a series of unit tests and system tests. Next, the code was validated by giving Airbus A320 values as input and comparing outcome values (such as fuselage length, weight, and wingspan) to information found in literature. The outcome of the validation was positive, and the results were stored.

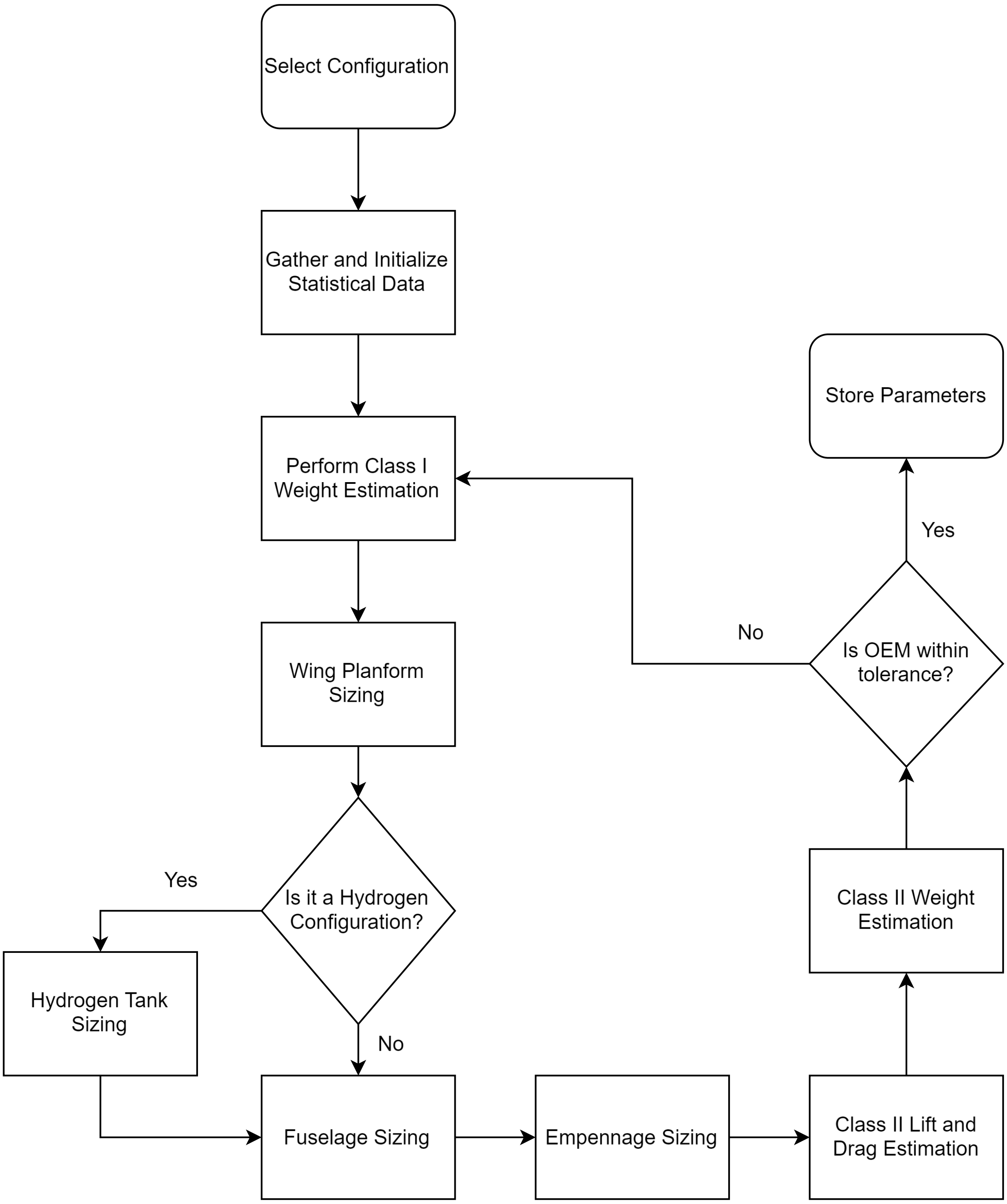

Figure 3.2: Flowchart of program structure used in the midterm report.

3.2. Initial Trade-Off Summary

The concept generation phase resulted in ten concepts entering the trade-off [2]. These options are listed in Table 3.1 and vary in cabin configuration and energy source/engine type.

Table 3.1: Design concepts entering trade-off.

No.	Airframe	Interior	Energy Source	Engine Type
1A	Conventional Tube-and-Wing	Single-Aisle	SAF	Turbofan
1B	Conventional Tube-and-Wing	Double-Aisle	SAF	Turbofan
2A	Conventional Tube-and-Wing	Single-Aisle	SAF	Turboprop
2B	Conventional Tube-and-Wing	Double-Aisle	SAF	Turboprop
3A	Conventional Tube-and-Wing	Single-Aisle	SAF	Turbo-electric
3B	Conventional Tube-and-Wing	Double-Aisle	SAF	Turbo-electric
4A	Conventional Tube-and-Wing	Single-Aisle	SAF	Propfan
4B	Conventional Tube-and-Wing	Double-Aisle	SAF	Propfan
5A	Conventional Tube-and-Wing	Single-Aisle	LH2	Turbofan
5B	Conventional Tube-and-Wing	Double-Aisle	LH2	Turbofan

To trade these options off, six criteria were selected based on the key requirements the design needs to fulfil. Subsequently, these criteria were assigned weights based on their relevance and importance. The criteria and their weights are summarised in Table 3.2.

The concepts were then scored on each criterion, with the results shown in Table 3.2. Additionally, a sensitivity analysis was performed to assess the robustness of this trade-off. This sensitivity analysis also identified opportunities and risks for further development, which will be addressed in Section 3.3.

The outcome of the trade-off showed that the LH2 aircraft were close contenders for winning the trade-off based on their strong performance on the sustainability criteria. However, the options scored unacceptable on *CRIT-DOC*, ruling them out as a winner. The overall winner ended up being the single-aisle SAF propfan concept, closely followed by the single-aisle SAF turbofan concept.

The sensitivity analysis confirmed these options as the most feasible but did not conclude which concept is superior. Thus, the result of the initial trade-off was too close to call. The concepts are developed further in Section 3.3 to make a final decision.

Table 3.2: Trade-off criteria, their respective related requirements, and their weight.

Identifier	Criteria	Requirements	Weight
CRIT-CO2	The amount of CO_2 emitted per ASK for the aircraft flying a distance of $1100\,\mathrm{km}$ in cruise	REQ-STK-11, REQ-STK-12	$25\,\%$
CRIT-NOX	The amount of NO_x emitted per ASK for the aircraft flying a distance of $1100\,\mathrm{km}$ in cruise	REQ-STK-11, REQ-STK-13	$25\,\%$
CRIT-EPN	The EPNdB of the aircraft at ”flyover”	REQ-STK-11, REQ-STK-14	15%
CRIT-TRL	The TRL level of the propulsion and fuel system	REQ-STK-07, REQ-STK-15, REQ-STK-17	$15\,\%$
CRIT-DOC	The direct operating cost for the aircraft including fuel, oil, and maintenance costs	REQ-STK-09	$10\,\%$
CRIT-GHT	The ground handling time of the aircraft including boarding and fuelling times	REQ-STK-08	$10\,\%$

Table 3.3: Trade-off summary.

Design options	CO2 (0.25)	NOX (0.25)	EPN (0.15)	TRL (0.15)	DOC (0.10)	GHT (0.10)	Total score
1A	2	2	3	4	4	3	2.75
1B	2	1	3	4	4	4	2.60
2A	1	1	2	4	3	3	2.00
2B	1	1	2	4	2	4	2.00
3A	1	1	2	1	1	3	1.35
3B	1	1	2	1	1	4	1.45
4A	3	2	2	4	4	3	2.85
4B	2	1	2	4	4	4	2.45
5A	4	3	3	2	1	2	2.80
5B	4	3	3	2	1	3	2.90

Criteria & weights

3.3. Concept Development

The trade-off showed that both concepts have to improve significantly on several metrics to meet the requirements. Both the propfan and turbofan options need to improve significantly with regard to CO_2 and NO_x emissions to meet the requirements. Furthermore, noise reduction remains a significant challenge for both options, but particularly for the propfan concept. In Subsection 3.3.1, technology improvements are identified and assessed before their integration into the concepts is discussed in Subsection 3.3.2 and Subsection 3.3.3.

3.3.1. Assessment of Technology Improvements

To address the shortcomings of the sustainability metrics, advanced engine architectures are considered. One such technology is the multi-fuel combustor concept. This concept uses stored LH2 as well as kerosene (or SAF), which are combusted in a multi-fuel combustor. On a retro-fit A320, this technology is estimated to reduce CO_2 emissions by up to $50\,\%$, according to Derwent[1]. The report by Derwent referenced above was part of their bid to be a part of the Cavendish project[2]. However, Rolls Royce has since taken the lead on this project and does not list Derwent as a partner[3]. The Cavendish project mainly aims to prototype and integrate full hydrogen combustion technologies in a Rolls Royce donor engine; the exploration of multi-fuel combustors is only listed as an additional objective [2].

Thus, there is little evidence that the multi-fuel combustor is pursued with sufficient funding and attention. Additionally, the concept would require significant development of hydrogen storage and distribution systems, which were also identified to be at a low TRL in the midterm report [3]. The combination of both the low confidence in the combustion technology development and the low TRL of hydrogen storage systems carries too much risk. Thus, the multi-fuel combustor is ruled out for integration in either of the concepts.

In a similar fashion, Fokker Next Gen is aiming to build an aircraft capable of operating on both $100\,\%$

[1] https://aviationweek.com/shownews/paris-air-show/derwent-unveils-dual-saf-hydrogen-combustor-conventional-narrowbodies

[2] https://cordis.europa.eu/project/id/101102000

[3] https://www.rolls-royce.com/media/our-stories/discover/2023/one-step-closer-to-climate-neutral-aviation.aspx

SAF (or kerosene) as well as $100\,\%$ hydrogen[4]. The benefit this provides is the fuel flexibility for the operator and the potential elimination of CO_2 emissions. The engines would have to be capable of operating on both hydrogen and SAF (or kerosene). A combustor operating on either hydrogen or SAF is being researched as part of the APPU project[5]. However, this technology is applied to the APU, not the main engines and is also a low-TRL technology. Additionally, this concept again relies on the storage of LH2, which is also considered to be a low-TRL technology. Again, the combination of these factors rules this option out.

The most promising option that was already identified during the sensitivity analysis is the implementation of water-injection combustion. This technology promises to reduce NO_x emissions by up to $90\,\%$ with respect to a conventional turbofan, as well as decreasing specific fuel consumption by 10 to $15\,\%$, at the cost of increased engine weight [7]. However, this advanced technology is inadvertently paired with a lower TRL and higher development risk.

Importantly, the water-injected turbofan (WIT) concept does not suffer from the combination of low TRL technologies, as the fuel system is identical to that of current turbofans. However, the engine itself is a significant step away from what is currently in operation due to the water-injection system and the heat-recovery systems. The significant development required necessitates strong evidence from within the industry that this technology is on target for entry-into-service in 2035.

MTU leads the European SWITCH project, with total funding of $€68\,\mathrm{million}$ [6]. The project partners include Pratt & Whitney, Collins Aerospace, GKN Aerospace and Airbus[7]. The project is scheduled to perform a full-system ground demonstration before the end of 2025, paving the way for entry into service in 2035. The project is thus well-funded and well-supported by important OEMs, providing the necessary confidence that this concept will deliver. Additionally, the WIT technologies may also be implemented in future hydrogen combustors. Thus, manufacturers' investments retain value long-term. Finally, the WIT technology is applicable to a much broader share of the aircraft market than multi-fuel technologies. Thus, in this regard, the potential return on investment for engine manufacturers is significantly higher. The factors outlined above provide sufficient confidence that the development of this technology will continue to meet expectations.

The WIT concept is elaborated on in a later stage of the report. Important to consider is that the core flow is cooled by the bypass flow to condense water. To this end, the core flow is routed through heat exchangers in the bypass flow, into the nacelle. Here, the condensed water is separated and the exhaust flow leaves through the nacelle. A similar arrangement is not implementable in the open-rotor design, as there is no nacelle. The water would have to be condensed through a different pathway, or else the water cycle cannot be closed. After brainstorming this issue, no feasible solution was conceived for implementing the WIT concept into the propfan concept. Thus, the water-injected combustion is considered to be applicable to the turbofan configuration only.

To address the shortcomings with respect to noise emissions, the overall aircraft configuration and integration of critical systems are to be assessed. The integration of the engines has the most significant impact on noise emissions, followed by the integration of the landing gear. Shielding of the engines must be considered, either by the main wing, the fuselage, or the horizontal tail. Additionally, the landing gear size should be minimised and ideally should be integrated into the fuselage as much as possible.

3.3.2. Propfan Concept Development

Based on preliminary estimations of the propfan noise, the propfan needs to be shielded to meet the noise requirement. Thus, it has to be placed above the wing, above the fuselage, or above the

[4]https://www.fokkernextgen.com/about-fokker-next-gen
[5]https://www.tudelft.nl/lr/appu
[6]https://cordis.europa.eu/project/id/101102006
[7]https://www.mtu.de/technologies/clean-air-engine/water-enhanced-turbofan/

horizontal tail. Therefore, the engine is to be mounted on large pylons. Based on the projections for the CFM RISE engine, the diameter of the propfan is estimated at $4\,\mathrm{m}$ [8]. For reference, this is the same diameter as the fuselage.

For the placement of the engine, two main locations are considered. The first location is above the main wing and fuselage in a high-wing configuration. The second location is above the horizontal tail-plane, at the back of the aircraft. The pros and cons of these options are summarised in Table 3.4 and Table 3.5. Adding it together, the tail-mounted propfan is, despite the structural challenge, deemed most feasible.

Table 3.4: Pros and cons of wing/fuselage-mounted propfan.

Pros	Cons
Longitudinally close to center of mass: structurally efficient.	Large vertical distance to center of mass: significant nose-down moment.
Large area (wing and fuselage) available for noise-shielding.	Divided fuselage due to high-wing structure: operationally impossible.
	Low accessibility for checks and maintenance: requires adaptation from MRO's.
	Landing gear integration: wing-mounted (high noise) or fuselage-mounted (high drag).

Table 3.5: Pros and cons of tail-mounted propfan.

Pros	Cons
Allows for low-wing: wing-mounted landing gear, uninterrupted fuselage.	Large longitudinal distance to center of mass: structurally inefficient, large CG shift.
Significant area available for noise-shielding	Large vertical distance to center of mass: significant nose-down moment.
	Reduced accessibility for checks and maintenance: requires adaptation from MRO's.

The performance of the propfan concept remains largely unchanged, as the WIT technology is not applicable; it is therefore non-compliant with both the CO_2 criterion and the NO_x criterion. However, due to the integration of the engines, it could comply with the noise requirement.

3.3.3. Turbofan Concept Development

For the turbofan concept, engine noise shielding also needs to be considered. The engine diameter is reduced compared to the propfan concept, so the pylons will not be as large. Besides this difference, the pros and cons of the engine positioning remain unchanged. The turbofan engines will thus also be integrated above the horizontal tail to provide noise shielding.

With the engines installed above the horizontal tail-plane, a conventional tail is not possible. The H-tail provides a good alternative that allows the engines to be close to the centerline of the fuselage, whilst providing sufficient directional stability. The one-engine-inoperative condition will likely not be a limiting condition for the H-tail sizing.

As the engines are placed at the back, the centre of mass of the aircraft is relatively far aft, pushing the wing backwards and increasing the CG shift during (un)loading. However, for a long single-aisle fuselage, this aft wing-position helps to increase the tail-strike angle, without necessitating long landing gear struts. As the landing gear struts have a significant impact on noise levels during landing, the aim is to minimise their size and optimize their integration into the airframe.

The turbofan concept will integrate the water-injected combustion concept. With this technology, the NO_x reduction comes well within reach. Additionally, the decreased specific fuel consumption will aid in meeting the CO_2 requirement. Finally, the concept promises to reduce contrail formation, increasing the overall climate benefit of this concept.

3.3.4. Concept Selection

To weigh up the (dis)advantages of both concepts, their performance on five metrics that have just been discussed is qualitatively summarised in Table 3.6. The comparison clearly shows that the turbofan with water-injected combustion is the way forward. The propfan disqualifies itself as it is unable to meet the performance requirements. It must be noted that in this regard, the turbofan concept is heavily dependent on the WIT combustion principle, which has a lower TRL. This is identified as a challenge going forward, potentially impacting development costs and risks. The assessment and mitigation of this risk will be discussed in Section 10.1, Chapter 13 and Chapter 15.

Table 3.6: Aircraft concept selection: a summary table.

Metric	Propfan Aircraft	Turbofan Aircraft
NO_x Emissions	non-compliant	compliant
CO_2 Emissions	non-compliant	feasible
Noise Emissions	challenging	compliant
TRL	compliant	challenging
Airframe Integration	challenging	feasible

3.4. Preliminary Design Parameters

The preliminary design of the aircraft is summarised in Table 3.7. The quantitative values have not yet been updated to reflect the changes made in the configuration development, as that process has been purely qualitative. The NO_x emissions are expected to drop significantly, and the OEM will rise due to the heavier engines and their integration. Similarly, due to the modified tail, the empennage parameters are expected to change. An artist impression is shown in Figure 3.3.

Table 3.7: Preliminary design parameters of X-300 concept aircraft.

Design characteristics	
Wing position	Low Wing
Engine type	Turbofan
Engine placement	Tail-mounted
Tail	H-Tail
Energy source	SAF
Fuselage parameters	
Outer fuselage diameter	$3.83\,\mathrm{m}$
Fuselage length	$54.22\,\mathrm{m}$
Seating configuration	3-3
Mass parameters	
OEM	$60\,080\,\mathrm{kg}$
MTOM	$122\,396\,\mathrm{kg}$
Maximum payload	$38\,971\,\mathrm{kg}$
Wing planform parameters	
Aspect ratio	8.5
Wingspan	$42.8\,\mathrm{m}$
Wing surface area	$215.65\,\mathrm{m}^2$
Leading-edge wing sweep	$2.86\,\mathrm{deg}$
Wing dihedral	$5.0\,\mathrm{deg}$
Root chord	$7.2\,\mathrm{m}$
Tip chord	$2.87\,\mathrm{m}$
MAC	$5.34\,\mathrm{m}$
Lift and drag	
Design C_L	0.487
Cruise L/D ratio	19.37
Empennage parameters	
Horizontal tail area	$49.86\,\mathrm{m}^2$
Horizontal tail span	$14.12\,\mathrm{m}$
Vertical tail area	$37.22\,\mathrm{m}^2$
Vertical tail span	$7.47\,\mathrm{m}$
Emission Indices	
CO_2	$3160\,\mathrm{g/kg}$
NO_x	<$11.16\,\mathrm{g/kg}$

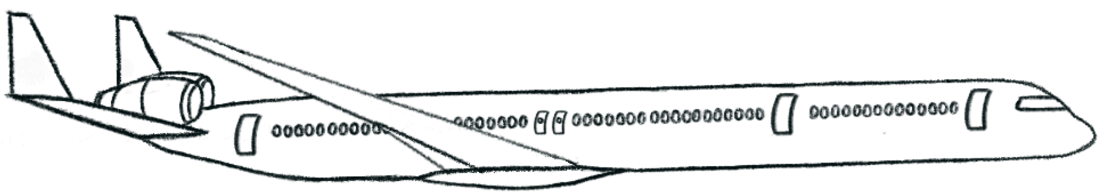

Figure 3.3: Preliminary design sketch of the chosen X-300 concept.

4
Functional Analysis

This chapter presents the functions of the X-300, which were first shown in the Baseline Report [2] and have now been updated to reflect the increased fidelity of the design. The functions are illustrated in two diagrams: a functional breakdown structure (Section 4.1) and a functional flow diagram (Section 4.2).

4.1. Functional Breakdown Structure

Figure 4.1 shows the functional breakdown structure of the X-300. This illustrates the program's functions in a hierarchical form. Here, "program" refers to the entirety of the aircraft's life cycle, from manufacture to disposal. As shown in the figure, four high-level functions have been identified:

1. Produce vehicle
2. Conduct flight operations
3. Conduct ground operations
4. Discontinue operations

All other functions which are dependent on these are listed on lower levels of the diagram. The system responsible for each function is indicated in the lower-left corner of each box (the meaning of each acronym is described in the legend). Details on some of these systems (IWETS, ECS, AFR) are presented in Chapter 5.

4.2. Functional Flow Diagram

Figure 4.2 (spreading over two pages) illustrates the functional flow diagram, which is a chronological order of the functions identified in the functional breakdown structure. Two gate operators are used in this diagram: "OR" gates, which indicate flows of activities dependent on particular conditions; and "AND" gates, which indicate flows of activity occurring in parallel. At the highest level ("LEVEL 1"), the flow of functions is as follows. First, the aircraft is manufactured (function F1.0). Then, it begins its operation on the ground (function F3.0). This is followed by an "OR" gate; if the aircraft is still in operation, it proceeds to perform a flight (F2.0). After the flight, the aircraft returns to the ground and conducts ground operations once again. This alternating cycle between ground and flight operations continues until the aircraft is decommissioned, at which point it proceeds from ground operations (F3.0), through the "OR" gate, to decommission (F4.0). Functional flows also occur at lower levels ("LEVEL 2", "LEVEL 3", and "LEVEL 4"). A miniaturised breakdown structure and dotted arrows show the hierarchical links between different levels.

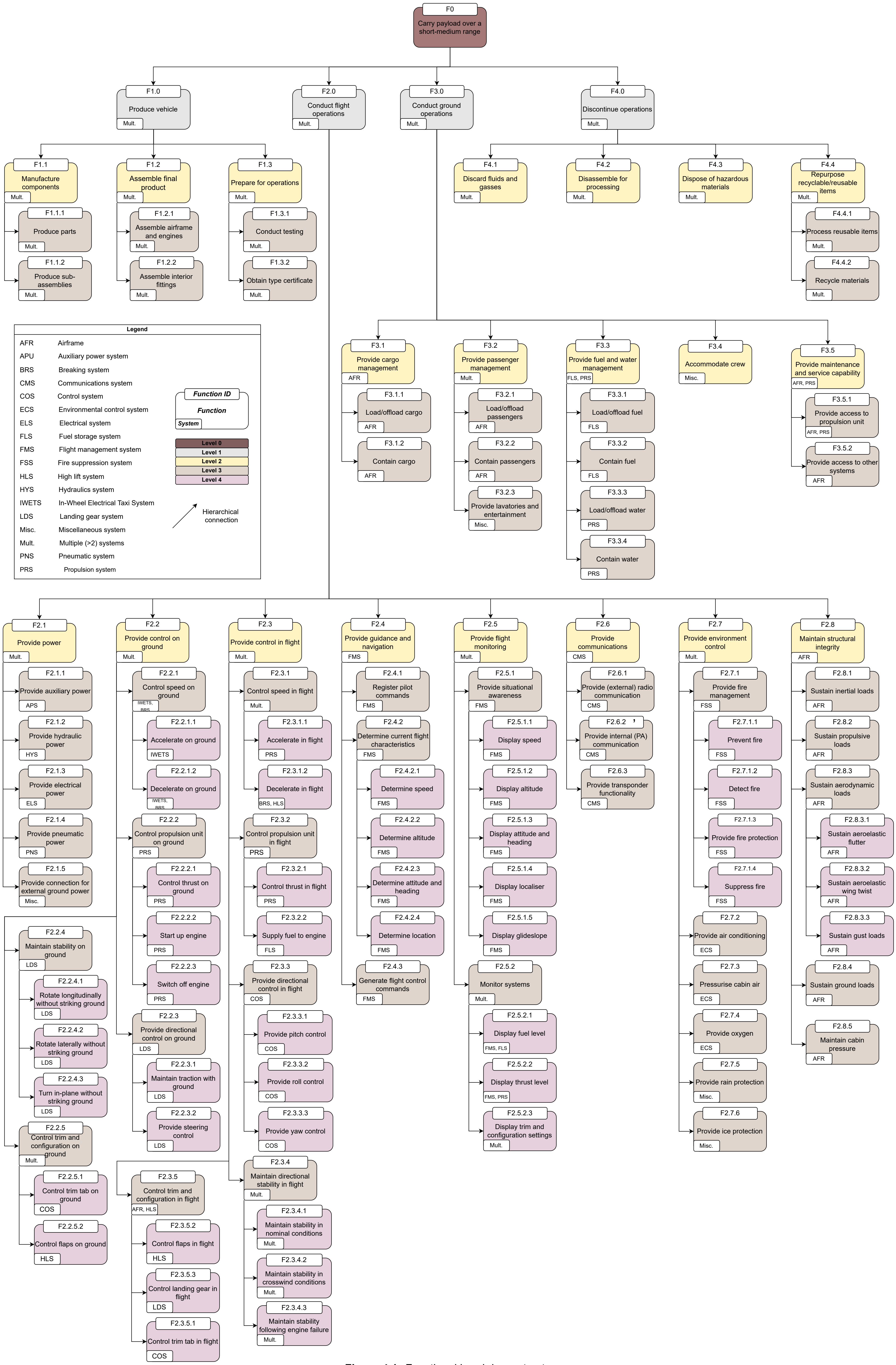

Figure 4.1: Functional breakdown structure.

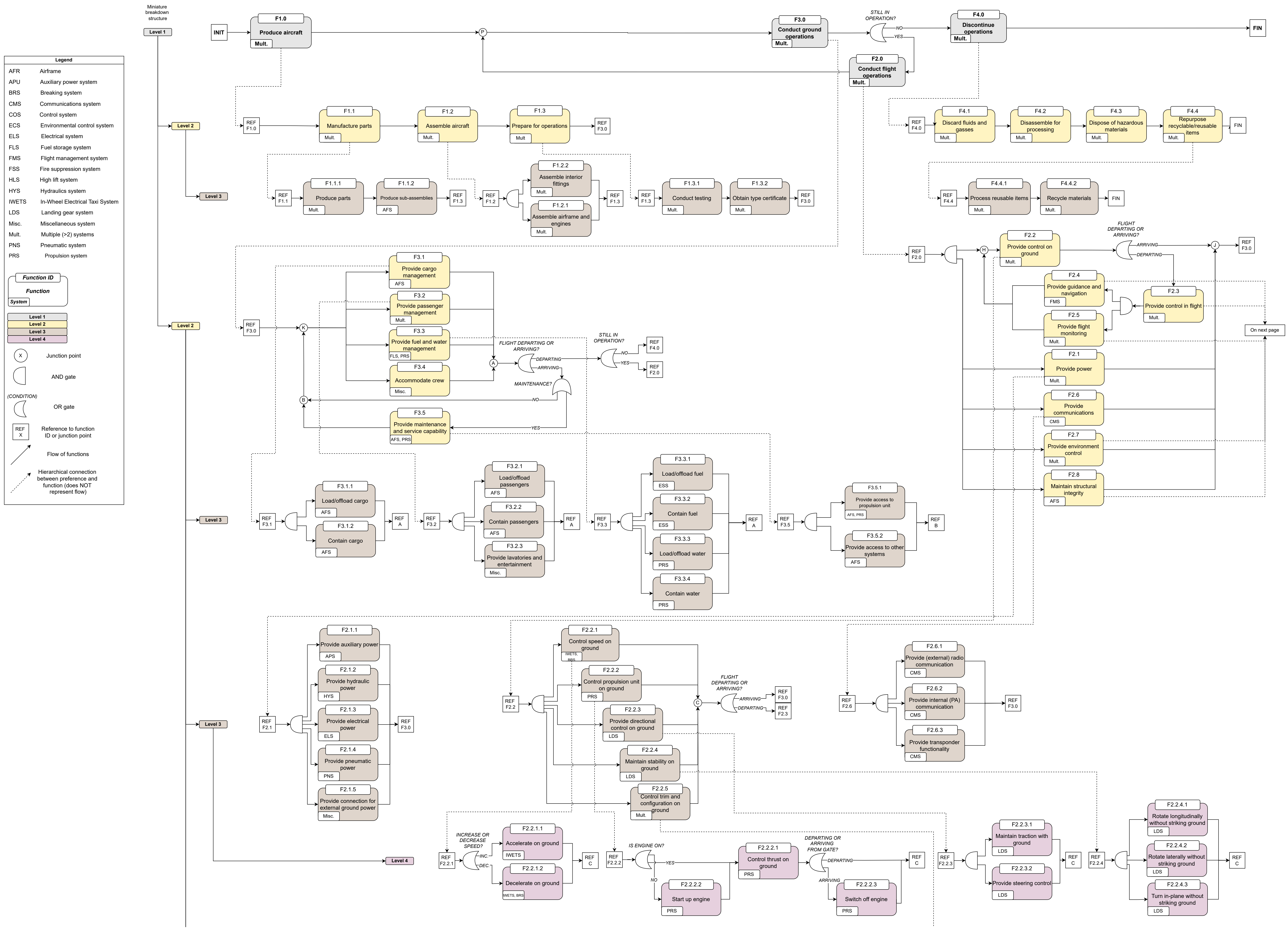

Miniature breakdown structure
Level 1
Level 2
Level 3
Level 2
Level 3
Level 3
Level 4
Legend
AFR Airframe
APU Auxiliary power system
BRS Breaking system
CMS Communications system
COS Control system
ECS Environmental control system
ELS Electrical system
FLS Fuel storage system
FMS Flight management system
FSS Fire suppression system
HLS High lift system
HYS Hydraulics system
IWETS In-Wheel Electrical Taxi System
LDS Landing gear system
Misc. Miscellaneous system
Mult. Multiple (>2) systems
PNS Pneumatic system
PRS Propulsion system
Function ID
Function
System
Level 1
Level 2
Level 3
Level 4
Junction point
AND gate
(CONDITION)
OR gate
REF X
Reference to function ID or junction point
Flow of functions
Hierarchical connection between preference and function (does NOT represent flow)
INIT
F1.0 Produce aircraft Mult.
F3.0 Conduct ground operations Mult.
STILL IN OPERATION?
NO
YES
F4.0 Discontinue operations Mult.
FIN
F2.0 Conduct flight operations Mult.
REF F1.0
F1.1 Manufacture parts Mult.
F1.2 Assemble aircraft Mult.
F1.3 Prepare for operations Mult
REF F3.0
REF F4.0
F4.1 Discard fluids and gasses Mult.
F4.2 Disassemble for processing Mult.
F4.3 Dispose of hazardous materials Mult.
F4.4 Repurpose recyclable/reusable items Mult.
FIN
REF F1.1
F1.1.1 Produce parts Mult.
F1.1.2 Produce sub-assemblies AFS
REF F1.3
REF F1.2
F1.2.2 Assemble interior fittings Mult.
F1.2.1 Assemble airframe and engines Mult.
REF F1.3
REF F1.3
F1.3.1 Conduct testing Mult.
F1.3.2 Obtain type certificate Mult.
REF F3.0
REF F4.4
F4.4.1 Process reusable items Mult.
F4.4.2 Recycle materials Mult.
FIN
REF F2.0
F2.2 Provide control on ground Mult.
FLIGHT DEPARTING OR ARRIVING?
ARRIVING
DEPARTING
REF F3.0
F2.4 Provide guidance and navigation FMS
F2.3 Provide control in flight Mult.
F2.5 Provide flight monitoring Mult.
On next page
F2.1 Provide power Mult.
F2.6 Provide communications CMS
F2.7 Provide environment control Mult.
F2.8 Maintain structural integrity AFS
REF F3.0
F3.1 Provide cargo management AFS
F3.2 Provide passenger management Mult.
F3.3 Provide fuel and water management FLS, PRS
F3.4 Accommodate crew Misc.
F3.5 Provide maintenance and service capability AFS, PRS
FLIGHT DEPARTING OR ARRIVING?
DEPARTING
ARRIVING
STILL IN OPERATION?
NO
YES
REF F4.0
REF F2.0
MAINTENANCE?
NO
YES
REF F3.1
F3.1.1 Load/offload cargo AFS
F3.1.2 Contain cargo AFS
REF A
REF F3.2
F3.2.1 Load/offload passengers AFS
F3.2.2 Contain passengers AFS
F3.2.3 Provide lavatories and entertainment Misc.
REF A
REF F3.3
F3.3.1 Load/offload fuel ESS
F3.3.2 Contain fuel ESS
F3.3.3 Load/offload water PRS
F3.3.4 Contain water PRS
REF A
REF F3.5
F3.5.1 Provide access to propulsion unit AFS, PRS
F3.5.2 Provide access to other systems AFS
REF B
REF F2.1
F2.1.1 Provide auxiliary power APS
F2.1.2 Provide hydraulic power HYS
F2.1.3 Provide electrical power ELS
F2.1.4 Provide pneumatic power PNS
F2.1.5 Provide connection for external ground power Misc.
REF F3.0
REF F2.2
F2.2.1 Control speed on ground IWETS, BRS
F2.2.2 Control propulsion unit on ground PRS
F2.2.3 Provide directional control on ground LDS
F2.2.4 Maintain stability on ground LDS
F2.2.5 Control trim and configuration on ground Mult.
FLIGHT DEPARTING OR ARRIVING?
ARRIVING
DEPARTING
REF F3.0
REF F2.3
REF F2.6
F2.6.1 Provide (external) radio communication CMS
F2.6.2 Provide internal (PA) communication CMS
F2.6.3 Provide transponder functionality CMS
REF F3.0
REF F2.2.1
INCREASE OR DECREASE SPEED?
INC.
DEC.
F2.2.1.1 Accelerate on ground IWETS
F2.2.1.2 Decelerate on ground IWETS, BRS
REF C
REF F2.2.2
IS ENGINE ON?
YES
NO
F2.2.2.1 Control thrust on ground PRS
F2.2.2.2 Start up engine PRS
DEPARTING OR ARRIVING FROM GATE?
DEPARTING
ARRIVING
F2.2.2.3 Switch off engine PRS
REF C
REF F2.2.3
F2.2.3.1 Maintain traction with ground LDS
F2.2.3.2 Provide steering control LDS
REF C
REF F2.2.4
F2.2.4.1 Rotate longitudinally without striking ground LDS
F2.2.4.2 Rotate laterally without striking ground LDS
F2.2.4.3 Turn in-plane without striking ground LDS
REF C

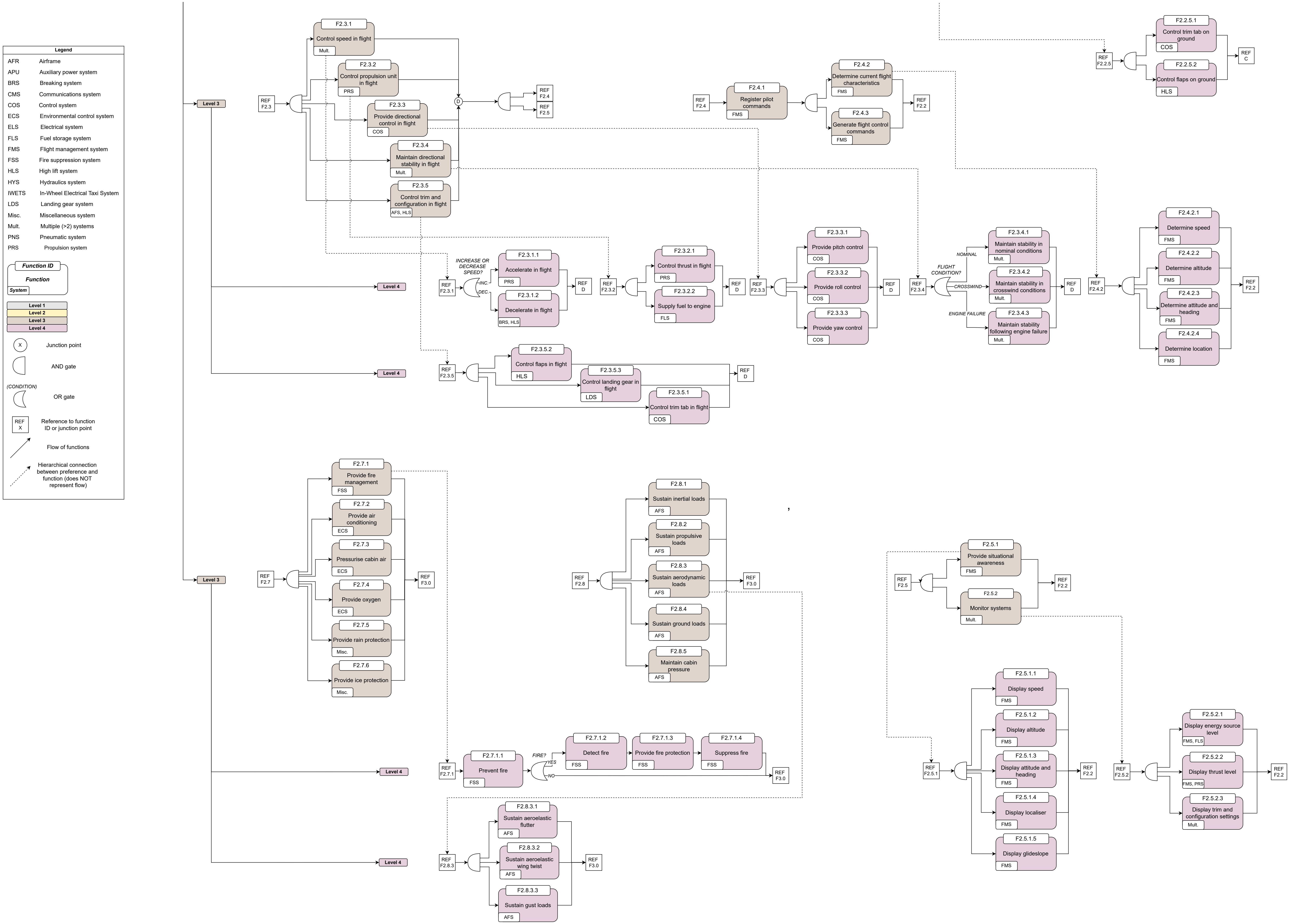

Figure 4.2: Functional flow diagram.

5 Detailed System Design

Starting from the preliminary design, the design is developed further to a higher degree of detail. First, the design of the propulsion system is described in Section 5.1, covering the engine performance and engine sizing. Then, the electrical power system is elaborated on in Section 5.2, covering the electrical power budget. In Section 5.3, the design of the fuel system is discussed, with a focus on operations and reliability. The innovative electric taxiing system is discussed in Section 5.4 and the fuel-saving environmental control system is the topic of Section 5.5. Finally, the development of the airframe is described in Section 5.6, covering the used materials, designed structures, aerodynamics, stability and control characteristics.

The detailed design of the X-300 is the result of an iterative process. Since the sizing of one system affects the sizing of the others, an iterator had to be constructed which allows for a clear link between each subsystem. In the context of this process, these subsystems which are to be iterated are called *modules*. The X-300 iterator comprises three modules: the electric taxiing system (Section 5.4), the aerodynamics module (Subsection 5.6.3), and the stability module (Subsection 5.6.4). Based on the preliminary design (Section 3.1), the iterator is run as long as the relative change in OEM is strictly less than a preset tolerance of 5×10^{-6}. The detailed design of the remaining subsystems such as the structural analysis, or environmental control is carried out based on the aircraft parameters resulting from the iterative process. For clarity and conciseness purposes, however, the remainder of this chapter discusses the design process based on these final values, so pertaining to the final, converged design.

5.1. Propulsion System

In this section, the propulsion system is developed. The propulsion system concept is outlined in Subsection 5.1.1. The design of the system involves the development of a thermodynamic model, described in Subsection 5.1.2. The model is then matched and validated with a similar existing model in Subsection 5.1.3 before the applicability to the X-300 is discussed in Subsection 5.1.4. The approach to verification and validation is discussed in Subsection 5.1.5. Finally, the engine sizing is the subject of Subsection 5.1.6.

5.1.1. Engine Performance: Concept

In the conceptual design, the water-injected-turbofan (WIT) concept was selected as the engine of choice for the X-300. In this section, the engine performance is analysed based on a thermodynamic model of the engine. In Subsection 5.1.6, the sizing of the engine in terms of weight and dimensions is discussed.

The principle of the WIT engine is to inject water vapour into the mixer before the combustor. This is to reduce combustion temperatures and increase the specific heat of the flow. As a result, the NO_x emissions are reduced and the specific work is increased, allowing for significant bypass ratios. Additionally, waste heat from the core-flow is recuperated through heat exchangers. In the first heat exchanger, the vaporizer, the core flow heats the water that is to be injected as steam. Then, the flow is cooled down through a heat exchanger in the bypass to the point that the water in it condenses. The water is then captured and pressurized before it is fed into the vaporizer. The vaporized water powers a steam turbine, which is connected to the low-power shaft powering the fan. Recuperating the waste-heat of the core flow helps to increase thermal efficiency. Overall, this technology promises to reduce NO_x emissions by over $90\,\%$ and TSFC by $15\,\%$ [7]. However, due to the weight of the extra components, the engine is expected to be significantly heavier, slightly off-setting the specific performance gains.

5.1.2. Engine Performance: Model Description

The thermodynamic model is based on a paper written by researchers at MTU [7]. The thermodynamic model described in the paper consists of 30 modules and corresponding stations. This includes a large number of 'ducting' modules, some of which are left out in the model developed here. Not only do these modules add extra complexity, but the quantification of their effects is also outside the scope of the current analysis. The simplifications lead to the model in Figure 5.1. The station numbers are kept consistent with those in the paper.

The formulas describing the thermodynamic relations are based on Power & Propulsion from the second year of the TU Delft Aerospace Bachelor (AE2230-II). Any deviations from this course will be clearly indicated. Pressure ratios are denoted by Π, whilst temperature ratios are denoted by τ. Total conditions are denoted by a zero-subscript, followed by the station number: $T_{0,x}$, $p_{0,x}$.

The equations are given for each type of module, but not for each module individually. For example, there are three nozzle modules that each use the nozzle calculations as described. To calculate the gas properties along the core flow path and for the bypass flow, NASA's CEA method is used [9]. To compute the properties of the water cycle, the IF97 standard is utilised [10]. The model is written in Python and existing Python packages are imported to use CEA[1] and IF97[2].

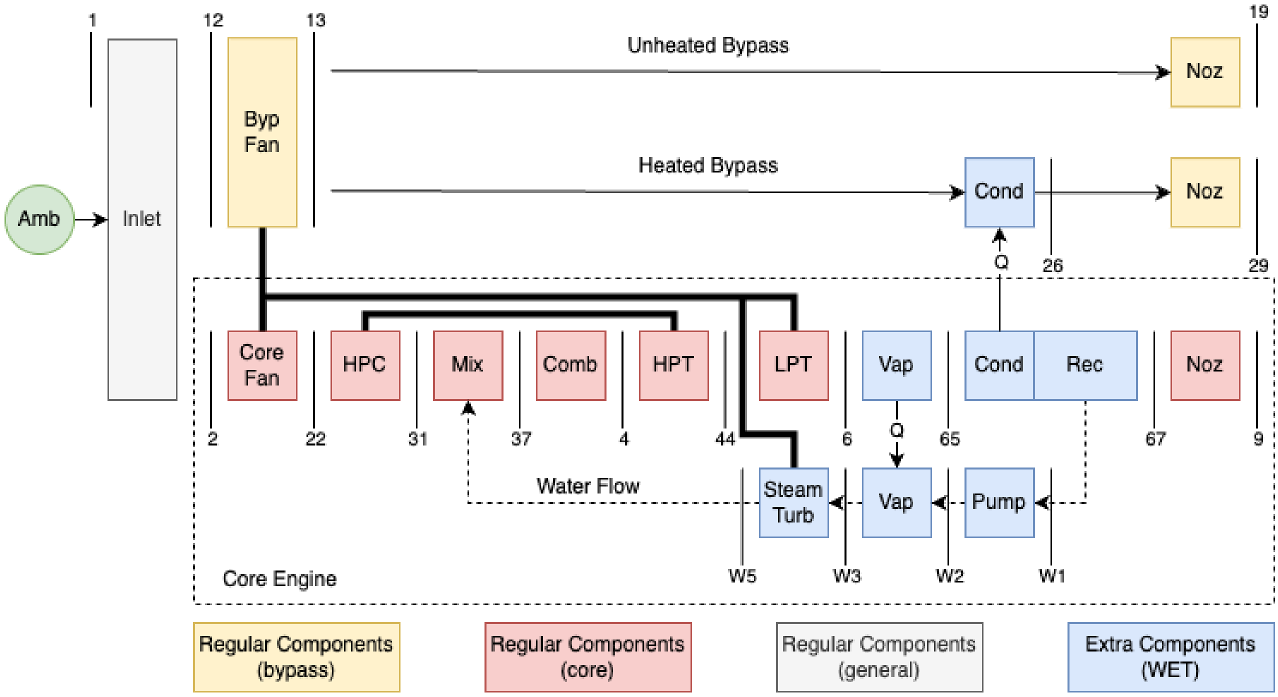

Figure 5.1: Thermodynamic model description of the WIT engine.

[1]https://github.com/civilwargeeky/CEA_Wrap
[2]http://www.coolprop.org/coolprop/wrappers/Python/index.html

Total Conditions

The total conditions are calculated using the standard relations that make use of the free-stream Mach number M_0 and the ratio of specific heats κ_a.

$$\tau_t = \frac{T_{0,1}}{T_a} = 1 + \frac{k_a - 1}{2} M_0^2 \qquad (5.1)$$

$$\Pi_t = \frac{p_{0,1}}{p_a} = \tau_r^{\frac{k_a}{k_a - 1}} \qquad (5.2)$$

Inlet

The inlet pressure ratio is calculated based on the inlet efficiency η_{inlet}. The total temperature remains constant across the inlet.

$$T_{0,2} = T_{0,1} \qquad (5.3)$$

$$\Pi_{in} = \frac{p_{0,2}}{p_a} = (1 + \eta_{inlet} \frac{k_a - 1}{2} M_0^2)^{\frac{k_a}{k_a - 1}} \qquad (5.4)$$

Fan

The pressure ratio of the fan is a specified parameter, based on which the pressure aft of the fan is calculated. Using the assumed isentropic efficiency of the fan, the temperature ratio across the fan is calculated. The work done on the fluid by the fan is calculated using the change in temperature, mass flow and specific heat of air.

$$\Pi_{fan} = \frac{p_{0,21}}{p_{0,2}} \qquad (5.5)$$

$$BPR = \frac{\dot{m}_{12}}{\dot{m}_2} = \frac{\dot{m}_1}{\dot{m}_2} - 1 \qquad (5.6)$$

$$\tau_{fan} = 1 + \frac{1}{\eta_{is,fan}} \left((\Pi_{fan})^{\left(\frac{k_a - 1}{k_a}\right)} - 1) \right) \qquad (5.7)$$

$$\dot{W}_{fan} = \dot{m}_2 c_{p,a} \left(T_{0,21} - T_{0,2} \right) \qquad (5.8)$$

Spool Power

The spool connects the fan, consisting of the core fan (CF) and the bypass fan (BPF), to the low-pressure turbine (LPT) and the steam turbine (ST). The mechanic efficiency of this setup is taken into account.

$$\dot{W}_{fan} = \dot{W}_{cf} + \dot{W}_{bpf} = (\dot{W}_{LPT} + \dot{W}_{ST}) \eta_m \qquad (5.9)$$

High pressure compressor

The high pressure has a specified compression ratio Π_{HPC}, based on which the aft pressure and temperature are calculated. The work done by the compressor is calculated analogously to how the work of the fan is calculated. The compressor is powered by and connected to the high-pressure turbine with a specified mechanical efficiency η_{mech}.

$$\Pi_{HPC} = \frac{p_{0,30}}{p_{0,22}} \qquad (5.10)$$

$$\dot{W}_{HPC} = \dot{m}_2 c_{p,a} \left(T_{0,30} - T_{0,22} \right) \qquad (5.11)$$

$$\tau_{HPC} = 1 + \frac{1}{\eta_{is,HPC}} \left(\Pi_{HPC}^{\frac{k_a - 1}{k_a}} - 1 \right) \qquad (5.12)$$

$$\dot{W}_{HPT} = \frac{\dot{W}_{HPC}}{\eta_{mech}} \qquad (5.13)$$

Mixer

In the mixer, the steam that has powered the steam turbine is injected. Perfect mixing is assumed, such that the flow is homogeneous. To calculate the properties of the gas entering the combustion chamber, the NASA CEA method is used, with a defined enthalpy problem. That is, the temperature of the air and steam, as well as their mass fractions, are inputs. The program outputs the resulting temperature of the mixture and the associated specific heats and ratios.

The mass flow of the injected water is calculated using a pre-set water-to-air ratio (WAR). This is an important design variable.

$$\dot{m}_{W5} = \dot{m}_2 WAR \tag{5.14}$$

$$\dot{m}_{W5} = \dot{m}_2 + \dot{m}_{W5} \tag{5.15}$$

Combustor

The combustor is assumed to be a constant-pressure combustor, with a small pressure loss modelled by the combustor pressure ratio. Based on the chosen equivalence ratio and stoichiometric fuel-to-air ratio, the mass flow of the fuel is calculated. The combustor outlet temperature, or turbine inlet temperature, can then be calculated. The resulting water-to-fuel ratio is calculated as well.

$$\dot{m}_f = \phi \cdot FAR_{stoich} \cdot \dot{m}_2 \tag{5.16}$$

$$\Pi_c = \frac{p_{0,4}}{p_{0,37}} \tag{5.17}$$

$$T_{0,4} = T_{0,37} + \frac{\dot{m}_f \cdot LHV \cdot \eta_{comb}}{\dot{m}_{37} \cdot c_{p,37}} \tag{5.18}$$

$$WFR = \frac{\dot{m}_{W5}}{\dot{m}_f} \tag{5.19}$$

Turbines

The turbine outlet temperatures are calculated based on the required power, the mass flow and the specific heat of the core flow. Using the turbine's isentropic efficiency, the pressure ratio is determined.

$$T_{0,out} = T_{0,in} - \frac{\dot{W}_T}{\dot{m} c_p} \tag{5.20}$$

$$\Pi_T = \left(1 - \frac{1}{\eta_T}(1 - \tau_T)\right)^{\frac{\kappa}{\kappa-1}} \tag{5.21}$$

Vaporizer

The vaporizer uses the heat contained in the core flow to heat the water flow. It does so through a heat exchanger. The heat exchanger effectiveness is defined as in Equation 5.22. The heat-exchanger effectiveness is highly dependent on the physical geometry and performance properties of such a heat exchanger. This value is thus not readily available. Instead, it is assumed that the vaporizer cools the core flow to within 5% or less of the temperature at which the water will start to condense for the given pressure. With this design decision, the required heat exchanger effectiveness is calculated. It is then checked that the heat exchanger effectiveness is between 0.3 and 0.6.

The potential heat flows are calculated using the respective mass flows and specific enthalpies. The specific enthalpies are obtained through CEA for the core flow and through IF97 for the water flow.

The water entering the vaporizer is first heated, then vaporized, after which the steam is heated. The heat transfer required for each of these is combined before the final steam temperature is calculated.

$$\epsilon = \frac{Q_{actual}}{\min\left\{\dot{m}_c \cdot \left(h_c\left(T_c\right) - h_c\left(T_w\right)\right),\, \dot{m}_w \cdot \left(h_w\left(T_c\right) - h_c\left(T_w\right)\right)\right\}} \tag{5.22}$$

$$T_{saturation} = CEA(p_{0,6}, T_{0,6}) \tag{5.23}$$

$$Q_{heatwater} = \dot{m}_{W2} \cdot c_{p,W2} \cdot (T_v - T_{W2}) \tag{5.24}$$

$$Q_{heatsteam} = Q_{actual} - Q_{heatwater} - Q_{vaporize} \tag{5.25}$$

$$Q_{actual} = \dot{m}_6 \cdot c_{p,6} \cdot (T_{0,6} - T_{saturation}) \tag{5.26}$$

$$Q_{vaporize} = \dot{m}_{W2} \cdot h_v \tag{5.27}$$

$$T_{W3} = T_v + \frac{Q_{heatsteam}}{\dot{m}_{W2} \cdot c_{p,steam}} \tag{5.28}$$

Condenser

The condenser is also a heat exchanger and is modelled using the same equation for heat exchanger effectiveness, Equation 5.22. As this effectiveness is not known, the assumption is made that the condenser condenses exactly enough water to close the water cycle. That is, the same amount of water is condensed as is injected. With this design point, the 'cooling product' (cp) is calculated. The cooling product is defined as the product of the heated bypass flow and the heat exchanger's effectiveness. With an assumed heat exchanger effectiveness of 0.5, the percentage of the bypass flow that cools the core flow is then calculated and verified to be less than $100\,\%$.

The change of specific enthalpy is calculated assuming that the potential heat flow from the bypass flow is designed to be smaller than the potential heat flow from the core flow. That is a valid assumption, as the engine would be designed such that the bypass flow is indeed limiting, in order to decrease the portion of the bypass flow that has to pass through the heat exchanger.

$$Q_{cooling} = \dot{m}_{65} \cdot c_{p,65} \cdot (T_{0,65} - T_{saturation}) \tag{5.29}$$

$$Q_{condense} = \dot{m}_{W1} \cdot h_v \tag{5.30}$$

$$cp = Q_{total}/\Delta h = \epsilon \cdot \dot{m}_{26} \tag{5.31}$$

$$\dot{m}_{67} = \dot{m}_{65} - \dot{m}_{W1} \tag{5.32}$$

$$Q_{total} = Q_{condense} + Q_{cooling} \tag{5.33}$$

$$T_{0,67} = T_{saturation} \tag{5.34}$$

$$\Delta h = h_{13}\left(T_{65}\right) - h_{13}\left(T_{13}\right) \tag{5.35}$$

$$T_{0,26} = T_{0,13} + \frac{Q_{total}}{\dot{m}_{26} \cdot c_{p,13}} \tag{5.36}$$

Nozzles

The nozzle performance is calculated using the standard method outlined in the mentioned course. First, it is determined if the flow is choked by comparing the pressure ratio to the critical pressure ratio.

$$\Pi_{cr} = \frac{1}{\left(1 - \frac{1}{\eta_{nozzle}}\frac{k-1}{k+1}\right)^{\frac{k}{k-1}}} \tag{5.37}$$

$$\Pi_{actual} = \frac{p_{0,noz}}{p_0} \tag{5.38}$$

If the flow is indeed choked, Equation 5.39 to Equation 5.43 are used to calculate the achieved thrust.

$$v_e = \sqrt{k \cdot R \cdot T_{out}} \tag{5.39}$$

$$A = \frac{\dot{m}RT_{out}}{p_{out}v_e} \tag{5.40}$$

$$T_{out} = \frac{2T_{0,noz}}{k+1} \tag{5.41}$$

$$p_{out} = \frac{p_{0,noz}}{\Pi_{cr}} \tag{5.42}$$

$$F_{thrust} = \dot{m}\left(v_e - v_0\right) + \left(p_{out} - p_a\right)A \tag{5.43}$$

If the flow is not choked, Equation 5.44 to Equation 5.47 are used to calculate the achieved thrust.

$$\Delta T = T_{0,noz}\eta_{noz}\left(1 - \frac{1}{\Pi_{actual}}\right)^{\frac{k-1}{k}} = T_{0,noz} - T_{out} \tag{5.44}$$

$$F_{thrust} = \dot{m}\left(v_e - v_0\right) \tag{5.45}$$

$$p_{out} = p_a \tag{5.46}$$

$$v_e = \sqrt{2c_p\Delta T} \tag{5.47}$$

Water Pump

The water pump efficiency can be calculated by calculating the enthalpy of the water entering and exiting the pump. This calculation is carried out by the `PropsSI` module from the Python `CoolProp` package [11]. In the code, the enthalpy is calculated using the pressure and temperature of the water. With the enthalpy known for inlet and exit conditions, the pump power can be calculated using Equation 5.48.

$$\dot{W}_{pump} = \dot{m}_w(h_{w,out} - h_{w,in}) \cdot \frac{1}{\eta_{pump}} \tag{5.48}$$

Maximum water pump efficiencies lay just below $90\,\%$ and are reached for high water flow rates ($500\,\mathrm{Ls^{-1}}$) [12]. Due to the lower water flow rate in the engine, the efficiency is lower. Thus the value used for the isentropic pump efficiency lowered to $75\,\%$, roughly coinciding with one of the data points in the study.

Steam Turbine

In the steam turbine, the (superheated) steam exits the vaporizer with a certain pressure and temperature. The outlet pressure is set slightly above the mixer stage pressure of the engine as this ensures a steam flow from the steam turbine into the mixing stage. Ideally, the steam is expanded isentropically to an outlet pressure, however, in reality, an isentropic efficiency needs to be taken into account. Using the outlet pressure the outlet temperature and the condensed steam percentage can be calculated. Manually, this would be done using steam tables. However, this is again automated in Python using `PropsSI` [11]. With the outlet conditions known the enthalpy of the steam entering and exiting the turbine is calculated. Lastly, the power output of the turbine is almost equal to Equation 5.48 with the exception that the isentropic turbine efficiency is to be multiplied instead of divided by. The formula for the steam turbine yields:

$$\dot{W}_{w,turbine} = \dot{m}_w(h_{w,out} - h_{w,in})\eta_{w,turbine} \tag{5.49}$$

Generally the larger a steam turbine the more efficient it is. A small turbine of $2\,\mathrm{kW}$ has shown the potential to reach $70\,\%$ isentropic turbine efficiency and this value is therefore used in the model [13].

NOx Emissions

The nitrous-oxide emissions are calculated using the method presented in the MTU paper [7]. The paper uses the relation for the emission index of NO_x as presented in GasTurb [14], and adjusts it with a technology factor TF, as well as a steam factor R_{STM}. The relation is presented in Equation 5.50. The technology factor is taken to be 0.72, based on state-of-the-art engines [15], assuming no technology improvements in this regard towards 2035. The steam factor is obtained through Equation 5.51 and is based on experimental data. It represents the ratio between NO_x emissions in a wet combustion process versus a dry combustion process, for varying levels of WAR.

$$EI_{NOx} = 32\frac{g}{kg} \cdot \exp\left(\frac{T_{37} - 826K}{194K}\right) \cdot \left(\frac{p_{37}}{2.965 \cdot 10^6 Pa}\right)^{0.4} \cdot TF \cdot R_{STM} \tag{5.50}$$

$$R_{STM} = \exp\left(\frac{-2.465WAR^2 - 0.915WAR}{WAR^2 + 0.0516}\right) \tag{5.51}$$

The wet combustion process achieves significant NO_x emission savings for three main reasons. First of all, the adiabatic flame temperature is reduced due to the presence of steam in the reaction process. Secondly, as the WIT engine operates at a reduced overall pressure ratio, the combustor inlet temperature and pressure are reduced. It does so because a lower overall pressure ratio leads to an increased turbine exit temperature, easing the extraction of heat from the core flow. And finally, the steam lowers the combustion inlet temperature even further.

To validate Equation 5.50 the NO_x emissions as calculated by this are compared to the LEAP-1A26 engine. The combustor inlet temperature and pressure (T37 and p37 respectively) for the LEAP-1A26 need to be obtained. As there is no data available on these internal conditions of the engine, conditions within the engine are modelled. The engine model created in this report performs insufficiently to be used for off-design points like take-off. Therefore a publicly available turbofan model is used [3]. For sea level static conditions the model yields T37 is $786\,\mathrm{K}$ and p37 is $3346\,\mathrm{kPa}$. No steam injection is used so the steam factor is simply 1.0 and a technology factor of 0.72 is used as the LEAP engine is state-of-the-art regarding NO_x emissions. Inputting these in Equation 5.50 yields an estimated take-off EI_{NOx} of $19.6\,\mathrm{g/kg}$ with the actual LEAP-1A26 having a value of $18.8\,\mathrm{g/kg}$ [15]. This is an overestimation of $4.3\,\%$ and is deemed an acceptable deviation. Similarly the EI_{NOx} of the LEAP-1A26 engines are found for cruise conditions at $10.7\,\mathrm{km}$ and $0.8\,\mathrm{Mach}$ yielding a more accurate LEAP-1A26 cruise EI_{NOx} estimation of $7.35\,\mathrm{g/kg}$

5.1.3. Engine Performance: Model Matching

To validate the accuracy of the performance model, it is attempted to replicate the results as presented by MTU. If that is achieved, the model parameters can be varied to optimize the engine for use on the X-300. All model input parameters are listed in Table 5.2. The source for each parameter is given.

Several parameters are not directly stated in the paper but have been obtained through calculations. The engine mass flow is calculated based on the given thrust value and specific thrust (Equation 5.52). The water-to-fuel ratio is said to be between 4 and 6 in the paper. The lower bound of this indication has been chosen, for a conservative estimate of emissions. Using this ratio, the water-to-air ratio is coupled to the equivalence ratio. The equivalence ratio is then obtained through Equation 5.53.

$$\dot{m}_1 = \frac{F_{thrust}}{T_{sp}} \quad (5.52) \qquad \phi = \frac{\dot{m}_{W5}}{WFR \cdot FAR_{stoich} \cdot \dot{m}_2} \quad (5.53)$$

In this way, the number of design variables to adjust is reduced to three: the overall pressure ratio OPR, the water pressure p_{W3} and the water-to-air ratio WAR. The goal is to approach the model outputs obtained by MTU and assess that design point. The objective function to be minimized is the sum of the absolute percentage differences over the four model outputs between this model and that of MTU: the 'performance' metric (Equation 5.54). To do so, an algorithm was run to explore the entire design space as described in Table 5.1. This is an expensive analysis, as it requires the analysis of thousands of design points.

$$p = \left(\left| \frac{\Delta T_{sp}}{T_{sp,MTU}} \right| + \left| \frac{\Delta TSFC}{TSFC_{MTU}} \right| + \left| \frac{\Delta T_{0,4}}{T_{0,4_{MTU}}} \right| + \left| \frac{\Delta EI_{NOx}}{EI_{NOxMTU}} \right| \right) \cdot 100\% \tag{5.54}$$

Table 5.1: Design space considered for results replication.

Parameter	Symbol	Lower Bound	Upper Bound	Sample Size
OPR	OPR	10	40	30
Water pressure	p_{W3}	$10\,\mathrm{bar}$	$40\,\mathrm{bar}$	20
Water-to-air ratio	WAR	0.05	0.25	20

Using this method, the design point as captured in Table 5.2 obtains the most optimal (lowest) value of the performance metric. The overall pressure ratio (26.4) is relatively low compared to current turbofan engines, which is expected. The water pressure ($25\,\mathrm{bar}$) is reasonable, but it should be noted that this is purely a thermodynamic model and does not optimize for the weight of the engine. Implementing a weight model for the engine would put a penalty on higher water pressures due to the

[3] https://www1.grc.nasa.gov/beginners-guide-to-aeronautics/enginesimu/

increase in heat exchanger mass. The water-to-air ratio (0.133) is well within the range of possible water-to-air ratios that are discussed in the paper.

Table 5.2: Model validation input parameters.

Parameter (known)	**Symbol**	**Value**	**Reference**
Mach number	M_0	0.78	MTU [7]
Altitude	h	$FL350$	MTU [7]
Ambient Temperature	T_a	$219\,\mathrm{K}$	ISA [4]
Ambient Pressure	p_a	$23\,842\,\mathrm{Pa}$	ISA [4]
Bypass ratio (BPR)	BPR	34.5	MTU [7]
Fan pressure ratio	Π_{fan}	1.32	MTU [7]
Fan diameter	d_{fan}	$2.2\,\mathrm{m}$	MTU [7]
Stoichiometric FAR	FAR_{stoich}	0.0681	CEA [9]
Lower heating value	LHV	$4.3 \times 10^6\,\mathrm{Jkg^{-1}}$	[16]
Engine mass flow	$\dot{m}_1$	$280\,\mathrm{kgs^{-1}}$	Equation 5.52
Water-to-fuel-ratio	WFR	4	MTU [7]
Equivalence ratio	ϕ	0.48	Equation 5.53
Thrust	F_{thrust}	$21\,\mathrm{kN}$	MTU [7]
Parameter (assumed)	**Symbol**	**Value**	**Reference**
Inlet efficiency	η_{inlet}	0.98	AE2230-II
Fan efficiency	$\eta_{is,fan}$	0.98	AE2230-II
Compressor efficiency	$\eta_{is,HPC}$	0.95	AE2230-II
Combustion efficiency	η_{comb}	0.99	AE2230-II
Pressure ratio combustor	Π_c	0.98	AE2230-II
Mechanical efficiency	η_m	0.99	AE2230-II
Turbine efficiency	η_T	0.95	AE2230-II
Core nozzle efficiency	$\eta_{noz,c}$	0.95	AE2230-II
Bypass nozzle efficiency	$\eta_{noz,f}$	0.98	AE2230-II
Water pump efficiency	η_{pump}	0.75	Article [12]
Steam turbine efficiency	η_{wt}	0.70	Article [13]
Parameter (design)	**Symbol**	**Value**	**n.a.**
OPR	OPR	26.4	-
Water pressure	p_{W3}	$25\,\mathrm{bar}$	-
Water-to-air ratio	WAR	0.133	-

Table 5.3: Model validation parameters and relative difference to MTU paper.

Parameter	**Symbol**	**Value Obtained**	**Value MTU**	**Model Difference**
Specific Thrust	T_{sp}	$80.5\,\mathrm{ms^{-1}}$	$75\,\mathrm{ms^{-1}}$	+$7.4\,\%$
TSFC	$TSFC$	$11.6\,\mathrm{gkN^{-1}s^{-1}}$	$12.56\,\mathrm{gkN^{-1}s^{-1}}$	-$7.2\,\%$
TIT	$T_{0,4}$	$1713\,\mathrm{K}$	$1700\,\mathrm{K}$	+$0.8\,\%$
NOx emission index	EI_{NOx}	$0.564\,\mathrm{gkg^{-1}}$	$0.557\,\mathrm{gkg^{-1}}$	+$1.3\,\%$

Within the considered design space, this value is known to be a global optimum, as the entire design space was explored. However, from this analysis, it is unclear if multiple design points lead to closely

[4] ISO 2533:1975

matched performance. To this end, the performance metric is plotted as a function of OPR and WAR. The water pressure for this analysis is kept constant, as it was shown to have relatively little influence on the performance. In Figure 5.2, a sub-set of the design space is visualized for this purpose. It can be seen that the model replicates MTU most accurately in one specific area where the performance metric is minimised. It is a clear region with smooth edges clearly showing that it is a global minimum of the performance metric. Therefore, this design point can be confidently chosen as the only design point that replicates the results of MTU.

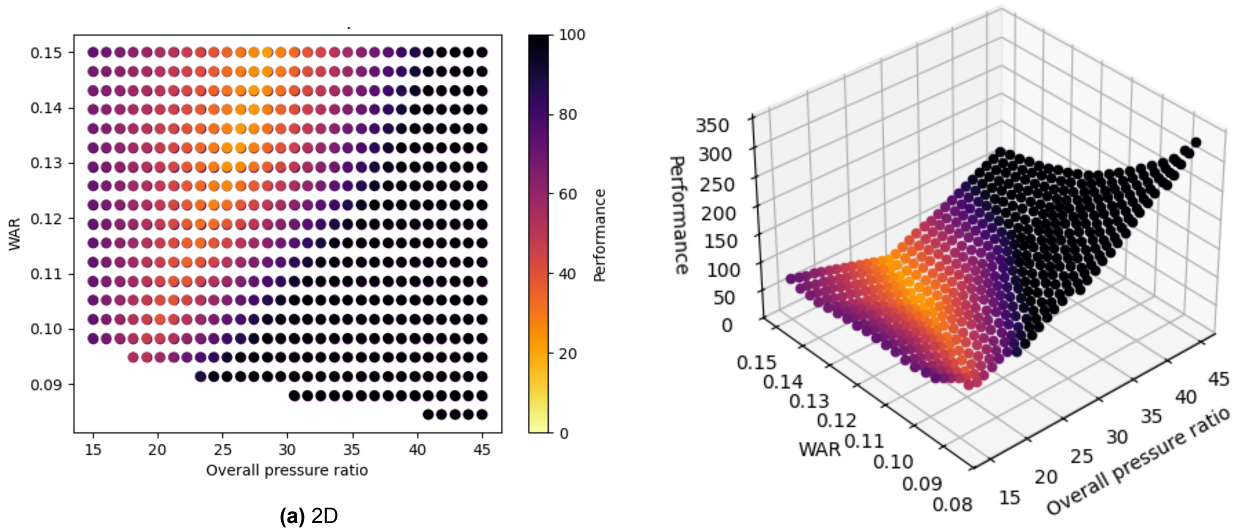

(a) 2D

(b) 3D

Figure 5.2: Plots showing the variations in the performance metric as a function of overall pressure ratio OPR and water-to-air ratio WAR for set water pressure (p_{W3} = $25\,\mathrm{bar}$).

The remaining differences between the obtained model and MTU's results can be explained well. As stated before, a lot of the ducting has been left out in this model, as well as the pressure drops over the heat exchangers. These differences would not influence TIT and EI_{NOx} significantly, which is why these closely match. These efficiency losses would impact the specific thrust and thrust-specific fuel consumption negatively, which explains why this model is too optimistic about these values.

5.1.4. Engine Performance: Model Application

With the validated model in place, adjustments are made to the engine operating conditions and design to make it suitable for the X-300. The complete list of operating conditions and model input parameters is shown in Table 5.4.

Table 5.4: X-300 engine design parameters (cruise).

Parameter	**Symbol**	**Value**	**Reference**
Mach number	M_0	0.65	X-300
Altitude	h	$FL290$	X-300
Ambient Temperature	T_a	$230.7\,\mathrm{K}$	ISA [5]
Ambient Pressure	p_a	$31\,485\,\mathrm{Pa}$	ISA [5]
Bypass ratio (BPR)	BPR	34.5	MTU [7]
Fan pressure ratio	Π_{fan}	1.32	MTU [7]
Stoichiometric FAR	FAR_{stoich}	0.0681	CEA [9]
Lower heating value	LHV	$4.3 \times 10^6\,\mathrm{J \cdot kg^{-1}}$	[16]
Engine mass flow	$\dot{m}_1$	$340\,\mathrm{kg \cdot s^{-1}}$	Equation 5.52
Water-to-fuel-ratio	WFR	4	MTU [7]
Equivalence ratio	ϕ	0.48	Equation 5.53
Parameter (design)	**Symbol**	**Value**	**n.a.**
OPR	OPR	31.5	-
Water pressure	p_{W3}	$25\,\mathrm{bar}$	-
Water-to-air ratio	WAR	0.1482	-
Water-to-fuel ratio	WFR	4.6	-

The operating conditions are different, as the X-300 will be cruising at a lower Mach number (0.65). The thrust output is also required to be higher, to overcome the $51\,\mathrm{kN}$ of drag during cruise. The mass flow is adjusted accordingly. Additionally, the electric power generation, necessary for the environmental control system, is taken into account. The required power for this system, $880\,\mathrm{kW}$, is added to the power generated by the low-power shaft.

The design parameters are then optimised for minimal $TSFC$ and minimal EI_{NOx}. In addition to the three design variables mentioned earlier, the water-to-fuel ratio is now also included. It is allowed to vary from four to six. The final design point is found by optimising for a specific thrust that matches the value obtained by MTU. This is done as the specific thrust is closely tied to the weight of the engine: the weight estimations performed by MTU remain valid if the specific thrust is closely matched. The results of these optimisations are captured in Table 5.5. This shows that the final design point is a reasonable middle-ground between optimisation for $TSFC$ and EI_{NOx}.

Table 5.5: X-300 engine design optimisation results.

Parameter (performance)	**Description**	**min.** $TSFC$	**min.** EI_{NOx}	**Final Design**
Specific Thrust	T_{sp}	$67.7\,\mathrm{ms^{-1}}$	$75.7\,\mathrm{ms^{-1}}$	$75.2\,\mathrm{ms^{-1}}$
TSFC	$TSFC$	$10.2\,\mathrm{gkN^{-1}s^{-1}}$	$11.95\,\mathrm{gkN^{-1}s^{-1}}$	$12.03\,\mathrm{gkN^{-1}s^{-1}}$
Combustor inlet temperature	$T_{0,37}$	$650\,\mathrm{K}$	$613\,\mathrm{K}$	$656\,\mathrm{K}$
NOx emission index	EI_{NOx}	$0.576\,\mathrm{gkg^{-1}}$	$0.252\,\mathrm{gkg^{-1}}$	$0.469\,\mathrm{gkg^{-1}}$
Parameter (design)	**Description**	**min.** $TSFC$	**min.** EI_{NOx}	**Final Design**
OPR	OPR	37.8	25.2	31.5
Water pressure	p_{W3}	$25\,\mathrm{bar}$	$25\,\mathrm{bar}$	$25\,\mathrm{bar}$
Water-to-air ratio	WAR	0.135	0.178	0.148
Water-to-fuel ratio	WFR	5.5	5.5	4.6

[5] ISO 2533:1975

The optimisations show the expected results. The EI_{NOx} optimal design is obtained at a higher water-to-air ratio and a lower pressure ratio. The combustor inlet temperature is decreased, in line with expectations. The $TSFC$ optimal design, on the other hand, benefits from lower water-to-air ratios and a significantly higher overall pressure ratio. However, due to this combination of factors, the EI_{NOx} is increased.

For the final design point, and with the input parameters as specified in Table 5.4, the final results are captured in Table 5.6.

Table 5.6: X-300 engine characteristics (cruise).

Parameter	Symbol	Value
Total engine thrust	F_{thrust}	$25.6\,\mathrm{kN}$
Total specific thrust	T_{sp}	$75\,\mathrm{ms^{-1}}$
Fan thrust	$F_{thrust,fan}$	$22.6 \times 10^3\,\mathrm{N}$
Core thrust	$F_{thrust,core}$	$2.9 \times 10^3\,\mathrm{N}$
TSFC	$TSFC$	$12.03\,\mathrm{gkN^{-1}s^{-1}}$
NOx emission index	EI_{NOx}	$0.469\,\mathrm{gkg^{-1}}$
Fan power	P_{fan}	$6.8 \times 10^6\,\mathrm{W}$
Compressor power	P_{HPC}	$3.9 \times 10^6\,\mathrm{W}$
Low pressure turbine power	P_{LPT}	$7.3 \times 10^6\,\mathrm{W}$
Steam turbine power	P_{steam}	$4.4 \times 10^5\,\mathrm{W}$
Steam power percentage	f_{steam}	$6\,\%$
Water pump power	P_{pump}	$3.0 \times 10^3\,\mathrm{W}$
Vaporizer effectiveness	ϵ_{vap}	0.54
Condenser effectiveness	ϵ_{con}	0.5
Heated bypass fraction	f_h	0.21

5.1.5. Engine Performance: Verification and Validation

To provide confidence that the methods used and code written produce reliable results, verification and validation is carried out in line with the plan outlined in the midterm report [3]. The verification approach includes a set of unit tests and (sub-)system tests. The validation has been discussed already; the comparisons with a similar model, such as that created by MTU, serve this purpose. It is recognized that this is a limited source of validation. An important part of further work would be to find alternative sources of validation.

The unit tests and (sub-)system tests are listed in Table 5.7 and Table 5.8. They are designed to provide full coverage of the entire code structure. That is, the unit tests assess all the thermodynamic modules individually, as well as the results from external code packages. Each module is modelled by a single function, so each function is subjected to at least one unit test. The (sub-)system tests are designed to cover the reliability of the interactions between the modules. The tests listed are all passed, and additional tests have been performed that have not been listed due to space constraints.

Table 5.7: List of unit tests performed on the thermodynamic engine performance model.

ID	Description	Explanation
T-UNI-01	All mathematical calculations are cross-checked once with hand-calculations	The outputs shall match hand calculation
T-UNI-02	The outputs of all functions are checked for correct units	All values shall be returned in SI units

Continues on next page

Table 5.7 – continues from previous page

ID	Description	Explanation
T-UNI-03	Zero-inputs, or other non-sensical inputs are intercepted	Value errors shall be raised for non-sensical inputs
T-UNI-04	For compressor modules (fan, HPC), the input and output pressure and temperature are compared	The output pressure and temperature shall exceed the input pressure
T-UNI-05	For turbine modules (HPT, LPT), the input and output pressure and temperature are compared	The output pressure and temperature shall be below the input pressure
T-UNI-06	For the combustor module, the input and output temperature are compared	The output temperature shall be above the input temperature
T-UNI-07	For the mixer module, the input temperatures and output temperature are compared	The output temperature shall be between the input temperatures of the water and air
T-UNI-08	For the inlet module, the input pressure and output pressure are compared	The input pressure shall exceed the output pressure
T-UNI-09	For the heat exchanger modules, the input and output temperatures are compared	The temperature of the hot side shall decrease across the heat exchanger. The temperature of the cold side shall increase across the heat exchanger
T-UNI-10	For the heat exchanger modules, the temperatures of the hot and cold side are compared	The output temperature of the cold side shall not exceed the input temperature of the hot side. The output temperature of the hot side shall not be lower than the input of the cold side
T-UNI-11	For all modules, the massflows are compared	Mass shall be conserved
T-UNI-12	The results from the external packages are compared to other sources for a varied set of input parameters	The external packages shall match the values obtained through other sources

Table 5.8: List of (sub-) system tests performed on the thermodynamic engine performance model.

ID	Description	Explanation
T-SYS-01	The modules are arranged to mimic two exam questions from AE2230-II	The outputs of the model shall match the answers of the exam
T-SYS-02	Parameters (bypass ratio, overall pressure ratio, equivalence ratio, lower heating value, Mach number, ambient temperature, ambient pressure, mass flow, water-to-fuel ratio, ...) are varied around the design point	Performance outputs shall vary smoothly and in the expected direction
T-SYS-03	The mass flows of the entire system are checked	Mass flow is conserved
T-SYS-04	The power values within the system are assessed	The power produced by relevant components shall match the power supplied by the relevant components, allowing for the mechanical efficiency

5.1.6. Engine Sizing: Model Description

To integrate the engines into the design mass flow, weight and diameter estimations have to be carried out.

Mass Flow Estimation

The first step to size the engine is estimating its (air) mass flow. This can be done using the Mass Flow Parameter (MFP) given by Equation 5.55 from [17]. Where T_t and p_t are the total temperature and pressure respectively. A is the area of the inlet throat.

$$MFP = \frac{\dot{m} \cdot \sqrt{T_t}}{p_t \cdot A} \tag{5.55}$$

The MFP is almost completely constant throughout the flight envelope of an aircraft. For modern turbofan engines the MFP is around 0.030 as shown in Table 5.9

Table 5.9: MFP values for multiple turbofan engines.

Engine	MFP	Condition
GE90	0.0291	Sea Level Static [6]
GE90	0.0306	Cruise at $10.7\,\mathrm{km}$ and $0.85\,\mathrm{Mach}$
CFM56-5C2	0.0294	Sea Level Static [7]
Trent 900	0.0295	Sea Level Static [8]
GEnx-1b70	0.0311	Sea Level Static [9]
WIT turbofan	0.0324	Cruise at $10.7\,\mathrm{km}$ and $0.78\,\mathrm{Mach}$ [7]

Using the 2 data points for the GE90 the model for the engine mass flow is validated by recognizing that the data points are almost exactly on the predicted engine air mass flow lines for an average MFP of 0.030 as shown in Figure 5.3. Thus, the WIT turbofan mass flow can be related to its MFP for every part of the flight.

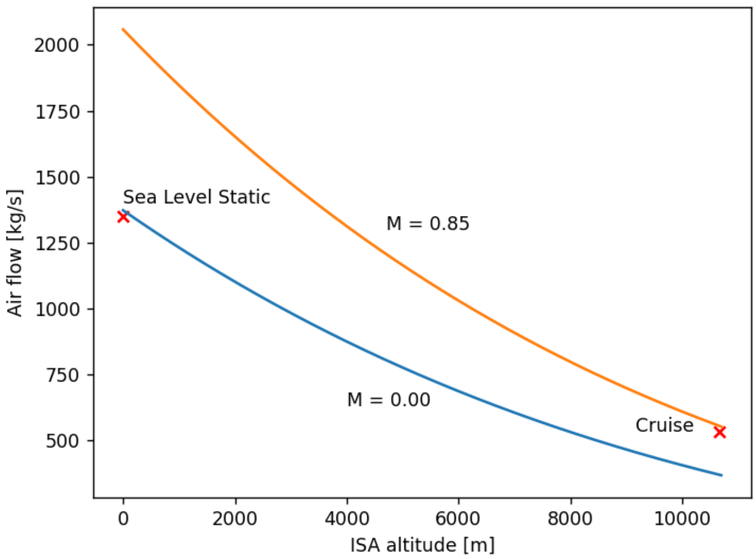

Figure 5.3: Mass flow data points for the GE90 engine and the predicted mass flow graphs.

Engine Diameter Estimation

The engine thrust determines the required mass flow. The mass flow can be calculated when the required thrust and the specific thrust are known using Equation 5.56

$$\dot{m} = \frac{F_{thrust}}{F_{specific_thrust}} \quad (5.56) \qquad A = \frac{\dot{m}\sqrt{T_t}}{p_t \cdot MFP} \quad (5.57)$$

If the MFP is known for an engine and the engine thrust dictates the required mass flow then the required inlet throat area can be calculated using Equation 5.57. The fan diameter is then simply converting the obtained area. The nacelle diameter of the engine is calculated by dividing by an additional factor to the fan diameter. This factor is taken to be 0.89 which is on the higher end for high bypass engines. The formulas for the fan and nacelle diameter Equation 5.58 and Equation 5.59 respectively.

$$D_{fan} = 2\sqrt{\frac{A}{\pi}} \quad (5.58) \qquad D_{nacelle} = \frac{D_{inner}}{0.89} \quad (5.59)$$

For the 2 WIT turbofans on the X-300 requiring a total take-off thrust of $405.7\,\mathrm{kN}$ this means that they have a fan and nacelle diameter of $2.68\,\mathrm{m}$ and $3.02\,\mathrm{m}$ respectively.

Mass Estimation

The mass of the engines has a significant influence on the aircraft's performance. It is vital to have an engine mass estimation. A study comparing multiple estimation methods found that the best-performing mass model is the Kuz'michev model [18]. This model outputs the mass of the engine including engine nacelle as a function of bypass ratio, overall compressor pressure ratio, air mass flow rate, turbine inlet temperature and fan pressure ratio. The calculations are straightforward to replicate from this model.

The challenging part of the engine weight estimation model is to account for the added mass of the WIT turbofan components like the heat exchangers and the water pump. After research on mass estimations for these parts accurately assessing this was deemed infeasible. The WIT turbofan concept analysis also mentions a mass increase in the order of $40\,\%$ compared to a generic extrapolated turbofan for 2030. In the engine mass estimation model for the X-300 WIT engines, this is implemented as a mass correction factor of 1.4

To verify that the Kuz'michev mass model is implemented correctly the values for the estimated mass over the actual mass are shown in Table 5.10 for some turbofan engines.

Table 5.10: Verification of the engine model implemented in the code. The (unitless) ratio of the estimated engine mass ($m_{\text{estimated}}$) over the actual engine mass (m_{actual}) is shown for various engine models.

Engine model	LEAP-1A26	GE90-76B	GEnx-70B
$m_{\text{estimated}}/m_{\text{actual}}$	0.78	0.97	0.91

These values show that it slightly under-predicts the engine mass for the lighter LEAP-1A-26 engines, but is more accurate for the heavier GE90-76B. Because the X-300 will use heavier engines than the LEAP-1A26 the model will converge more to the accurate engine mass.

The resulting engine mass per engine with each WIT turbofan having to provide $203\,\mathrm{kN}$ is $7853\,\mathrm{kg}$

5.2. Electrical System Power Budget

Table 5.11 shows the power budget of the X-300 at this stage of the design with estimates for the power requirements of various systems. Since the aircraft can generate power with its engine generators and its APU, a power requirement has been determined for each. The total power requirement for the engine generators (namely, $880\,\mathrm{kW}$) is accounted for in the virtual engine model. While not included here, a power requirement for a ram air turbine (i.e. an emergency generator) must also be established at a later stage in the design.

Table 5.11: Electrical power budget.

System/component	Power (kW)
ECS	380
Avionics	20
IWETS charging	100
Cabin appliances	40
Wing de-ice	90
Fly-by-wire	200
Misc. Engine	50
TOTAL (engine)	880
Engine starter	150
Misc. APU	100
TOTAL (APU)	250

The reasoning behind these estimates is summarised below:

- As detailed in Section 5.5, the X-300 features an electrical Environment Control System (ECS), meaning the system replaces pneumatic power (or bleed air) with electrical power. The power demands were estimated based on a study by Herzog [19], who suggests a power requirement of $150\,\mathrm{kW}$ for a 100-passenger airliner and $400\,\mathrm{kW}$ for a 350-passenger airliner. The estimated value of $380\,\mathrm{kW}$ is obtained by linear extrapolation.
- Because bleed air is no longer used, the aircraft requires an electric engine starter (as discussed in Section 5.5). A value of $150\,\mathrm{kW}$ was estimated; for reference, the Boeing 787, which uses a similar ECS, utilizes $180\,\mathrm{kW}$ of power for engine start-up [20]. This value must be supplied by the APU, not the engine generators since it is necessary for starting of the engines.
- Similar to above, the leading edge of the wing must be de-iced using an electrical system, as bleed air is not available. Based on the $100\,\mathrm{kW}$ system found on the Boeing 787 [20], a power requirement of $90\,\mathrm{kW}$ was estimated.
- Power demands for the remaining items which are reliant on the engine generators (avionics, cabin appliances, fly-by-wire) were estimated by engineering judgement based on a relative comparison of these systems presented by Seresinhe and Lawson [21]. A notable entry is the power allocation for IWETS charging, which, at $100\,\mathrm{kW}$, would allow for the system to be completely charged by the engine generators in $99\,\mathrm{minutes}$. Any system which is not included in the current budget falls under *"Misc. Engine"*, for which a power of $50\,\mathrm{kW}$ has been allocated. A similar allocation has been made for unforeseen components which draw power from the APU (labelled *"Misc. APU"*). A power budget of $100\,\mathrm{kW}$ has been set, higher than the power allocated to *"Misc. Engine"*, to account for the APU having to provide power to critical systems in the event of an engine/generator failure.
- The total power requirement for the engine generators is $880\,\mathrm{kW}$, while for the APU generators it is $250\,\mathrm{kW}$. As a point of comparison, the engine generators on Boeing 787 generate $1\,\mathrm{MW}$ of power, while its APU generates $450\,\mathrm{kW}$ [20]. Therefore, the estimates are considered to be within reasonable bounds.

5.3. Fuel System

A conventional fuel storage arrangement is used that comprises wing tanks and a central fuselage tank. Initially, an aft fuselage tank was considered as well due to a lack of confidence that only the forward tanks would be sufficient for storing the maximum required fuel. This could also potentially be used for the active longitudinal centre of gravity control system implementation. However, as the design was finalised, the need for such a tank disappeared, deciding not to unnecessarily increase the weight and complexity of the fuselage. From a CG perspective as well, it is already located very aft due to the engine position so a fuel tank that is rear-located would not help with this.

One important issue that has to be addressed in the design of this system is the concerns of CG shifts due to fuel migration resulting from pitch attitude changes. The fuel tends to move aft during the climb phase, reducing the static stability margin of the aircraft. This effect can be mitigated by dividing the wing tank into multiple compartments that block the fuel migration outboard but allow inboard flow. This is accomplished with the help of baffle check valves as depicted in Figure 5.5 [22]. In the presence of dihedral, during level flight, the fuel automatically moves to the inner tanks. However, as this phenomenon is not as significant for an unswept wing of the X-300, the wing will only be divided into an inner and an outer tank (also for wing load alleviation). The inner tanks together with the central tank will serve as the main feeding tanks for the engines and the APU system.

Another key consideration is the need for surge tanks. Commercial aircraft make use of an ”Open vent system” to enable a connection between the ullage above the fuel in each tank and outside air. If this does not exist, very large pressure differences develop resulting in massive forces on the structures. Also for safety reasons during the refuelling process, in order to avoid spillage of fuel outside a surge tank/vent box is there to capture the overflow [22]. These are normally located close to the wingtips and in case of the proposed aircraft will occupy $5\,\%$ of the total wingspan.

The arrangement of the main fuel tanks is presented in Figure 5.4. The fuel capacity of each is further demonstrated in Table 5.12. As the surge tank is designed to capture the fuel spill and not carry additional fuel, its capacity is not included in the total fuel capacity of the aircraft.

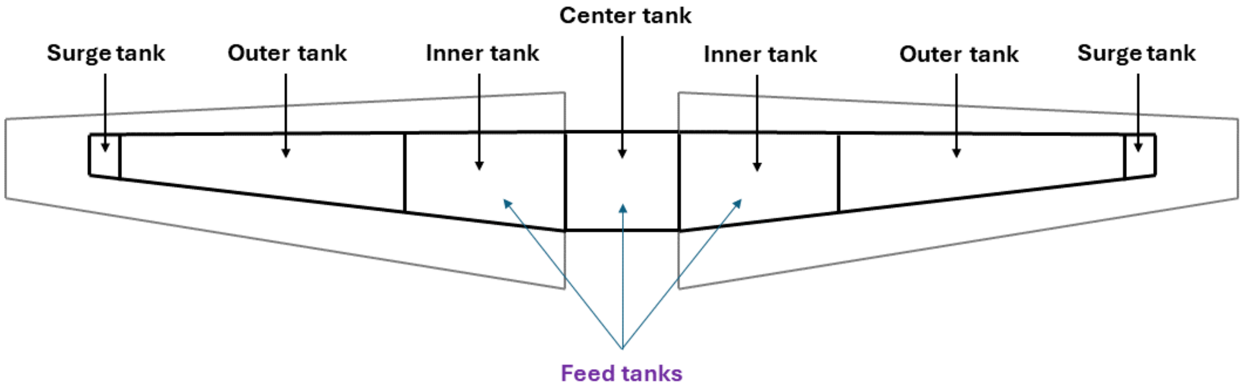

Figure 5.4: Fuel storage arrangement.

Table 5.12: Usable fuel capacity of the tanks. *surge tank fuel capacity is not used in the total calculations.

Fuel capacity	Inner tanks	Outer tanks	Center tank	Surge tanks*	Total
Volume (l)	2 $\times$ 4656	2 $\times$ 6823	5281	2 $\times$ 335	28239
Mass (kg)	2 $\times$ 3725	2 $\times$ 5458	4225	2 $\times$ 268	22591

The maximum fuel that can be required for a mission on X-300 is estimated to be $19\,403\,\mathrm{kg}$, also taking into account some amount of trapped fuel. From the numbers in Table 5.12 it is apparent that the designed fuel tanks will be able to accommodate the maximum amount of fuel with a sufficient margin. The fuel system is further detailed in Figure 5.5, with simplified schematics of the fuel feed, transfer and refuelling subsystems.

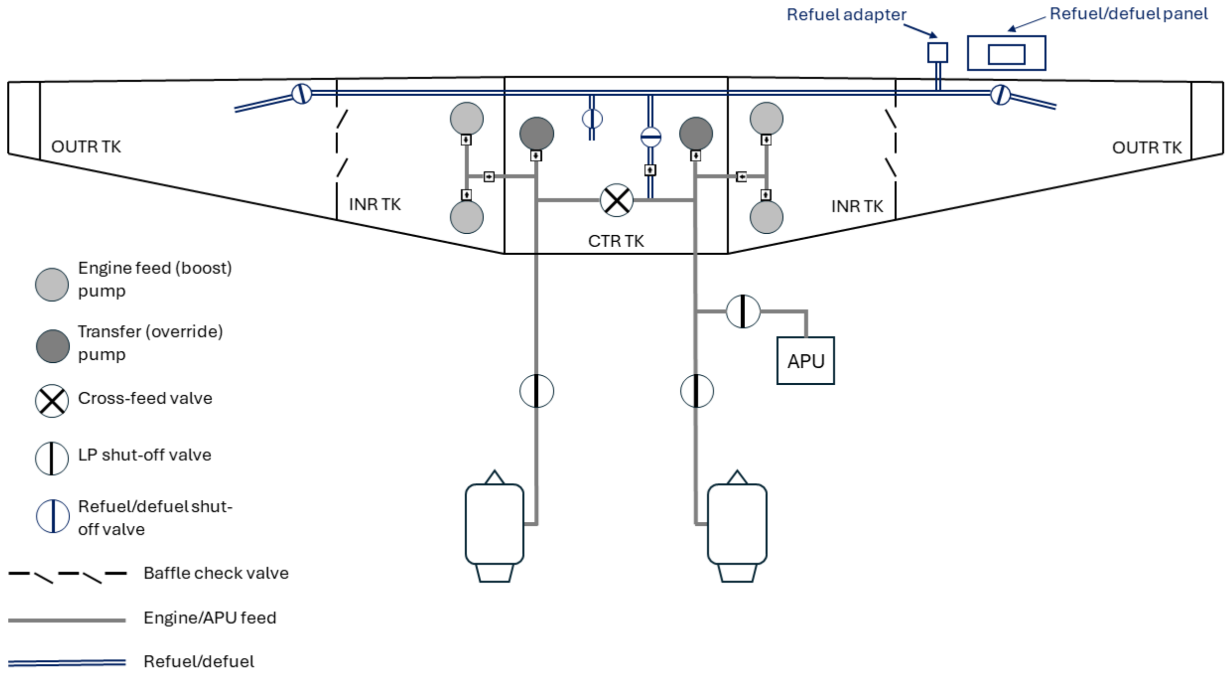

Figure 5.5: Feed, transfer and refuel/de-fuel system schematics.

Feed System

As demonstrated in Figure 5.5, each engine is fed from two motor-driven pumps located in the inboard-forward and inboard-aft of inner tanks and one located in the central tank. The former is done to minimise the unusable fuel, as the aft pump will be covered in the climb phase of the flight with fuel flowing to the back of the tank, while the forward pump will support the climb phase [22]. The APU is fed from the right engine feeding system. Each engine and APU have their own dedicated LP shut-off valves.

The engine feeding is completed following a sequence of central tanks - inner tanks - outer tanks (fuel is transferred to inner tanks and fed from there). The fuel in the outer tanks is kept full during most of the flight and is burnt last for wing load alleviation reasons. A full outboard tank results in a reduced bending moment on the wing. Furthermore, for safety purposes, a cross-feed system is present to enable the fuel of the failed engine tank to be fed into the other operating engine.

Transfer System

The fuel feeding sequence requires the central fuselage tank to be consumed first. For this reason, the transfer (override) pumps in the central tank produce significantly larger feed line pressures than the wing boost pumps are able to, thus keeping the wing pumps' outlet check valves closed by the override pump pressure. When the central tank is emptied, the transfer pumps are switched off allowing the fuel in wing tanks to flow to engines [22].

Then to consume the fuel in outer tanks in the last phases of the flight, the fuel has to be transferred to the inner tanks as outboard ones are not feed tanks. This, as explained before, is accomplished automatically with the use of baffle check valves in the presence of dihedral and available space in the inner tanks.

Refueling/Defueling System

The refuelling process is done with the refuel lines that reach the outer tanks as well as the central tank. Three shut-off valves are present (one for each) and a standard refuel adapter. The refuelling is started with fuel flow to the central tank and the most outboard compartments, whereupon filling up, the uplifted fuel flows into the inner tanks through the baffle check valves.

Defueling, normally done for maintenance purposes, is completed by suction applied at the ground refuel adapter through the dedicated line.

5.4. In-Wheel Electrical Taxiing System (IWETS)

The X-300 features an In-Wheel Electrical Taxiing System (IWETS), which powers electrically four of the eight wheels on the main landing gear. This system allows the aircraft to taxi at airports (both prior to take-off and after landing) without using engine power or consuming fuel. Furthermore, the system eliminates the aircraft's dependency on a tow vehicle for pushback from a gate space (as the IWETS also allows it to move in reverse), meaning the aircraft is not affected by vehicle unavailability at the airport. While a tow is no longer required, a ground operator must still be present to monitor the aircraft during the pushback process. In Chapter 10 the operational aspect of this will be further addressed.

A simplified schematic of the IWETS diagram is shown in Figure 5.6. Four motors of $84.5\,\mathrm{kW}$ each are powered by a $162\,\mathrm{kWh}$ battery, with the power supply being facilitated by a power distribution unit and an inverter. The motors drive the two outer wheels on each strut of the main landing gear. A controller located in the cockpit allows the pilot to command different motor speeds. The battery stack is charged between every flight via a DC ground connection while the aircraft is at the gate. A single charge is sufficient both for the taxi-in and taxi-out phases. If necessary, the engine generators can also be used to charge the battery in flight. This ensures that there is sufficient energy in the battery both for the taxi-out and taxi-in phase. In case the system fails, the engines may still be used for taxiing. However, because of the inclusion of the system, the aircraft no longer carries fuel dedicated to taxi. Therefore, if an engine taxi is required, it must use reserve fuel.

Energy and power requirements for the system were derived based on a method by Vratny and Kling [23]. First, the wheel friction force during taxi, R_{taxi}, is calculated as follows:

$$R_{taxi} = MTOM \cdot g \cdot \mu_D, \tag{5.60}$$

which is a function of the aircraft's MTOM and coefficient of rolling friction, μ_D. Aerodynamic friction/drag is neglected, and the dry ground conditions are assumed. A $1.5\,\%$ incline (or $\gamma = 0.015\,\mathrm{rad}$) is applied to account for unevenness in the tarmac (this is done by multiplying Equation 5.60 by the term $\cos\gamma + \sin\gamma$). The required electric motor torque T_{motor} can be calculated by using the number of electrified wheels, $n_{e-wheel}$, and the radius of each wheel, r_{wheel}, as shown below:

$$T_{motor} = \frac{R_{taxi}}{n_{e-wheel}} r_{wheel}. \tag{5.61}$$

The required motor power, P_{motor}, is then calculated by multiplying T_{motor} with the forward speed of the wheel it is attached to. This speed is equivalent to the taxi speed of the aircraft v_{taxi}:

$$P_{motor} = T_{motor} \cdot v_{taxi}. \tag{5.62}$$

The limiting case for the motor power is the maximum taxi speed, for which a value of $20\,\mathrm{kts}$ is assumed.

The required energy from the battery, $E_{bat,rq}$, is calculated as follows:

$$E_{bat,rq} = n_{e-wheel} \cdot P_{motor} \cdot t_{taxi}, \tag{5.63}$$

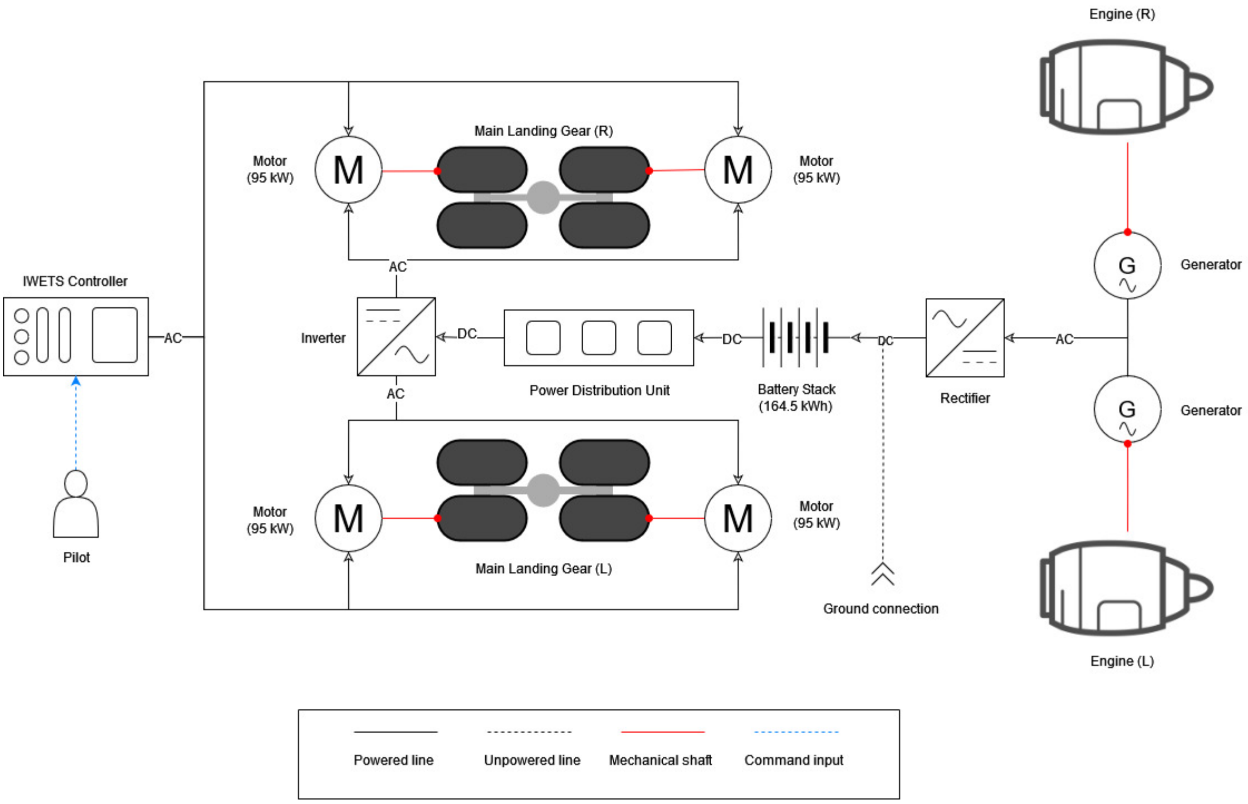

Figure 5.6: Simplified schematic of X-300's IWETS.

with t_{taxi} being the duration for which the battery must provide power to the motors (i.e. the duration of the taxi). In the previously established mission profile, a combined taxi time (i.e. taxi-in and taxi-out) of $26\,\mathrm{minutes}$ was determined [2] and is used in this calculation. It should be noted that the engines must warm up for approximately $5\,\mathrm{minutes}$ prior to the take-off run [24], meaning that the IWETS would only operate for $21\,\mathrm{minutes}$, but the value of $26\,\mathrm{minutes}$ is nevertheless used as a conservative estimate.

The required mass of the battery, $m_{battery}$, is calculated as follows:

$$m_{battery} = \frac{E_{bat,rq}}{E_{bat,sp}},$$

where $E_{bat,sp}$ is the battery's gravimetric energy density, for which a value of $300\,\mathrm{Wh/kg}$ is used [25]. For the remainder of the system's mass, Vratny and Kling [23] present the following relation:

$$m_{no-bat,T} = 0.05 \cdot (P_{mot,tot})^{1.1} + (T_{motor})^{0.49} + 0.025 \cdot T_{motor}, \tag{5.64}$$

$$m_{no-bat,P} = 0.38 \cdot P_{mot,tot} + 0.014 \cdot T_{motor} + 43.82, \tag{5.65}$$

$$m_{no-bat} = \max(m_{no-bat,T}, m_{no-bat,P}), \tag{5.66}$$

where $P_{mot,tot}$ is simply P_{motor} multiplied by $n_{e-wheel}$. Finally total mass of the system, m_{IWETS}, is given by the addition of $m_{battery}$ to m_{no-bat}.

To ensure that the wheels roll rather than slip across the surface, the following check is conducted to see whether the dynamic friction exceeds the static friction on the electrified wheels:

$$\frac{MTOM \cdot g}{n_{wheel}} \cdot 0.92 \cos \gamma \mu_S > \frac{R_{taxi}}{n_{e-wheel}}, \tag{5.67}$$

where n_{wheel} is the total number of wheels on the main landing gear, and μ_S is the coefficient of static friction. A factor of 0.92 is applied to account for the fact that the main landing gear carries only $92\,\%$ of the aircraft's weight. If the relation above holds, then the wheels roll across the tarmac as required.

The numbers used in the IWETS sizing process are shown in Table 5.13. Note that the final weight of the system is the iterated result.

Table 5.13: Inputs and outputs for IWETS sizing.

(a) Inputs.

Parameter	Value	Unit
MTOM	$123\,448$	kg
μ_D	0.3	–
μ_S	0.8	–
n_{wheel}	8	–
$n_{e-wheel}$	4	–
r_{wheel}	0.635	m
v_{taxi}	20	kts
t_{taxi}	26	min
γ	0.015	rad
$E_{bat,sp}$	300	Wh/kg

(b) Outputs.

Parameter	Value	Unit
T_{motor}	5852.5	rad/s
P_{motor}	95	kW
$E_{bat,rq}$	164.5	kWh
$m_{battery}$	548	kg
m_{no-bat}	270	kg
m_{IWETS}	818	kg

The net fuel savings due to the IWETS under the nominal mission profile were calculated as the difference between the removal of fuel dedicated to taxi and the addition of fuel to carry the extra weight of the IWETS system (which can be considered "dead" weight as the system is not operational during flight). Under the nominal mission profile, the IWETS results in a net fuel saving of $837\,\mathrm{kg}$ (or a $9.25\,\%$ reduction in required fuel for the nominal mission profile).

5.5. Environmental Control System (ECS)

The Environmental Control System (ECS) is responsible for the pressurisation and thermal control of the fuselage as well as the supply of air to the passengers and crew. Traditional ECS architecture uses bleed air from the compressor stages of the engine to pressurise the aircraft. The APU can also be bled for the same purpose. Since bleed air presents a pressure loss in the engine compressor, the engine's performance is reduced. To avoid this pressure loss, the X-300 uses a bleedless architecture similar to the one found on the Boeing 787. A simplified schematic of the ECS is shown in Figure 5.7

What is different in this system compared to a traditional one is that the "primary airflow" (marked with red arrows) no longer originates in the engine compressor. Rather, ambient air is channelled into an electrical compressor by an inlet (located on the wing fairing) before flowing into a heat exchanger. To achieve the correct temperature and pressure, the air passes through a second compressor and heat exchanger before it is expanded by a turbine for mixing with recirculated cabin air. The mixed airflow is fed into the fuselage; subsequently, some of it is vented or leaked by the fuselage while the rest is filtered for re-circulation. As evident from Figure 5.7, the ECS relies on electrical power from the engine generators. In the event of an engine and/or generator failure, the APU can also power the system, albeit at a lower level of performance, since the APU generator cannot produce sufficient power. In that case, the emergency oxygen system would have to be deployed.

The removal of bleed air from the engines and APU has two other implications. First, the engines can no longer be started using APU bleed air, hence an electrical starter must be integrated into the engines and powered by the APU during the start-up procedure. Second, there is no possibility

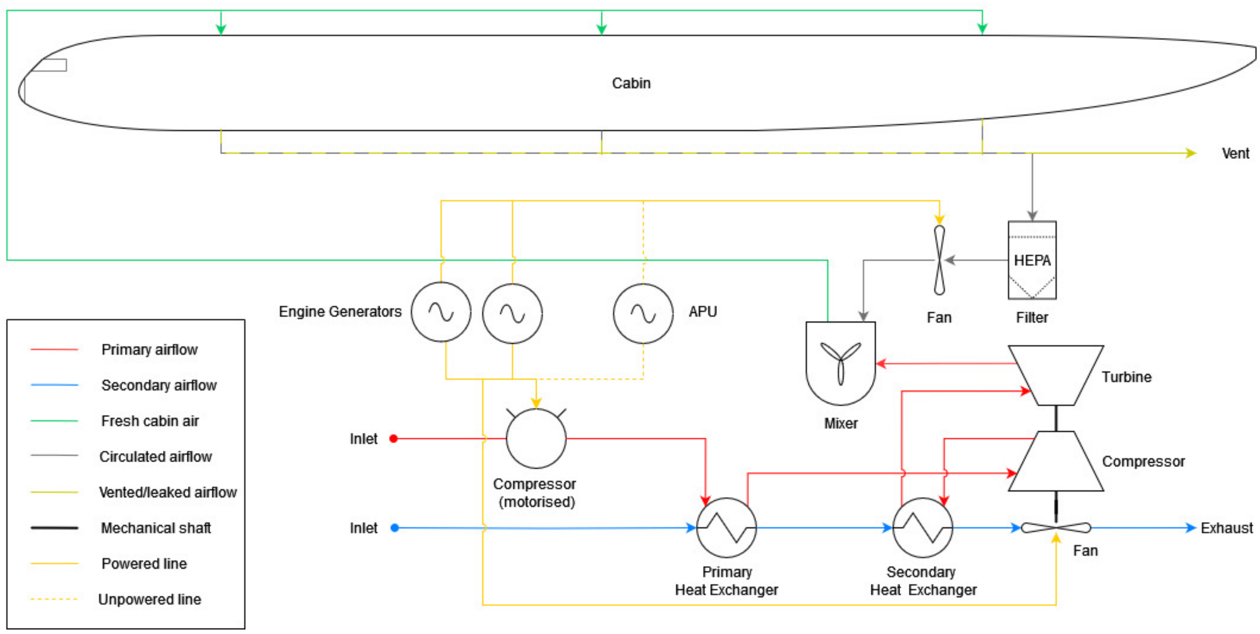

Figure 5.7: Simplified schematic of the X-300's ECS. Valves and air conditioning lines are not shown. Modelled after Planés et al [26].

of using bleed air for de-icing of the wing's leading edge, thus necessitating an electrical de-icing installation in the wing. These design modifications are also present on the Boeing 787 which uses an electrical ECS [20], and they are accounted for in the electrical power budget (see Table 5.11).

It is not possible to quantify the exact effects of the electrical ECS on the X-300's fuel consumption at this stage of the design. Boeing claims that the 787 sees a reduction in fuel burn of approximately $3\,\%$ [27]. Holmgren et al [28] report a fuel saving of $5\,\%$ for a 300-passenger aircraft (up to $6.6\,\%$ for an electrical ECS which uses a vapour cycle machine). In a case study of an Airbus A321, Ercan et al [29] found that the implementation of an electrical ECS would bring fuel savings of between 4 and $4.5\,\%$. Therefore, it is reasonable to assume that the X-300 also yields fuel savings of at least $3\,\%$. Although an exact value for the reduction in fuel consumption was not established, the integration of the ECS is taken into account in the virtual engine model in two ways: it is assumed that there are no pressure losses related to bleed air in the compressor, and the ECS's power demand is subtracted from the power generated by the engine's shaft.

5.6. Airframe

This section will give insights into the detailed design of the airframe that was conducted to assess the various configuration options in order to choose the most optimal configuration. First, the material selection will be presented, followed by the structural analysis that was performed. Lastly, the aerodynamic, stability and control characteristics are analysed.

5.6.1. Material Characteristics

To make an aircraft an attractive option for airliners to consider, sustainability is one of the main points of consideration in the current market. A lot of emphasis is mainly put on the reduction of CO_2 emissions and other emissions during operation like NO_x and noise, however, one of the aspects which is often overlooked is the life cycle impact of an aircraft. One important aspect of the life cycle is the recyclability of all the parts used in the aircraft.

Due to the high recyclability of the A320neo, The same material has been applied to most of the airframe structural components. However, new materials have also been incorporated into the design in an effort to improve the structural characteristics and lower the weight of the aircraft. The first material that is used is the aluminium - Lithium metal. This is due to the fact that the material has a high strength-to-weight ratio and can be recycled, therefore helping contribute to the overall sustainability of the aircraft. AL-LI 8090 also excels in compressive strength so components that will experience high compressive loads will comprise of this material.

Components that will undergo very high stresses will primarily be made of Titanium alloys, as they generally possess a much higher yield strength than aluminium alloys [30]. In addition to this, the final material that is utilised is carbon-fibre-reinforced-polymers. This material has a relatively lower weight than aluminium and titanium alloys and therefore helps in lowering the operational empty weight and maximum takeoff weight of the aircraft. Lowering the weight of the aircraft will result in less thrust being needed so that less fuel is burned over the course of a full flight mission. An overview of the materials that are utilised in the various aircraft systems can be seen in Table 5.14.

Table 5.14: Material choice for selected aircraft structures.

Part	Al-Li 8090	CFRP	Ti-6Al-4V	Ti-10V-2Fe-3Al
Wing				
Wing box			X	
Leading edge	X			
Empennage				
Tailplane		X		
Elevator		X		
Fuselage				
Skin, stringers, frames	X			
Bolts, seat rails			X	
Floor		X		
Floor struts	X			
LG				
LG struts				X
Engine				
Pylon				X
Nacelle		X		
Fan blades, fan case			X	
Compressor blades			X	

As can be seen from the table, There is a rather even distribution of the allocation of materials to the aircraft systems. Titanium alloys are used on the heavy duty components such as stringers, fasteners and engine blades. Aluminium is then used on compressive components as well as components that require a high strength to weight ratio such as the wing leading edge and fuselage skin, stringers and frames. The carbon-fibre-reinforced-polymer material is then implemented on components where weight reduction is key and relatively high strength is not necessarily needed. Due to the fact the aircraft is already tail heavy (due to the engine placement and consequential tail size, which is elaborated upon Subsection 5.6.4), it was decided that the empennage will comprise CFRP. This will help in reducing the weight of the tail and therefore making the aircraft less tail-heavy. Other components that also comprise CFRP are the floor and engine nacelles, as these are not considered to be heavy duty components.

The Airbus A320neo comprises of $92\,\%$ of recyclable materials [31]. Since the same materials have been used with the addition of CFRP, it is expected that the recyclability of the X-300 is comparable to that of the A320neo. However, as CFRP has been utilised in some components, the recyclability is expected to be slightly lower than the recyclability of the A320neo. The next section will give an overview of the structural analysis of the X-300 that was conducted.

5.6.2. Structural Characteristics

In this subsection, the structural considerations of the design are to be discussed. The approach is as follows. Since the aircraft is primarily conventional, the structural analysis will concentrate on the components undergoing the most significant changes. Therefore, the fuselage and empennage have been selected for detailed examination. This is because of the length of the fuselage accommodating the single-aisle configuration, as well as the placement of the engines on the top part of the rear fuselage. Moreover, the H-tail has been included in the structural analysis due to its construction. Although the wing is acknowledged to be influenced by the rear-mounted engines, it has been deemed unnecessary to focus on a detailed structural analysis. This decision is justified by several factors. Firstly, the weight increase due to the rear-mounted engines has already been accounted for in the Class II weight estimation from Roskam [6]. Additionally, preliminary studies indicate that the structural integrity of the wing remains within acceptable limits under the modified configuration. Furthermore, there are existing aircraft designs that do not have engines mounted on the wings, demonstrating the feasibility and safety of such configurations. These considerations collectively support the decision to deprioritise further structural analysis of the wing in this context.

The outline of the structural analysis for both the fuselage and the tail is as follows. First, the most limiting loading cases are identified based on CS25 regulations. Then, the internal loading diagrams are constructed for each of the load cases. Based on the internal moment, the required skin thickness is calculated so that the total mass can be determined. Based on that, a weight estimation is performed and the results are analysed. Lastly, the deflections of the fuselage are computed for in-flight and on-ground conditions and the feasibility of the design is confirmed.

Before this is done, however, a body-centered coordinate system is introduced for an accurate description of the internal loading diagrams. Its orientation is presented in Figure 5.8.

Figure 5.8: Body-centered coordinate system.

The x-axis is positioned along the fuselage, with its positive direction towards the nose, and the y-axis is placed in the wing plane and directed towards the right wing. The z-axis complements the right-handed coordinate system and points downwards as shown above. The origin of the axes is located at the rear end of the fuselage.

Load Cases

In this subsubsection, the critical load cases are defined for which the internal loading diagrams will be constructed. This is done in a descriptive way. Each load case will be given its identifier (ID) starting with *LC-*. The considered forces and load factors applied to the indicated forces are tabulated in Table 5.15.

Table 5.15: Definition of load cases. Based on [32].

ID	Loading Condition	Present Forces	Load Factor
LC-01	TO	lift, drag, structural weight, thrust	$n_W = n_L = 1.7$
LC-02	Cruise	lift, drag, structural weight, thrust	$n_W = n_L = 2.5$
LC-03	Landing on MLG	main landing gear normal force, lift, drag, structural weight	$n_{MLG} = n_W = n_L = 2.6$
LC-04	Landing on NLG	main landing gear normal force, nose landing gear normal force, lift, drag, structural weight	$n_{NLG} = n_W = n_L = 2.6$

The subscript in the load factor n indicates to which force the specified factor is applied: W refers to the weight, L to the lift, MLG to the main landing gear normal force, and NLG to the nose landing gear normal force. Lift, drag, structural weight and thrust are modelled as uniformly distributed loads with the magnitude of $w := F/d$, where F is the magnitude of each force and d the distance over which it acts. The structural weight of the fuselage is distributed over its full length, lift and drag are distributed over the length of the root chord at its appropriate position along the fuselage acting in according directions. The forces from the main and nose landing gear are in turn modelled as point loads in the negative z-direction.

Internal Loading Diagrams

Now that all the load cases are defined, it is possible to construct the internal loading diagrams based on the loading conditions as explained above. An example of such a diagram for *LC-02* is shown in Figures 5.9, 5.10, and 5.11.

In Figure 5.9, N_x refers to the normal force the x-direction. V and M with the subscripts refer to the shear and bending moments in appropriate directions, respectively. Units on both axes are in SI.

Moreover, similar diagrams are produced for the empennage, such that the bending moment and internal shear force are known at each point along it. Also, the fuselage is modelled as a straight tube with a constant radius, except for the tail and nose cones for which the radius r is modelled to vary linearly. This way, $r(x)$ is known.

Determining the Minimum Thickness and Mass

Having determined the internal loads, the design for minimum fuselage thickness can be carried out. This is done as follows. For a given load case, at each x-position along the fuselage, its structural cross section is modelled as a circle with a constant thickness. This takes into account both the fuselage skin and other structural elements such as stringers. The thickness is then allowed to vary along the x-coordinate, and is found such that the cross-sectional area moment of inertia and thickness limit the bending and shear stresses to within the yield and shear strengths of the chosen material: Aluminium-Lithium alloy Al-Li 8090. Its properties are found to be as tabulated in Table 5.16.

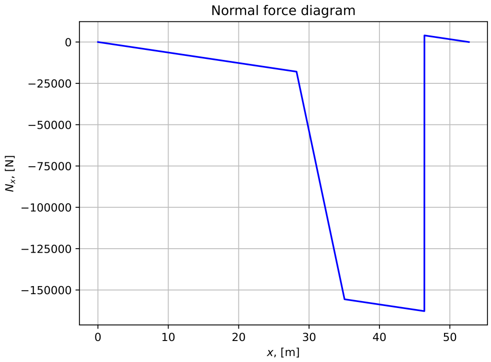

Figure 5.9: *LC-02* normal force diagram. Single-aisle configuration.

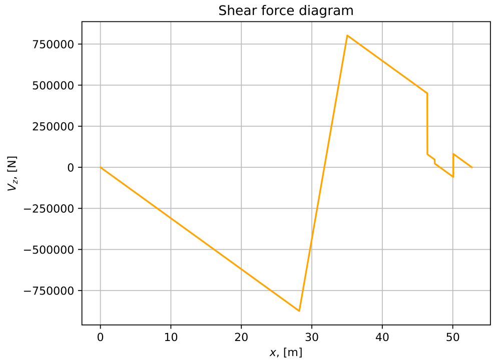

Figure 5.10: *LC-02* shear force diagram. Single-aisle configuration.

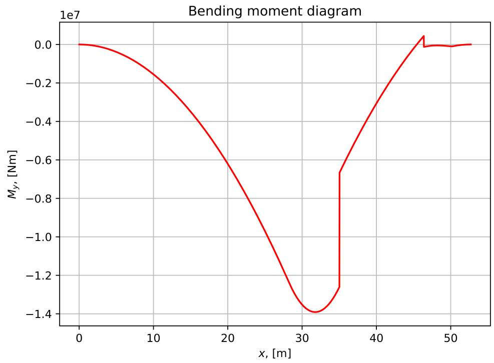

Figure 5.11: *LC-02* internal bending diagram. Single-aisle configuration.

Table 5.16: Material properties of Al-Li 8090.

Property	Symbol	Value	Unit	Source
Yield Strength	σ_y	370	MPa	[33]
Shear Strength	τ_y	270	MPa	[33]
Density	ρ	2540	$\mathrm{kg/m^3}$	[33]

Furthermore, the axial stress due to cabin pressurisation is accounted for and calculated according to (5.68) [34]:

$$\sigma_{ax} = \frac{\Delta pr}{2t}, \tag{5.68}$$

where $\Delta p = 44\,\mathrm{kPa}$ is the pressure differential, r is the radius of the fuselage at each x-coordinate, $\sigma_{ax} = \sigma_y$ and the thickness t is to be found.

This procedure is repeated for *LC-01* through *LC-04*. Denoting the resulting thickness variation of the i-th load case (*LC-0i*), $i = 1, \ldots, 4$ by $t_i(x)$, the point-wise maximum is finally determined such that the conservative estimate of the minimum required thickness $t_{min}(x)$ is computed according to (5.69):

$$t_{min}(x) = \max_{i=1,\ldots,4} t_i(x). \tag{5.69}$$

In other words, the conservative estimate is assumed. Though the resulting thickness distribution may be overestimated, the design is guaranteed to be feasible. Furthermore, the described procedure above is carried out for both the single- and double-aisle configuration for comparison purposes as shall be discussed later.

The resulting minimum fuselage thickness at each x-coordinate for the single- and double-aisle configurations are presented in Figure 5.12 and Figure 5.13, respectively.

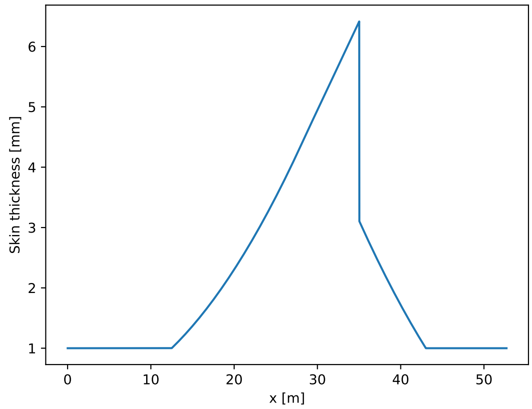

Figure 5.12: Thickness variation as a function of position along the fuselage. Single-aisle configuration.

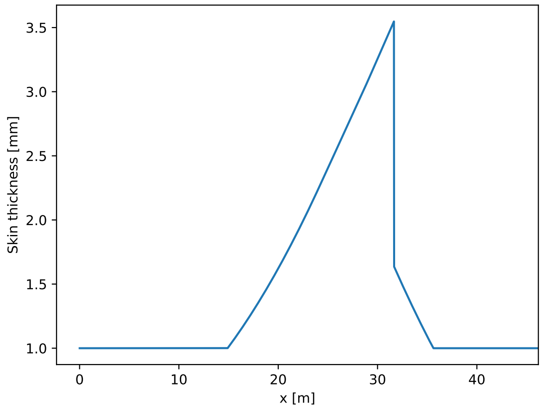

Figure 5.13: Thickness variation as a function of position along the fuselage. Double-aisle configuration.

A lower limit of $1.0\,\mathrm{mm}$ on the thickness has been imposed throughout due to manufacturing limitations. The occurrence of the maximum thickness (around $6.5\,\mathrm{mm}$) in Figure 5.12 is correctly predicted at the coordinate of maximum internal bending stress My in Figure 5.11 (around $35\,\mathrm{m}$) which serves as a sanity check of the analysis.

The described methodology is also applied to the horizontal stabiliser. There, the cross-section of the aerofoil is modelled as an ellipse due to the chosen aerofoil being symmetric, as discussed in Subsection 5.6.3. The resulting minimum thickness is smaller than the set minimum $1\,\mathrm{mm}$, so the thickness is chosen to be $1\,\mathrm{mm}$ throughout the full length of the horizontal stabiliser.

With the thickness distributions known, it is now possible to compute the total mass of the structural material. Comparing the resultant masses for the single- and double-aisle configurations, it has been concluded the previously estimated structural mass of the fuselage as described in [3] which was based on [6] had been underestimated by roughly $23\,\%$. To shift the design to the more conservative side, a margin has been applied and the structural mass of the fuselage was increased by $25\,\%$. This yielded the final fuselage mass of $m_{fus} = 15\,156\,\mathrm{kg}$. Similarly, the final empennage mass was found $m_{emp} = 1556\,\mathrm{kg}$.

Fuselage Deflection

Another crucial structural consideration is the stiffness of the fuselage, especially for such a slender fuselage. The deflections are hence analysed to ensure the feasibility of the single-aisle configuration and its estimated skin thickness. The most critical load cases for the deflection analysis were found to be the following.

- *LC-02* to assess how much the front of the fuselage deflects over its length compared to the aerodynamic centre point. The criticality of this load case derives from the aft located wing that leaves a very long part of the aircraft in front unsupported.
- *LC-03* to assess how much the fuselage deflects around the main landing gear as a support point. This case was most of the time the most critical for the bending analysis therefore is

considered crucial for stiffness feasibility as well.

The obtained results are demonstrated in Figure 5.14. Note that downward deflection is marked as positive.

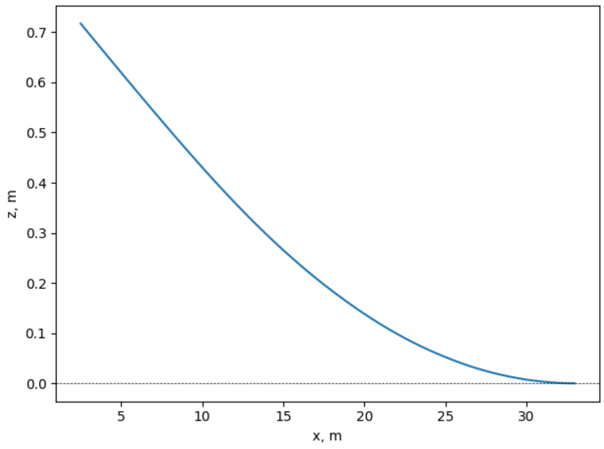

Figure 5.14: Front fuselage deflection for in-flight load case. The x-coordinate is inverted here and goes from $x = 0\,\mathrm{m}$ (the nose) to $x = x_{ac} = 33.1\,\mathrm{m}$ (aerodynamic center).

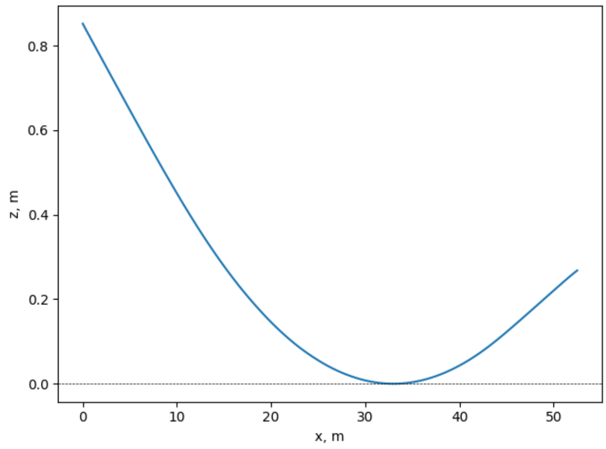

Figure 5.15: The fuselage deflection for main gear landing load case. The x-coordinate is inverted here and goes through the entire length of the aircraft.

From the plot, it is evident that for the critical in-flight case (with a load factor of 2.5), the maximum deflection at the very front of the fuselage is $0.72\,\mathrm{m}$. Considering that this deflection occurs over a length of over $33.1\,\mathrm{m}$, this yields a slope of around $1.2\,°$. As for the landing case (with a load factor of 2.6), the maximum deflection is also at the front of the fuselage, $0.85\,\mathrm{m}$. This, over a length of $32.9\,\mathrm{m}$, results in a deflection angle of $1.5\,°$.

As these are the maximum deflections that occur only at the most critical load cases, the deflection and therefore the stiffness of the fuselage are thus deemed acceptable for this phase of the design.

Verification and Validation

Finally, the code used for the analysis as discussed above needs to be verified and validated. Since the procedure consists of mainly two steps: determining the internal loading diagrams and deflections, the verification procedure is two-fold.

Firstly, the loading diagrams are verified by analytically solving a simply-supported beam and finding all the loadings by hand. The result is then cross-checked with the code output. It has been confirmed the two results were identical. Moreover, the maximum bending and shear stresses for a sample loading case have been looked up in [34] and consulted with the code outcome. Once again, the results coincided.

Secondly, the verification and validation of the tool used for determination of the fuselage deflection was done similarly, i.e., a sample case (cantilever beam) was considered and the deflection was compared to the standard solutions found in [34]. Moreover, some loads were eliminated from the fuselage so that a simpler case could be analysed by hand and the results were then cross-checked with the numerical output; the outcomes were acceptably close.

5.6.3. Aerodynamic Characteristics

Aerofoil Trade-Off

Before conducting the aerodynamic analysis, one must first select a proper aerofoil to be used for the wing. As a first iteration, it was assumed that a single aerofoil along the whole wingspan was utilised. Nevertheless, in post-DSE activities, the possibility of having multiple aerofoils along the wing will be analysed.

Since the aircraft is operating at relatively low subsonic speeds (i.e. non-transonic speeds), it was decided that a simple NACA asymmetrical would be chosen. Therefore, a trade-off was performed for both the NACA 2412, NACA 2414 and NACA 2415.

After analysing multiple aerodynamic parameters for each aerofoil, it was decided to trade off based on four different parameters that differed per aerofoil and which were more relevant to the design. For each parameter, a given weight was chosen and each aerofoil was rated from 1 to 3 (relative to each other, 1 meaning worst and 3 meaning best) on each of these parameters. The parameters used for the trade-off were the following:

- **Maximum thickness to chord ratio ($25\,\%$):** A higher thickness to chord ratio (t/c) results in more space for the fuel tanks and other necessary components of the wing system, as for example the flaps system, cabling, etc.
- **Maximum lift coefficient ($30\,\%$):** A higher maximum lift coefficient ($C_{l_{max}}$) means that the requirements for High Lift Devices (HLDs) are not as stringent, resulting in a potential weight reduction in the wing system.
- **Minimum drag coefficient ($30\,\%$):** A lower minimum drag coefficient is favourable since then the required thrust will in principle be lower.
- **Angle of attack at $(C_l/C_d)_{max}$ ($30\,\%$):** Preference was given to an angle of attack closer to what is expected during normal operations cruise conditions (approximately $1\,\mathrm{deg}$ to $4\,\mathrm{deg}$) such that the wing area could be reduced to a minimum, hence reducing the overall weight of the wing system.

As can be seen in Table 5.17, the best-performing aerofoil appears to be the NACA 2412, therefore this aerofoil will be further analysed for the remainder of this subsection.

Table 5.17: Wing airfoil trade-off.

Parameter (weight)	**NACA 2412**	**NACA 2414**	**NACA 2415**
Maximum thickness to chord ratio (25%)	0.12 (score of 1)	0.14 (score of 2)	0.15 (score of 3)
Maximum lift coefficient (30%)	1.6 (score of 2)	1.55 (score of 1)	1.55 (score of 1)
Minimum drag coefficient (30%)	0.006 (score of 2)	0.007 (score of 1)	0.007 (score of 1)
Angle of attack at $(C_l/C_d)_{max}$ (15%)	$4\,\mathrm{deg}$ (score of 3)	$5\,\mathrm{deg}$ (score of 2)	$6\,\mathrm{deg}$ (score of 1)
Overall Score	1.9	1.4	1.5

It is important to note that although the choice for the NACA 2412 was made for the wing, the winglets do have a different aerofoil. This is because the aerodynamics of the winglets have a very big influence on the overall performance, stability and controllability of the aircraft. To account for this, an LS(I)-0413 aerofoil was chosen, as this aerofoil has been tested to have very good laminar flow behaviour, resulting in an improved aerodynamic performance of the winglets. [35]

2D Aerofoil Analysis

To perform an analysis of the NACA 2412 aerofoil, a Computational Fluid Dynamics (CFD) analysis was conducted with the help of the Ansys Fluent software. It was decided to evaluate, for multiple angles of attack, both the lift coefficient (C_l), drag coefficient (C_d), moment coefficient (C_m), and the pressure coefficient (C_p) distribution along the chord of the aerofoil. This was performed for both cruise and landing conditions, which simulate therefore the airplane operating at maximum and minimum operating speeds.

Before actually getting the CFD simulation up and running, one must first set up a proper mesh around the aerofoil being analysed, such that it provides accurate results in the end. For this, mesh spacing with respect to the wall of the aerofoil (Δy) must be properly defined. To do this, a choice of a Y+ parameter is chosen likewise. As can be seen in Figure 5.16, how much this spacing should be exactly is dependent on a previously chosen Y+ parameter as well as other external affecting parameters, such as freestream velocity (u) and atmospheric conditions. The Y+ parameter should be within 1 and 30 to account for an accurate result, although a lower Y+ within these boundaries should result in slightly more accurate results.[10] The Y+ parameter was chosen to be 1 for this simulation to generate more accurate results at the cost of few more computational resources.

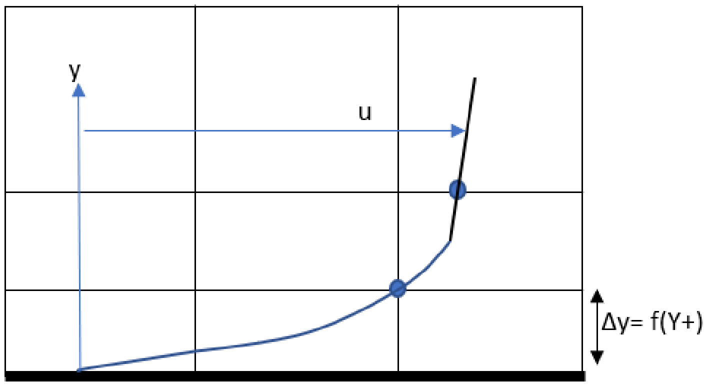

Figure 5.16: Mesh wall spacing based on Y+.

For the analysis itself, the k-omega (k_ω) method was used to the best of its abilities to predict the aerodynamic performance of the NACA 2412 aerofoil. This method is capable of simulating a turbulent airflow around the aerofoil by approximating the Reynolds-Averaged Navier Stokes (RANS) equations. Due to time constraints regarding the duration of the DSE project, a few assumptions and simplifications had to be made with regard to the aerodynamic analysis. These are the following:

- The aerofoil was individually analysed at a chord of $1\,\mathrm{m}$ and neither at real chord lengths nor at different chord lengths. The results presented in this report are therefore based on this aerofoil.
- A complete wing or aircraft aerodynamic analysis using CFD would be unfeasible considering the short time frame given during the DSE project, hence a semi-empirical method was used to translate the results obtained during the aerofoil CFD simulation to those of the wing of the aircraft.

After having successfully analysed the aerofoil itself, it is important to convert this data to its whole wing equivalent. As earlier stated, this was done using semi-empirical methods, rather than analysing the wing using CFD. The methods used for these conversions are proposed by J. Roskam [36].

The lift coefficient analysis results can be observed in Figure 5.17. As expected, due to the asymmetrical properties of the NACA 2412 aerofoil, at an angle of attack of $0\,\mathrm{deg}$, there is some minimal lift. When translating the aerofoil results to the wing, it can also be noticed that the maximum lift coefficient of the wing ($C_{L_{max}}$) is slightly lower than the aerofoil's equivalent as expected. It is important to note that the aerofoil's zero lift angle of attack (α_{0_l}) is $-2.1\,\mathrm{deg}$.

In Figure 5.18, the results of the C_L/C_D analysis can be observed for both the aerofoil CFD and wing estimation. One can see that although the aerofoil CFD model results seem reasonable, the conversion to the wing however seems a bit far off. Nevertheless, a full-wing CFD analysis could be

[10]https://resources.system-analysis.cadence.com/blog/msa2023-y-boundary-layer-thickness

required to prove this is indeed the case. It is important to note regardless that the optimal angle of attack of the wing in this case is $3.5\,\mathrm{deg}$, which is optimal from a cruise point of view.

By looking at Figure 5.19, one can read the results for the moment coefficient (evaluated at $x = 0.25c$) with respect to the angle of attack, for both the aerofoil and the wing. It can be noted that the wing curve is steeper, meaning that C_{m_α} of the wing is also higher. It is also important to note that the aerodynamic centre has been computed to be located at $x = 0.22245c$.

Lastly, in Figure 5.20 the pressure coefficient distributions along the aerofoil chord for different angles of attack are depicted. The results appear to be reasonable, and as expected, the difference in pressure distribution at higher angles of attack is more accentuated to account for a higher lift coefficient.

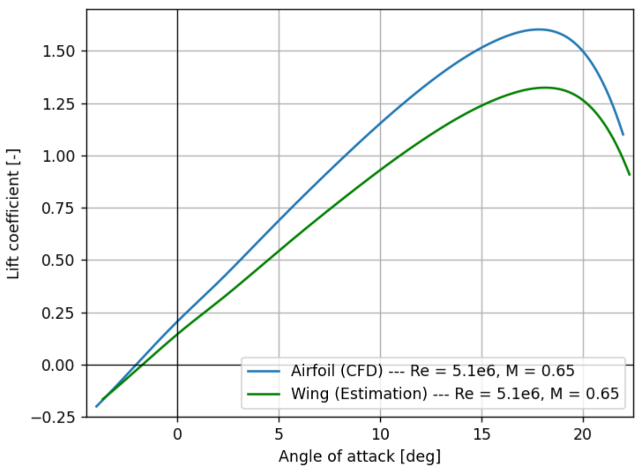

Figure 5.17: aerofoil Lift Coefficient (C_l) variation with Angle of Attack (α) at cruise conditions (chord of $1\,\mathrm{m}$).

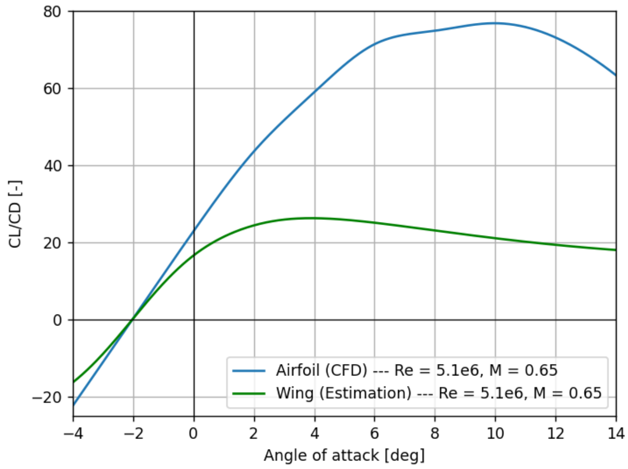

Figure 5.18: C_l/C_d variation with angle of attack (α) at cruise conditions (chord of $1\,\mathrm{m}$).

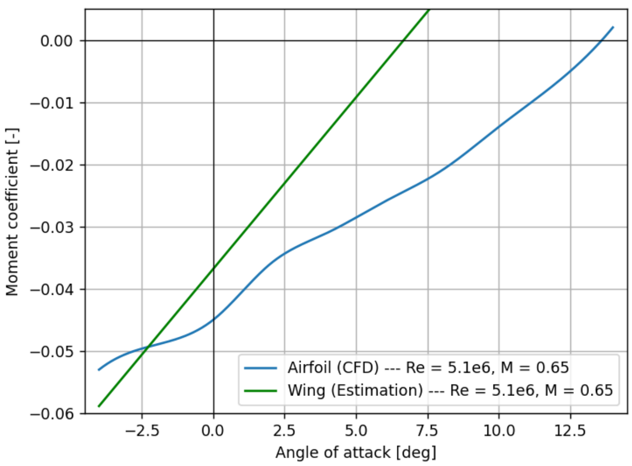

Figure 5.19: aerofoil Moment Coefficient (C_m) variation with Angle of Attack (α) at cruise conditions (chord of $1\,\mathrm{m}$).

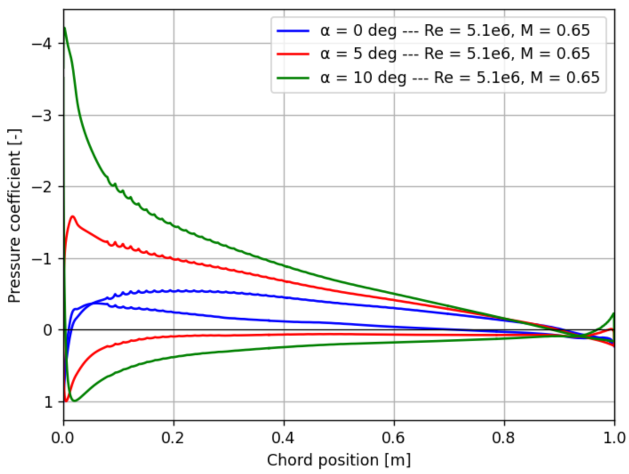

Figure 5.20: Pressure Coefficient (C_p) distribution at different angles of attack (α), at cruise conditions (chord of $1\,\mathrm{m}$).

In addition to these previous analyses, a depiction of the velocity magnitude around the aerofoil was generated and can be read from Figure 5.21. This analysis was conducted at an angle of attack of $10\,\mathrm{deg}$, since this is the angle of attack for which the C_l/C_d of the aerofoil is maximum.

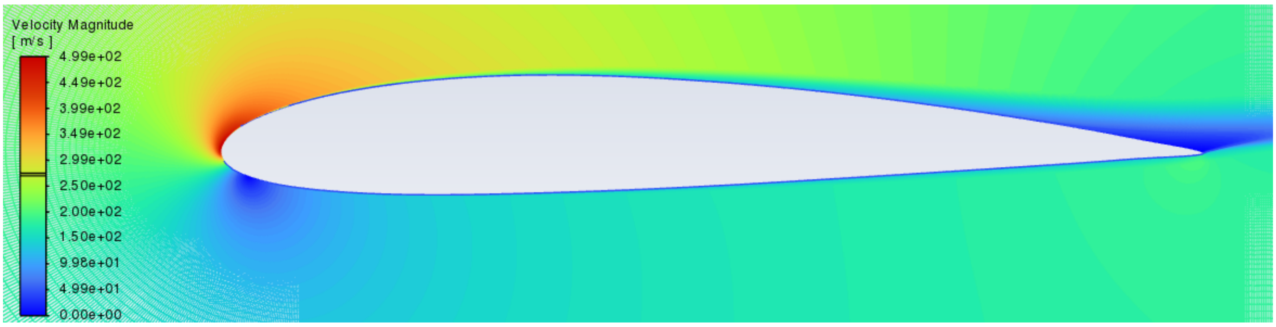

Figure 5.21: Velocity magnitude distribution around the aerofoil at $\alpha = 10\,\text{deg}$, $Re = 5.1 \times 10^6$ and $M = 0.65$.

After all the analyses have been performed, the most important parameters have been gathered in Table 5.18.

Table 5.18: Summary of the most important wing airfoil characteristics.

Parameter	Value	Unit
$C_{l_{max}}$	1.60	$-$
$C_{L_{max}}$	1.32	$-$
C_{l_α}	0.0946	deg^{-1}
C_{L_α}	0.0784	deg^{-1}
$(C_l/C_d)_{max}$	76.8	$-$
$(C_L/C_D)_{max}$	26.3	$-$
$C_{d_{min}}$	0.008	$-$
$C_{D_{min}}$	0.0085	$-$
C_{m_α}	2.97	deg^{-1}
C_{M_α}	5.51	deg^{-1}
$C_{m_{ac}}$	-0.051	$-$

Verification & Validation

The use of the k-omega method for CFD modelling of the NACA 2412 aerofoil is prone to large errors and uncertainties if not properly used. Because of this, the model was firstly verified by both increasing and decreasing the initially used $Y+ = 1$ and later validated by comparing the CFD results with those of experimental data.

As earlier stated, during a CFD analysis an appropriate Y+ value must be chosen such that the simulation runs smoothly and the results are accurate enough. To verify that an optimal Y+ has been chosen for the analysis of the aerofoil, it has been decided to run the same model with a $Y+ = 0.5$ and another run with a $Y+ = 15$. The expected outcome is that, in both cases, the model will likely predict less accurate results, although not by a large margin. The simulation was run for three different angles of attack and their respective lift coefficients were computed to compare the difference, which can be seen in Table 5.19. As can be easily drawn from this table, the differences are negligible, although these are worse for $Y+ = 0.5$ as expected, since this value is already out of the recommended range of $Y+$.

Table 5.19: Wing airfoil verification.

Angle of attack (deg)	**Original** C_l	C_l **at** $Y+=0.5$	C_l **at** $Y+=15$
0	0.18	0.17	0.18
5	0.69	0.67	0.68
10	1.15	1.14	1.15

Secondly, the model has also been validated, using experimental data retrieved from NASA regarding NACA2412 [37]. It was decided to validate the data obtained at cruise conditions, and since the Reynolds number (Re) at these conditions is just over 5 million, the data from experiments was used at Re = 5.7 million, since this is the closest reported Reynolds number value of for such experiments for this specific aerofoil. It is expected that the small difference will not be significant enough to cause large deviations, however. The data from both the experimental and CFD model can be compared in Figure 5.22, Figure 5.23 and Figure 5.24. It can be easily concluded that most of the key parameters predict somewhat accurately. Nevertheless, for high angles of attack, the lift coefficient computations seem to be a bit off, most likely due to the difference in Reynolds number, but also because this is a known limitation of the k-omega method [38]. Additionally, the drag coefficient might be not accurately predicted due to the difference in Reynolds number on top of the fact that the used aerofoil in the experimental data has a grid, which can influence the drag coefficient slightly.

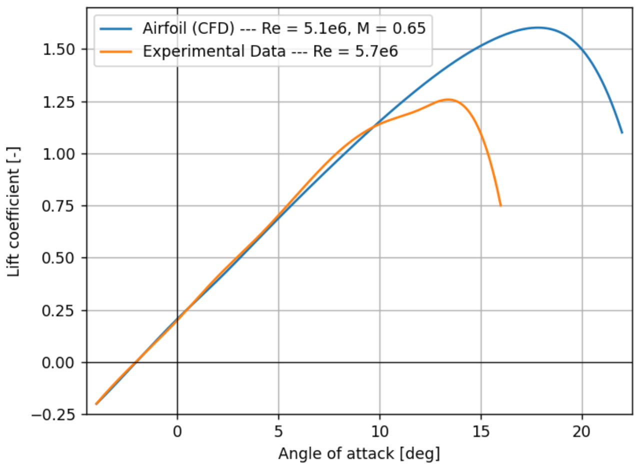

Figure 5.22: C_l-α curve comparison between the CFD model results and Experimental Data.

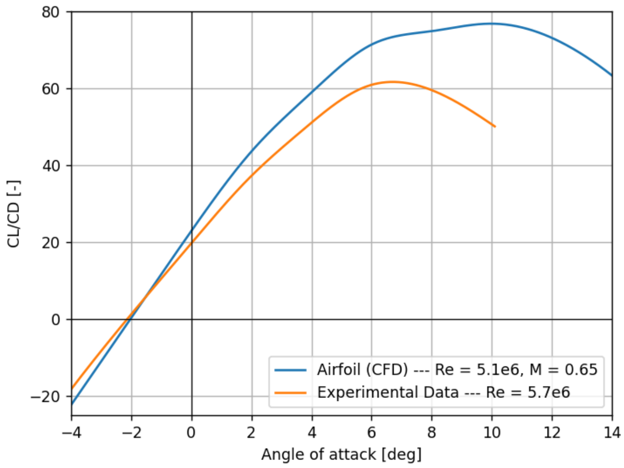

Figure 5.23: C_l/C_d-α curve comparison between the CFD model results and Experimental Data.

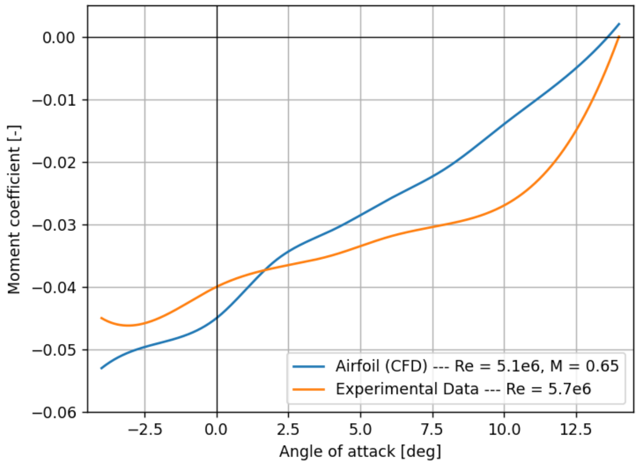

Figure 5.24: C_m-α curve comparison between the CFD model results and Experimental Data.

Horizontal Stabiliser Aerodynamics

For the Horizontal Stabiliser, the only requirement when choosing the aerofoil was that it should be symmetrical for easy controllability, hence the NACA 0012 aerofoil was chosen.

A CFD analysis was performed on the NACA 0012 aerofoil in the same way it was conducted on the NACA 2412 aerofoil chosen for the wing. The results were however only analysed for the lift coefficient since this is an important parameter that has to be analysed before conducting the Stability and Control Analysis presented in Subsection 5.6.4. It has been considered, mainly due to time constraints that an analysis of the drag coefficient, as well as of the moment coefficient of the horizontal stabiliser would be negligible for the performance of the overall aircraft. The results of the lift coefficient analysis of the NACA 0012 aerofoil can be seen in Figure 5.25.

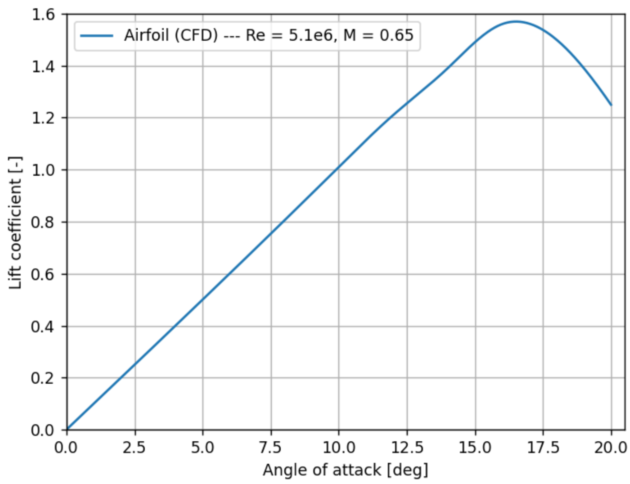

Figure 5.25: C_l - α curve for the NACA 0012 at cruise conditions (chord of $1\,\mathrm{m}$).

5.6.4. Stability and Control Characteristics

In this section, the ailerons, horizontal and vertical tail will be designed and sized to ensure that the aircraft is both stable and controllable during all phases of flight and most extreme centre of gravity positions on the aircraft. First, the sizing of the horizontal tail for longitudinal stability and control will be discussed, followed by the sizing of the vertical tail for lateral stability and control. Aerodynamic characteristics determined from the aerodynamic analysis of the wing and tail were utilised in order to form the control and stability curve as a function of the tail size and centre of gravity position. The specific parameters used to generate and analyse these curves will also be presented in order to clarify what the behaviour of the control curve and stability curves depend on.

Roll Control Surface Design

The two primary functions of the roll control system are to provide manoeuvrability as well as provide stability and control. Following these functions are certain roll requirements depending on the type and size of the aircraft. In order to comply with the latter of the requirements, the adverse yaw needs to be minimised as much as possible. Consequentially, differential ailerons were selected in an effort to minimise these effects. The requirement in which the aileron sizing and positioning is derived is that the aircraft shall achieve a roll angle of $30\,°$ in $1.5\,\mathrm{seconds}$. Firstly, the location of the front and aft spar needed to be determined in order to identify the aileron placement relative to the wing chord. Based on statistical data provided by Roskam [6], it was decided to have a front and aft spar location at $20\,\%$ and $75\,\%$ of the chord respectively. This means that the ratio of the aileron chord to wing chord is 0.25. From this value, the aileron effectiveness is then determined. Initially, it is assumed that the ailerons start at $70\,\%$ and end at $95\,\%$ of the half wingspan.

Using the aileron effectiveness, the gradient of the lift curve as well as the zero-lift drag coefficient of the selected aerofoil discussed in the previous section, the aileron control derivative ($C_{l_{\delta a}}$) and the aileron roll damping coefficient (C_{l_p}) are then determined using the following equations. The aileron control derivative is found using:

$$C_{l_{\delta a}} = \frac{2c_{l_\alpha}\tau}{Sb}\int_{b1}^{b2} yc(y)dy \tag{5.70}$$

The roll damping coefficient is found with:

$$C_{l_p} = \frac{4(C_{l_\alpha} + C_{d_0})}{Sb^2}\int_{0}^{b/2} y^2c(y)dy \tag{5.71}$$

Both equations can then be combined with the average aileron deflection to determine the roll rate:

$$P = -\frac{C_{l_{\delta a}}}{C_{l_p}}\frac{2V}{b}\delta_{a_{max}} \tag{5.72}$$

Where $\delta_{a_{max}}$ is the average max deflection angle of the differential ailerons. This can vary for different aircraft based on their mission profile and requirements that need to be met. By looking at aircraft with a similar size and mission profile to the one being designed, an idea of the range of possible deflection angles was achieved. It was initially decided to have an average max deflection angle of $25\,°$. From the roll rate, the time to reach the desired roll angle could be computed as follows

$$\Delta t = \frac{\Delta\phi}{P} \tag{5.73}$$

where ϕ is the roll angle, which is required to be $30\,°$ for class III aircraft. An if statement was implemented in the code in order to notify the user if the roll requirement is not met. Initially, an error was raised as the initial sizing and max deflection angle of the ailerons was not large enough to meet the roll rate requirement. As a result, the maximum deflection angle was increased to $30\,°$ and the start position of the ailerons were slightly altered to start at $66\,\%$ of the half wingspan rather than at $70\,\%$. When running the code with these new parameters, a sufficient roll rate was achieved as the aircraft takes just under $1.5\,\mathrm{seconds}$ to reach a bank angle of $30\,°$

the table below shows the final type of roll control system used as well as its sizing characteristics

Table 5.20: Table showing the dimensions of roll control system.

Parameter	Value
Type	Differential ailerons
Roll rate	$8.6\,\mathrm{deg/s}$
Length	$1.5\,\mathrm{m}$
Start position	$20.0\,\mathrm{m}$
End position	$22.5\,\mathrm{m}$
Max deflection	$30\,\mathrm{deg}$

Sizing Horizontal Tail for Longitudinal Stability and Control

In order to size the horizontal tail, a more detailed centre of gravity excursion of the aircraft had to be performed. First, the operational empty weight of the aircraft was determined, stemming from the preliminary design with the following equation.

$$x_{CG_{OEW}} = \frac{(x_{CG_{wing}} \cdot W_{wing}) + (x_{CG_{fuselage}} \cdot W_{fuselage})}{(W_{wing} + W_{fuselage})} \tag{5.74}$$

As payload and fuel is loaded into the plane, the centre of gravity of the aircraft as a whole will vary, depending on the locations at which the fuel or payload is loaded. In order to account for this, the new centre of gravity is calculated with the following equation.

$$x_{CG_{new}} = \frac{(x_{CG_{old}} \cdot W_{old}) + (x_{CG_{item}} \cdot W_{item})}{(W_{old} + W_{item})} \tag{5.75}$$

Where $x_{CG_{old}}$ and W_{old} is the centre of gravity and the total weight of the aircraft prior to the loading of the payload, while $x_{CG_{item}}$ and W_{item} is the local centre of gravity of the item being added with respect to the aircraft and the individual weight. In order to determine the variation of the centre of gravity, a certain order of loading the payload and fuel had to be established. The following order of loading was assumed.

1. Loading of cargo
2. Loading of passengers
3. Loading of fuel

Due to the aft location of the aircraft's wing, it was decided that there be one large front cargo hold and no aft cargo holds, as this would be sufficient to hold the expected volume of cargo to be loaded as well as help in shifting the centre of gravity forwards. In addition to this, the loading of the passengers is such that window seat passengers are loaded first, followed by the aisle seat passengers. Lastly, the middle seat passengers then board the aircraft. Using Equation 5.74 and Equation 5.75 with the loading process, a loading diagram can be constructed to identify the most forward and aft centre of gravity.

The centre of gravity limits were then retrieved from the loading diagram, based on the initial wing positioning and horizontal tail size. However, a safety margin of 5% was also applied to both the forward and aft centre of gravity.

Following this, the scissor plot was constructed. This plot assesses the controllability and stability of the aircraft. By using the same dimension on the x-axis for the control and stability curve as the loading diagram, it can then be assessed whether the aircraft's current tail size is sufficient enough to control and stabilise the aircraft within the determined centre of gravity limits. The following equation was used to determine the stability curve.

$$\frac{S_h}{S} = \frac{\overline{x}_{CG}}{\left(\frac{C_{L_{\alpha_h}}}{C_{L_{\alpha_{A-h}}}}\right)\left(1-\frac{d\epsilon}{d\alpha}\right)\frac{l_h}{MAC}\left(\frac{V_h}{V}\right)^2} - \frac{\overline{x}_{AC} - 0.05}{\left(\frac{C_{L_{\alpha_h}}}{C_{L_{\alpha_{A-h}}}}\right)\left(1-\frac{d\epsilon}{d\alpha}\right)\frac{l_h}{MAC}\left(\frac{V_h}{V}\right)^2} \tag{5.76}$$

Where $C_{L_{\alpha_{A-h}}}$ and $C_{L_{\alpha_h}}$ are the rate of the lift coefficients of the aircraft body without the tail and the horizontal tail respectively. These parameters have been determined for cruise conditions so that the stability of the aircraft is assessed in cruising conditions, as this is the most demanding and critical condition for stability. The ratio of the speed of the airflow over the horizontal tail compared to the wing takes into account the type and placement of the horizontal stabiliser. A rather unconventional H-tail, fuselage-mounted horizontal stabiliser will be used and so this is taken into account in this ratio. This is also taken into account in the downwash gradient experienced at the tail. For example, for a T-tail configuration, $\left(\frac{V_h}{V}\right)^2 = 1$ compared to $\left(\frac{V_h}{V}\right)^2$ of the H-tail which is 0.85, as the local velocity of the airflow over the horizontal tail is lower than that of a T-tail due to the perturbing presence of the fuselage.

The controllability of the aircraft was assessed in landing conditions as this is the most limiting condition in regards to controlling the plane. The controllability of the X-300 was characterised by the following equation.

$$\frac{S_h}{S} = \frac{\overline{x}_{CG}}{\left(\frac{C_{L_h}}{C_{L_{hA-h}}}\right)\frac{l_h}{MAC}\left(\frac{V_h}{V}\right)^2} + \frac{\frac{C_{m_{ac}}}{C_{L_{A-h}}} - x_{ac}}{\frac{C_{L_h}}{C_{L_{hA-h}}}\frac{l_h}{MAC}\left(\frac{V_h}{V}\right)^2} \tag{5.77}$$

where the aerodynamic parameters of the horizontal tail were determined during the aerodynamic analysis once again. In addition to this, a plot of how the centre of gravity varies with the wing position was constructed. By overlaying this plot with the scissor plot, an optimal wing position as well as an optimal horizontal tail sizing could then be determined. From this, a new optimal wing position and tail size could then be implemented in the design. The scissor plot showing the optimal wing placement and tail size can be seen below. The corresponding loading diagram is also presented below, showing the resulting centre of gravity range.

The region to the left of the controllability curve is the uncontrollable region and the unstable region is to the right of the stability curve. It is therefore crucial that the wing position and tail size allow for the aircraft to be controllable and stable within a centre of gravity range that falls between the two curves.

From the plots, the resulting tail size and wing position were determined to be $38.2\,\mathrm{m}$ and $29.1\,\mathrm{m}$ respectively. The corresponding front and aft centres of gravity were $-0.4\,\mathrm{MAC}$ and $0.32\,\mathrm{MAC}$, allowing for a centre of gravity range of $0.72\,\mathrm{MAC}$. However, due to further design choices that were made, both the wing position as well tail size had to be altered in order to aid in the functionality of the aircraft as a whole.

The first design choice that the horizontal tail had to cater for was the placement and size of the engines. Due to the engines being located above the horizontal stabiliser, the tail is less effective as a part of the effective area of the tail is covered by the engines. This was accounted for by determining the percentage of wetted area taken up by the engines and adding this percentage to the optimal size of the tail. Due to the large diameter of the engines, this increased tail size would

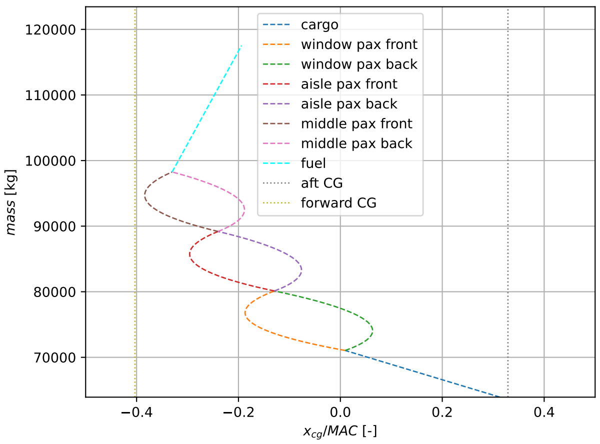

Figure 5.26: Figure showing the optimal centre of gravity range.

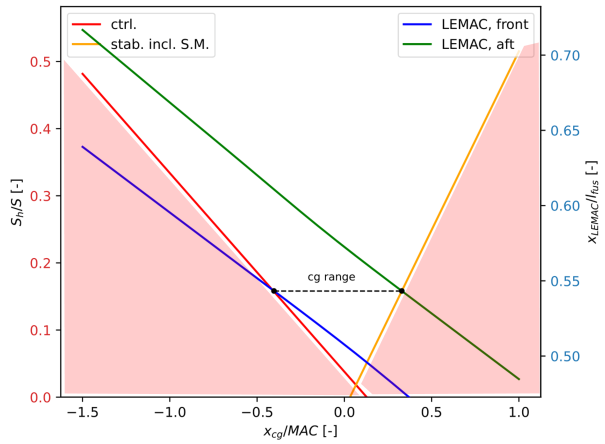

Figure 5.27: Figure showing the optimal wing position and tail sizing.

also be effective in shielding noise. In addition to this, the engine location moves the centre of gravity further aft. The wings therefore need to be placed further back to ensure that the centre of gravity lies in front of the neutral point to have longitudinal static stability in flight.

In addition to the engine placement, the optimal wing location also posed issues in regards to static ground stability and the landing gear position. With the current wing location, it cannot accommodate the full landing gear when retracted as they are not aligned. By moving the leading edge location of the wing to $32.5\,\mathrm{m}$ the landing gear is able to be retracted and stored within the wing while complying with a scrape angle of $15\,\mathrm{deg}$. Another benefit of this wing placement is that it moves the centre of gravity of the aircraft further aft in an absolute sense, meaning it moves closer to the main landing gear. With this, the static ground stability is then satisfied. The centre of gravity and the landing gear are then at a distance of $10\,\%$ from each other. Most aircraft design for this value to be between $10\,\%$ $15\,\%$ in order to ensure static ground stability [36].

The final reason for moving the wing further aft is due to the findings from the sensitivity analysis in Section 6.5. When considering this, it can be concluded that moving the wing position further back relative to the fuselage will also decrease the overall operative empty weight of the aircraft. As a result, many benefits can be taken advantage of by moving the wing position back.

When taking these factors into account, a new set of outputs in regards to the tail sizing and centre of gravity range was generated. The updated scissor plot and loading diagram are presented below.

By looking at the scissor plot above, it can be seen that after the changes made to the tail size and wing position, the tail is now over-engineered. At the new tail size and wing position, the aircraft is controllable and stable within a centre of gravity range of $-0.21\,\mathrm{MAC}$ to $0.7\,\mathrm{MAC}$ but it only needs to be within a range of $-0.21\,\mathrm{MAC}$ to $-0.96\,\mathrm{MAC}$. This is due to the fact that the centre of gravity has moved further forward relative to the neutral point of the wing. As a result, the aircraft has become even more stable but at the cost of reduced controllability. This is seen in Figure 5.29 where the tail size has become approximately twice as big as the optimal tail size in order to ensure the aircraft is still controllable at the new wing position. This was expected and can be easily justified by the fact that the tail needs to produce a larger down-force in order to control the aircraft. Consequently, the aircraft is stable in a much larger centre of gravity range than needed. It can therefore be concluded that the aircraft is more than capable of being stable and controllable within the desired centre of gravity range. It is also assured that the aircraft can remain controllable and stable in the unlikely event of the centre of gravity moving very far aft, up to $0.7\,\mathrm{MAC}$. The tail being over-engineered would suggest a larger tail mass and larger overall operational empty weight. However, from the

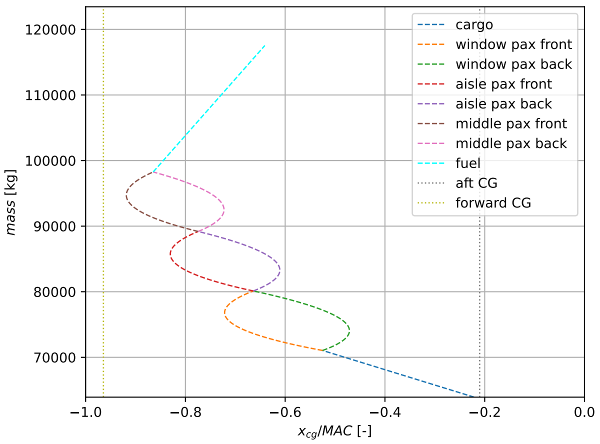

Figure 5.28: Figure showing the updated potato plot.

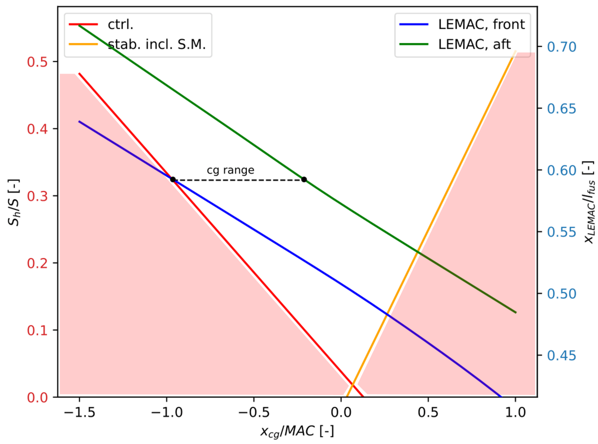

Figure 5.29: Figure showing the updated scissor plot.

sensitivity analysis in Section 6.5, the altered wing position results in weight savings from other subsystems, resulting in a lower overall operational empty weight.

The two tables below give an indication of the inputs used in the Python tool and the resulting outputs of the aircraft's stability and control characteristics.

Table 5.21: Inputs for stability and control.

(a) Inputs.

Parameter	Value	Unit
S	224.75	m^2
X_{ac}	33.10	m
$C_{L_{\alpha_h}}$	0.12	–
$C_{L_{\alpha_{A-h}}}$	4.84	–
$\frac{d\epsilon}{d\alpha}$	0.41	rad^{-1}
l_h	18.71	m
MAC	5.03	m
$\left(\frac{V_h}{V}\right)^2$	0.85	–
C_{L_h}	−1.5	–
$C_{L_{A-h}}$	1.1	–
$C_{m_{ac}}$	−0.05	–

(b) Outputs.

Parameter	Value	Unit
$X_{CG_{OEM}}$	31.39	m
$X_{CG_{front}}$	27.67	m
$X_{CG_{aft}}$	31.44	m
X_{LEMAC}	32.5	m
S_h	72.65	m^2
A_h	3	–
$span_h$	16.21	m
$taperratio$	0.5	–

Sizing Vertical Tail for Lateral Stability and Control

The dimensions of the two vertical tails were determined for the midterm report and were based on statistical relations from [6]. Another crucial factor that was taken into account when determining the size was the fact that the aircraft shall possess directional stability both on the ground and in flight. the area of each vertical tail is $9.89\,\mathrm{m}$, meaning a total vertical tail area of $19.77\,\mathrm{m}$. The span of each vertical tail is $3.85\,\mathrm{m}$ while a chord root of $3.42\,\mathrm{m}$ was used. Lastly, an aspect ratio and taper ratio of 1.5 and 0.5 was used respectively.

Verification and Validation

In order to verify the Python tool that was created to analyse the stability and control characteristics of the aircraft, both unit tests and subsystem tests were performed on the module of code. Unit tests were performed by analytically calculating the outputs of all equations that have been utilised and comparing these values to the numerical solutions provided by the tool. Different methods of subsystem tests were also performed. The curves that were plotted were checked against the corresponding equations in order to assess whether they comply with each other and make sense. The loading diagram and scissor plot were also compared against one another. As they both utilise the same x-axis, the CG range on both plots should be the same. Verifying that these were indeed the same ensured that the curves and limits were plotted correctly.

To validate the tail sizing, it was decided that the tail area to wing area ratio would be compared to that of reference aircraft which are in operational use. First data was collected on the wing and tail size of various aircraft from an aircraft database [39]. These aircraft only consist of a conventional tail rather than an H tail, however. This is due to the fact that there is not a sufficient amount of available data for aircraft with H tails, as this is currently an uncommon configuration for passenger aircraft. Some ratios of various passenger aircraft are given in the table below.

Table 5.22: Ratio between tail area and wing area (unitless) for a range of transport aircraft.

AC type	A320-200	A321-200	A330-300	B737-300	B757-300	B767-300
S_h/S	0.25	0.25	0.2	0.34	0.27	0.27

When considering the optimal tail sizing generated by the code, it is expected that an H tail will have a smaller S_h/S ratio. The optimal sizing ratio for the X-300 is $S_h/S = 0.16$, which is lower than all values presented in the table. This is due to the increased effectiveness of an H tail in comparison to a conventional tail. This results from the fact that the H tail is positioned out of the airflow behind the wing, meaning it experiences less downwash and is therefore more effective [40].

After changing the wing position, the resulting increase in the size of the horizontal stabiliser (including the engine noise shielding considerations), the ratio then becomes $S_h/S = 0.34$, which is larger than all reference aircraft except for the B737-300. This is also an expected result as the X-300 needs to be able to accommodate the engines and shield noise emissions via the horizontal tail planform. This increase in size is also a consequence of moving the leading edge of the main wing further aft. This alteration means the tail size has to be slightly increased as larger control surfaces on the horizontal tail are needed to manoeuvre and control the aircraft.

6 Performance Analysis

In this chapter, the performance properties of the X-300 are analysed. Section 6.1 presents the flight performance characteristics. This is followed by Section 6.2 and Section 6.3 which discuss the CO_2 and NO_x emissions of the aircraft respectively. Section 6.4 analyses the noise emissions of the EcoFlyer and is followed by a sensitivity analysis in Section 6.5.

6.1. Flight Performance

This section will present the flight performance characteristics of the aircraft. This includes a payload-range diagram, airfield performance and climb performance.

6.1.1. Payload Range

The payload range diagram shows different loading cases for the aircraft. The most important points are the harmonic range, range with maximum fuel and ferry range. Harmonic range is the maximum range with maximum payload and ferry range is the maximum range with no payload. Figure 6.1 Shows the payload range diagrams for the X-300 EcoFlyer and Airbus A320[41]. The diagram also displays the important coordinates, which are formatted as *(range, payload)*. It can be seen that the EcoFlyer has a higher payload capacity for similar ranges, which aligns with the aim of this aircraft design.

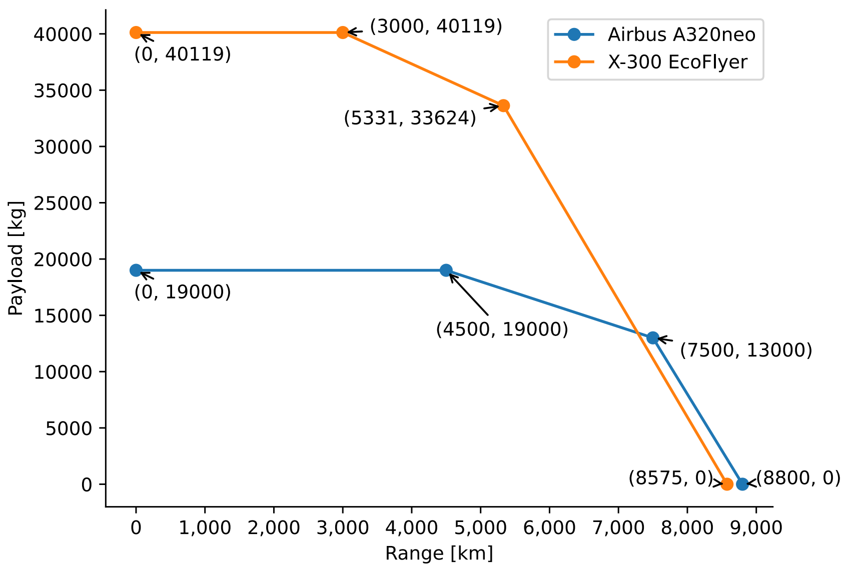

Figure 6.1: Payload Range diagram of the EcoFlyer and A320neo.

6.1.2. Airfield Performance

Airfield performance consists of calculating take-off and landing distances. The calculations presented are based on literature[42].

Take-Off

Take-off distance contains 3 parts: Ground roll, transition distance and clearance distance.

The ground roll is the distance the aircraft covers from being stationary to lift off. It is calculated using Equation 6.1. The coefficients K_A, K_T are defined in Equation 6.2 and Equation 6.3 respectively where μ is the ground friction coefficient and is taken as 0.02[42].

$$s_G = \frac{1}{2gK_A} \ln\left(\frac{K_T + K_A V_{LOF}^2}{K_T}\right) \tag{6.1}$$

$$K_A = \frac{T}{W} - \mu \tag{6.2}$$

$$K_T = \rho \frac{-C_{D_0} - C_L^2/\left(\pi A e\right) - \mu C_L}{2\left(\frac{W}{S}\right)} \tag{6.3}$$

Next, the transition distance is calculated. This is the distance between when the aircraft is at lift-off speed and climb speed. This is done by using Equation 6.4. R, γ are defined in Equation 6.5 and Equation 6.6 respectively. n is the load factor during take-off and is taken as 1.2 [42]. Equation 6.7 shows the equation used to determine the aircraft's height at the end of the transition. V_{LOF} is the liftoff speed which is $1.1\,\mathrm{t}$imes the stall speed at take-off, while V2 is the climb speed which is 1.2 times the take-off stall speed.

$$s_T = R\gamma \tag{6.4}$$

$$R = \frac{\left(V_{LOF} + V_2\right)^2}{4g(n-1)} \tag{6.5}$$

$$\gamma = \arcsin\frac{T - D}{W} \tag{6.6}$$

$$h_T = R\frac{\gamma^2}{2} \tag{6.7}$$

During take-off, the aircraft must be able to clear an obstacle which has a height of $35\,\mathrm{ft}$[32]. This is known as screen height. Using Equation 6.7, it is known that this aircraft already passes the obstacle during the transition phase. Therefore, the distance taken to clear the obstacle after lift-off is calculated using Equation 6.8, where h_s is the screen height.

$$s_s = \sqrt{(R + h_s)^2 - R^2} \tag{6.8}$$

The total take-off distance is the sum of the ground roll and distance to clear the screen. The sum is multiplied by a factor of 1.15 to account for operational variability [32]. Table 6.1 shows the inputs used for the calculations and the final take-off distance of $1669\,\mathrm{m}$. This result complies with the requirement that the maximum take-off distance shall be less than $2100\,\mathrm{m}$.

Table 6.1: Take-off distance calculation input and final result.

Parameter	Value	Unit
$C_{L_{TO}}$	1.98	$-$
Maximum take-Off Weight	$1\,211\,023$	N
Wing area	224.7	m^2
μ_{TO}	0.02	$-$
Aspect ratio	10	$-$
Oswald factor	0.8	$-$
$V_{stall_{TO}}$	73.7	$\mathrm{m/s}$
Take-off thrust	$405\,706$	N
Take-off distance	1669	m

Landing

Calculating landing distance follows a similar procedure compared to calculating take-off distance. The phases of landing consist of approach, flare, free roll and ground roll. The approach angle, γ_A, was set as $3\,°$ [42].

The approach distance is the distance covered from the start of the approach until the start of the flare. The start of the approach is when the aircraft is at screen height, which is $50\,\mathrm{ft}$ for landing [32]. The distance was calculated using Equation 6.9 and Equation 6.10. V_F is the flare velocity and is 1.2 times the landing stall speed. The flare radius, R, was found using Equation 6.11. With this, the distance during flare was calculated using Equation 6.12.

$$s_A = \frac{h_s - h_F}{\tan \gamma_A} \tag{6.9}$$

$$h_F = R\frac{\gamma_A^2}{2} \tag{6.10}$$

$$R = \frac{V_F^2}{g(n-1)} \tag{6.11}$$

$$s_F = R\gamma_A \tag{6.12}$$

On the ground, the aircraft rolls for a few seconds after touchdown before the brakes are applied. This time was taken as $2\,\mathrm{s}$ [42] and the distance covered is the product of the time and touchdown speed. The ground distance needed for the aircraft to come to a complete stop was calculated using Equation 6.1 where the thrust was set to the thrust of thrust reversers.

In order to reduce the landing distance, thrust reversers are used during landing. The thrust from the thrust reversers is up to $28\,\%$ of the maximum static thrust [43]. The ground coefficient of friction, μ, was chosen as 0.5 [42]. The lift of the aircraft is assumed to be zero due to the deployment of spoilers.

The total landing distance is the sum of all the components combined and then multiplied by 1.66 to account for operational and pilot variability [32]. Table 6.2 shows the inputs used to calculate the landing distance, which was $1427\,\mathrm{m}$. This complies with the landing distance requirement of $1500\,\mathrm{m}$.

Table 6.2: Landing distance calculation input and final result.

Parameter	Value	Unit
$C_{L_{land}}$	2.6	$-$
Maximum Landing Weight	$956\,976$	N
μ_{land}	0.50	$-$
$V_{stall_{land}}$	57.22	m/s
Reversers thrust	$-113\,597$	N
Landing distance	1475	m

6.1.3. Cruise Performance

The cruise performance is analysed to give the maximum altitude when flying at cruise speed and the maximum speed when flying at cruise altitude. The calculations presented are taken from literature[44].

The design cruise altitude for this aircraft is $29\,000\,\mathrm{ft}$ ($8840\,\mathrm{m}$). This is a lower altitude than most modern airliners [1]. Flying lower reduces the climate impact of the aircraft, such as a reduction in contrail effects by up to $60\,\%$ if flying $2000\,\mathrm{ft}$ lower than current aircraft [45].

The first step to finding if the aircraft meets the required design conditions was determining the power available and required for the aircraft. The power available changes with altitude which are accounted for using Equation 6.13, where the sea level power is the maximum thrust multiplied by the velocity at which it is calculated.

$$\frac{P_n}{P_{SL}} = \sqrt{\frac{\rho_n}{\rho_{SL}}} \tag{6.13}$$

The power required for the aircraft to fly was calculated using Equation 6.14. The drag was calculated using Equation 6.15. The power required and available was calculated for altitudes $0\,\mathrm{m}$ up to $10\,000\,\mathrm{m}$ at $1000\,\mathrm{m}$ intervals. Figure 6.2 shows the power required and power available during cruise for different velocities. From Figure 6.2, it can be seen that the maximum velocity at which the aircraft can fly at a cruise altitude of $8840\,\mathrm{m}$ is $200\,\mathrm{m/s}$.

$$P = DV \tag{6.14}$$

.

$$D = \frac{1}{2}\rho V^2 S C_D \tag{6.15}$$

[1] https://calaero.edu/aeronautics/aircraft-performance/how-high-do-commercial-planes-fly/

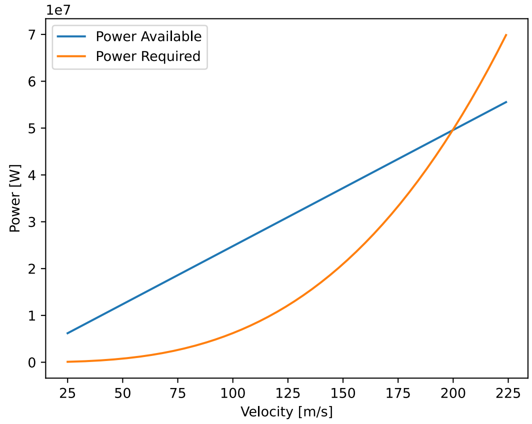

Figure 6.2: Power Available and Power Required curves for a cruise altitude of $8840\,\mathrm{m}$.

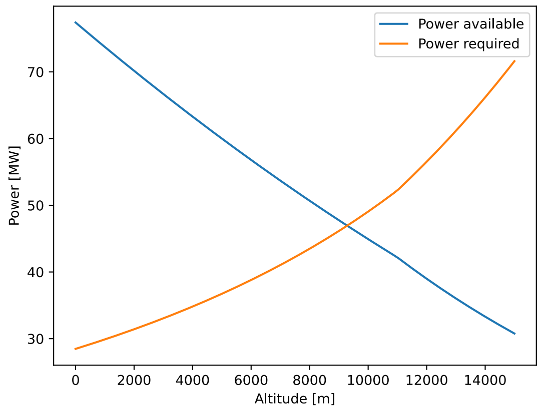

Figure 6.3: Power available and power required for different altitudes at a speed of $194\,\mathrm{m/s}$.

In order to find the maximum height X-300 can fly at a cruise speed of $194\,\mathrm{m/s}$, the power required and power available for different altitudes at the cruise speed were calculated. This can be seen in Figure 6.3, where the theoretical ceiling of the aircraft is at $9280\,\mathrm{m}$.

6.1.4. Verification and Validation

In order to ensure the Python program gives reliable results, the code must be verified and validated. Code verification was done by conducting a series of unit tests for the individual functions where the results from the code were compared with hand calculations. Additionally, the code was validated by using sample aircraft data from Jenkinson [42]. Table 6.3 displays the validation results for the take-off and landing distance calculations.

Table 6.3: Results of program using reference data.

Parameter	Value from simulation	Value from source [42]	Difference
Take-off ground roll	$1586.84\,\mathrm{m}$	$1586\,\mathrm{m}$	$0.05\,\%$
Distance to screen take-off	$283.52\,\mathrm{m}$	$284\,\mathrm{m}$	$0.17\,\%$
Total take-off distance	$2150.9\,\mathrm{m}$	$2150\,\mathrm{m}$	$0.04\,\%$
Landing approach distance	$228.2\,\mathrm{m}$	$228.4\,\mathrm{m}$	$0.09\,\%$
Landing ground roll	$671.8\,\mathrm{m}$	$672\,\mathrm{m}$	$0.03\,\%$
Total landing distance	$1915.7\,\mathrm{m}$	$1916\,\mathrm{m}$	$0.02\,\%$

6.2. CO_2 Emissions

Using the total fuel consumption computed by the model and the CO_2 reduction percentage for an average forecasted SAF blend from Section 9.3 the CO_2 emissions can be calculated and are shown in Table 6.4.

Table 6.4: CO_2 emission results for a $1100\,\mathrm{km}$ mission.

Parameter	A320neo (modeled)	X-300 (no SAF)	X-300, $6\,\%$ SAF blend
CO_2 reduction by use of SAF	$0\,\%$	$0\,\%$	$4.6\,\%$
Total fuel consumed kg	6672.5	8120.1	8120.1
Total CO_2 emissions kg	$21\,085$	$25\,943$	$24\,750$
Available Seats	194	330	330
CO_2 g / ASK	98.8	71.5	68.2
CO_2 g / ASK reduction compared to modeled A320neo	$0\,\%$	$27.7\,\%$	$31.0\,\%$

As shown in the table solely, the performance improvement of the design is sufficient to meet the $25\,\%$ reduction in CO_2 emissions per ASK.

6.3. NO_x Emissions

In this section, the NO_x emissions are separately calculated for LTO and cruise.

6.3.1. LTO NO_x Emissions

Using the engine model, its subsequent NO_x model and the nominal mission profile the amount of NO_x emissions that the X-300 emits during LTO were to be calculated. However, the engine model was not robust enough to yield probable values for off-design points of the WIT turbofan engine. As the engine's design point is the cruise phase, the LTO NO_x emissions can not be calculated using the engine model. Therefore the engine emissions of the WIT turbofan are calculated using a highly conservative assumption so as to not overestimate its NO_x reduction potential. The NO_x calculations are shown below in Table 6.5. The notes below clarify values in Table 6.5.

1. LEAP-1A26 EINOx values are taken from the ICAO engine emissions database [15].
2. A highly conservative EINOx reduction factor for the WIT turbofan compared to the LEAP-1A26 is calculated being $50\,\%$ The steam factor is excluded, only the lower T37 and p37 contributions of $45\,\%$ and $16\,\%$ are used leading to this figure [7].
3. Even though the WIT has a higher TSFC the fuel mass flow is assumed to only scale linearly with the max take-off thrust of the engine which is a conservative assumption.
4. This time is given by the ICAO LTO cycle definition [2].
5. The taxi time is reduced to only 4 minutes of idling due to engine warm-up, the rest of the taxiing is done electrically by the IWET system.
6. This total NO_x value is **per engine**. This is done because the ICAO has standards that relate the maximum allowed NO_x to the take-off engine thrust. The total LTO NO_x emissions for the A320neo and X-300 are double these values.

With conservative estimates on the LTO NO_x emissions the engine, producing a maximum thrust of $203\,\mathrm{kN}$ and a pressure ration of 26, has a Dp / Foo NO $_x$ of $9.56\,\mathrm{g/kN}$. This makes the WIT engine compliant with the future ICAO NO_x standard for 2027 shown in Figure 6.4 [3]

6.3.2. NO_x Cruise Emissions

The NO_x cruise emissions can be calculated by multiplying the total cruise fuel burn with the cruise EINOx. The EINOx for cruise has been calculated to be $0.564\,\mathrm{g\,kg^{-1}}$. The model yields a total fuel for

[2] https://www.icao.int/environmental-protection/Pages/LAQ_TechnologyStandards.aspx
[3] https://www.icao.int/environmental-protection/Documents/EnvironmentalReports/2019/ENVReport2019

Table 6.5: NO_x emissions for the LTO cycle, comparison between the A320neo and the X-300 engine. The notes are mentioned in Subsection 6.3.1.

Emissions per LTO phase	LEAP-1A26	WIT turbofan	Percentage of LEAP-1A26	Note
EINOx Take-off g/kg	18.77	9.46	50 %	1,2
Fuel Flow kg/s	0.86	1.43	167 %	3
Time s	42	42	100 %	4
NO_x Take-off kg	0.67	0.57	84 %	
EINOx Climb out g/kg	11.16	5.62	50 %	1,2
Fuel Flow kg/s	0.71	1.18	167 %	3
Time s	132	132	100 %	4
NO_x Climb out kg	1.04	0.87	84 %	
EINOx APP g/kg	8.67	4.37	50 %	1,2
Fuel flow kg/s	0.24	0.40	167 %	3
Time s	240	240	100 %	4
NO_x Approach kg	0.50	0.42	84 %	
EINOx Idle g/kg	4.63	2.33	50 %	1,2
Fuel flow kg/s	0.09	0.15	167 %	3
Time s	1560	240	15 %	5
NO_x Idle kg	0.64	0.08	13 %	
Total NO_x kg	**2.85**	**1.94**	**68%**	6

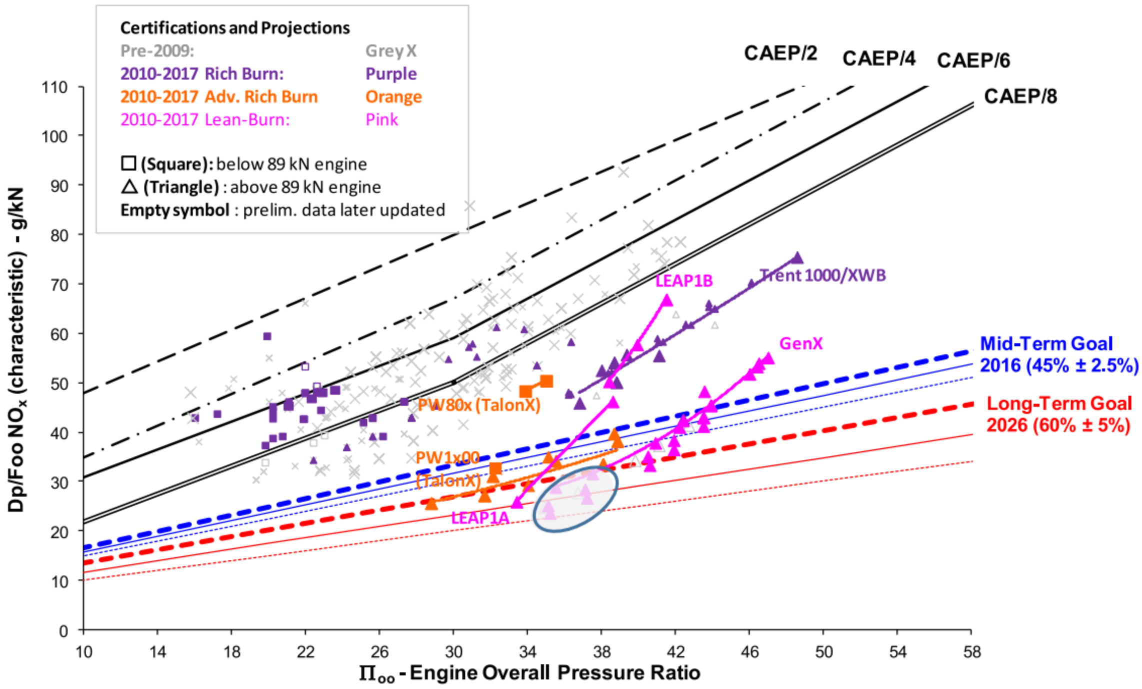

Figure 6.4: ICAO NOx engine standards (taken from [3]).

the nominal mission of 8120.1 kg. As the fuel used for calculating NO_x emissions of LTO should not be counted double the total LTO fuel is subtracted. Using Table 6.5 the LTO fuel can be calculated to be 1089.9 kg which yields a cruise fuel burn of 7030.2 kg. This results in a cruise NO_x emission of 3965 g. The same can be done for the modelled A320neo yielding 44 280 g.

6.3.3. NO_x Emissions Results

The results of the NO_x calculations are shown in Table 6.6.

Table 6.6: NO_x emissions results for a $1100\,\mathrm{km}$ mission.

Parameter	A320neo (modeled)	X-300
NO_x emissions LTO g	5704	3880
Cruise EINOx $\mathrm{g/kg}$	7.35	0.469
NO_x emissions Cruise g	$44\,280$	3321
Total NO_x emissions g	$44\,285$	7201
Available Seats	194	330
NO_x g / ASK	0.208	0.020
NO_x g / ASK reduction compared to modeled A320neo	$0\,\%$	$90.5\,\%$

The NO_x emissions reduction per ASK is $90.4\,\%$. This is in line with the NO_x reduction potential of more than $90\,\%$ mentioned in the WIT turbofan concept analysis [7].

6.4. Noise Emissions

This section presents an analysis of the X-300's noise emissions. Although there are several analytical and semi-empirical noise prediction models (e.g. ANOPP [46], NRM [46], and PANAM [47]), these models cannot be applied to the X-300 for two reasons. First, as this is a feasibility study, many of the input parameters necessary for the aforementioned models are not defined yet (these are very specific design parameters, such as the clearance between compressor stages in the engine). Second, the models cater to traditional aircraft configurations with low wings and wing-mounted engines, which makes them less robust, if not inapplicable, for our aircraft's design.

Due to this limitation, noise emissions for the X-300 were predicted using a combination of publicly available experimental data and literature. First, the applicable noise limits for the aircraft were established as per ICAO guidelines (Subsection 6.4.1). Then, using experimental data from the ICAO Noise Database[4], statistical formulas were computed relating noise levels to aircraft design characteristics such as maximum take-off mass (MTOM) and sea-level static thrust (SLST) among others (Subsection 6.4.2). These relations were used to establish the baseline noise level of our aircraft without any noise-reducing modifications. To quantify the effects of the modifications (i.e. fan noise shielding and a podded landing gear), literature sources were used to determine the reduction in noise achieved by their implementation (Subsection 6.4.3). The final noise levels are calculated by subtracting these reductions from the baseline noise level (Subsection 6.4.4). As a final note, the metric used here to quantify noise is Effective Perceived Noise Level, EPNL, measured in decibels (dB, also appears as EPNdB)

6.4.1. Applicable Noise Limits

The noise limits considered for this analysis are the ones provided by ICAO in *"Annex 16, Volume I to the Convention on International Civil Aviation"*[5]. Since 2013, the latest limits are defined by Chapter 13, and they prescribe a reduction in noise of $7\,\mathrm{EPNdB}$ (cumulative) relative to the preceding Chapter 4 limits. The latter is determined, per certification point (i.e. independently at flyover, lateral, and approach), by formulas specific to jet aircraft which take the aircraft's MTOM as input. The formulas can be found in Annex 16, Volume 1. Using the X-300's MTOM of $123.4\,\mathrm{t}$, the calculated EPNL values (for Chapter 4 limits) can be found in Table 6.7. The cumulative EPNL is simply an addition

[4]https://noisedb.stac.aviation-civile.gouv.fr/

[5]https://www.icao.int/environmental-protection/pages/Reduction-of-Noise-at-Source.aspx

of the three certification points. The Chapter 13 limit is then obtained by subtracting $7\,\mathrm{EPNdB}$ from the cumulative Chapter 4 limit.

Since the X-300 is due to enter service by 2035, future noise limits are also of interest. In 2019, an Independent Experts Panel on behalf of the ICAO Committee on Aviation Environmental Protection (CAEP) agreed on scenarios for future aircraft noise performance based on the development outlook for noise-reduction technologies [6]. While these are not hard limits, they offer an indication of the expected noise performance of future aircraft. Predictions for 2037 foresee a reduction in cumulative EPNL of as much as $25\,\mathrm{dB}$ relative to current Chapter 13 limits. As a point of reference, a 2037 target noise performance is tabulated in the last row of Table 6.7

Table 6.7: Noise limits for X-300 (with MTOM = $123.448\,\mathrm{t}$).

Parameter	EPNdB	**Notes**
Flyover (Chapter 4)	94.4	Used formula: $69.65 + 13.29 \cdot \log(MTOM)$
Lateral (Chapter 4)	98.7	Used formula: $80.87 + 8.51 \cdot \log(MTOM)$
Approach (Chapter 4)	102.2	Used formula: $86.03 + 7.75 \cdot \log(MTOM)$
Cumulative (Chapter 4)	295.4	Addition of flyover, lateral, and approach
Cumulative (Chapter 13)	288.4	$-7\,\mathrm{EPNdB}$ lower than Chapter 4
Cumulative (2037 target, not limit)	263.4	$-25\,\mathrm{EPNdB}$ lower than Chapter 13

It should be noted that the values in Table 6.7 are not considered limiting, because most aircraft tend to perform well below their prescribed noise limits. For example, based on data from the ICAO Noise Database, the A320neo averages a margin to its cumulative EPNL limit of approximately $30\,\mathrm{EPNdB}$ (i.e. its certified noise level is $30\,\mathrm{EPNdB}$ below its prescribed noise limit). So, while these limits are useful for ensuring the aircraft meets industry noise standards, common practice shows that it is always the case.

6.4.2. Baseline Noise Level

In this subsection, a baseline noise level for the X-300 is determined using experimental data from the ICAO Noise Database. Here, the word "baseline" is used to refer to the X-300 without any noise-saving measures such as fan-noise shielding and a podded landing gear. The reason for this assumption will be explained later. This analysis aims to identify which design parameters have the strongest correlation to EPNL, derive statistical relations between them and EPNL, and finally, use these relations on our aircraft by inserting its design parameters to obtain an EPNL value.

Depending on which EPNL measurement point is considered, an aircraft's measured noise will be dominated by a different aircraft element. For example, at take-off (i.e. flyover measurement), the engines operate at or close to full power, hence engine noise is the biggest contributor to the EPNL measurement at flyover [46]. A similar thing applies to the later measurement, which is recorded by a microphone to the side of the runway during an aircraft's take-off run. On the other hand, on approach (i.e. approach measurement), the engines operate at a lower power setting, hence airframe noise is the biggest contributor to the EPNL measurement on approach. Bertsch et al [48] have identified a number of aircraft parameters which contribute to aircraft noise at all the measurement points. Based on this study, the following design parameters were selected for further investigation as potential predictors of EPNL:

- Six engine parameters (to characterise noise originating from the engine): bypass ratio (`BR`), number of fan blades (`N_blades`), rotational speed of the low-speed spool at take-off (`N1`, in rpm), rotational speed of the high-speed spool at take-off (`N2`, in rpm), fan diameter (`D_fan`, in cm), and total sea-level static thrust (`SLST`, in kN).

[6] https://www.easa.europa.eu/eco/eaer/topics/technology-and-design/aircraft-noise#certified-noise-levels

- Six airframe parameters (to characterise noise originating from the airframe): wing area (`S`, in m^2), aspect ratio (`AR`), slat deflection angle on landing (`d_S`, in deg), flap deflection angle on landing (`d_F`, in deg), number of wheels on main landing gear (`N_wheel`), diameter of wheels on main landing gear (`D_wheel`, in in).
- Two other parameters (to characterise overall aircraft noise): maximum take-off mass (`MTOM`, in t), maximum landing mass (`MLM`, in t).

Data was gathered on each of these 14 parameters for 21 different aircraft models, spanning a wide range of weight categories and all having entered in service from 2006 onwards. The full data set can be found in Appendix A. Note that for some aircraft types, multiple aircraft models have been tabulated (e.g. for the A320neo aircraft type, the following models have been included: A320-251N, A320-271N, A320-272N, and A320-273N). This has been done with the aim of diversifying the range of engine options present in the analysis in order to see how a given aircraft type performs when powered by different engines. The MTOM and MLM values specified for each entry are the exact values for which the given EPNL measurements were made. In some cases, there are multiple entries for the same aircraft model (e.g. there are three entries for the Boeing 787-8, two entries for the A350-941, three entries for the Embraer E195-E2, etc.). Once again, this is done to investigate how a given aircraft model performs under different MTOM and MLM conditions. Finally, for each entry, a record number has been specified, linking it to the location in the ICAO Noise Database where it was retrieved.

A Pearson correlation coefficient (PCC) was calculated for each combination of design parameter and cumulative EPNL. The results are shown in Table 6.8. PCC values range from -1 to $+1$; positive correlation is indicated by positive numbers, while negative correlation is indicated by negative numbers. The closer the PCC is to ±1, the stronger the correlation.

Table 6.8: PCC for each combination of design parameter and EPNL measurement point.

Parameter	PCC for cumulative EPNL
BR	-0.50551
N_blades	0.59875
N1	-0.74876
N2	-0.88400
D_fan	0.88220
SLST	0.93279
MTOM	0.95147
MLM	0.95269
S	0.93418
AR	-0.85485
d_S	0.34052
d_F	-0.38952
N_wheel	0.87402
D_wheel	0.89868

As evident from the table above, the parameters which exhibit the strongest correlation to cumulative EPNL for the gathered data are the maximum landing mass (`MLM`), maximum take-off mass (`MTOM`), wing area (`S`), and sea-level static thrust (`SLST`). Using the data from Appendix A, polynomial best-fit curves were constructed for each of the four parameters. The formulas describing these curves are given below, along with a coefficient of determination (R^2), which measures how well the formulas replicate the data (the closer R^2 is to 1, the better the fit of the curve).

$$EPNL\ (MTOM) = -1 \cdot 10^{-4} \cdot MTOM^2 + 0.1148 \cdot MTOM + 250.65, \qquad R^2 = 0.9593 \tag{6.16}$$
$$EPNL\ (MLM) = -1 \cdot 10^{-4} \cdot MLM^2 + 0.1463 \cdot MLM + 249.87, \qquad R^2 = 0.9353 \tag{6.17}$$
$$EPNL\ (S) = -3 \cdot 10^{-5} \cdot S^2 + 0.0657 \cdot S + 251.08, \qquad R^2 = 0.903 \tag{6.18}$$
$$EPNL\ (SLST) = -1 \cdot 10^{-5} \cdot SLST^2 + 0.0432 \cdot SLST + 249.03, \qquad R^2 = 0.8986 \tag{6.19}$$

Using these formulas and the relevant input parameters, four estimates for the baseline EPNL (cumulative) were computed. A final estimate was calculated using a weighted average, with the R^2 values of each formula serving as weights. The results are shown in Table 6.9

Table 6.9: Baseline noise calculation.

(a) Inputs.

Parameter	Value	Unit
MTOM	123.448	t
MLM	108.025	t
S	224.75	m^2
SLST	405.71	kN

(b) Outputs.

Cumulative EPNL	Note
263.7 EPNdB	from MTOM, using Equation 5.16
264.5 EPNdB	from MLM, using Equation 5.17
264.3 EPNdB	from S, using Equation 5.18
264.9 EPNdB	from SLST, using Equation 5.19
264.4 EPNdB	using a weighted average of the above

The value in the last row of Table 6.9b, 264.4 EPNdB, is the final estimate for the baseline noise of the X-300. Once again, “baseline” refers to the noise of the aircraft without accounting for noise reduction technologies. For reference, the A320neo, across all its variations, averages 258.6 EPNdB, meaning the baseline X-300 is louder by 6.3 EPNdB. In the next section, noise reduction will be applied to close this difference.

6.4.3. Effects of Noise-Reducing Design Modifications

The main noise reducing measure implemented in the X-300 is the concept of fan noise shielding (or more broadly, engine noise shielding). The principle behind noise shielding is that of sound reflection, whereby a surface placed in close proximity to a sound source reflects that sound away from the source. In aircraft with engines mounted on the underside of the wing, that underside reflects the noise away from the engine and orients it downwards (i.e. towards the ground). To achieve fan noise shielding, a surface must reflect the noise such that perceived noise on the ground is reduced. Logically, a surface reflecting the noise upwards (i.e. away from the ground) achieves that effect. In a conventional tube-and-wing aircraft, possible surfaces for that purpose include the upper surface of the wing, the upper surface of the fuselage, and the upper surface of the horizontal stabilizer. As explained in Chapter 3, the X-300 uses the horizontal stabilizer to achieve engine noise shielding.

Due to the lack of means to evaluate the effect of noise shielding analytically, literature has been used to inform an educated guess on the potential savings from noise shielding. Table 6.10 presents an overview of reported noise reductions (as cumulative EPNL) from shielding.

Table 6.10: Potential noise savings from engine shielding as reported by literature.

Source	$\Delta\mathrm{EPNdB}$	Characteristics of studied aircraft
Bertsch et al [49]	-22.1	MTOM = $76.2\,\mathrm{t}$; configuration with high wing and engines mounted on top of the wing (at wing root); engine intake shielded entirely by the upper surface of the wing box; engine exhaust shielded only by the fuselage; uses a geared turbofan engine.
Noeding and Bertsch [50]	-31.8	Re-assessment of Bertsch et al [49]; same characteristics as above.
Bertsch et al [49]	-12.7	MTOM = $82.5\,\mathrm{t}$; configuration with high wing and engines mounted on top of the wing (at wing root); engine intake shielded entirely by the upper surface of the wing box; engine exhaust shielded only by the fuselage; uses a non-geared turbofan engine.
Noeding and Bertsch [50]	-15.2	Re-assessment of Bertsch et al [49]; same characteristics as above
Gyunn and Olson [51]	-33.0	MTOM = $135.3\,\mathrm{t}$; configuration with high wing and engines mounted on top of the wing; engine extends beyond the leading edge of the wing, but fan is shielded by a scarfed intake; engine exhaust shielded by the upper surface of the wing;
Greco et al [47]	-3.59	MTOM approximately $75\,\mathrm{t}$; only accounts for flyover and approach measurements (i.e. not lateral); actual cumulative EPNL is likely around -5 to $-5.5\,\mathrm{EPNdB}$; configuration with high wing and engines mounted on top of the wing (at wing root); engine intake is located at the wing's trailing edge; engine exhaust shielded only by the fuselage.

Based on these findings, the $\Delta\mathrm{EPNL}$ from engine noise shielding alone was estimated to be $-10\,\mathrm{dB}$. Some considerations behind this estimate include:

- The studies presented in Table 6.10 involve aircraft which use the wing for noise shielding rather than the horizontal stabiliser as the X-300. The wing is a larger surface, hence it is expected that it achieves better shielding than the horizontal stabilizer. As such, it is unlikely for the X-300 to yield noise savings higher than $-30\,\mathrm{EPNdB}$ as some of the studies report.
- On account of the higher MTOM of the X-300 relative to the aircraft from the literature studies, it is expected that the implementation of engine noise shielding will bring lower noise savings on the X-300 compared to the studied aircraft.
- By having the engines on top of the fuselage, there is no noise generated by the interaction between engine exhaust flow and the trailing edge of the flaps. Additionally, since the engines are mounted at the rear of the fuselage (rather than close to the wing similar to the aircraft from the studies), there is also no noise generated by the interaction between engine exhaust flow and the upper side of the fuselage.
- The vertical stabilizers also provide lateral shielding of the aircraft noise, something not present on the aircraft from the studies.

6.4.4. Final Noise Level

With a baseline noise level of EPNdB, and a noise reduction of $10\,\mathrm{EPNdB}$ brought about by engine noise shielding, the final cumulative EPNL of the X-300 is $254.3\,\mathrm{dB}$. This is $4.2\,\mathrm{EPNdB}$ lower than the a320neo, which corresponds to a noise reduction of $25.3\,\%$. Furthermore, the margin to the Chapter 13 cumulative EPNL limit (limits were reported in Table 6.7) is $34.0\,\mathrm{EPNdB}$. There is scope for further noise reduction with more advanced landing gear fairings and flap designs, and this can be investigated in a future design phase.

6.5. Sensitivity Analysis

In this section, the sensitivity analysis conducted for the model is discussed. For the sensitivity analysis, a Monte-Carlo simulation was performed for selected parameters of the aircraft and their effect on the Operating Empty Weight was assessed.

Monte-Carlo Simulation

A Monte-Carlo simulation was conducted to analyse the potential sensitivity of the design to changing key parameters. In this, an aircraft parameter is varied between a certain interval by multiplying it with a randomly generated factor. This allows for a high number of runs (up to 1000) which can give a better view of any inconsistencies in the code at any point. A particular distribution method was created to get the factor, for which a peak value (currently estimated value), a minimum value and a maximum value would be defined a priori. These minimum and maximum values define approximately a $95\,\%$ confidence interval. This means that $95\,\%$ of the parameters will be varied between the upper and lower bounds which allows the introduction of a slight bias towards a higher value. This was done because the aircraft parameters such as weight or wing area are expected to increase in later stages of design, therefore it is possible to analyse from the presented graphs whether a specific value for the parameter that could affect the mass drastically is likely or not to be chosen.

An example distribution can be seen in Figure 6.5 where the mean is 200, the upper bound is 250 and the lower bound is 190. The bias towards values higher than 200 is visible, as well as cases where the outcome is outside the $95\,\%$ interval. This logic is used for the rest of the sensitivity analysis.

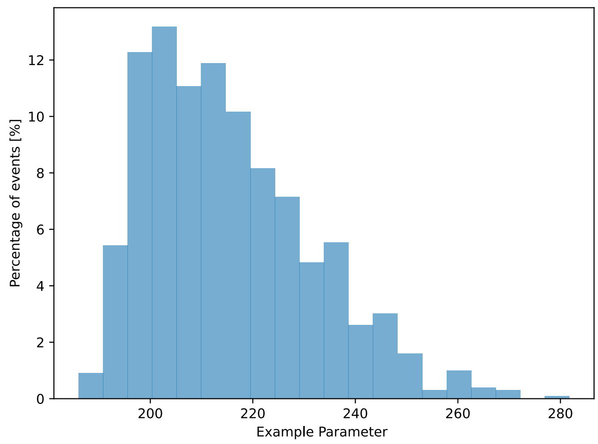

Figure 6.5: Example of the distributed method applied with a peak of 200, and 95% confidence interval within 190 and 250.

Setup and Results

The parameters which were analysed were the wing area, thickness-to-chord ratio of the wing and the position of the wing along the fuselage. For each parameter, 1000 samples were run with individually defined means and confidence intervals. These values can be found in Table 6.11.

Table 6.11: List of parameters analysed in sensitivity analysis.

Parameter	Mean	Lower bound	Upper bound
Wing Area $[m^2]$	224.8	210	250
Thickness-to-chord ratio $(\frac{t}{C})$ [%]	18	12	24
Position of wing along the fuselage (x_{LEMAC}) [m]	32.5	30	35

This sensitivity analysis aims to see the effect of changing the parameters in Table 6.11 on the Operating Empty Mass (OEM) of X-300. The reason the OEM was chosen as an output of this analysis is that it is directly related to the aircraft cost as seen in Chapter 11. Additionally, the Maximum Takeoff Mass(MTOM) is directly proportional to the OEM which in turn is related to the total fuel consumption. A higher OEM leads to a higher MTOM which leads to a higher fuel consumption. The CO_2 and NO_x emissions are directly related to fuel consumption, so a higher fuel consumption leads to higher emissions.

In Figure 6.6, one can analyse the change in OEM with increasing Wing Area. As expected, this will result in a heavier aircraft. Nevertheless, the difference within the $95\,\%$ confidence interval is not very substantial, therefore it can be concluded that the design outcome is not very sensitive to the wing area. It should be noted however that there is a high likelihood the wing area can increase the OEM by approximately $300\,\mathrm{kg}$. Additionally, the computation of the OEM fails when the wing area falls beyond $245\,\mathrm{m}^2$, likely due to code inconsistencies.

The sensitivity analysis for the positioning of the Leading Edge Mean Aerodynamic Chord (LEMAC) can be observed in Figure 6.7. As can be deduced from the graph, it might be beneficial to shift the wing further back, so that the Operating Empty Weight can reduce. Moreover, in this situation, the OEM is relatively sensitive to a difference in the positioning of the LEMAC. Besides this, it appears that for values of x_{LEMAC} bellow $31.4\,\mathrm{m}$, some inconsistencies in the code exist, resulting in unexpected values for the OEM.

Figure 6.8 shows the results of the sensitivity analysis when the thickness-to-chord ratio of the wing is varied. It can be seen that the code is very sensitive to this parameter and the OEM values fluctuate greatly. The values seem to be stable after a value of $0.16\,\%$ and show a decreasing trend. It can be concluded that the code is very sensitive to the thickness-to-chord ratio and it is therefore recommended to modify the program.

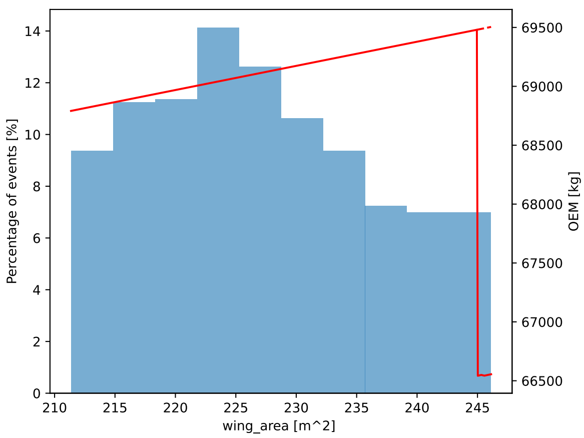

Figure 6.6: Sensitivity analysis on Wing Area (S); solid curve depicts the OEM depending on wing area; intermittent curve represents expected behaviour.

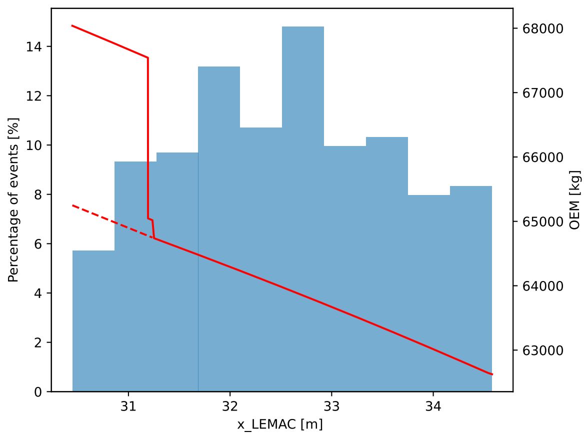

Figure 6.7: Sensitivity analysis on position of the LEMAC (x_{LEMAC}); solid curve depicts the OEM depending on x_{LEMAC}; intermittent curve represents expected behaviour.

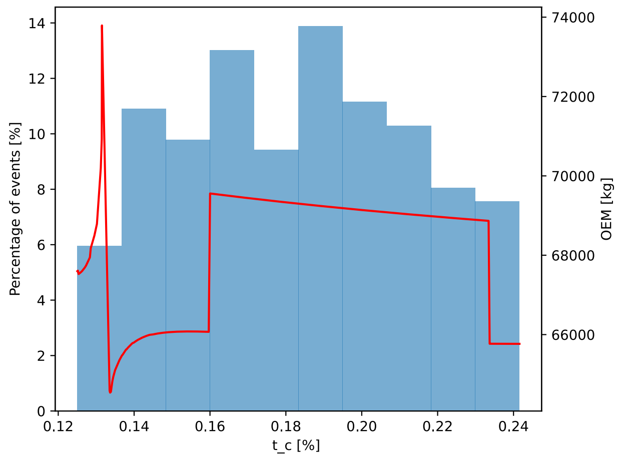

Figure 6.8: Sensitivity analysis on thickness to chord ratio (t/c); solid curve depicts the OEM depending on t/c.

7 Final Design Specification

In this chapter, the final design will be presented, which will serve as the basis for the analysis presented in the upcoming chapters. In Section 7.1 the internal configuration will be shown with values, followed by the external layout in Section 7.2. Section 7.2 also summarises the design specifications and it includes a technical drawing.

7.1. Internal Configuration

In Figure 7.1 the cross-section of the fuselage of the EcoFlyer is depicted. All internal dimensions are also displayed in Table 7.1. The aircraft has a single aisle with 6 seats abreast, using a seat width of $17\,\mathrm{in}$, aisle width of $18\,\mathrm{in}$, armrest width of $2\,\mathrm{in}$ and $1\,\mathrm{in}$ clearance on both sides. Combining this with a shoulder height of $50\,\mathrm{in}$, headroom of $65\,\mathrm{in}$, and an aisle height of $80\,\mathrm{in}$. The cross-section of the fuselage was such designed that it could accommodate 11 of the LD3-45W containers, which are widely used on the A320 model.

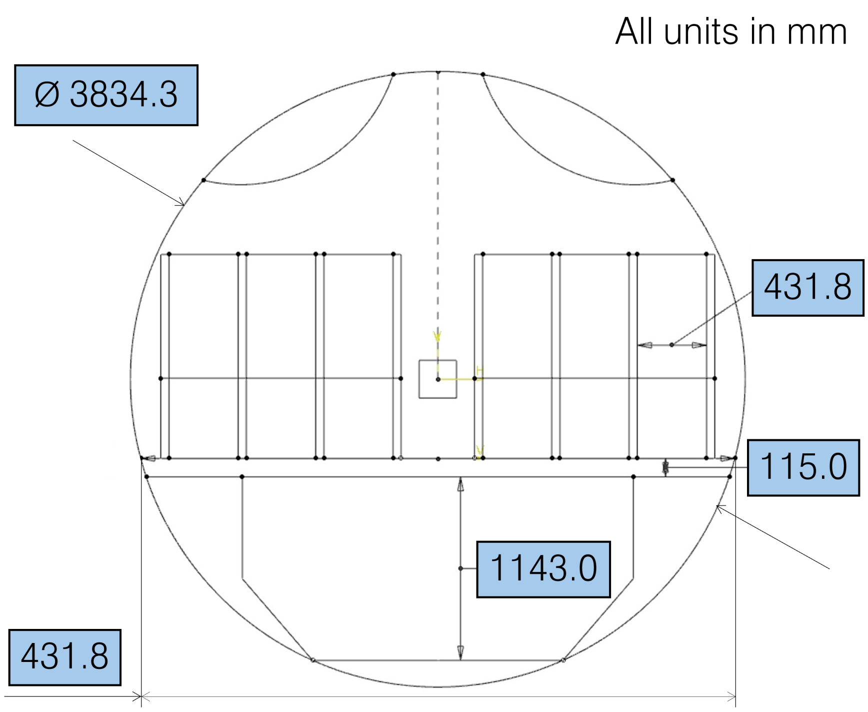

Figure 7.1: Internal dimensions of cabin and cargo bay.

In Figure 7.2 a 3D view of the internal layout of the aircraft is given. The seat pitch is $28\,\mathrm{in}$, resulting in 55 rows of seats in a single class high-density configuration (330 PAX). Next to that the cabin includes 6 toilets (orange) and 2 galleys (yellow). In Figure 7.3 a top view is presented.

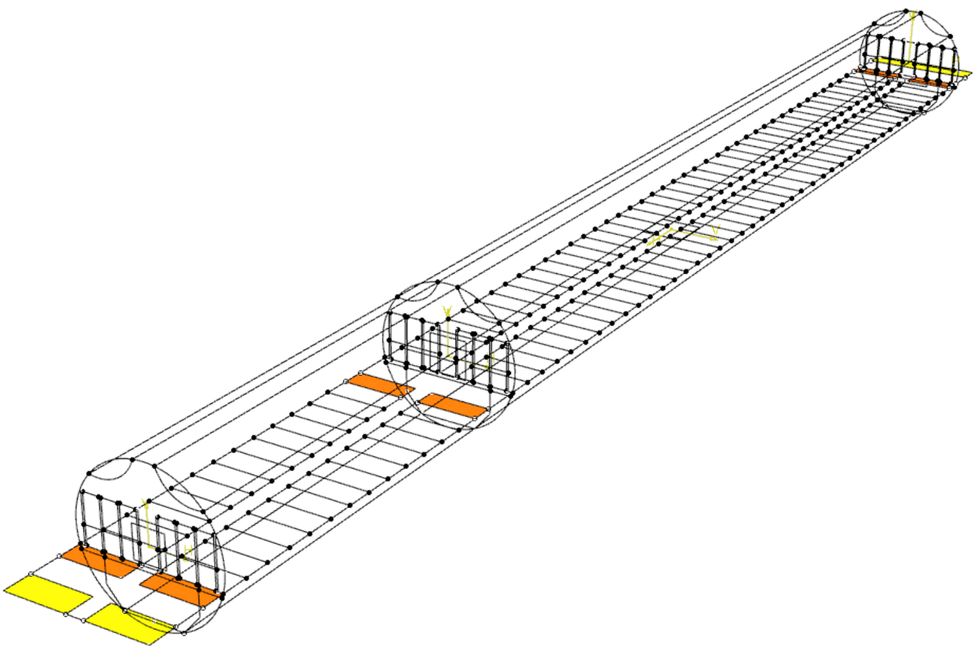

Figure 7.2: 3D view of cabin and cargo bay.

Table 7.1: Summary of internal dimensions.

(a) General aircraft parameters.

Parameter	Value	Unit
Pilots	2	-
Cabin Crew	8	-
PAX	330	-
Seats Abreast	6	-
Container Type	LD3-45W	-
Number of Containers	11	-
Number of Toilets	6	-
Number of Galleys	2	-
Number of Rows	55	-

(b) Internal dimensions.

Parameter	Value	Unit
Seat Width	0.431	m
Shoulder Height	1.27	m
Headroom Height	1.65	m
Aisle Height	2.03	m
Inner Fuselage Diameter	3.8	m
floor Thickness	0.115	m
Floor Width	3.76	m
Type A aisle	1.07	m
Type B aisle	0.812	m
Toilet Width	0.609	m
Galley Width	0.762	m

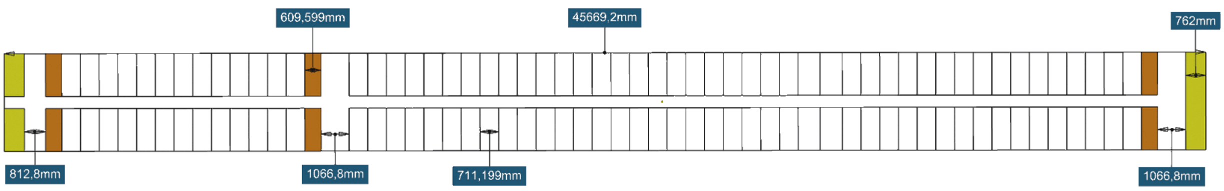

Figure 7.3: Internal top view of floor plan of the cabin.

7.2. External Configuration

Regarding the exterior of the fuselage, the X-300 has an additional type A exit, positioned at a quarter of the fuselage. This would be the main boarding door if single-door boarding is assumed. Next to that, there is a front type B exit and aft type A exit. Next to that every emergency exits also includes a emergency slide. There are two additional type 3 exits positioned over the wing. These exits are sufficient to comply with CS-25 and should improve boarding times. Figure 7.4 displays the outer geometry of the aircraft, with Table 7.2 showing the outer parameters.

Table 7.2: Overview of Design Parameters for the X-300 EcoFlyer.

Parameter	Value	Unit
Fuselage		
Fuselage Length	54.9	m
Wing Mounting	low wing	-
Fuselage Outer Diameter	4.09	m
Type A Exit	4	-
Type B Exit	2	-
Type III Exit	4	-
Main Wing		
Surface Area	225	m^2
Quarter Chord Sweep	0	deg
Span	47.4	m
Root Chord Length	6.8	m
Tip Chord Length	2.7	m
Dihedral	5	deg
Aerofoil	NACA 2412	–
x_{lemac}	32.5	m
Vertical Stabiliser		
Surface Area	19.8	m^2
Leading Edge Sweep	2.45	deg
Span	5.4	m
Root Chord Length	4.8	m
Tip Chord Length	2.4	m

Parameter	Value	Unit
Undercarriage		
Strut Height LG	1.5	m
CoG Offset Nose gear	27.5	m
CoG Offset Main Gear	5.6	m
Wheel Diameter Nose	0.762	m
Wheel Diameter Main	1.27	m
Propulsion		
Number of Engines	2	-
Engine Type	Turbofan	–
Engine Diameter	3	m
Engine Offset	1	m
Engine Mass	7853	kg
Horizontal Stabiliser		
Surface Area	87.6	m^2
Quarter Chord Sweep	20	deg
Span	16.2	m
Root Chord Length	7.2	m
Tip Chord Length	3.6	m
Aerofoil	NACA 0012	–
Stability Margin	5%	–

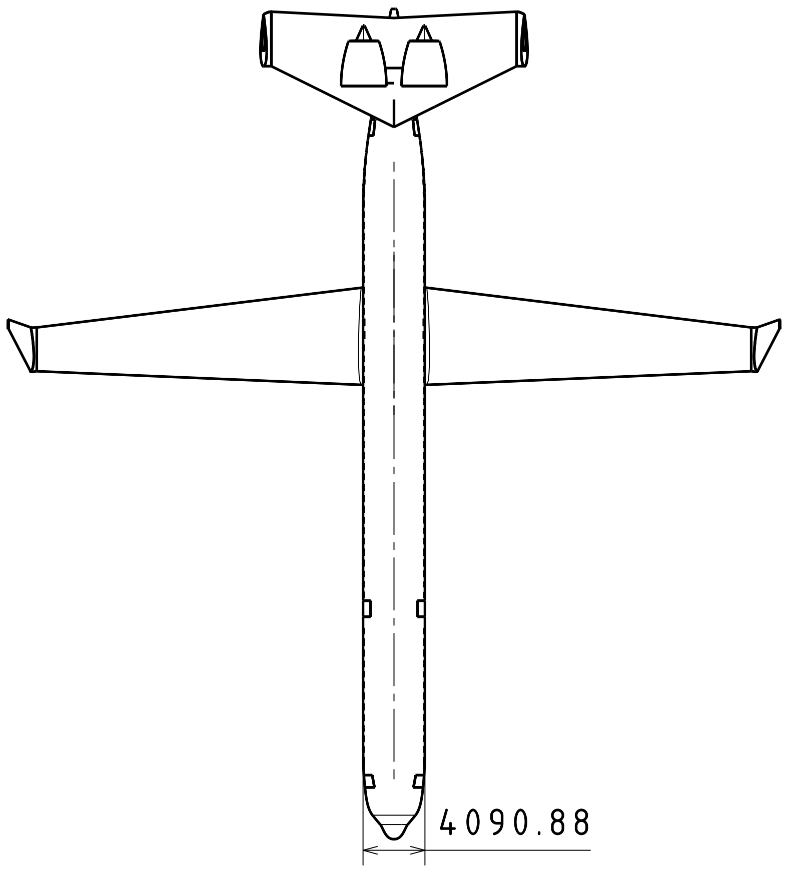

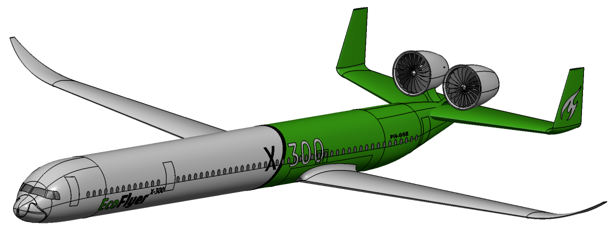

Item No.	Quantity	Name
1	2	Set of Type III Over-Wing Emergency Exits
2	2	Set of Type A Doors
3	1	Set of Type B Doors
4	1	Set of Water Injected Turbofan Engines

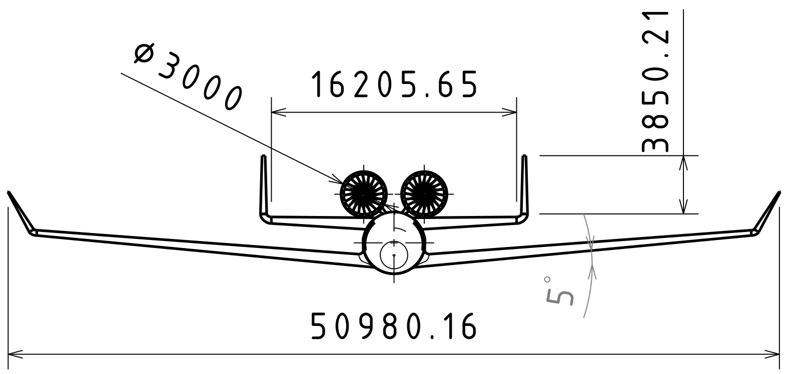

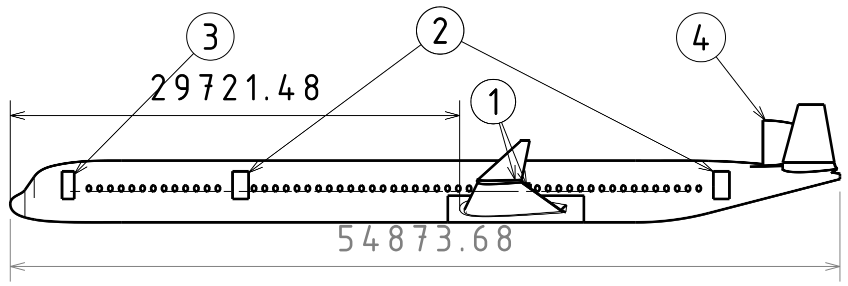

DRAWN BY Bram Verweij	DATE 25-6-2024	Description: A three view drawing of the X-300
CHECKED BY Jakub Bartmański	DATE 25-6-2024	SIZE A3 · Title DSE Assembly · REV 1.A
DESIGNED BY DSE Group 29	DATE 25-6-2024	SCALE 1:500 · WEIGHT(kg) 63926 · SHEET 1/1

TU Delft

8
Manufacturing, Assembly, and Integration Plan

The purpose of this chapter is to provide a clear outline of the activities that are performed to construct the aircraft and its constituent parts. A time ordered process of the activities will be explained and visually displayed in a manufacturing and assembly timeline. In addition to this, information regarding the quality and inventory control to be conducted will be provided.

8.1. Manufacturing, Assembly and Integration Timeline

The figure below shows the general timeline of the activities that are performed to produce the aircraft. Additionally, a number of various aircraft parts and subsystems which are constructed in each process are also indicated. The aircraft production is estimated to begin in 2034. The aircraft parts are manufactured in batches whereas the assembly of the aircraft is conducted using the line production process, which would allow for a production of at least 625 units.

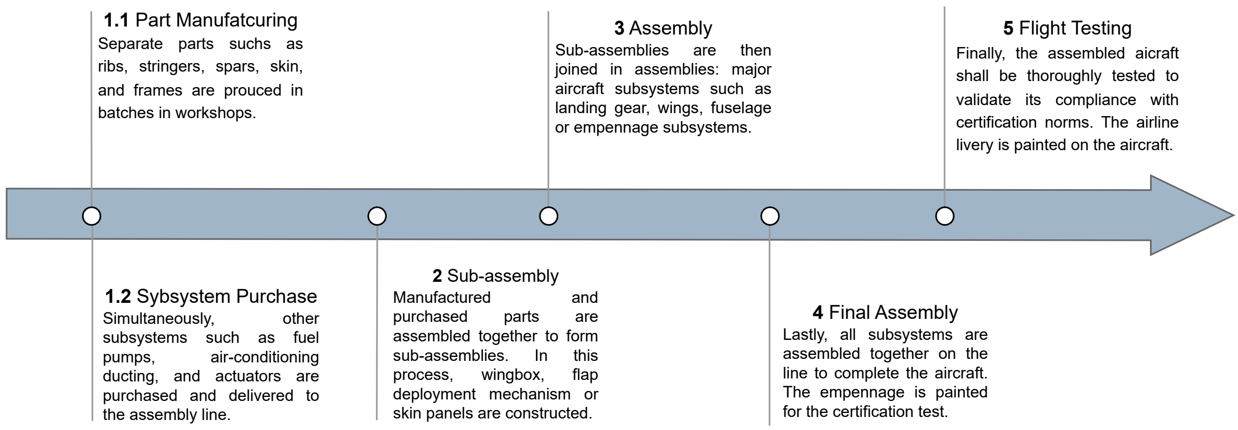

Figure 8.1: Figure showing the time ordered process of constructing the aircraft.

Initially, individual parts are manufactured in parallel to the purchasing of certain equipment and subsystems needed for the aircraft. Parts which are initially manufactured include important structural components such as stringers and skins, as can be seen in the diagram. Due to the fact that the wing, fuselage and tail of the aircraft involve structural elements such as stringers, different sizes and types will need to be manufactured depending on where in the aircraft they are utilised. Many various methods can be used to manufacture the aircraft parts. These include methods such as sheet metal forming processes, for skins and stringers for example, and machining to possibly refine and remove chips from the parts.

Running in parallel to the manufacturing of specific aircraft parts, various equipment and subsystems not made by the manufacturer need to be ordered. This involves ordering electrical equipment to facilitate the functionality of systems such as:

- Avionics
- Auxiliary fuel pump
- Flight control system
- Engine starter motor

Following from this, additional equipment including interior furnishing (carpets and interior panels), flight control equipment and fasteners such as bolts and rivets need to be ordered. Lastly, the water-injected turbofan (WIT) engines which will provide propulsion for the aircraft, are ordered.

After the aircraft parts are manufactured and the subsystems and equipment have been received, the sub-assembly stage can then commence. This involves connecting the manufactured and ordered parts to form larger structures. Structures such as the wingbox, skin panels and actuator subsystems are constructed during this sub-assembly stage. These sub-assemblies can then be integrated together to form the larger structures. The assembly of different systems and structures are categorised into mounting and manufacturing divisions. The manufacturing divisions are divisions where components need to be replaced and so they are assembled with removable joints. The mounting division uses permanent joints as these assemblies do not need to be disconnected in regards to maintenance and inspection.

The smaller sub-assemblies are then used to form the larger systems of the aircraft. This involves assembling the landing gear as a whole, the different wing sections, fuselage sections and the empennage. Once this phase is complete, The final stage of assembly can begin. The final assembly stage then consists of assembling the previously mentioned larger systems of the aircraft together to form the final, complete aircraft. Once the construction of the aircraft is complete, it can enter the final testing phase where the aircraft is put through various tests to determine if it functions as intended and to ensure all design and mission requirements are met. This is also done to certify the aircraft such that it can enter the market.

8.2. Inventory and Quality Control

The various parts of the aircraft will be manufactured in batches. This means that all specific parts are made in one go in dedicated workshops, which are located outside of the assembly lines. The batches are then stored in the warehouse, where it acts as a buffer, supplying the desired parts to the assembly line. A reorder point is established to ensure that the stock available in the warehouse does not decrease below a point to ensure there is not a supply shortage. The figure below indicates how the stock varies with time as a result of the reorder point. The blue arrow indicates the time it takes for the new stock to be supplied while N_{max} is the maximum capacity and N_{min} is the capacity at which a new order needs to be placed.

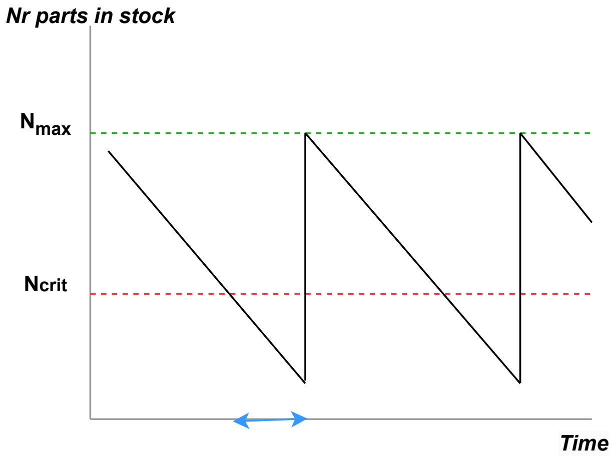

Figure 8.2: Figure showing the variation of the warehouse capacity with time.

In addition to this, the size of the batches is determined such that a sufficient amount of parts can be supplied to the assembly line each time so that the assembly process is not delayed. The parameters that primarily determine the size include the delivery interval, the number of identical parts being used in the aircraft as well as the size and price of the product.

In addition to the methods used to monitor and control the inventory, quality tests need to be performed on the manufactured parts. This is to ensure that there are no damaged or defective parts that could reduce the functional capabilities of the aircraft. Non-destructive methods are used to assess the quality of the parts. This includes methods such as:

- Visual inspection
- Ultrasonic measurements
- Thermography
- Acoustic emission analysis
- Utilising fluorescent penetrant
- Utilising magnetic ink

The next chapter will provide information on the use and support of the aircraft as a whole. Concepts involving the maintenance and ground support as well as the intended operational use of the aircraft will be discussed.

9 Sustainable Development Strategy

In this chapter the sustainability impact of the X-300 EcoFlyer is presented including potential savings due to SAF usage. Next, the forecasted development, availability, price and equivalent life-cycle CO_2 emissions of different SAF types are assessed. Leading up on this, the preferable SAF type for airports is discussed. Lastly, the potential life-cycle CO_2 reduction is calculated.

9.1. X-300 Sustainability Impact

The major sustainability goals of the X-300 are listed below [2]

- **REQ-STK-12** The aircraft's operational CO_2 emissions per passenger per kilometer shall be $25\,\%$ lower than those of the Airbus A320neo.
- **REQ-STK-13** The aircraft's operational NO_x per passenger per kilometer emissions shall be $50\,\%$ lower than that of the Airbus A320neo.
- **REQ-STK-14** The cumulative effective perceived noise level (EPNL) of the aircraft shall be $20\,\%$ lower than that of the Airbus A320neo.

The resulting savings of the X-300 are shown in Table 9.1. Additionally NO_x emissions not only pollute the air around airports, at higher atmosphere NO_x particles can contribute to global warming. The Global Warming Potential (GWP) of a gas can be expressed in iequivalent grams of CO_2 GWP per gram, $CO_{2,eq}$. The $CO_{2,eq}$ GWP of NO_x for a time horizon of 20 years is 31.5 [52]. Combining the NO_x / ASK times its global warming potential and the CO_2 / ASK yields an GWP $CO_{2,eq}$ / ASK parameter showing the contribution of the aircraft to global warming. This GWP parameter is included in Table 9.1.

Table 9.1: Major sustainability achievements of the X-300.

	X-300	A320Neo	Reduction to the A320Neo	Target Reduction
CO_2 $\mathrm{g/ASK}$	71.5	98.9 [1]	$27.7\,\%$	$25\,\%$
NO_x $\mathrm{g/ASK}$	0.020	0.208	$90.5\,\%$	$50\,\%$
GWP $CO_{2,eq}$ $\mathrm{g/ASK}$	72.2	105.5	$31.6\,\%$	-
Cumulative EPNL dB	254.3	258.6	$25.3\,\%$	$20\,\%$

Obtaining these savings and prioritising sustainability within the design process was achieved by various measures. Specific sustainability criteria for the trade-offs have been implemented. Extensive research on design options to reduce the environmental impact of the X-300 has been carried out. At all times the impact of design choices on the environment were an important factor in the decision making.

[1] value for modeled A320Neo for better comparison with the modeled X-300

The adoption of the X-300 by airlines to replace their long-range wide-body aircraft on busy short-haul routes will reduce the CO_2 emissions per ASK on these routes. This contributes to reducing the carbon footprint of the aviation sector. Furthermore the local air quality around those airports would ameliorate due to the lower NO_x emissions. On top of this the aircraft is quieter than an A320Neo reducing the negative impact of local communities in the vicinity of airports. The X-300 EcoFlyer is a more sustainable replacement for the current aircraft flying these busy short-haul routes.

9.2. Contrail & Cirrus Cloud Formation

Soot and sulfate nuclei emitted by aircraft engines can lead to contrail cloud formation in the short term (hours). The soot and sulfate nuclei can linger in the atmosphere for days and induce the formation of cirrus clouds [53]. These clouds contribute due to their radiative forcing to global warming. WIT engines have the potential to pass the complete exhaust flow through a soot filter and thereby lower the cloud formation. Subsequently, the X-300 would have a lower contribution to global warming.

However, several issues have impeded a more thorough analysis on this effect. The climate impact of these clouds is difficult to assess. The formation of contrails into cirrus clouds is difficult to model [54]. Modeling this requires more insight on soot and sulfate nuclei present in the exhaust than the development state of the WIT engines can currently provide.

The possibly employed soot filters in the WIT engine will reduce contrail formations. Also flying at lower altitude, as the X-300 is optimised for, can lower cloud formations. It is therefore expected that the global warming per ASK due to cloud formation by the X-300 will be lower than it is for current aircraft. However quantifying this effect is not carried out in this report.

9.3. SAF Adoption Goals

Worldwide there are numerous organisations that are targeting future SAF adoption goals. Several of those are listed below. In the case of a full road-map of SAF adoption, specifically the targets around the entry into service year of the aircraft of 2035 are mentioned. Because most targets are stated for 2030 the adoption targets for this year are considered. The 5 more years until the aircraft enters service will be considered as a safety margin.

- **Japan:** ANA and Japan Airlines co-signed the 2030 Ambition Statement to substitute 10% of aviation fuel by SAF by 2030 [2].
- **Europe:** The European Union requires airports to supply 6% SAF blend by 2030 and 20% by 2035 [3].
- **China:** According to companies that prepare SAF production in China, a mandate requiring a SAF blend of 2% to 5% is expected to be unveiled this year by China. [4].
- **Australia:** Qantas targets a SAF adoption of 10% by 2030.[5]
- **Singapore:** Singapore Airlines plans to implement a SAF adoption between of 3% to 5% [6]
- **United Kingdom:** The United Kingdom targets at least a 10% SAF blend by 2030. [7]

[2] https://www.anahd.co.jp/group/en/pr/pdf/20211008-1-1.pdf - 2024-06-13

[3] https://centreforaviation.com/analysis/reports/eu-parliament-approves-sustainable-aviation-fuel-mandate-up-from-2-in-2025-to-70-in-2050-661409 - 2024-06-13

[4] https://www.reuters.com/sustainability/climate-energy/chinese-firms-invest-green-jet-fuel-anticipating-blending-rule-2024-05-16/ - 2024-06-13

[5] https://www.qantas.com/au/en/qantas-group/sustainability/our-planet/sustainable-aviation-fuel.html - 2024-06-13

[6] https://www.hydrocarbonprocessing.com/news/2024/02/asias-saf-projects-and-agreements/ - 2024-06-13

[7] https://assets.publishing.service.gov.uk/media/662938db3b0122a378a7e722/creating-the-UK-saf-mandate-consultation-response.pdf - 2024-06-14

Within the European Union a union wide SAF blend of 6% is targeted. However, no route in the top 60 busiest routes flies to an EU airport. Hence, this is not the major targeted market of the aircraft. Therefore, despite contributing to advancements for SAF adoption in the upcoming years, the EU market is discarded in the SAF availability analysis. Although the United Kingdom has a few (international) flights in the top 60 busiest routes, these are all well outside of the range of the designed aircraft.

domestic Japanese, South Korean, Australian, Chinese and international Singaporean flights make up almost half of the top 60 busiest routes by yearly passengers. The targeted SAF adoptions within each country are shown in Table 9.2.

Table 9.2: Targeted SAF blends by 2030 for different operators and countries.

Country	PAX per year share of 60 busiest routes	Targeted SAF blend by 2030
Japan	$14.74\,\%$	$10\,\%$ (by two major carriers)
South Korea	$7.63\,\%$	- (no concrete target)
Australia	$5.84\,\%$	$10\,\%$ (by major carrier)
China	$14.31\,\%$	$2\,\%$ (predicted, national flights)
Singapore	$5.31\,\%$	$3\,\%$ (all flights)
Total	$48\,\%$	-

Japanese short-haul flights account for $15\,\%$ of the passenger movements for the top 60 busiest routes in the world. The $10\,\%$ SAF adoption target signed by the two major national carriers means that the availability of SAF at major Japanese airports is predicted to be there. The same holds for Australian short-haul flights making up $6\,\%$ of the top 60. With Qantas being committed to $10\,\%$ SAF adoption Australian airports presumably will have infrastructure for SAF as well. The conservatively expected 2030 SAF blends of China and Singapore of $2\,\%$ and

9.4. Economically Efficient SAF

To lower the CO_2 emissions with more expensive SAF the CO_2 reduction per extra invested dollar should be maximized. There are different types of SAF. Fischer-Tropsch (FT), Hydroprocessed Esters and Fatty Acids (HEFA), Alcohol To Jet fuel (AFJ), Hydroprocessed Fermented Sugars (HFS) and Catalytic Hydrothermolysis Jet fuel (CHJ). Their price and LCA CO_2 emissions are shown in Table 9.3.

Table 9.3: CO_2 reduction and price increase for different SAF types, adapted from [55].

Technology	$\$/\mathrm{L}$	Price increase	CO_2 $\mathrm{g/MJ}$	CO_2 reduction	Reduced CO_2 $\mathrm{g/MJ/\$}$
FT	2.08	$320\,\%$	7.8	$92\,\%$	52
HEFA	1.12	$120\,\%$	65	$27\,\%$	39
ATJ	1.69	$240\,\%$	39	$57\,\%$	43
HFS	3.99	$700\,\%$	42	$53\,\%$	14
CHJ	1.30	$160\,\%$	21	$77\,\%$	86
Conventional	0.50	$0\,\%$	89	$0\,\%$	-

As can be seen in Table 9.3 the fuel type that yields the best CO_2 reduction per invested dollar is CHJ. Therefore it is assumed that airports invest in this type of SAF. This fuel has a price of $1.30\,\$/\mathrm{L}$. Another study found a similar average price for multiple feedstock for CHJ, being $1.25\,\$/\mathrm{L}$ [56]. The CHJ SAF is 2.6 times more expensive than conventional jet fuel. If airlines use a $6\,\%$ CHJ SAF blend this results in a fuel price increase of $9.6\,\%$ compared to conventional jet fuel. However, this price increase applies to all flights and airlines operating from this airport and would therefore have a relatively low impact on the competitive position of the airlines within this airport.

9.5. Fuel Life-Cycle Analysis

One of the requirements for the X-300 is that it should reduce CO_2 $\mathrm{g/ASK}$ by $25\,\%$. Thus far in the design process, it was aimed to achieve this reduction purely by performance improvements and excluding fuel life-cycle emissions. The CO_2 reductions including life-cycle emissions in a more realistic use-case will be calculated now. A $6\,\%$ CHJ SAF blend with a $77\,\%$ reduction in equivalent CO_2 emissions is used. This yields a reduction of equivalent life-cycle CO_2 emissions for the aircraft of $4.6\,\%$.

10 Operations and Logistics

This chapter discusses the reliability, availability, maintainability and safety (RAMS) characteristics of the X-300 EcoFlyer. This is explained in Section 10.1. Section 10.2 then provides the operational and logistical concept description of the X-300.

10.1. RAMS Characteristics

This section will provide insight into the reliability, availability, maintainability and safety of the aircraft. Subsection 10.1.1 will characterise the reliability of the aircraft as well as its recently developed new subsystems while Subsection 10.1.3 will discuss how the aircraft is maintained as well as its maintenance schedule. Lastly, Subsection 10.1.4 will provide the safety features and the redundancy philosophy which has been implemented.

10.1.1. Qualitative Reliability

This subsection will discuss the reliability of the X-300 EcoFlyer. The reliability of this aircraft is comparable to that of the Airbus A320neo as there are many similar and conventional subsystems that both aircraft use. However, various new subsystems have been implemented in the design to improve the aircraft's performance and reduce its emissions, as well as to meet requirements. The reliability of these subsystems needs to be assessed in order to determine if they negatively or positively affect the reliability of the X-300 EcoFlyer. The IWETS, ECS and WIT engines are the main subsystems which have been implemented in the design. The reliability of each of these subsystems will be further explained in the following three subsections.

IWETS

As previously discussed, the IWET system is a very new, currently underdeveloped system which enables the aircraft to taxi to the runway electrically. The reliability of this system is comparably lower to the standard taxiing on fuel system due to its underdevelopment and limited research that has been conducted. However, it does not affect the reliability of the taxiing system as a whole. This is because if the IWET system fails, the aircraft can easily switch to taxiing on fuel. An additional factor which decreases the reliability of the IWET system is the fact that it is located on the landing gear. This could result in debris getting caught in the motors, which could therefore disable the functionality of the system.

The system also includes fairings which could aid in preventing debris from entering the motor. However, the fairings may also reduce the airflow into the IWET system. In combination with the heat produced from braking and the reduced airflow, the system may experience temperatures which are too high and could therefore overheat, resulting in a possible failure.

A possible approach to increase the reliability of this subsystem would be to implement monitoring systems in order to monitor the flow of power as well as the applied torque. This would ensure that the provided power and torque do not exceed a certain limit. Furthermore, retractable fairings could be implemented in order to improve the airflow and sufficiently cool the system.

ECS
As explained in Section 5.5, the Environmental Control System is used instead of the bleed air subsystem. In terms of reliability, this has mostly positive effects. This is because the ECS compressors are currently being used in the Boeing 787 aircraft and have not been a cause of any serious incidents so far. On the other hand, due to the lack of a bleed air system, the engines now must be started using electrical motors, which may require large amounts of power. This has been, however, taken into account and a power margin is implemented in all systems.

WIT
Since the propulsive system consists of turbofan engines equipped with the WIT technology, their reliability shall be discussed. By introducing the water injection system, the engines become more complex and include more components, such as water pumps, heat exchangers, water injectors and condensers. This higher complexity may initially lower the reliability of the propulsive system. To circumvent that, a redundancy philosophy is applied as well as predictive maintenance. This is, however, explained in Figure 10.1.4. It is furthermore expected the novel engine concept will be thoroughly certified in the future, so events of begin-of-life failures will not be of any concern. Moreover, the reliability is partially increased due to the repositioning of the bleed air system from the engine to the fuselage as mentioned above, which reduces the effective complexity.

It can be concluded that when compared to the A320neo, the reliability of the X-300 is slightly lower. This stems from the fact that the X-300 possesses newer and underdeveloped systems such as the IWET system and the WIT engines. As these systems are further developed with time, it is expected that the reliability of the X-300 will then be on par with the A320neo.

10.1.2. Quantitative Reliability
This subsection will discuss the reliability of the new systems from a quantitative perspective, where the technology readiness level of each of the three new systems is evaluated. Figure 10.1 shows the different readiness levels, where a TRL of 7-9 is indicative of a reliable system.

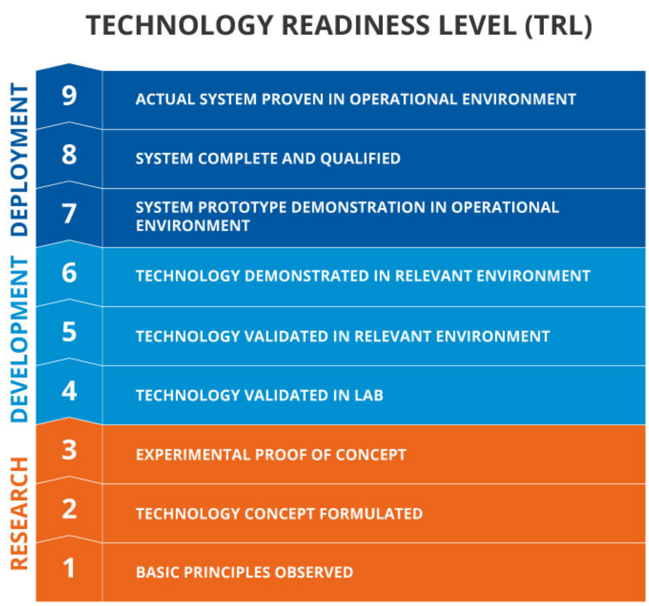

Figure 10.1: Figure showing the technology readiness levels [57].

When analysing the TRL of the WIT engines, various aspects of the engine can be considered to have a relatively high TRL. For example, the fuel system is identical to the fuel system used in current turbofans, indicating that this subsystem has a high TRL. The fuel itself can also be considered to have a high TRL as kerosene and SAF blends are already being used in some aircraft. However, The introduction of new, under-developed components such as the water-injection and heat-recovery systems. These systems still require further development and are not in operational use yet, suggesting an overall TRL of 5 for the WIT engines.

The ECS which has been implemented in the X-300 EcoFlyer, as previously explained, differs from the traditional ECS that uses bleed air and has its own compressor at the inlet. Although contrasting with the traditional ECS, this electronic ECS is already in operational use on the B787. When referring back to Figure 10.1, this indicates that the electronic ECS has a TRL of 9.

In regards to the IWETS, the realisation of such a concept is already possible with current technology. From a technical point of view, the TRL of the IWETS is sufficient and can be given a score of 7. This cannot be higher as this system has not been qualified and put in operational use. However, further improvements of the system are currently being explored, such as improving electrical, structural and aerodynamic characteristics to enhance the taxiing performance it can provide [23]. Based on this, a total TRL of 6 was given for the IWET system.

The table below outlines the TRL of the new systems. As previously mentioned, the aircraft as a whole can be comparable to the A320neo in terms of reliability and has therefore initially been given a TRL level of 9. When taking into account the implementation of the IWETS and WIT engines, these are expected to lower the overall TRL of the aircraft, coming to a final value of level 6.

Table 10.1: Table showing the technology readiness level of the X-300 and its new systems.

System	TRL
IWETS	6
WIT engines	5
ECS	9
X-300 EcoFlyer	**6**

The next section will analyse how the X-300 EcoFlyer fairs with other aircraft regarding maintenance and availability of materials and systems.

10.1.3. Availability and Maintainability

Due to the use of varying materials, fuel types and subsystems compared to conventional aircraft, the availability of these elements needs to be analysed in order to assess whether they can be readily implemented into the X-300 EcoFlyer.

When considering the materials that the aircraft will comprise, all of these materials are commonly used on currently operating aircraft. It can therefore be concluded that the availability of these types of materials will not be an issue when constructing the X-300 EcoFlyer. However, the aircraft will use sustainable aviation fuel as its fuel source. Due to the fact that many current aircraft operate only on kerosene-based fuel, the availability of SAF may be limited as proper supply chains need to be established to supply this fuel to airline companies' aircraft Section 9.3.

When taking into consideration the availability of future technology such as the IWETS and WIT engines, availability may be limited as these systems are still being developed. However, the X-300 EcoFlyer is set to enter the market in 2035. It then becomes apparent that the design concepts may become more available closer to the entry year as they are further developed.

The ECS implemented in the X-300 EcoFlyer is identical to the ECS the Boeing 787 uses. Due to the fact that this system is already implemented in currently operational aircraft, it is expected that the system is sufficiently developed and readily available. From this, it can be concluded that the ECS can be integrated into the design without any significant issues regarding the availability of the system.

Finally, the maintainability of the X-300 shall be discussed. Just as is the case for existing aircraft, the EcoFlyer will be subjected to both expected and unexpected maintenance inspections, which shall be referred to as *checks*. Since the X-300 is in a great part comparable to the baseline A320neo aircraft, only the maintainability of the alternative subsystems is to be covered.

The IWET system maintenance is not expected to be excessively time- or workforce-consuming. This is because it is conveniently accessible and, if properly designed, the disassembly and assembly can be rather straightforward. On the other hand, the WIT engines may pose difficulties in regular maintenance. Their positioning on top of the fuselage makes it challenging for periodic checks. The most time-consuming, heavy check can be however improved in terms of planning by implementing state-of-the-art predictive maintenance schedules, such as the one found in [58]. Lastly, the aircraft is planned to be equipped with an extensive monitoring system, with an emphasis on the WIT engines, which will bring the maintenance classification to expected or at least predictable.

Finally, the ABC check system is to be employed with the schedule as follows [59]:

- **A check:** every 500 flight hours;
- **B check:** every 7 months;
- **C check:** every 20-24 months;
- **D check:** every 6-10 years.

This all is on top of the regular on-ramp maintenance checks such as the pre-flight or service checks. The checks are also incorporated in the post-DSE development logic in Chapter 15.

10.1.4. Safety

This section will identify the potential system failures that can occur during flight operations of the X-300, through the construction of a fault tree. It is presented in Figure 10.2. There are various ways in which many subsystems on the aircraft can fail. As a result, the most crucial and significant failures of the subsystems will be identified. It is important to note the presented tree as seen in Figure 10.2 is not complete, since many more failures can be potentially identified. They have not been given for compactness. From this tree, system failures which will directly influence the safety of the X-300 can be identified. The redundancy philosophy that will be applied to the X-300 to overcome the mentioned system failures will then be discussed.

Safety Critical Functions

From the failure tree, the safety critical systems can then be derived; some of them are listed below:

- Fuel and water pumps;
- Hydraulic system;
- Flight control system;
- Main and landing gear;
- Primary flight Controls;
- Communication system;
- ECS;
- Hydraulic system;
- Primary airframe structure;
- Aircrew life-support system;
- Heat exchangers
- Emergency systems.

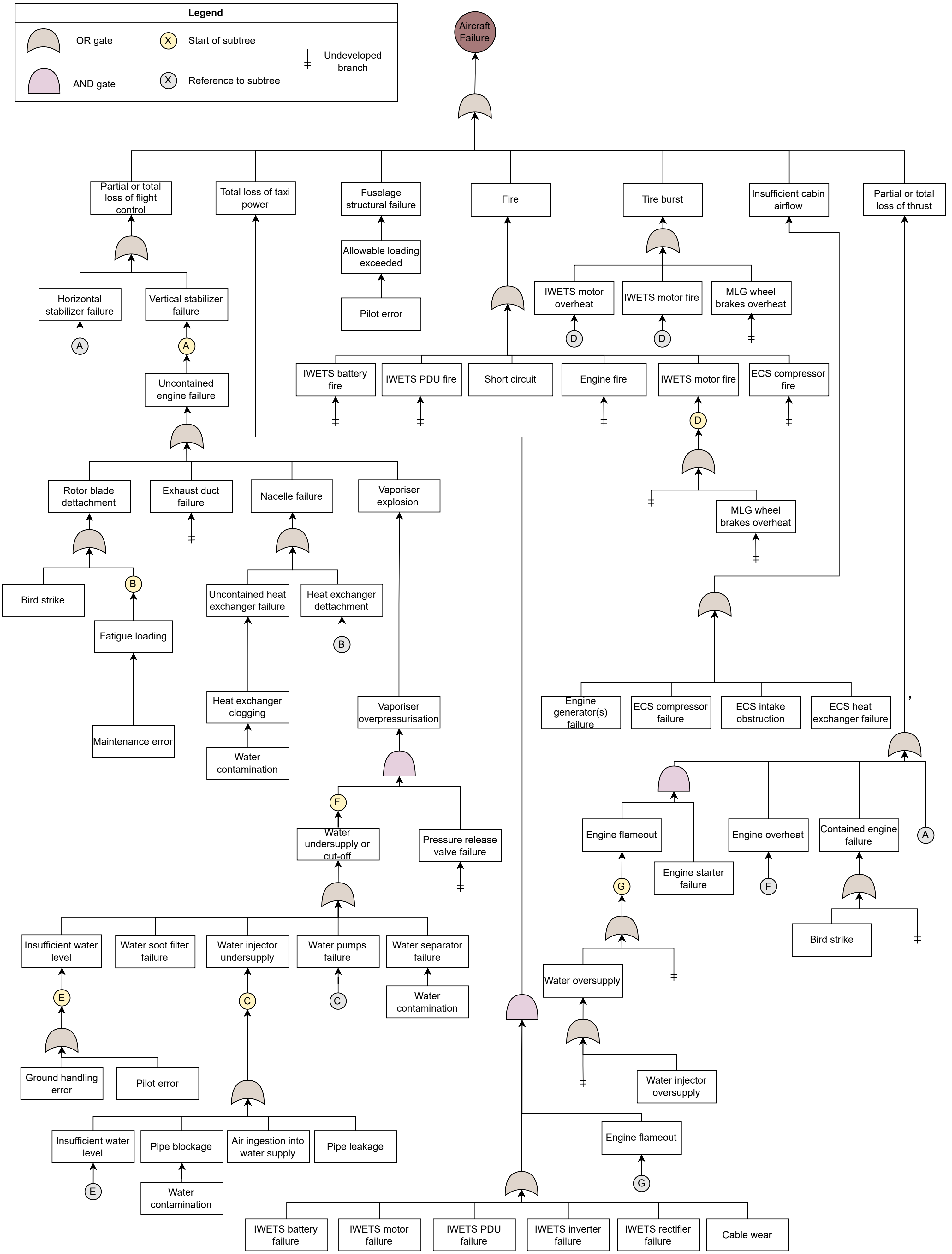

Figure 10.2: Preliminary failure tree (including engine, IWETS, ECS, and fuselage related failures).

Again, other critical subsystems may be identified, and only twelve are given for brevity. These include the most important aircraft subsystems in terms of providing safety-critical functions. For instance, the hydraulic system provides pressure to the brakes, actuators, high-lift devices, rudder, elevator and spoilers. The emergency systems such as emergency slides or functioning emergency doors are also safety-critical. The flight control system includes, for instance, the Primary Flight Computers. ECS and aircrew life-support guarantee, amongst others, cabin pressurisation and oxygen supply.

The failure tree also aids in identifying the safety critical systems stemming from the implementation of nontraditional systems such as the WIT engines. It is clear from the tree that the heat exchangers and water pumps need to be made redundant systems as failure of these systems can lead to an uncontained engine failure. The following section will discuss how redundancy has been applied to components such as the aforementioned water pumps and flight control system computers.

Redundancy Philosophy

The implementation of a redundancy philosophy ensures that the X-300 is still able to operate as intended when experiencing a system failure. With these systems being critical for safety, the redundant systems also oversee each other as well as detect possible failures and isolate these failures. By looking at the previously identified safety-critical functions, it can be determined which systems need to have redundancy. Similar and dissimilar redundancy may both be incorporated into some safety-critical functions.

A very important system which must contain redundancy is the flight control system. As the aircraft is a fly-by-wire aircraft, electrical actuators are used to control the aircraft. As a result, the electrical actuators will be made double redundant, containing three redundant systems. There will also be a simple redundant hydraulic system, consisting of two systems. This system can be used in the case of the failure of all three electronic actuator systems.

Two flight control system (FCS) computers will be implemented. Making this system double redundant will ensure the aircraft is always controllable in case of a system failure. In an effort to further enhance the safety of the aircraft, a similar redundancy philosophy to Airbus in regards to the FCS will be used. Dissimilar redundancy will be applied. Two further backup systems will be available, which aid in isolating the faulty system. These two systems will slightly differ from each other as they will run software made by a different team. They will also run on different processors and be supplied by two different suppliers. The reason for applying dissimilar redundancy to the FCS computers is that systematic errors that occur due to a common malfunction can then be nullified.

As previously mentioned in Subsection 10.1.1, due to the higher complexity of the WIT engines, redundancy will be applied to some of the components the engine comprises. The fuel pumps will be made into a simple dissimilar redundant system in a parallel configuration. The two sets of fuel pumps will be supplied by different suppliers and engineered by different groups once again. This will ensure that the engines will remain fully operative without any issues in the case of a failure of the first set of fuel pumps. This will include, Additionally, two sets of water pump systems are implemented in the WIT engine. The secondary system not only serves as a backup system but also monitors the functionality of the primary system. This will ensure that over-pressurisation will not occur, thereby preventing any possible explosions.

Another safety-critical system that was identified is the hydraulics of the aircraft which account for the functionality of many systems such as brakes, landing gear and flap deployment. The hydraulic system will be made a double redundant system, ensuring that all systems relying on hydraulics can be safely operated in the case of one or even two hydraulic system failures.

As previously mentioned in Subsection 10.1.1, due to the higher complexity of the WIT engines, redundancy will be applied to some of the components the engine comprises. This will include, for example, having two sets of water pumps in the WIT engine in which the secondary system not only serves as a backup system but also monitors the functionality of the primary system.

10.2. Operations and Logistic Concept Description

This section presents the refined operational analysis. In Subsection 10.2.1 an update for the concept of operations diagram will be provided. Subsection 10.2.2 describes what effect the chosen subsystems have on the day-to-day operations of the X-300.

10.2.1. Concept of Operations

Figure 10.3 provides the updated concept of the operations diagram. In the upper part, the nominal flight mission is described with all aspects of the operation. It is an update of the diagram presented in the midterm report [3] as the design is finalised. In the diagram, the interactions between the aircraft and external parties (airport, ATC, airline) are depicted throughout the operation in blue. The biggest changes are related to the IWET system and maintenance operations. The addition of maintenance considerations (detailed flow diagram at the bottom) is due to including some advanced subsystems in the design that can potentially make the process more complex. This has already been discussed in the RAMS characteristics (Section 10.1).

10.2.2. Operational and Logistic Considerations

The design of the EcoFlyer can cause some deviations regarding the day-to-day operations of the aircraft, compared to the current aircraft operations. In the following sections, the most severe deviations will be elaborated on, including the change in taxi and engine start-up operations, as well as the turn-around process. Effects of another major deviation which is the use of SAF on airport operations and logistics have already been discussed in Section 9.3.

IWET system

The IWET system, introduced in Section 5.4, causes severe deviations from the day-to-day aircraft operations. The biggest advantage is the fact that the engines are not started at pushback, and instead, the IWET system is turned on. As seen in Figure 10.3, the start-up of the engines is done prior to take-off. As the engines still need time to warm up, this process is started simultaneously with the taxi phase to minimize ground manoeuvring time.

The same applies to the process after landing. Immediately after landing, the engines are turned off, and the IWET system is used to taxi the aircraft back to the gate. A similar principle for electric taxi is already in practice with certain Taxi bots.[1] The only difference here is that, with the Taxibot, the mechanism that propels the aircraft is not inside the aircraft itself but involves an external push-and-pull vehicle. Also, with the TaxiBot the aircraft is being brought as close to the runway as possible, where the engines are started. The advantage of the IWET system is that no external vehicle is necessary.

The process of the aircraft 'powering back' from the gate using the IWET system might be more difficult to implement from an operational perspective. In itself, an aircraft using its own propulsion to manoeuvre back from the gate is not new. As an example in the 1980's this was actually more common. This was mostly the case for aircraft with fuselage-mounted engines, as one of the severe risks is that debris is sucked into the engine. Another downside is the fact that reversing near a gate is extremely loud and consumes fuel [2]. On the contrary, these described downsides are not applicable to the IWET system as it is electric, and not using the engines directly. The risk for the aircraft to tip-back, when braking under reversing, however, is a significant risk. Also, support for the pilots would be necessary to 'reverse'. This could be resolved by ground personnel 'guiding' the pilots. Next to that, most airports do not allow for powering back from the gate, and a future change

[1] https://taxibot-international.com
[2] https://nci.edu/2022/08/22/how-do-airplanes-go-in-reverse.

in regulations, as well as further research into the risks, is necessary to make use of this advantage of the IWET system. In the meantime, the X-300 fits in current operations with a normal pushback truck required.

Turn-around time

Due to the choice of a single-aisle cabin configuration, the boarding and as a result turnaround times can be negatively affected. From an initial market analysis, a mission requirement of an average turnaround time of less than $60\,\mathrm{min}$ (**REQ-MIS-033**) was derived. In the midterm trade-off phase, the maximum turnaround time for a $100\,\%$ load factor scenario resulted in an estimated $62\,\mathrm{min}$ of turnaround and was marked under the category of "Correctable deficiencies" [3]. However, as the requirement states an average time, a more common occurring scenario of $85\,\%$ load factor is assumed in order to assess the feasibility. The study based on a simulating model yields a time of $51\,\mathrm{min}$ in this case, which takes into account the reduction that is achieved by the use of an enlarged door (-$4\,\mathrm{min}$ due to Type A quarter-door) [60]. This then complies with the introduced market requirement.

However, even with the requirement met, the turnaround is relatively longer than the market average and potentially worse than what the customers would expect. Especially for low-cost operations, this time is critical. For that, a number of potential solutions can be implemented by the airlines. The main effective modification is the use of 2- or even 3-door boarding. The X-300 is designed to have a quarter-door that is sized as a full boarding door. For 2-door boarding, the quarter and rear doors can be used as the front one has a smaller size, but in the case of 3-door boarding the front one can be used as well. This as the study suggests, has the potential to lower the boarding and turnaround times by around $20\,\%$ when using a dual door boarding ($-13\,\mathrm{min}$) [60]. Nonetheless, since multiple-door boarding is not the default procedure in most airports, these changes are not taken into account for requirement compliance; they only serve as a suggestion in case the customer needs to lower the boarding times for their operations. Another possible modification is making the aisle wider. The seat width is currently designed with $1\,\mathrm{in}$ margin from minimum, so if needed, this can be used for increasing the aisle width instead, which will potentially result in another $4\,\%$ reduction of turnaround time [60].

A remark should be made on the refuelling process. This is considered to be performed in parallel to other boarding activities, as regulations for SAF and Jet-A kerosene allow it [61]. Therefore, the refuelling time does not fall under the critical path of turnaround. However, in case an airline opts not to do this simultaneously, an estimation of refuelling time is obtained. For a maximum range mission, assuming a $15\,\mathrm{kg/s}$ refuelling rate, this time will be $21.4\,\mathrm{min}$. If the airline performs the refuelling completely separately from the boarding, this will account for $25.7\,\%$ of the total turnaround time, also complying with **REQ-SYS-048**.

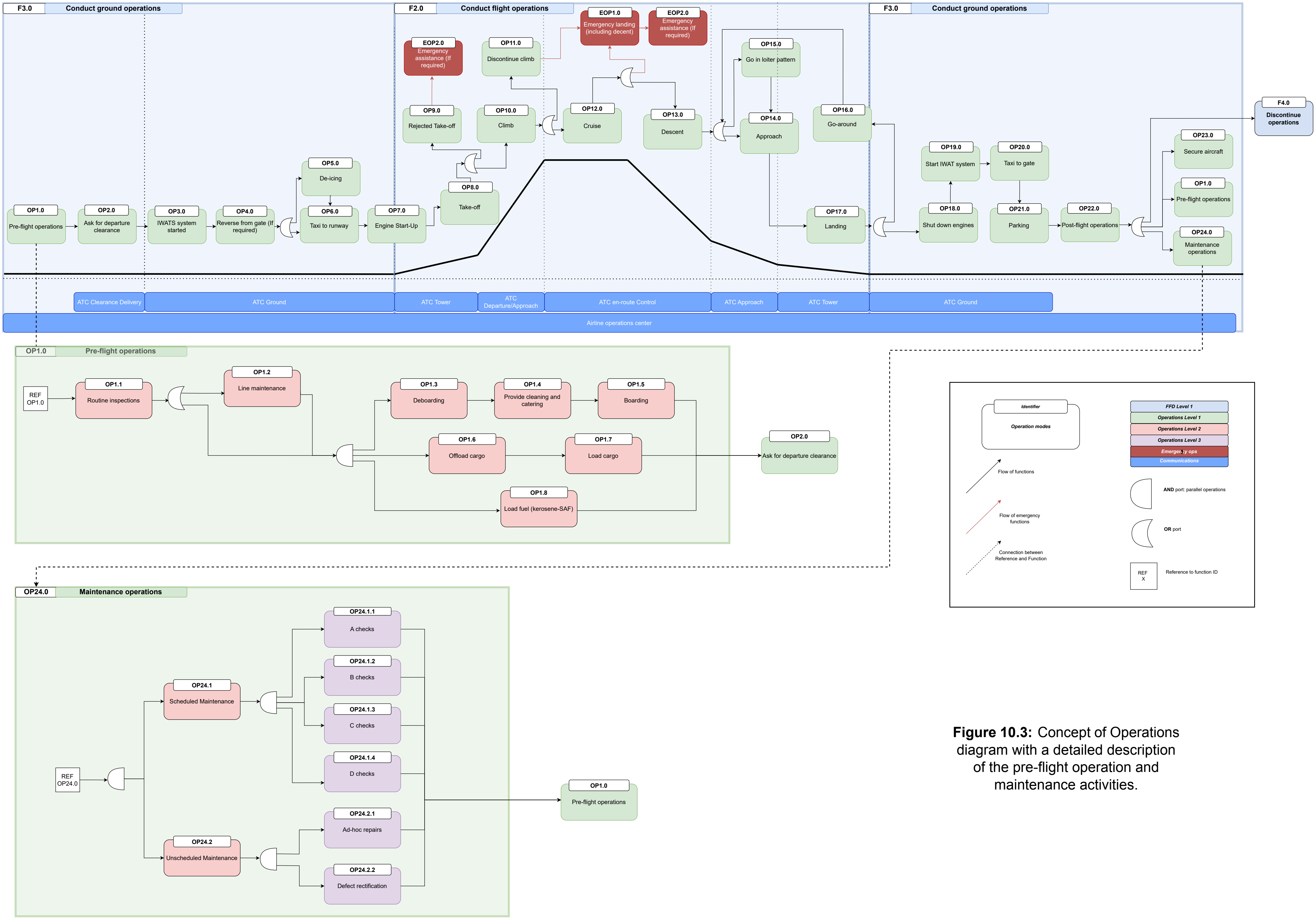

Figure 10.3: Concept of Operations diagram with a detailed description of the pre-flight operation and maintenance activities.

11
Business Case

In this chapter, the business case of the established design will be analysed to investigate the feasibility of the proposed aircraft from the market and financial perspectives, as well as identify the key aspects that may affect these. The market is first defined and the main stakeholders are discussed in Section 11.1. Further, the product's position and its share in the future market are estimated in Section 11.2 to obtain an expected number of aircraft deliveries. Based on this analysis, the production, development and operating costs of the aircraft are computed and pricing for the X-300 is obtained in Section 11.3. Finally, sales and return on investment estimations are provided in Section 11.4.

11.1. Market Analysis

To start the analysis, the targeted market will be discussed and the rationale behind it will be explained. Additionally, the main stakeholders who are involved will be assessed.

11.1.1. Target Market

A key aspect of the current commercial aviation market is that a significant share of growing air transport demand is concentrated on a relatively small number of short-range routes. Regarding the world's top 60 busiest routes, the vast majority of which (with only 3 transatlantic exceptions) are less than $3000\,\mathrm{km}$, thereby generating almost $15\,\%$ of the global air traffic demand (in terms of annual passengers)[1]. These routes are demonstrated in Figure 11.1. This demand, however, is not directly fulfilled by any of the existing aircraft types as can be seen in Figure 11.2.

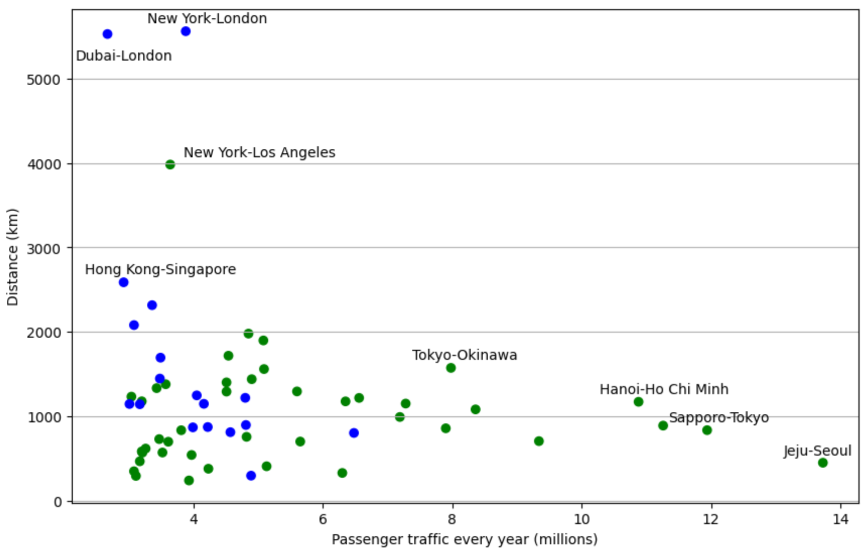

Figure 11.1: Passenger capacity (annual) to range comparison for the world's 60 busiest routes in 2018-2023.

[1] `https://www.oag.com/busiest-routes-world-2023` - 2024-05-06

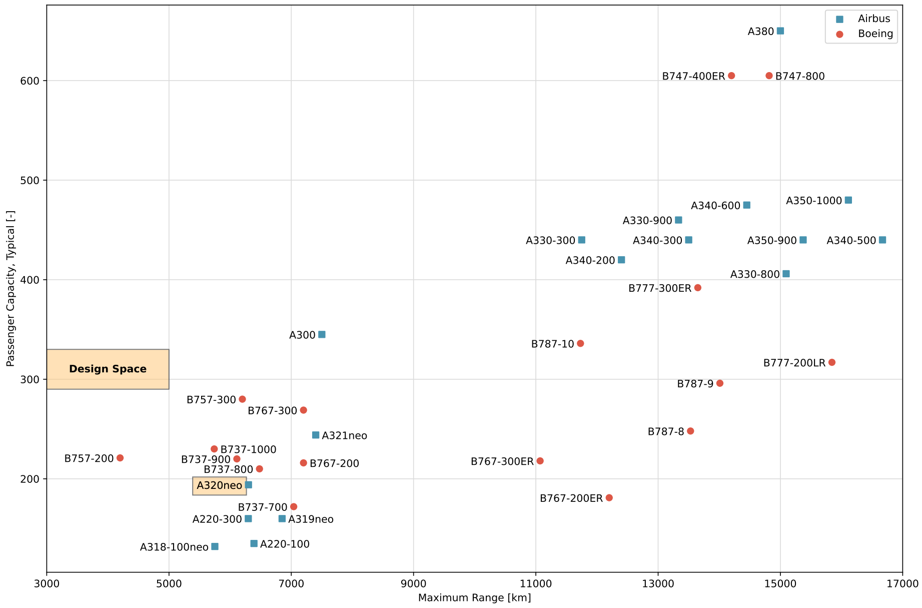

Figure 11.2: Passenger capacity to range comparison for the airliners currently in operation [2].

As demonstrated in Figure 11.2, there is a market gap for an aircraft that could carry more than 200 passengers but fly a relatively short range. Therefore the goal of the design is to fill this market gap.

The number and demand for the targeted routes already imply that the defined market size is substantial. In 2014, $50\,\%$ of the flights with aircraft of more than 300 seats had a distance of less than $4500\,\mathrm{km}$, and by 2050 it is projected that this number will grow to $80\,\%$. As depicted in Figure 11.3, the forecast predicts the biggest growth in the market for more than 300-seat aircraft. Furthermore, the aircraft within the design range of this study (300 passengers and maximum range of $3000\,\mathrm{km}$) is expected to be responsible for the largest share of the CO_2 emissions in 2050, therefore demonstrating a need for a cleaner alternative, especially with the upcoming sustainability regulations.

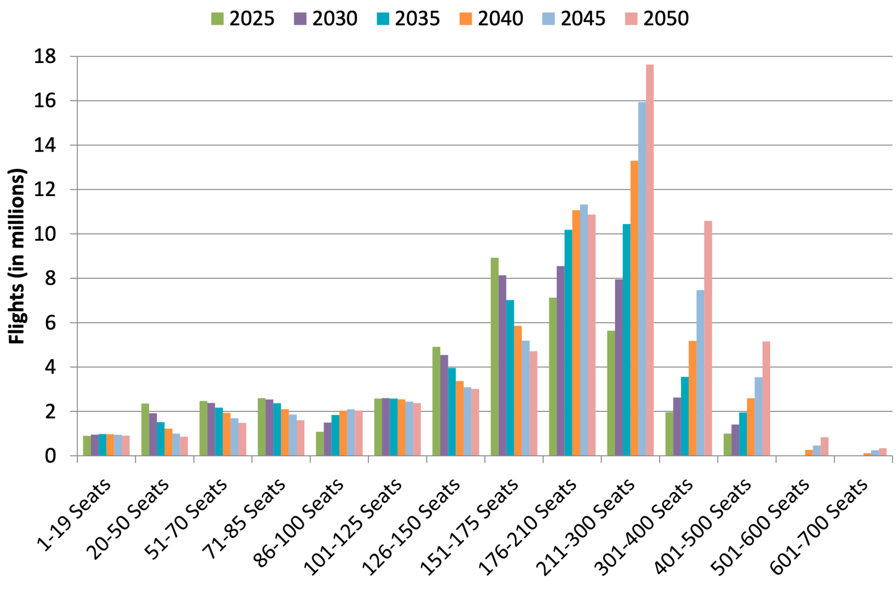

Figure 11.3: Flights by Aircraft Size Classes in the DLR Forecast 2025-2050 [62].

Another noteworthy aspect of the current market is the dominance of the Asian continent, which has the highest share of the total airline passenger traffic ($31\,\%$ for Asia-Pacific and $9\,\%$ for Middle

East in 2023) [2] and is predicted an even bigger market share in the future as Airbus Commercial Market Outlook estimates total of 18,670 expected new deliveries in that region for 2023-2042 [3]. More importantly, the dominance of the Asia-Pacific market is specifically evident in such very high-capacity routes with Japan, South Korea and China leading the way. Hence the primary focus of the mission in these markets.

11.1.2. Stakeholders Analysis

The main stakeholders that are affected by the outcomes of the aircraft design project are presented in Figure 11.4. The interests and considerations of each of the stakeholders that may influence the design are also demonstrated in Figure 11.4. The stakeholders are also plotted on a stakeholder map in Figure 11.5 with interest versus influence on the project axes in order to determine the attitude towards them. According to the matrix, they are divided into key (in case of both high interest and great influence) and non-key, marked in both figures as *K* and *NK* respectively. A discussion about the most important points for the key stakeholders follows.

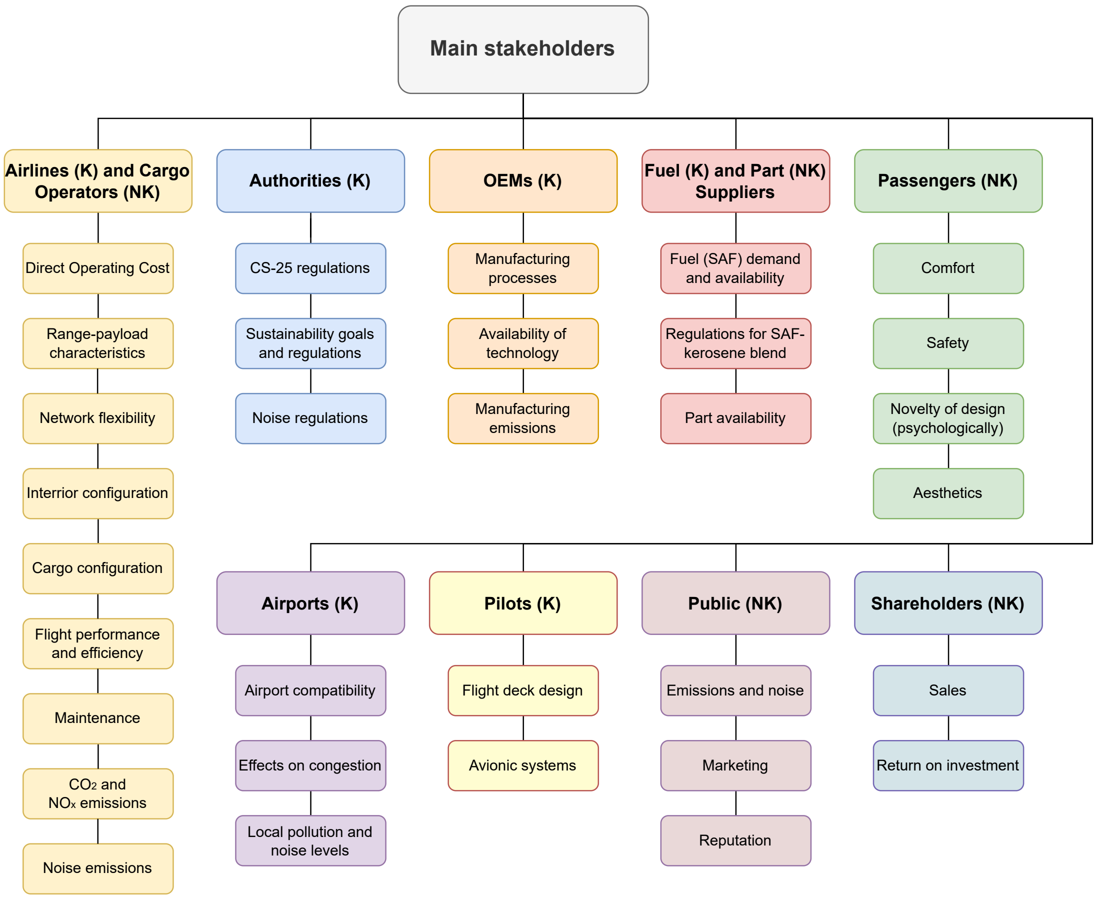

Figure 11.4: Main stakeholders breakdown.

[2] `https://www.statista.com/statistics/619777/air-passenger-traffic-by-region` - 2024-05-06
[3] `https://www.airbus.com/en/products-services/commercial-aircraft/market/global-market-forecast` - 2024-06-17

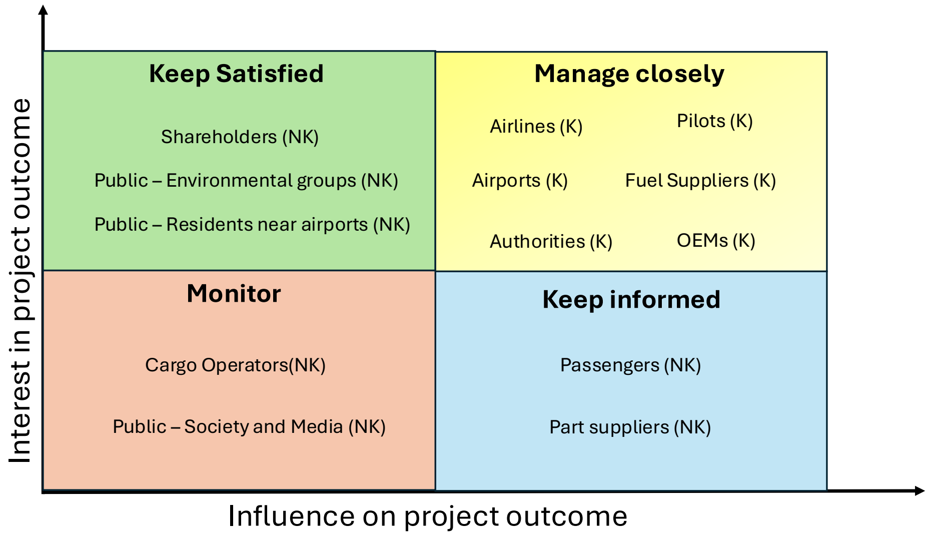

Figure 11.5: Stakeholder map: interest in project outcome vs influence on project outcome.

Airlines and Cargo Operators

The airlines are the main customers of the proposed X-300 and have a large interest in and influence on the design outcome, therefore are considered to be the primary stakeholders. The cargo operators on the other hand are considered non-key stakeholders since cargo transportation is not as demanded on such short ranges. The main concerns of these stakeholders are as follows.

- The Direct Operating Cost (DOC) shall be as low as possible for profitability. A comparison with other state-of-the-art aircraft as well as potential future designs will be performed in Section 11.3 and Section 11.2 respectively.
- The payload-range characteristics and network flexibility imply that the design has to be compatible with the airline's network. Therefore specific market of airlines is targeted that will be discussed in Section 11.2.
- The internal configuration shall be such to grant airlines freedom of cabin layout choices and meet the turnaround and boarding time needs. The latter has been analysed more in-depth in Chapter 10.
- The cargo configuration, although not as crucial, shall comply with standard container geometries (same as the A320neo chosen for the X-300) that airlines would expect.
- Flight performance determines the efficiency of the aircraft operations and hence is of great interest to the airlines.
- Ease of maintenance is another feature that is taken into consideration by the airlines as it directly affects their operations and DOC. The effects of a water-injected turbofan engine choice on maintenance are addressed in Section 10.1.
- The CO_2, NO_x and noise emissions of the airlines influence their compliance with the sustainability regulations. As a practical example, the airlines have to meet the offsetting requirements under CORSIA that almost all of the targeted states have committed to (except China) [4]. Furthermore, some airports implement landing charges that contain noise and emissions fees[5].

[4] https://www.icao.int/environmental-protection/CORSIA/Pages/default.aspx
[5] https://www.easa.europa.eu/eco/eaer/topics/market-based-measures

Authorities

The other primary stakeholders are the regulatory authorities. The design has to comply with all the regulations set by them in order to successfully receive certification and enter into service, therefore they have a very large influence on the design. This function is accomplished by the European Aviation Safety Agency (EASA), for which compliance with the CS-25 regulations needs to be proved. Furthermore, there are a growing number of sustainability and noise regulations that also can greatly affect the new aircraft design. The requirements for CO_2 and NO_x emissions have been discussed and ensured to be met in Section 9.3 and Section 6.3. The noise regulations and goals as well have been addressed in Section 6.4.

Manufacturers (OEMs) and Suppliers

Manufacturers and suppliers are also both considered to be key stakeholders as the development and utilisation of the final product heavily rely on them. The main concern for this category is related to the fuel suppliers, as in the case of the use of SAF-kerosene blend as fuel, the issues and price volatility of SAF can yield serious problems for operations. Based on conservative predictions, a $6\,\%$ blend is estimated to be used by the X-300 aircraft upon entry into service. For more details, refer to Section 9.3.

Airports

All of the aircraft operations are directly linked to the airports hence the compatibility with them is another vital consideration. Particularly, the X-300 aircraft is designed to fit into Category D airports (wingspan of $47.4\,\mathrm{m}$), that form majority in the targeted Asian market. Furthermore, the high capacity of the aircraft contributes to the possibility of lowered congestion at the airports by enabling reduced frequencies for the airlines. The effects of IWET system implementation on airport logistics are addressed in Section 10.2.

11.2. Product Positioning

In this section, the X-300 aircraft's position in the targeted market will be analysed. Market predictions for the year 2035 will be made, based on which the market share of the proposed aircraft is estimated.

11.2.1. Market Size

The main purpose of the proposed design is to replace the existing widebodies that are used on short but very busy routes with an aircraft that carries the same amount of passengers but is specifically optimized for such ranges and hence is more fuel and cost-efficient. Therefore, the total market size can be estimated based on an analysis of the share of widebodies that are used by airlines on ranges of less than $3000\,\mathrm{km}$. For this, the fleet and network of a list of chosen Asian airlines are studied.

A special consideration has to be made for the Japanese airlines as the X-300 characteristics perfectly fit into their network. This is due to the phenomenon of domestic widebody configurations widely implemented into the fleet of All Nippon Airways (ANA) and Japan Airlines in particular. A considerable part of their twin-aisle aircraft is operated only on domestic routes, making it possible for a direct replacement by the EcoFlyer.

As for the other airlines from the Asia-Pacific, Middle East and India, the trend of using widebodies over very short distances is present as well. However, due to reduced flexibility, the replacement with the proposed design will require some network adjustments, as these airlines now tend to not have aircraft that are utilised only on some specific ranges. Nevertheless, these airlines will also be included in the market size since the increased efficiency and profitability of the X-300 are expected to compensate for these losses of flexibility (the effects are discussed more in the next subsection).

The data for 12 major Asian airlines are presented in Table 11.1[6]. In addition to this, the current widebody orders of these airlines are included, as an indicator of their future fleet developments.

[6] https://www.flightradar24.com/

For Japan, only the percentage of the domestic configuration widebodies is demonstrated, meaning the aircraft that are solely used on short ranges. This will later be reflected in the estimations of the market share.

Table 11.1: Short-range widebody fleet of Asian airlines.

Airline	Region	Share of short-range	Current total fleet	Total orders
ANA	Japan	43.6 %	130	35
Japan Airlines	Japan	35.3 %	101	43
Emirates	Middle East	11.8 %	249	305
Qatar Airways	Middle East	8.4 %	188	52
Saudia	Middle East	24.7 %	91	49
Air China	China	39.0 %	130	0
China Southern	China	56.4 %	94	3
China Eastern	China	8.8 %	99	2
Singapore Airlines	Rest of Asia	24.7 %	120	41
Korean Air	Rest of Asia	12.9 %	93	60
Cathay Pacific	Rest of Asia	26.4 %	142	21
Air India	Rest of Asia	10.2 %	60	64

The trends for each of the regions are evident from Table 11.1. The Japanese and Chinese markets are the dominant. The market share estimation in Subsection 11.2.3 for each region will be partially based on these shares as well as the fleet and orders of the airlines.

11.2.2. Position and Share in Future Market

The data analysed in the previous subsection represents only the current market. However, it may undergo significant changes until 2035. This will be investigated in this subsection. Two cases for the market entry of the EcoFlyer will be discussed: the so-called ”best-case” (one-on-one competition) and ”worst-case” (highly competitive market) scenarios.

For the best-case scenario, it is assumed that the new design will have only one direct competitor, essentially serving as a potential replacement for it. As a reference, the case of the relatively new Airbus A220 family against the Embraer E-Jet family is used. The main similarity between the reference and real cases is the fact that A220 as well was marketed as a more efficient and sustainable alternative to the existing designs (25 % better fuel burn than similarly sized aircraft)[7]. Analysing the number of orders and deliveries of both aircraft types, and the number of E-Jets retired, a market share of **54%** was estimated, 33 % of which was for replacing the older similar type and 21 % for expansion purposes[8,9].

As for the more realistic and competitive future scenario, a market of 4 directly competing aircraft types is considered. Besides the X-300 EcoFlyer, Next Generation (2035) widebodies and narrowbody hydrogen aircraft are assumed to operate. The Next Gen widebodies are predicted to replace the current ones, having very similar characteristics but offering considerably lower fuel burns and emission improvements. As no major manufacturing player shift is expected in the upcoming decade (newly emerging Comac will be discussed for the Chinese market), two such aircraft are assumed to be present, from Boeing and Airbus respectively. As for the hydrogen plane, the predictions align with Airbus' initiative of introducing ZEROe concept single-aisle (<200 passengers) aircraft with two hybrid-hydrogen turbofan engines[10]. Even though the hydrogen design was discarded from the

[7] `https://aircraft.airbus.com/en/aircraft/a220/a220-purpose-built-for-maximum-profitability`
[8] `https://aircraft.airbus.com/en/aircraft/a220/a220-purpose-built-for-maximum-profitability`
[9] `https://www.embraercommercialaviation.com/orders-and-deliveries/`
[10] `https://www.airbus.com/en/innovation/low-carbon-aviation/hydrogen/zeroe`

trade-off phase for the X-300 as too risky of an option, Airbus promises to bring it to market by 2035, therefore it is considered as a competitor. This aircraft is considered to compete with the X-300 from the environmental point of view, providing an alternative fuel-powered design that can be deemed more appropriate for the future market and sustainability regulations.

All the options are then scored from 1 to 5 against three main criteria to obtain a rough estimate of their market shares. Score 1 refers to a significantly worse performance than the reference A320neo aircraft, while score 5 indicates a substantial improvement compared to the reference. The criteria, based on the stakeholders' analysis, include market suitability, direct operating costs and emissions. The results are presented in Table 11.2. The properties of the Next Generation widebodies are found relative to the current Airbus A350 aircraft [63]. As we assume there are 2 of those aircraft competing, the market share is doubled relative to the score. For the hydrogen aircraft, a study comparable to Airbus ZEROe characteristics is used [64]. The percentage differences of the aircraft properties are with respect to the reference A320neo. Also, note that this is only a first estimation of the market share and hence the trade-off is performed in a quite simplified manner, however, the use of two different methods and further iterative process with the cost analysis should yield reliable results.

Table 11.2: The market shares trade-off of the competing aircraft types in 2035.

Property	**X-300 EcoFlyer**	**2 Next Gen widebodies**	**ZEROe narrowbody**
Range (nm)	1620	8000	1500
Max pax capacity	330	440	180
DOC ($\$/\mathrm{ASK}$)	0.061 (-11%)	0.065 (-6%)	0.084 (+21%)
CO_2 ($\mathrm{g/ASK}$)	74.0 (-25%)	52.6 (-47%)	0 (-100%)
NO_x ($\mathrm{g/ASK}$)	0.020 (-91%)	0.688 (+213%)	0.292 (-16%)
Score on market suitability	4	3	2
Score on DOC	4	3	1
Score on sustainability	5	1	5
Total score	13	2×7	8
Market share	**37%**	40%	23%

The scores for the direct operating cost and sustainability are directly derived from the aircraft's performance in these criteria. Note that the DOC for the X-300 will be obtained in the Section 11.3, however as it depends on the number of expected deliveries, the value used in the end is an outcome of a few iterations. The market suitability, however, comprises several aspects, therefore the score will be discussed in more detail. For the defined market, the main properties for compatibility are the range and passenger capacity, both of which X-300 is optimised for, while the widebodies and hydrogen option are designed for other types of missions. The reason for not receiving the highest score for the EcoFlyer however is due to the use of a few advanced subsystems as the WIT engine and SAF for fuel. These might affect the utilisation of the aircraft and therefore not be favoured by the customers. Although the hydrogen aircraft, being a more sustainable alternative, is designed also for short ranges, its very low single-aisle capacity does not suit well with the targeted extremely busy routes, which is why the score of 2.

The outcome of the analysis is the predicted share of **37%** for the X-300 aircraft in the highly competitive scenario, which is scaled according to the total scores obtained in the trade-off. Combining this with the more optimistic predictions that were presented in the beginning yields an average product share of **46%**.

11.2.3. Expected Number of Deliveries

In order to further analyse the costs and sales of the product, an expected number of deliveries for the X-300 EcoFlyer has to be estimated based on the obtained market size and share information. The

Boeing Commercial Outlook serves as a demonstration of the expected number of total widebody aircraft deliveries per region for the coming 20 years[11]. Based on these values, the number of fleets dedicated to short ranges is found, using the ratios presented in Table 11.1. From this, with the market share estimated in the previous subsection, the actual number of proposed aircraft deliveries is computed.

The market share, as already mentioned, is alternated based on the region under consideration and its market characteristics. So for Japan, considering the very high ratio ($40\,\%$ on average) of the aircraft that are only used for short-range routes, the product share is multiplied by a factor of 1.5. On the other hand, in the Chinese market, despite again relatively high portion of short-range aircraft, the emergence of a new local manufacturer, is expected to negatively affect the EcoFlyer's share. The Comac C929 long-range widebody airliner is expected to enter service in 2027[12]. If considering as a reference the single-aisle competition between Airbus/Boeing narrowbodies and Comac C919, the Chinese airlines have placed almost half ($48\,\%$) of the orders from their national manufacturer. Extrapolating this into our market results in a share of $24\,\%$ for the X-300 in China. For the Middle Eastern and Rest of Asia airlines, the trend is present quite evenly in all major airlines, therefore the share of $44\,\%$ remains unchanged.

In addition to this, another market opportunity that is considered is the replacement of narrowbodies (such as the reference A320neo) that are operated at very high frequencies, by providing similar capacities in total but reducing congestion at the airports. Especially in Asia, the congestion of such hubs is a growing issue, therefore the X-300 could be used as a partial solution to this[13]. To account for this market as well, a factor of $20\,\%$ is added to the previously obtained number. Finally, to obtain a number for the whole world, another factor of another $25\,\%$ is added to the Asian number of deliveries as there are some tendencies of the targeted routes appearing in North America, Australia and eventually in Europe too.

The total number of deliveries assumes a production period of 30 years, based on data from already discontinued aircraft (Airbus A300 and Boeing 727). According to future market forecasts of a SAF/kerosene aircraft, the demand for such an aircraft is predicted to reach its peak in 2047, growing linearly up to that point and further decreasing linearly until 2065, that is the end of production period [65]. The estimation of the total number of deliveries is hence based on this model. All the results of this analysis are presented in Table 11.3.

Table 11.3: Number of deliveries for different target regions. *only contribution of ANA and Japan Airlines considered as other airlines operate wide bodies on longer ranges.

Market	Total forecast (2023-2042)	Total short-range (2023-2042)	X-300 share	Yearly X-300 (2035)	Total X-300
Japan	323	117*	$68\,\%$	4.79	176
Middle East	1350	174	$46\,\%$	4.75	174
China	1550	539	$24\,\%$	7.68	282
Rest of Asia	1347	219	$46\,\%$	5.98	219
Rest of world	-	-	-	5.80	213
Total	-	-	-	**29.01**	**1063**

[11] https://www.boeing.com/commercial/market/commercial-market-outlook
[12] https://aviationweek.com/air-transport/comac-foresees-future-intelligent-aircraft
[13] https://pecc.org/resources/infrastructure-1/845-air-transport-in-the-asia-pacific-challenges-opportunities-and-options/file

11.3. Cost Analysis

In the following section, the cost analysis concerning the final design will be presented. The life cycle cost, as well as a detailed analysis of the production and development cost, will be presented. Also the direct operating costs, as well as the price are estimated, and concluded by a sales estimation.

11.3.1. Cost Breakdown Structure

As part of the cost analysis of the EcoFlyer, all costs related to the life cycle are analysed. The life cycle cost can be broken down into the research and development cost, acquisition cost, operating cost and disposal cost. In Figure 11.6 the cost breakdown structure is depicted. Here the life cycle cost breakdown proposed by Raymer [66] and Roskam [67] are combined.

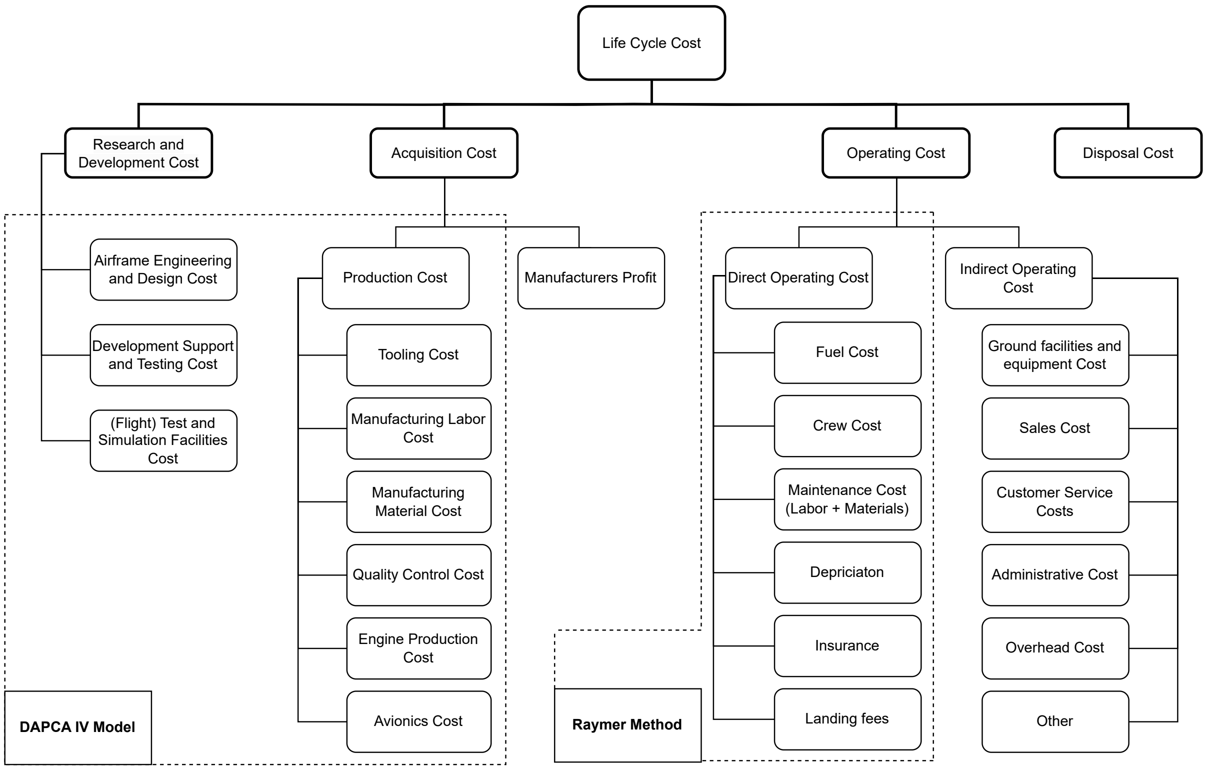

Figure 11.6: Cost breakdown structure of life-cycle cost of new aircraft design.

The reason for analysing the life cycle cost within this study serves two purposes. As a starting point, the research, development, test and evaluation cost (RDT&E) directly influence the unit cost when divided by the total number of aircraft produced. In Subsection 11.3.2 the DAPCA IV model (development and procurement costs of aircraft) proposed by Raymer [66] will be used to estimate the related cost. The RDT&E cost together with the production cost and manufacturers' profit determines the price per aircraft. For potential buyers, the operating cost, especially the direct operating cost (DOC), is an extremely important factor for the attractiveness of the design. In Subsection 11.3.4 the Raymer method will be used to have an estimate for the DOC that can be compared to other aircraft designs.

11.3.2. Production and Development Cost

The RAND DAPCA IV model combines the development with the production cost in certain cost estimate relationships. The method is widely known to provide reasonable results for civil transport aircraft. DAPCA estimated the hours required for RTD&E and production by the engineering (H_E), tooling (H_T), manufacturing (H_M) and quality control (H_Q) groups. These are multiplied by the appropriate hourly rates to yield cost. Development support (C_D), flight-test (C_F), avionics ($C_{avionics}$) and manufacturing material cost (C_M) are directly estimated. Equation 11.1 is than used to calculate the total invested cost (C_{inv}):

$$C_{inv} = H_E R_E + H_T R_T + H_M R_M + H_Q R_Q + C_D + C_F + C_M + C_{eng} N_{eng} + C_{avionics} \tag{11.1}$$

As input the model uses the operating empty weight, maximum velocity and the number of aircraft produced in 5 years. From Subsection 11.2.3 it followed that over a period of 30 years, 1063 aircraft will be produced, resulting in a production rate of 177 aircraft every 5 years.

DAPCA assumes that the engine cost (C_{eng}) is known, and if that is not the case it provides a formula to estimate the price based on inlet temperature and and maximum thrust. However since the method is not very accurate for modern engines, it will not give an accurate estimate for the water-injected engine, as this is a future engine concept. To estimate the price of the engine, a study was conducted to determine the average price increase associated with an improvement in engine efficiency. This involved analyzing and comparing various older engines with their replacements to establish a relationship.

Table 11.4 shows an example where the popular CFM 56 engine, used on the A320ceo is compared to the leap 1A engine and the PW1000G geared turbofan, which are both used on the A320neo and therefore serve as a direct replacement of the CFM 56 [14]. To make an accurate comparison between for instance the bigger GE90 engine used on the 777 the price is normalised by the maximum thrust. Also, inflation is taken into account.

Table 11.4: Engine comparison CFM 56 with successors.

Engine model	**SFC** ($g\backslash kNs$)	**Max thrust** (kN)	**price** (million \$)	**SFC compared to CFM 56**	**Price compared to CFM 56**
CFM 56	15.4	104	10	0	0
LEAP 1A	14.43	155	15	$-6.3\,\%$	$50\,\%$
PW1000G	14.4	147	14.5	$-6.5\,\%$	$45\,\%$

From Table 11.4 it can be seen that approximately an increase in efficiency of $6\,\%$ results in a significant price increase of almost $50\,\%$. When more engines and their successors are taken into account such as the G9X, with a 10% lower SFC and price increase of $40\,\%$, replacing the GE90 on the 777x. Or looking at the Trent7000 replacing the Trent700 on the a330neo, a general trend can be approximated to give a more accurate price indication for the engine. From the analysis, it followed that as a rough estimation an efficiency increase of $10\,\%$ results in a price increase of $50\,\%$. To be conservative on the estimation of the price this $50\,\%$ price increase is added to the value that followed from the DAPCA method to account for the improved technologies. Next to that, it must be noted that the method is not considering the development cost of the engine itself, it is therefore assumed that the engine is bought from a third party.

According to the method the cost for avionics accounts for $10\,\%$ of the production cost. Raymer suggests increasing the hours predictions and cost estimations of the DAPCA method by about $20\text{-}40\,\%$ for the most advanced aircraft designs. Due to the slightly unconventional design of the EcoFlyer with the engines at the back and the H-tail, in combination with a preferred over prediction of the development cost, a 1.4 factor is applied to all predictions. Next to that, the model assumes an all-aluminium design, where the design is an aluminium-lithium design with a composite tail, an

[14] https://booksite.elsevier.com/9780340741528/appendices/data-b/table-1/default.htm

additional factor of 1.2 is applied to the manufacturing material cost. Lastly, the model is corrected for inflation from 1999 to 2024 by a factor of 1.88 [15]. All components that contribute to the development and production cost are presented in Table 11.5. The production cost is an estimation for all 923 aircraft and for 1846 engines. Only the production costs are given per aircraft. This results in an estimated investment cost for the entire program of:

$$C_{inv} = \textbf{\$ 116 Billion}$$

Table 11.5: Breakdown of RDT&E and production cost.

Cost component	**Symbol**	**Cost (USD)**
Engineering	$H_E RE$	9.2 billion
Development Support	C_D	0.91 billion
Flight Test	C_F	0.6 billion
Total RTD&E Cost		**10.7 billion**
Tooling	$H_T R_T$	5.8 billion
Manufacturing Labor	$H_M R_M$	19 billion
Materials	C_M	8.0 billion
Quality Control	$H_Q R_Q$	2.8 billion
Avionics	$C_{avionics}$	9.5 billion
Engine	$C_e N_e$	60 billion
Total production cost per aircraft		**98.7 million**
Total	C_{inv}	**116**

11.3.3. Market Price

The market price is dependent on two values, the production cost per aircraft and the manufacturers' profit. Raymer suggests multiplying the production cost by a certain investment cost factor of 1.1-1.4 to arrive at the market purchase price. This includes the 'cost of money' and manufacturers' profit. The manufacturer's profit directly influences your break-even point and should therefore be carefully chosen. A margin of $30\,\%$ is chosen, as a lower manufacturer's profit would result in a too little return on investment (explained later). A higher profit would result in the price not being competitive or meeting the requirement. This results in a selling price in the year 2024 of:

$$\textbf{Market price} = \textbf{\$ 128 million}$$

In Section 11.4 the price, break-even point and return on investment will be elaborated on.

11.3.4. Direct Operating Cost

The direct operating cost is an important aspect of the cost analysis as it directly influences the attractiveness of the design for potential buyers. A relatively more expensive plane, but with significantly lower DOC can still be very attractive. In the following sections, the breakdown of the DOC will be discussed, as well as compared to planes that are operating on the target routes of the proposed design.

The DOC is typically expressed in cost per block hours. The block hours include flight time, taxi time, ground hold time, etc. To come up with the block time Raymer suggests adding 21 minutes to the flight time (15 min for ground maneuver and 6 min for air maneuver), resulting in a nominal block time of 1.99 block hour (BH).

[15] https://smartasset.com/investing/inflation-calculator

Fuel Cost

One of the biggest contributions to the DOC normally comes from fuel. To calculate the fuel used per block hour the fuel usage of $5.98\,\mathrm{kg/km}$ is used, as calculated in Chapter 6. This includes the fuel reduction of the IWET system of $9.25\,\%$, from Section 5.4. This is then multiplied by the nominal mission distance, with a 2.5% addition for the fact that the flight is not assumed to be in a straight line, and multiplied by the fuel price. Here a fuel price of $0.87\,\$/\mathrm{kg}$ is used. This includes a 6% SAF blend as explained in Section 9.3. The total fuel per block hour is then calculated, as shown in Equation 11.2.

$$C_{fuel} = \frac{5.98 \cdot 1127.5 \cdot 0.87}{1.99} = \$2,678.47/BH \tag{11.2}$$

Crew Cost

The flight deck crew cost per block hour is estimated by Equation 11.3 from [66] for a two-man crew based on the cruise speed and MTOW.

$$C_{crew} = 54 \cdot \left(V_c \cdot \frac{W_{MTOW}}{10^5}\right)^{0.3} + 122 = \$1,002.90/BH \tag{11.3}$$

Maintenance Cost

Maintenance activities, including scheduled and unscheduled maintenance, are lumped together under Maintenance Man hours per Fight Hour (MMH/FH) which is roughly proportional to the weight. Next, it is strongly influenced by the utilization. Typical values for the MMH/FH for civil transport are in the range of 5-15 according to Raymer ranging from a very easily maintainable aircraft to an aircraft that is very difficult to maintain with advanced large composite structures and complex systems. As explained in Subsection 10.1.3 the X-300 faces some difficulties regarding maintenance and therefore a value of 12 has been chosen as the aircraft is still somewhat conventional, but more difficult to maintain with the less accessible engines. The MMH/FH is then multiplied by the labour cost to predict the total manufacturing labour cost per flight hour.

The total cost for materials used in the maintenance process per flight hour is calculated by Equation 11.4, from [66]. The formula uses as input the aircraft cost less engine (C_a), the cost per engine (C_e) and the number of engines (N_e).

$$\frac{materialcost}{FH} = 3.3 \cdot \left(\frac{C_a}{10^6}\right) + 10.2 + \left(58 \cdot (\frac{C_e}{10^6}) - 19\right) \cdot N_e = \$3,493.52/BH \tag{11.4}$$

The total manufacturing cost is the sum of the materials cost and manufacturing labour cost:

$$C_{man} = MMH/FH \cdot R_{man} + \frac{materialcost}{FH} = \$1,649.68/BH \tag{11.5}$$

Insurance, Depreciation and Landing Fees

For commercial aircraft, the depreciation is considered a part of the operating expenses. As a first estimate, it is assumed that the reseal price is 10% of the original value over the 30-year lifespan of the aircraft. Here the unit cost is assumed to be the total investment cost, divided by the total number produced and minus the cost of the engine, as the engine resale value can be neglected for initial analysis [66].

$$C_{dep} = \frac{0.9 \cdot unitcost/30}{1.98 \cdot 5 \cdot 365} = \$591.22/BH \tag{11.6}$$

Insurance costs for commercial aircraft add approximately 1% to the cost of operations [66].

Landing fees are on average about 33% of the fuel cost. [66].

Comparison

It is interesting to see how the X-300 is performing with respect to the other aircraft operating on the target routes that were analysed in Subsection 11.2.1. In Table 11.6 the DOC breakdown of the X-300 and its direct competitors are depicted. To make a fair comparison, the same method is used to calculate the DOC for the other aircraft types operating on the target routes. Finally, the DOC is normalised per flight hour and per passenger to compare. The table is discussed in the market positioning (Section 11.5).

Table 11.6: Comparison of the X-300 wit its direct competitors.

	X-300	**A320neo**	**A330-300**	**777-300-ER**	**B787-8**	**A350-900**
PAX	330	154	262	344	248	315
Cost ($/block hour)						
Fuel	2678	1592	3670	5134	3352	3643
Crew cost	1003	944	1240	1368	1236	1282
Maintenance labor	1650	1100	1375	1374	1512	1512
Maintenance Materials	3494	1911	3362	4493	3636	3724
Depreciation	591	774	2066	3163	2005	2614
Landing fee	893	531	1223	1711	1117	1214
insurance	103	68	129	172	129	140
Total DOC	10,442	6,931	13,065	17,418	12,987	14,130
DOC/ASK	0.0613	0.0686	0.0739	0.0736	0.0748	0.0646

11.4. Sales Estimation

To summarise the cost analysis performed above the X-300 has a unit cost of a $\$109\,\mathrm{million}$, market price of $\$128\,\mathrm{million}$ and $\$0.0613\,\mathrm{ASK}$ direct operating cost. With this, the return on investment (ROI) can be calculated:

$$ROI = \frac{marketprice \cdot N_{sold} - C_{inv}}{C_{inv}} \cdot 100\% = \frac{128,311,527 \cdot 1063 - 115,591,087,684}{115,591,087,684} \cdot 100\% = \mathbf{18\%}$$

This results in a total profit for the entire program after 30 years of4$\$21\,\mathrm{billion}$. Also, the break-even point can be calculated. The program starts making money after the total RTD&E cost of $\$10.7\,\mathrm{billion}$ is recovered. Since the profit per aircraft sold is $30\,\%$ of the production cost, the expected break-even point is at aircraft number **360**.

11.5. Final Market Positioning

To analyse the final market position, the market price of the EcoFlyer is compared to the state-of-the-art A320neo. From the cost analysis a unit cost prediction of $\$109\,\mathrm{million}$ for 2024 was found. **REQ-STK-15** asks for a unit cost estimation for 2035 in euros. When a cumulative inflation of 31.21% from 2024-2035 [16] is used and converted from dollars to euros this would result in a unit cost prediction for 2035 of **€133 million**. This would mean that the requirement is not met as the maximum unit cost could only be $€130\,\mathrm{million}$. It is difficult to compare the unit cost with the unit cost of the

[16]https://smartasset.com/investing/inflation-calculator

A320neo, as there is no reliable information available publicly. It is however possible to compare the price estimation of $\$128\,\text{million}$ for 2024 with the price of an A320neo of $\$110\,\text{million}$. The $17\,\%$ price increase can be explained by several factors. Most of the reasons have been explained in the previous cost analysis parts. To summarise, the aircraft has a significant increase in size and therefore increased material and manufacturing costs. Next to that the aircraft has a significant increase in efficiency and therefore engine price. If you compare the market price with the wide-bodies it is actually significantly lower. Therefore it is justified why the requirement is not met and why the price is higher than the A320neo.

When analysing the DOC/ASK, depicted in Table 11.6 it can be seen that the X-300 performs very well on DOC compared to the other aircraft. The X-300 shows a $11\,\%$ reduction in DOC/ASK compared to the A320neo. This mainly comes from the fact that the aircraft is more fuel efficient resulting in smaller fuel cost per passenger. As expected the X-300 performs even better compared to the wide-bodies. This is a result of the optimised design for a higher capacity but with narrow-body comparable emissions. Also, the fact that the unit cost of the aircraft is significantly lower than the wide-bodies results in a significant reduction in depreciation.

All the previously analysed properties of the aircraft in terms of its market competitiveness are reflected in the SWOT analysis, presented in Figure 11.7.

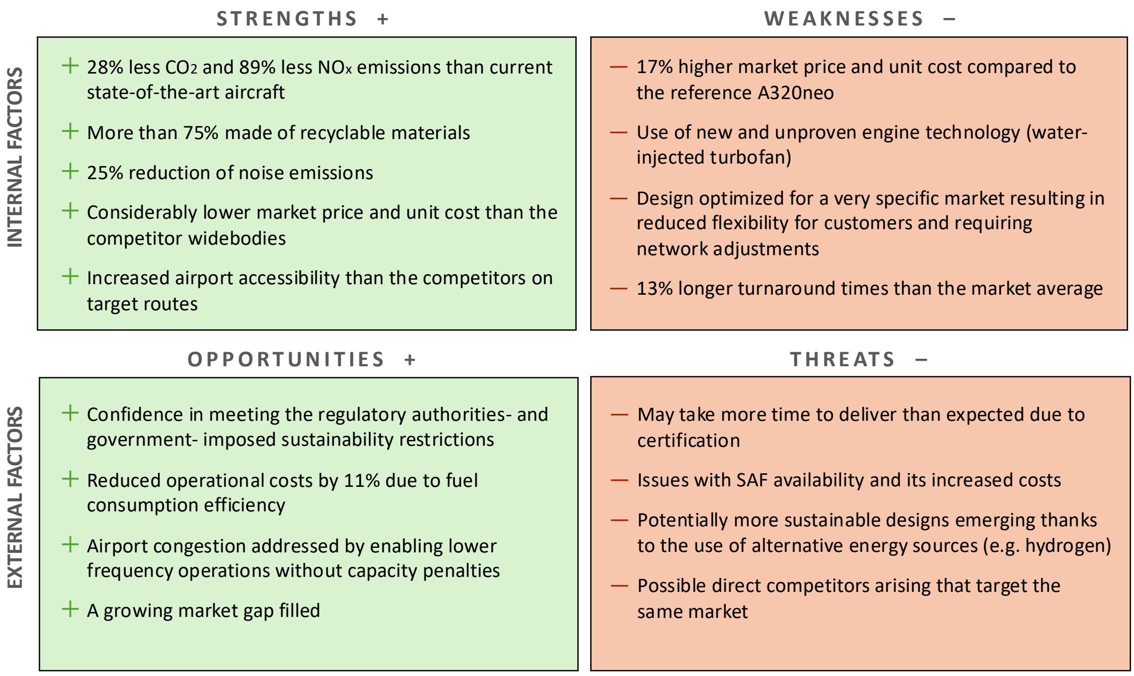

Figure 11.7: Mission SWOT analysis for final market positioning.

From the cost and market analysis, it can be concluded that the X-300 EcoFlyer is a serious competitor for the current and future market with a lower DOC(/ASK) and a very competitive, yet realistic market price. Despite some potential weaknesses and threats, it can be reasserted that the proposed aircraft will fit well in the future market, having a substantial market share and as a result yielding profitability.

12 Resource and Budget Breakdown

In this chapter, the allocation of critical technical resources established in the beginning of planning phase, will be re-evaluated based on the detailed design. The primary resources which have been analysed are the mass, cost and power of the X-300 EcoFlyer. The cost and power breakdowns are already presented in Section 11.3 and Section 5.2 respectively. Therefore, in this chapter only the detailed breakdown of the mass budget is provided. Tables 12.1 and 12.2 indicate the OEW and MTOW breakdowns per subsystem.

Table 12.1: X-300 operating empty mass budget.

System	Sub-System	Mass (kg)	Percentage
Fuselage group	Fuselage	15 156	23.71 %
	Systems (IWETS, hydraulics, etc)	21 989	34.40 %
	Empennage	1556	2.43 %
	Powerplant	15 705	24.57 %
Wing group	Wing	5452	8.53 %
Total		63 926	100 %

Table 12.2: X-300 maximum take-off mass budget.

System	Sub-System	Mass (kg)	Percentage
Fuselage group	Fuselage	15 156	12.3 %
	Systems (IWETS, hydraulics, etc)	21 989	17.8 %
	Empennage	1556	1.26 %
	Powerplant	15 705	12.7 %
	Payload (incl. cargo)	40 120	32.5 %
Wing group	Wing	5452	4.42 %
	Undercarriage	4873	3.95 %
	Fuel	19 279	15.62 %
Total		123 448	100 %

As expected, the systems (including IWETS, fuel, hydraulics, etc.), the fuselage, and the propulsion unit are the largest contributors to the empty weight. This aligns with the initial budget breakdown predictions. The landing gear and empennage are also very similar to the initial estimations and the predefined contingencies have mostly disappeared. The wing weight, on the other hand, is likely to be an underestimation and therefore needs a more detailed structural analysis to obtain an accurate value. For the MTOW, the fuel and payload have not been budgeted previously. However, considering that the aircraft is designed for a short mission but a very large capacity, the correlation obtained is comparable with the design characteristics.

The evolution of the contingencies applied for these technical resources is demonstrated in Table 12.3.

Table 12.3: Updated contingencies of critical technical resources.

Design Phase	**OEW** (t)	**Unit Cost** ($\mathrm{million}\ \$$)	**Power** (kW)
Conceptual	40 %	27 %	40 %
Preliminary	33 %	13 %	35 %
Current	28 %	11 %	22 %
Detailed	10 %	5 %	8 %
Manufacturing	5 %	2 %	5 %
Production	0 %	0 %	0 %
Current value	63.9	133	1130
Target value	89.3	150	1450

The target value for the OEW is derived from **REQ-MIS-043**. The unit cost is also from a mission requirement, **REQ-STK-15**, however the initial market analysis showed that this value is unrealistic for 2035. This was later confirmed by more detailed cost analysis at the current stage. Therefore, a new target value of $150 million has been chosen. As for the power budget, it follows from **REQ-SYS-030** and **REQ-SYS-035**, and the target is derived from comparable aircraft properties (Boeing 787-8) [20].

As shown in Table 12.3, so far the resources have been correctly allocated and the current values lie in between the initial and target values. There is a sufficient margin left that will gradually decrease to zero throughout the upcoming post-DSE phases.

13 Technical Risk Assessment

In this chapter, a technical risk assessment is performed for the X-300 at its current stage in the design process. This is first done by identifying potential risks for different subsystems, followed by making a risk matrix to identify the most critical risks. Finally, the mitigation measures for the necessary risks will be presented.

Table 13.2 displays the technical risks related to the product. The columns L, C, and R correspond to the likelihood, consequence and risk scores. Risk is calculated as the product of likelihood and consequence. The risk identifiers refer to CON - Control and Stability, AER - Aerodynamics, MAT - Materials, ECT - Electric, NOI - Noise, ENG - Engine, PER - Flight Performance and STR - Structures. Table 13.1 shows the criteria used to score the risks.

Table 13.1: Criteria used to allocate scores for risk assessment.

Score	Likelihood	Consequence
1	Highly Unlikely	Negligible
2	Unlikely	Marginal
3	Possible	Critical
4	Highly Possible	Catastrophic

Table 13.2: Technical risk assessment with identifiers, scores and responsible departments.

Identifier	Risks	Impact	L	C	R	Responsible department
R-CON-01	The wings of the aircraft are more aft than existing aircraft	The aircraft requires a large tail to maintain controllability	3	2	6	Control and Stability
R-CON-02	Eigenmotions are not analysed in depth	Since there is an H-tail, assumptions for conventional aircraft configurations may not be representative	4	2	8	Control and Stability
R-AER-01	Semi-empirical methods are used for 3D wing analysis	Wing aerodynamic coefficients may by inaccurate	3	3	9	Aerodynamics
R-AER-02	CFD model is used for airfoil analysis	Model may not represent real conditions	4	2	8	Aerodynamics

Continues on next page

Table 13.2 – continues from previous page

Identifier	Risks	Impact	L	C	R	Responsible department
R-MAT-01	Recyclability of material is assumed to be the same as that for A320neo	Assumptions may not be valid	3	1	3	Materials
R-MAT-02	Composites may have better recyclability methods in the next $10\,\mathrm{years}$	Composites are lighter so the aircraft may be heavier than competitors	3	4	12	Materials
R-ECT-01	Motors are placed in the wheels	May be overheated during braking	3	3	9	Power and propulsion
R-ECT-02	Electric taxi system is designed for $26\,\mathrm{minutes}$	If time to taxi is longer, fuel reserved for loiter will have to be used	4	3	12	Power and propulsion
R-ECT-03	Environment Control Unit is electrically powered and can fail	Failure results in low oxygen supply and is an additional probable cause for an emergency	1	4	4	Power and propulsion
R-NOI-01	Literature used to estimate noise reduction has a wide range of values	Estimations may not be accurate and may be biased	4	2	8	Sustainability
R-ENG-01	Engines which are placed on the horizontal tail may fail	Engine failure may impact tail performance due to damage	1	4	4	Risk
R-ENG-02	Engine is only designed for one design point	Engine performance may differ from the model for other design points such as wet or icy conditions	3	3	9	Power and propulsion
R-ENG-03	Weight factor of 1.4 is taken from one source	Engine weight could be underestimated or overestimated.	3	3	9	Power and propulsion
R-ENG-04	Engine technology may not be available by 2035	Delay in aircraft delivery or choosing another engine	3	4	12	Power and propulsion
R-PER-01	Flight ceiling of $10\,000\,\mathrm{m}$ may limit airspace accessibility in conflict zones	Reduction in route network flexibility	3	2	6	Performance
R-PER-02	Power available used for calculations is scaled for altitude using literature	Power available may be different than calculated which affects the cruise calculations	3	1	3	Performance
R-STR-01	Fuselage weight estimation is based on statistical data	Weight could be underestimated	4	2	8	Structures
R-STR-02	Wing structural analysis is not performed which does not account for engine weight relief	Wing may need more structural reinforcement than it currently has now	3	3	9	Structures

The identified risks were then plotted on a risk map. The risk map has coloured legends; Green - Negligible, Yellow - Marginal, Red - Unacceptable. The risk map can be seen in Figure 13.1

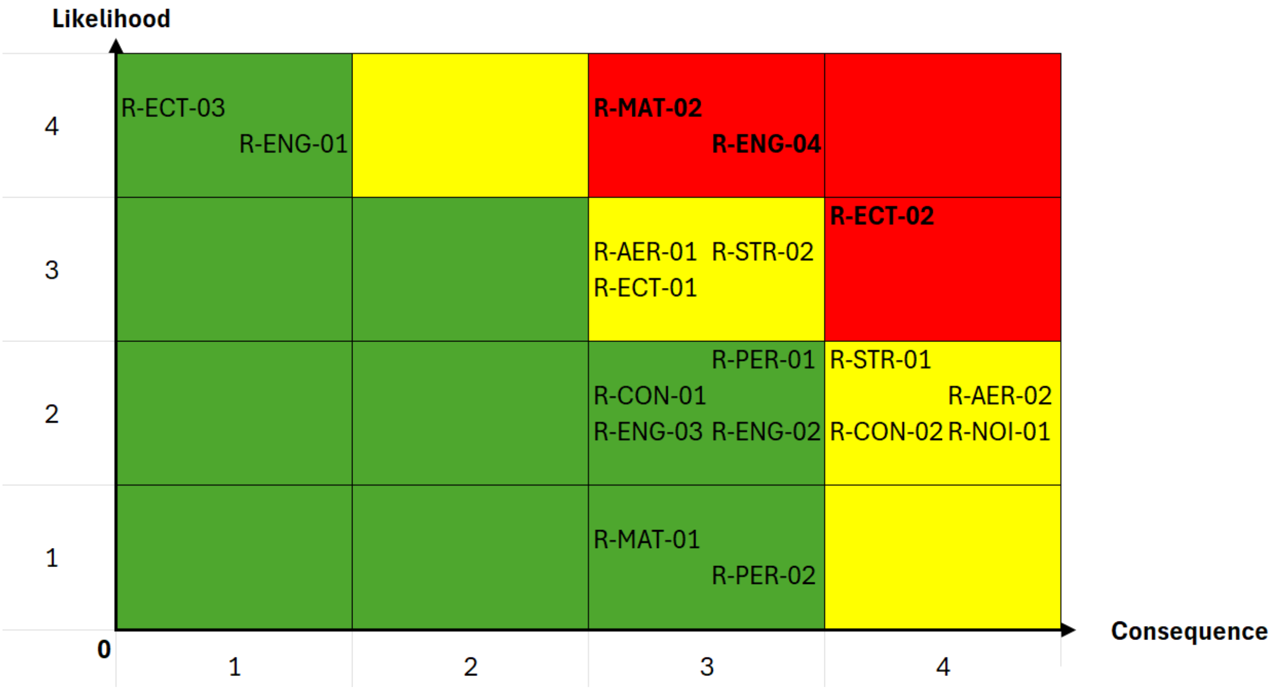

Figure 13.1: Risk map before mitigation measures are derived.

From Figure 13.1, it can be seen that the unacceptable risks are R-MAT-02, R-ENG-04 and R-ECT-02. In an effort to use resources optimally, mitigation measures are developed only for the unacceptable risks.

Table 13.3: Unacceptable risks which require mitigation/contingency.

ID	Mitigation	Contingency	L	C	R
R-MAT-02	Conduct more detailed analysis on potential recycling measures available in the next 10 years and reconsider material choice if necessary	If composite technology improves then change the material of the plane	1	4	4
R-ENG-04	Tie up with an engine manufacturer with a target year before 2035 before proceeding with more detailed design	Delay delivery of the aircraft	2	4	8
R-ECT-02	Improve taxi planning procedures in airport operations	Carry extra fuel on the aircraft	2	2	4

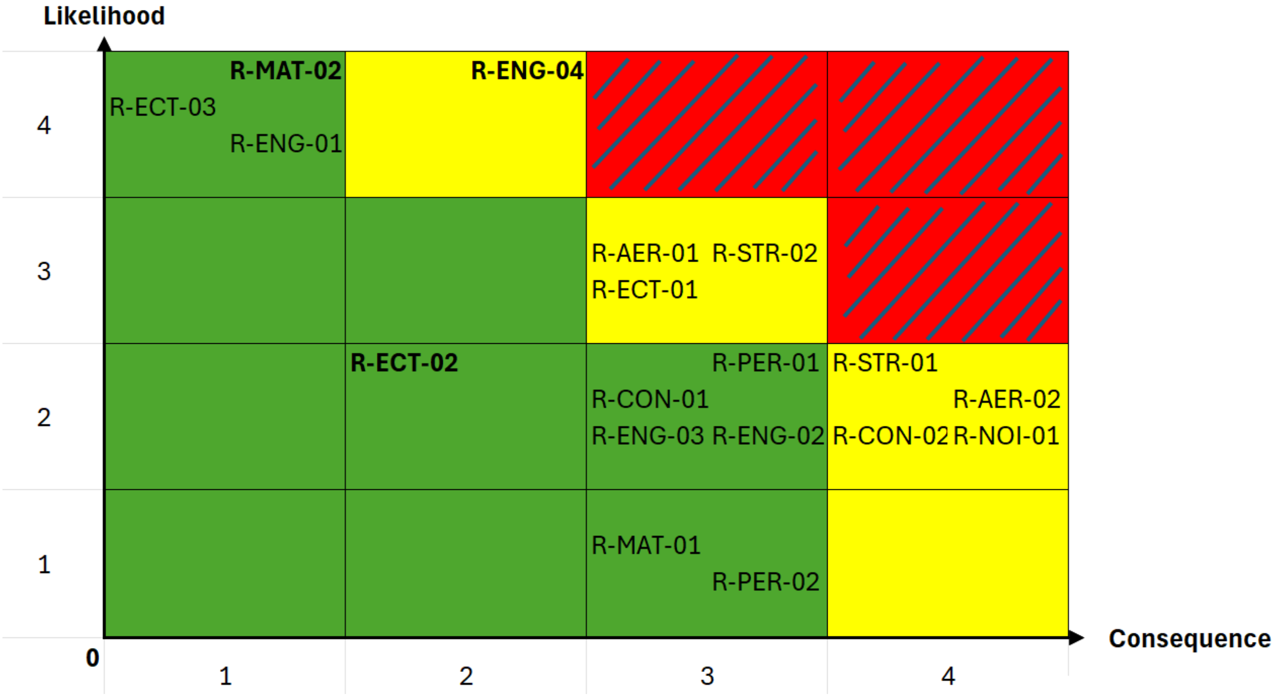

Figure 13.2: Risk map after mitigation measures are applied.

Figure 13.2 shows the risk map after mitigation measures are applied to the most critical risks. To meet the requirement that at least $75\,\%$ of the aircraft shall be recyclable, the material chosen was an Aluminium-Lithium alloy. If recycling technology can improve for composites they could prove to be a more advantageous choice for aircraft due to the relatively low weight of this material. Assuming recycling technology does indeed improve, this will affect sales if future competitors choose to use composites.

Another requirement for the aircraft is that it has to enter into service by 2035. Since the X-300 uses a new engine technology (WIT), there is a risk that the engine is not available in time. The mitigation measure for this is also discussed in Chapter 15.

The aircraft uses an electric taxi system for ground operations, which means it has to carry less fuel. However, taxi times can often exceed the designed $26\,\mathrm{minutes}$ in busy and larger airports which means the aircraft needs to use the reserve fuel for loitering. This would either mean a having a lower loiter reserve or carrying more fuel, where the latter lowers the potential benefit of the IWETS.

14 Compliance Matrix

This section will analyse whether all previously established requirements have been met by the final design, through the use of a compliance matrix. The compliance matrix discusses the requirements of the aircraft [3] and if they have been met at this stage of the design. If the requirement is satisfied, the ”Compliant” column has 🟢, and if the requirement is not met the ”Compliant” column has 🔴. If the requirement has not been analysed yet but is expected to be met at later design stages, it is marked with 🟡. If the stakeholder and mission requirements have been marked with 🟡, the method of verification post-DSE has been indicated. The compliance matrix can be seen below in Table 14.1.

Table 14.1: List of mission requirements.

Identifier	**Requirement description**	**Compliant**
REQ-STK-01	The aircraft shall have a maximum range of $3000\,\mathrm{km}$ or above	🟢
From Section 6.1, the aircraft can fly for up to $8575\,\mathrm{km}$		
REQ-STK-02	The aircraft shall have a maximum endurance of $6\,\mathrm{hours}$ or above	🟢
From Chapter 7, the maximum endurance of this aircraft is $7.5\,\mathrm{hours}$		
REQ-STK-03	The aircraft shall cruise at a ground speed of 700 km/h or more	🟢
From Section 6.1, the aircraft can cruise up to a speed of $720\,\mathrm{km/h}$		
REQ-STK-04	The maximum cruise flight level shall be FL290 or above	🟢
From Section 6.1, the maximum altitude the aircraft can fly at cruise speed is FL300		
REQ-STK-05	The required take-off distance shall be $2100\,\mathrm{metres}$ or below	🟢
From Section 6.1, the take-off distance is $1669\,\mathrm{m}$		
REQ-STK-06	The required landing distance shall be $1500\,\mathrm{metres}$ or below	🟢
From Section 6.1, the landing distance is $1427\,\mathrm{m}$		
REQ-STK-07	The aircraft shall comply with the CS-25 regulations	🟡
The aircraft does not yet comply with every regulation, but it is expected to do so in further stages of design. Post-DSE Verification: Test		
REQ-STK-08	The operational reliability of the aircraft shall be equal or higher than the A320neo	🟢
From Section 10.1, the reliability of X-300 is comparable to the A320neo		
REQ-STK-09	The aircraft shall have no required additional maintenance compared to the A320neo	🔴
From Chapter 11, the maintenance cost of X-300 is higher than A320neo mainly due to a more complex engine		
REQ-STK-10	$75\,\%$ or more of the materials used in the aircraft parts shall be recyclable/re-processable	🟢
From Subsection 5.6.1, the material used leads to that aircraft being more than $75\,\%$ *to recycle*		
REQ-STK-11	The total environmental impact of the aircraft’s life-cycle shall be less than that of the A320neo	🟡

Continues on next page

Table 14.1 – continues from previous page

Identifier	Requirement description	Compliant
The lifecycle has still not been analysed at this stage of design. Post-DSE Verification: Test, Analysis		
REQ-STK-12	The aircraft's operational CO_2 emissions per passenger per kilometer shall be $25\,\%$ lower than those of the Airbus A320neo	🟢
From Section 6.2, the CO_2 emissions satisfy this requirement		
REQ-STK-13	The aircraft's operational NOx per passenger per kilometer emissions shall be $50\,\%$ lower than those of the Airbus A320neo	🟢
From Table 6.5, the NO_x emissions satisfy this requirement		
REQ-STK-14	The cumulative effective perceived noise level (EPNL) of the aircraft shall be $20\,\%$ lower than that of the Airbus A320neo	🟢
From Section 6.4, the noise emissions is $25.3\,\%$ lower than the A320.		
REQ-STK-15	The unit cost of each aircraft shall be less than $130\,\mathrm{million\ EUR}$ in 2024	🔴
From Section 11.3, the unit cost exceeds that of the requirement. It is explained in Section 11.3		
REQ-STK-16	The aircraft shall be able to accommodate an amount of 290 to 330 passengers	🟢
From Chapter 7, the aircraft can carry a maximum of 330 passengers.		
REQ-STK-17	The aircraft shall be in service in 2035	🟡
While TRL level was analysed in Section 3.2, the exact timeline is expected to be known in later design stages. Post-DSE Verification: N/A		
REQ-MIS-001	The aircraft shall provide power during all phases of its mission profile.	🟢
From Section 6.1, it is seen that the aircraft has enough power available and thrust for take-off, landing and cruise at design cruise altitude and speed		
REQ-MIS-002	The aircraft shall have means of accelerating while on the ground.	🟢
From Section 5.4, the aircraft has an electric taxi system.		
REQ-MIS-003	The aircraft shall have means of decelerating while on the ground.	🟢
From Chapter 6, the aircraft has brakes and thrust reversers		
REQ-MIS-004	The aircraft shall provide directional control on the ground.	🟡
This aspect of ground movement has still not been analysed, but the requirement shall still be met in later design stages. Post-DSE Verification: Review of design		
REQ-MIS-005	When stationary, the aircraft shall possess static ground stability between the OEW and MRW.	🟢
From Subsection 5.6.4, the aircraft is stable on ground during loading.		
REQ-MIS-006	The aircraft shall have means of accelerating at speeds below the maximum speed for a given flight condition.	🟢
From Section 6.1, the aircraft has more power available than required for cruise condition, take-off and landing		
REQ-MIS-007	The aircraft shall have means of decelerating at speeds above the minimum speed for a given flight condition.	🟡
Although in some cases the simple action of reducing thrust could result in a speed reduction, the spoilers have yet not been designed, therefore this requirement hasn't been fully met. Post-DSE Verification: Analysis		
REQ-MIS-008	The aircraft shall provide directional control in all phases of flight.	🟢
From the midterm report[3], the aircraft has ailerons		
REQ-MIS-009	The aircraft shall possess negative static stability in all phases of flight.	🟢

Continues on next page

Table 14.1 – continues from previous page

Identifier	Requirement description	Compliant
From Subsection 5.6.4, the aircraft satisfies this requirement.		
REQ-MIS-010	The aircraft shall possess inertial navigation capabilities	
Even though this is an expected capability of the aircraft, the sub-system has still not been designed. Post-DSE Verification: Review of design		
REQ-MIS-011	The aircraft shall assist the pilots in controlling the vehicle using autopilot software	
Even though this is an expected capability of the aircraft, the sub-system has still not been designed. Post-DSE Verification: Review of design		
REQ-MIS-012	The aircraft shall provide transponder functionality	
Even though this is an expected capability of the aircraft, the sub-system has still not been designed. Post-DSE Verification: Review of design		
REQ-MIS-013	The aircraft shall sustain a maximum of 330 passengers during nominal flight at cruise altitude	
The aircraft weight when analysing performance is at maximum payload which is 330 passengers		
REQ-MIS-014	The aircraft shall have fire safety (prevention, detection, protection, and suppression) equipment	
Even though this is an expected capability of the aircraft, the sub-system has still not been designed. Post-DSE Verification: Review of design		
REQ-MIS-015	The aircraft shall be statically stable on the ground during the nominal loading sequence.	
From Subsection 5.6.4, the aircraft satisfies this requirement		
REQ-MIS-016	The aircraft shall be operated by 2 pilots.	
From Chapter 7, the cockpit is large enough to accommodate 2 pilots		
REQ-MIS-017	The aircraft shall enable the pilots to communicate with external parties like ATC and airline operations centre	
Even though this is an expected capability of the aircraft, the sub-system has still not been designed. Post-DSE Verification: Review of design		
REQ-MIS-018	The aircraft shall be capable of flying under (S)VFR conditions	
Some essential sub-systems to fly in such conditions have not yet been designed. Post-DSE Verification: Review of design		
REQ-MIS-019	The aircraft shall be capable of flying under IFR conditions	
Some essential sub-systems to fly in such conditions have not yet been designed. Post-DSE Verification: Review of design		
REQ-MIS-020	The aircraft shall be capable of flying in rain of up to $4\,\mathrm{mm}$ per hour	
Such a simulation/analysis has not yet been conducted due to the early stage of design Post-DSE Verification: Analysis		
REQ-MIS-021	The aircraft shall be capable of performing a take-off with a crosswind speed of up to $65\,\mathrm{kts}$.	
Even though this is an expected capability of the aircraft, the sub-system has still not been designed Post-DSE Verification: Simulation		
REQ-MIS-022	The aircraft shall be capable of performing a take-off with a tailwind speed of up to $65\,\mathrm{kts}$.	
Even though this is an expected capability of the aircraft, the sub-system has still not been designed. Post-DSE Verification: Simulation		
REQ-MIS-023	The aircraft shall be capable of performing a take-off with a headwind speed of up to $65\,\mathrm{kts}$.	

Continues on next page

Table 14.1 – continues from previous page

Identifier	Requirement description	Compliant
Even though this is an expected capability of the aircraft, the sub-system has still not been designed. Post-DSE Verification: Simulation		
REQ-MIS-024	The aircraft shall be capable of performing a landing with a cross-wind speed of up to $65\,\mathrm{kts}$.	🟡
Even though this is an expected capability of the aircraft, the sub-system has still not been designed Post-DSE Verification: Simulation		
REQ-MIS-025	The aircraft shall be capable of performing a landing with a tailwind speed of up to $65\,\mathrm{kts}$.	🟡
Even though this is an expected capability of the aircraft, the sub-system has still not been designed. Post-DSE Verification: Simulation		
REQ-MIS-026	The aircraft shall be capable of performing a landing with a head-wind speed of up to $65\,\mathrm{kts}$.	🟡
Even though this is an expected capability of the aircraft, the sub-system has still not been designed. Post-DSE Verification: Simulation		
REQ-MIS-027	The aircraft shall be capable of operating in ambient air temperatures of minimum $-45\,°\mathrm{C}$ at sea level.	🟡
Although the logic of the Environmental Control System has been designed, the operating characteristics have not yet been computed at this stage of design. Post-DSE Verification:Analysis		
REQ-MIS-028	The aircraft shall be capable of operating in ambient air temperatures of a maximum of $55\,°\mathrm{C}$ at sea level.	🟡
Although the logic of the Environmental Control System has been designed, the operating characteristics have not yet been computed at this stage of design. Post-DSE Verification: Analysis		
REQ-MIS-029	The aircraft shall be capable of operating in ambient air temperatures of minimum $-70\,°\mathrm{C}$ at FL290 or higher.	🟡
Although the logic of the Environmental Control System has been designed, the operating characteristics have not yet been computed at this stage of design. Post-DSE Verification: Analysis		
REQ-MIS-030	The aircraft shall accommodate a net cargo volume of $30\,\mathrm{m}^3$.	🟢
From Chapter 7, the cargo capacity of the X-300 is $44.5\,\mathrm{m}^3$		
REQ-MIS-031	The aircraft shall have an exit limit of $330\,\mathrm{p}$assengers	🟢
From Chapter 7, the aircraft can carry up to 330 passengers		
REQ-MIS-032	The aircraft shall contain a sufficient amount of energy source to fly a range of at least $3000\,\mathrm{km}$ when taking off at MTOW.	🟢
From Section 6.1, the aircraft has enough fuel capacity to fly $3000\,\mathrm{km}$		
REQ-MIS-033	The average nominal turnaround time of the aircraft shall not be more than $60\,\mathrm{minutes}$.	🟢
The turnaround time of the aircraft has been computed in Subsection 10.2.2 to be $51\,\mathrm{minutes}$*, complying therefore with the requirement.*		
REQ-MIS-034	The aircraft shall accumulate an annual maintenance cost less than $9.48\,\mathrm{million\ EUR}$.	🔴
The annual maintenance cost of each unit has been computed in Subsection 11.3.4 to be approximately $18\,\mathrm{million\ EUR}$ *per year. This largely surpasses the requirement, therefore it has to be reconsidered later in the design process.*		
REQ-MIS-035	The total environmental impact of the aircraft's life-cycle shall be less than that of the A320neo when evaluated using ISO 14040/14044 standards.	🟡
The lifecycle has still not been analysed at this stage of design. Post-DSE Verification: Analysis		
REQ-MIS-036	The aircraft shall have a service life of minimum 30 years.	🟡

Continues on next page

Table 14.1 – continues from previous page

Identifier	Requirement description	Compliant
This parameter was still not fully assessed at this stage of design. Post-DSE Verification: Analysis		
REQ-MIS-037	The manufacturing method shall accommodate a product series of minimum 625 units.	
This requirement has been met when establishing the manufacturing plan in Chapter 8.		
REQ-MIS-038	Series production shall begin in 2035 at the latest.	
As specified in Chapter 8, the series production should begin in 2034.		
REQ-MIS-039	Gross development costs shall not exceed $20\,\mathrm{billion\ EUR}$.	
The gross development costs have been computed in Subsection 11.3.2 to be $9.2\,\mathrm{billion\ EUR}$		
REQ-MIS-040	Manufacture of components shall comply with safety factors established in CS-25 regulations.	
This compliance has still not been checked at this moment of design. Post-DSE Verification: Review of design		
REQ-MIS-041	The aircraft shall maintain a cabin altitude of at most $6000\,\mathrm{ft}$ during cruise.	
Although the logic of the Environmental Control System has been designed, the operating characteristics have not yet been computed at this stage of design.		
REQ-MIS-042	$75\,\%$ of the aircraft's OEM shall be either recyclable (with energy input) or reusable (without energy input).	
From Subsection 5.6.1, the aircraft satisfies this requirement		
REQ-MIS-043	The OEW of the aircraft shall be at least $25\,\%$ lower than that of the Boeing 787-8	
From Chapter 7, the OEW of the X-300 is $38.6\,\%$ *lower than the Boeing 787-8*		
REQ-MIS-044	The aircraft shall have a cumulative EPNL of no more than $255\,\mathrm{dB}$.	
From Section 6.4, the aircraft has a cumulative EPNL of $254.3\,\mathrm{dB}$		
REQ-MIS-045	The aircraft shall emit less than $46.4\,\mathrm{g/ASK}$ of CO_2 when operating under the nominal mission profile.	
From Section 6.2, the aircraft meets this requirement.		
REQ-MIS-046	The aircraft shall emit less than $0.112\,\mathrm{g/ASK}$ of NOx when operating under the nominal mission profile.	
From Section 6.3, the aircraft satisfies this requirement		
REQ-MIS-047	The maximum ground speed of the aircraft during cruise shall be less than $592\,\mathrm{kts}$.	
From Section 6.1, the maximum speed of the aircraft at cruise is $389\,\mathrm{kts}$ Simulation		
REQ-MIS-048	The aircraft's energy source shall have a TRL of at least 6	
From Section 3.2, the aircraft satisfies this requirement		
REQ-MIS-049	The energy source chosen for the aircraft shall have predefined safety regulations.	
From Section 3.2, the aircraft uses kerosene/SAF which satisfies this requirement		
REQ-MIS-050	The wingspan of the aircraft shall be less than $52\,\mathrm{m}$	
From Chapter 7, the wingspan is $47.4\,\mathrm{m}$		
REQ-SYS-001	The airframe shall be able to resist corrosion at the atmospheric conditions of its operational flight envelope.	
From Subsection 5.6.1, the aircraft satisfies this requirement		
REQ-SYS-002	The landing gear shall be able to withstand at least $20\,000$ repeated landing cycles without failing.	
Even though this is an expected capability of the aircraft, this has not been analysed yet.		
REQ-SYS-003	The aircraft shall be equipped with a wing de-icing system.	

Continues on next page

Table 14.1 – continues from previous page

Identifier	Requirement description	Compliant
Even though this is an expected capability of the aircraft, the sub-system has still not been designed.		
REQ-SYS-004	The aircraft shall be equipped with a propulsion unit de-icing system.	🟡
Even though this is an expected capability of the aircraft, the sub-system has still not been designed.		
REQ-SYS-005	The aircraft shall have pitch control surfaces.	🟢
From Chapter 7, the aircraft has elevators		
REQ-SYS-006	The aircraft shall have yaw control surfaces.	🟢
From Chapter 7, the aircraft has a rudder		
REQ-SYS-007	The aircraft shall have roll control surfaces.	🟢
From Chapter 7, the aircraft has ailerons		
REQ-SYS-008	The landing gear shall be able to retract and deploy below the airspeed of $100\,\mathrm{m/s}$.	🟡
Even though this is an expected capability of the aircraft, this function has still not been designed.		
REQ-SYS-009	The aircraft shall be equipped with a GPS receiver.	🟡
Even though this is an expected capability of the aircraft, the sub-system has still not been designed.		
REQ-SYS-010	The aircraft shall be equipped with a fly-by-wire control system.	🟢
From Section 10.1, the aircraft meets this requirement		
REQ-SYS-011	The aircraft shall have autopilot capabilities (heading/track hold, altitude hold, speed/Mach hold, vertical speed/flight patch hold).	🟡
Even though this is an expected capability of the aircraft, this function has still not been designed.		
REQ-SYS-012	The aircraft shall be equipped with at least 3 VHF units.	🟡
Even though this is an expected capability of the aircraft, this function has still not been designed.		
REQ-SYS-013	The aircraft shall be equipped with at least 3 HF units.	🟡
Even though this is an expected capability of the aircraft, this function has still not been designed.		
REQ-SYS-014	The aircraft shall be equipped with 2 Primary Flight Displays.	🟡
Even though this is an expected capability of the aircraft, this function has still not been designed.		
REQ-SYS-015	The aircraft shall be equipped with 2 Navigation Display.	🟡
Even though this is an expected capability of the aircraft, this function has still not been designed.		
REQ-SYS-016	The aircraft shall be equipped with at least $2\,\mathrm{FMS}$ units.	🟡
Even though this is an expected capability of the aircraft, this function has still not been designed.		
REQ-SYS-017	The aircraft shall be capable of performing automated landings up to ILS CAT IIIc.	🟡
Even though this is an expected capability of the aircraft, this function has still not been designed.		
REQ-SYS-018	The aircraft shall be equipped with at least 3 angle of attack sensors.	🟡
Even though this is an expected capability of the aircraft, this function has still not been designed.		
REQ-SYS-019	The aircraft shall be equipped with at least 3 pitot tubes.	🟡
Even though this is an expected capability of the aircraft, this function has still not been designed.		
REQ-SYS-020	The aircraft shall be equipped with at least 6 static ports.	🟡
Even though this is an expected capability of the aircraft, this function has still not been designed		
REQ-SYS-021	The propulsion unit shall provide sufficient thrust to accelerate the aircraft (at MTOW) to a rotation speed of minimum 140 kts over a distance of 2100 m at sea-level conditions (ISA).	🟢
From Section 6.1, the aircraft satisfies this requirement		

Continues on next page

Table 14.1 – continues from previous page

Identifier	Requirement description	Compliant
REQ-SYS-022	The propulsion unit shall provide sufficient thrust to enable the aircraft (at MTOW) to climb at a minimum rate of $2500\,\mathrm{ft/min}$ at sea-level conditions (ISA)	🟢
From Section 6.1, the aircraft meets this requirement		
REQ-SYS-023	The propulsion system shall provide a minimum thrust of $405\,\mathrm{kN}$ at sea-level conditions (ISA)	🟢
From Chapter 7, the aircraft satisfies this requirement		
REQ-SYS-024	The aircraft shall be equipped with an auto-throttle.	🟡
Even though this is an expected capability of the aircraft, this function has still not been designed.		
REQ-SYS-025	The propulsion unit shall have a fire suppression system.	🟡
Even though this is an expected capability of the aircraft, this function has still not been designed.		
REQ-SYS-026	The aircraft shall possess an APU system.	🟢
From Section 5.2, the aircraft satisfies this requirement		
REQ-SYS-027	The APU system shall be equipped with a fire suppression system.	🟡
Even though this is an expected capability of the aircraft, this function has still not been designed.		
REQ-SYS-028	The propulsion unit shall be capable of providing reverse thrust.	🟢
From Section 6.1, the aircraft has this capability		
REQ-SYS-029	The propulsion unit shall be capable of being (re)started during flight.	🟢
From Section 5.1, the aircraft satisfies this requirement		
REQ-SYS-030	The propulsion-unit-driven generator(s) shall supply a minimum power of $880\,\mathrm{kW}$ under nominal cruise conditions.	🟢
From Section 5.1, the aircraft satisfies this requirement		
REQ-SYS-031	The emergency generator(s) shall supply a minimum power of $20\,\mathrm{kW}$ under propulsion unit inoperative conditions.	🟡
The emergency generators have not yet been designed at this stage.		
REQ-SYS-032	All exits shall be equipped with evacuation slides.	🟢
As mentioned in Chapter 7, every single emergency exit possesses an emergency slide as well.		
REQ-SYS-033	The environmental control unit shall maintain a cabin/cockpit temperature within a range of 18 to 25 °C.	🟡
Although the logic of the Environmental Control System has been designed, the operating characteristics have not yet been computed at this stage of design.		
REQ-SYS-034	The cabin shall have an overhead storage capacity of $16.2\,\mathrm{m}^3$.	🟡
The sizing of the overhead storage bins has not yet been performed at this stage of design.		
REQ-SYS-035	The APU generator shall deliver a power of at least $250\,\mathrm{kW}$ during sea level ISA conditions.	🟡
Although the power budget has already been properly stipulated, the actual power generated by the APU remains to be assessed.		
REQ-SYS-036	The aircraft's control surfaces shall sustain the aerodynamic loads experienced within the aircraft's flight envelope.	🟡
Since the elevators and rudder still need to be sized, this requirement is yet to be met.		
REQ-SYS-037	The aircraft's control surfaces shall guarantee that the aircraft is stable within its flight envelope.	🟡
Since the elevators and rudder still need to be sized, this requirement is yet to be met.		
REQ-SYS-038	The aircraft shall enable deceleration during all phases of flight using aerodynamic breaking.	🟡

Continues on next page

Table 14.1 – continues from previous page

Identifier	Requirement description	Compliant
Aerodynamic breaking has neither been designed nor implemented in the aircraft at this stage of design.		
REQ-SYS-039	The ailerons shall be able to achieve a roll rate of at least $0.1496\,\mathrm{rad/s}$.	🟢
This requirement has already been met in the Midterm Report [3], when designing the ailerons.		
REQ-SYS-040	The elevators shall be able to achieve a pitch rate of at least $0.0698\,\mathrm{rad/s}$.	🟡
The elevators have not yet been sized to account for this requirement.		
REQ-SYS-041	The rudder shall be able to achieve a yaw rate of at least $0.0873\,\mathrm{rad/s}$.	🟡
The rudder has not yet been sized to account for this requirement.		
REQ-SYS-042	The aircraft tip-back angle shall be more than $15\,°$.	🟢
This angle is exactly $15\,\mathrm{deg}$ as explained in Subsection 5.6.4.		
REQ-SYS-043	The aircraft turnover angle shall be less than $55\,°$.	🟡
This angle has still not been measured at this stage of design.		
REQ-SYS-044	The landing gear shall enable a minimum turn radius of $25\,\mathrm{m}$ or less at MTOW at with no slip angle.	🟡
The nose wheel turning characteristics have not yet been designed.		
REQ-SYS-045	The aircraft landing gear shall be able to withstand the lateral strains during normal operating conditions.	🟡
At this stage of design, the undercarriage has not yet been tested to withstand these conditions.		
REQ-SYS-046	The aircraft shall have clearly identifiable exterior lights as prescribed by CS-25	🟡
Even though this is an expected capability of the aircraft, the sub-system has still not been designed		
REQ-SYS-047	The propulsion system shall be accessible for maintenance by removing a single layer of nacelle panels without any tooling.	🟡
The accessibility of the engine for maintenance personnel has still not been analysed at this stage of design.		
REQ-SYS-048	The loading of the energy source shall occur within $50\,\%$ of the turnaround time.	🟢
As specified in Subsection 10.2.2, the fuel loading process takes about $25.7\,\%$ of the whole turnaround time (non-parallel loading).		
REQ-SYS-049	The airframe shall withstand all CS-25 specified load limits without resulting in permanent deformation.	🟡
Even though this is an expected capability of the aircraft, the sub-system has still not been designed.		
REQ-SYS-050	The aircraft shall have a sufficient number of emergency exits to allow for an evacuation of 330 people within 90 seconds in case half of the emergency exits are unusable.	🟡
To fulfil this requirement an on-person simulation with the full-model aircraft has to be conducted. Nevertheless, the emergency doors were designed and positioned in such a way that this requirement is most likely met.		
REQ-SYS-051	The access door to the cockpit shall be reinforced as prescribed by CS-25.	🟡
Even though this is an expected capability of the aircraft, the sub-system has still not been designed		

Continues on next page

Table 14.1 – continues from previous page

Identifier	Requirement description	Compliant
REQ-SYS-052	The propulsion unit shall be certified by 2033 at the latest.	●
The exact timeline of the availability of the Water-Injected Turbofan is unknown		
REQ-SYS-053	The aircraft shall be compatible with a $400\,\mathrm{Hz}$ ground power connection.	●
From Section 5.5, the aircraft is compatible with a ground connection		

15
Post-DSE Development Logic

The post-DSE activities are a continuation of the development cycle of the aircraft. The development cycle outlined by Airbus, in which maturity gates form clear technological milestones, is taken as the basis for further activities [1]. On the following pages, the logical flow of this process is outlined, sub-activities are elaborated upon and the timeline is set out using a Gantt-chart.

The DSE forms the start of the development cycle and covers maturity gates 1 to 4. This includes the identification of market opportunities, the establishment of standards and requirements, the selection of an aircraft-concept and the establishment of the aircraft configuration. The baseline- and midterm-reports cover these maturity gates (1-2 and 3, respectively). Altogether, these activities comprised the feasibility and concept phase of aircraft development.

The end of the DSE nears in on maturity gate 5, the validation of the detailed A/C concept. Depending on final reviews and implementation of feedback, this gate may be passed upon the completion of the DSE. However, depending on stakeholder satisfaction and internal continuity, this gate may not be passed. With the passing of gate 5, the instruction to proceed is given, resulting in the commitment of resources towards the continuation of the project.

What follows after maturity gate 5 is the definition phase, in which aircraft specifications and commercial properties are finalized. This should result in the completion of maturity gate 6 and the 'authorization to offer', meaning the aircraft is ready to be marketed to potential buyers.

If the market response to the aircraft upon offering is positive, the detailed design of all aircraft components, but also of the manufacturing and testing systems is conducted. This work culminates in the launch of the aircraft to the general public, as all component level designs have been completed.

The project then moves into the development phase, which comprises maturity gates 8 to 13. This phase includes the start of manufacturing, the first production units, as well as the certification testing of the aircraft, leading to the first flight (MG11), the type certificate (MG12) and the entry into service (MG13).

The phase that follows is the operational phase, in which a growing (and then shrinking) aircraft fleet is in operation. Key internal activities during this phase include upholding production rates and general support of the existing aircraft fleet. This is in support of the external parties that operate the fleet (operators) and maintain the fleet (MRO partners).

Finally, the first aircraft and eventually the entire fleet retire: end-of-life. Recycling of aircraft materials and re-use of components in this stage is key to achieving the set sustainability targets.

[1] https://www.airbus.com/en/newsroom/news/2017-02-aircraft-lifecycle-from-design-to-operations

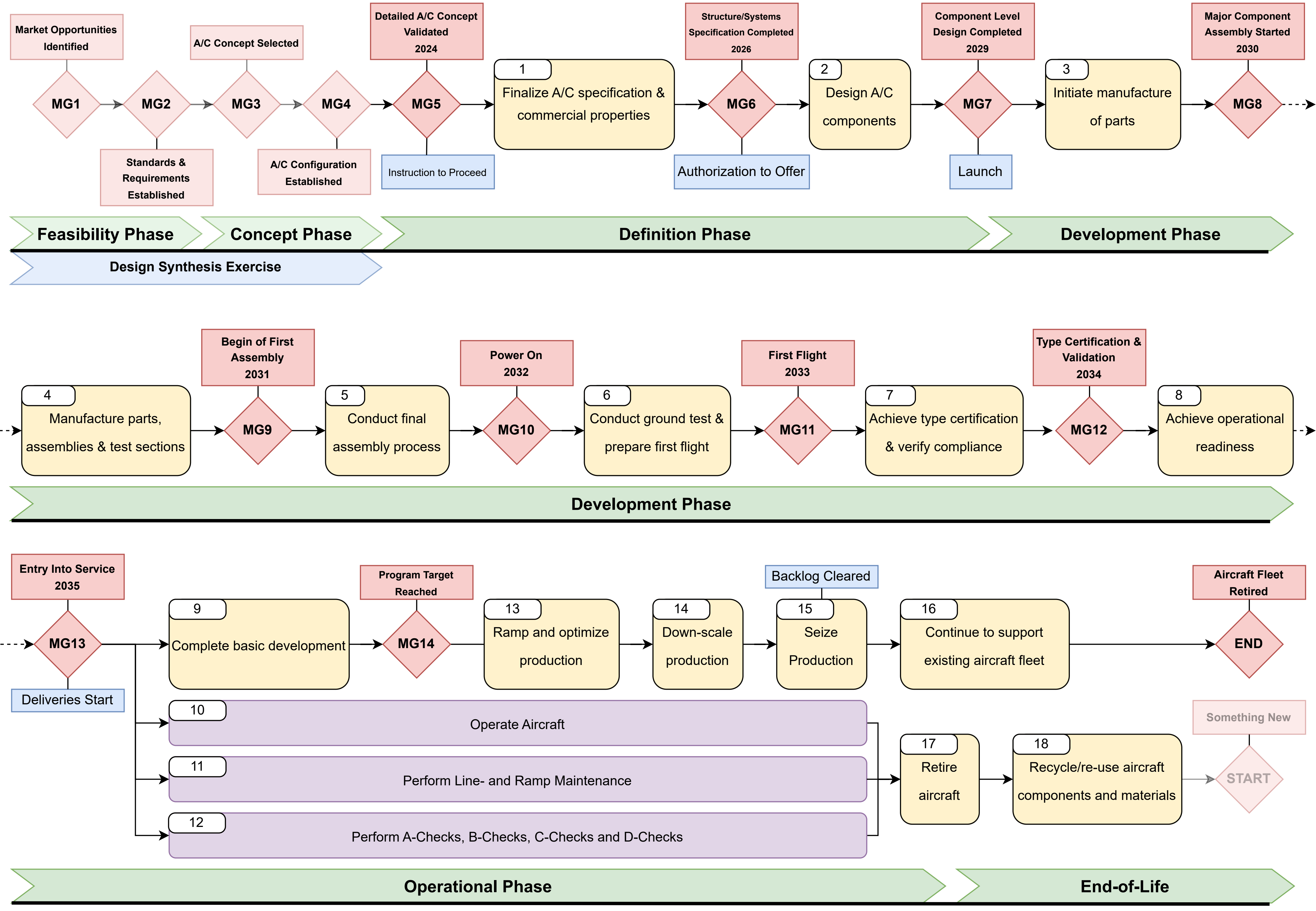

Market Opportunities Identified
MG1
MG2
Standards & Requirements Established
A/C Concept Selected
MG3
MG4
A/C Configuration Established
Detailed A/C Concept Validated 2024
MG5
Instruction to Proceed
1 Finalize A/C specification & commercial properties
Structure/Systems Specification Completed 2026
MG6
Authorization to Offer
2 Design A/C components
Component Level Design Completed 2029
MG7
Launch
3 Initiate manufacture of parts
Major Component Assembly Started 2030
MG8
Feasibility Phase
Concept Phase
Definition Phase
Development Phase
Design Synthesis Exercise
4 Manufacture parts, assemblies & test sections
Begin of First Assembly 2031
MG9
5 Conduct final assembly process
Power On 2032
MG10
6 Conduct ground test & prepare first flight
First Flight 2033
MG11
7 Achieve type certification & verify compliance
Type Certification & Validation 2034
MG12
8 Achieve operational readiness
Development Phase
Entry Into Service 2035
MG13
Deliveries Start
9 Complete basic development
Program Target Reached
MG14
13 Ramp and optimize production
14 Down-scale production
Backlog Cleared
15 Seize Production
16 Continue to support existing aircraft fleet
Aircraft Fleet Retired
END
10 Operate Aircraft
11 Perform Line- and Ramp Maintenance
12 Perform A-Checks, B-Checks, C-Checks and D-Checks
17 Retire aircraft
18 Recycle/re-use aircraft components and materials
Something New
START
Operational Phase
End-of-Life

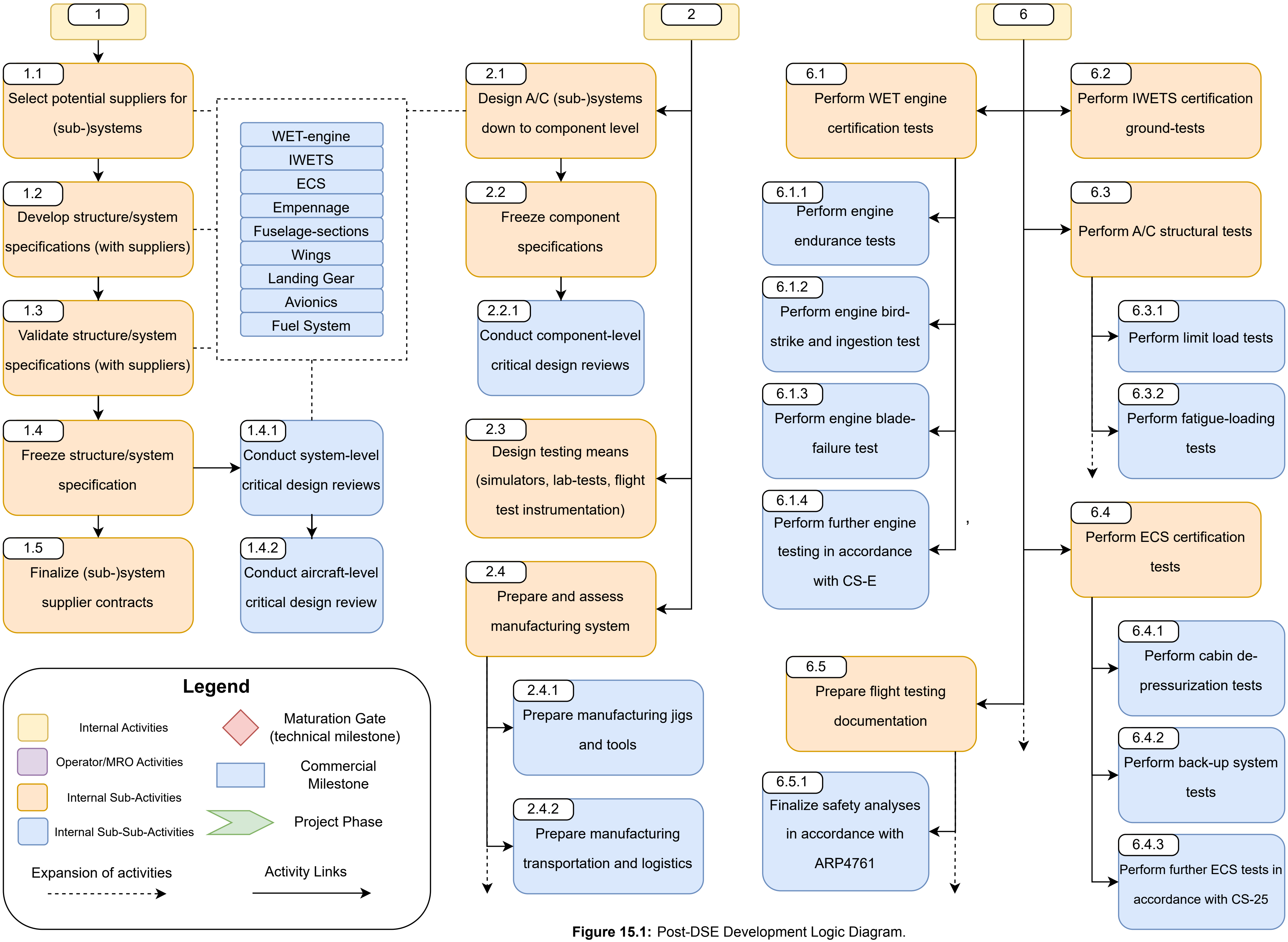

Figure 15.1: Post-DSE Development Logic Diagram.

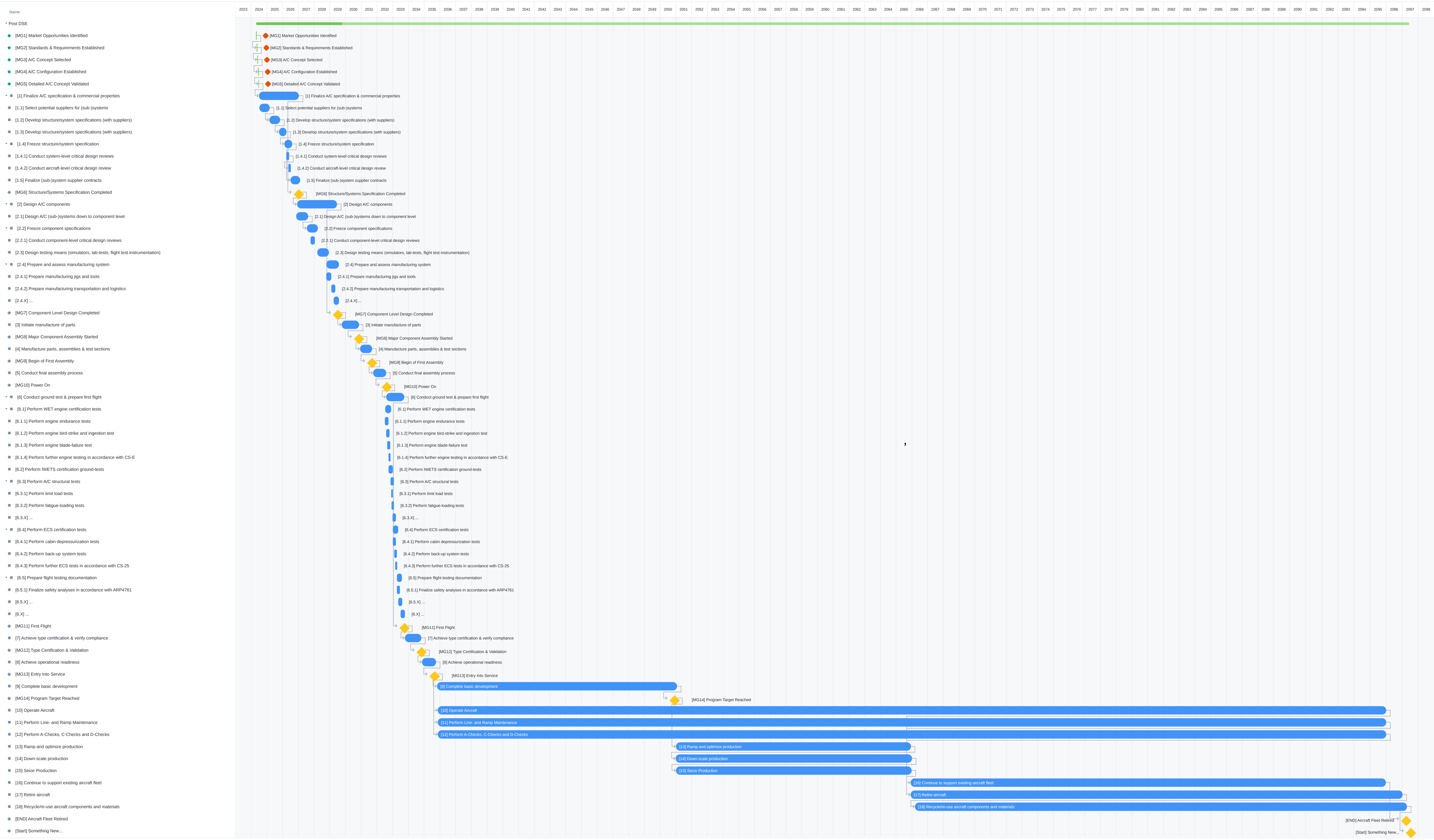

Figure 15.2: Post-DSE Gantt chart.

16 Conclusion

In response to anticipated future demand for high-capacity short-to-medium range passenger aircraft, the aim of this report is to study the feasibility of an airliner with such capabilities and a lower environmental impact compared to current state-of-the-art aircraft. The proposed *X-300 EcoFlyer* offers a maximum capacity of 330 passengers and a harmonic range of $3000\,\mathrm{km}$ while yielding $27.7\,\%$ lower CO_2 emissions, $90.5\,\%$ lower NO_x emissions, and $25.3\,\%$ lower noise emissions compared to the Airbus A320neo. To achieve these performance metrics, the aircraft features a fuselage designed for engine noise shielding, a novel water-injected turbofan engine, an in-wheel electrical taxing system, and an electrical environmental control system.

In relation to the market gap and technical challenges which the X-300 is designed to address, this study has proven the following:

- While common practice suggests that aircraft designed for 300 passengers or more should have a twin-aisle configuration, the design of the X-300 demonstrates that a high-capacity single-aisle fuselage is technically feasible and advantageous, given its lower fuel consumption compared to an equivalently-sized twin-aisle alternative.
- The performance of the WIT engine shows that there is potential for reduction in NO_x emissions without resorting to alternative fuels such as hydrogen. Given the engine's compatibility with hydrogen fuel as well as SAF, there is a compelling case for further investment in this technology to develop it for full-scale operations in the industry.
- Re-configuring traditional tube-and-wing aircraft to enable engine noise shielding is an effective way of reducing an aircraft's noise emissions, independent of the engine noise itself.
- A purpose-built aircraft for high-demand short-haul routes yields superior operating economics compared to the high-capacity long-range aircraft which currently operate said routes. Given that the mismatch between aircraft capability and route characteristics is expected to grow in the coming decades (as mentioned previously, in 2050 some $80\,\%$ of the demand for high-capacity long-range aircraft will be for high-demand short-haul routes), there will be a strong incentive for operators to purchase purpose-built aircraft such as the X-300.
- While a SAF-kerosene blend can contribute to lowering the CO_2 emissions of a given aircraft, this potential is hampered by operational constraints, as it relies on all airports (which the given aircraft operates from) to be equipped with a SAF supply infrastructure. If only select airports in an aircraft's route network can offer SAF, the overall reduction in CO_2 emissions of that aircraft will be insignificant in the context of its operational lifetime.

What this study shows is that there is ample scope for the project to succeed in the anticipated future state of the commercial air transport sector. Nevertheless, further development of the X-300 EcoFlyer is necessary for the aircraft to achieve full technical and market readiness by 2035. A few critical points that must be addressed in the subsequent development of the aircraft include:

- The engine model must be expanded to include off-design points, transient effects and a wider set of operating conditions. Additionally, higher-fidelity mass models for the heat exchangers should be developed. The models should be expanded and linked to enable a multidisciplinary optimisation of the engine integrated with the aircraft.
- Additional sources of validation for the engine model should be considered and eventually experiments should be carried out to validate the performance metrics.
- A more representative fuselage cross section must be analysed to improve the accuracy of the structural analysis. While the current cross-section (which comprises solely fuselage skin) served the purpose of a first-order analytical estimation of the fuselage's weight, a more elaborate analysis would involve a fuselage made of skin and stiffening elements with a more detailed assessment of the shear stress in the skin and the bending stress in the stiffening elements.
- An structural analysis of the wingbox must be conducted in order to obtain an analytical (rather than empirical) estimate of the wing's weight.
- The horizontal stabilizer is larger than necessary because of the constraints imposed by the landing gear and wing positioning as well as its noise shielding purpose. The combination of a nontraditional tail design and a rear engine placement necessitates a closer examination of the control and stability characteristics, not least because the current stability analysis relies heavily on empirical methods.
- The current noise analysis relies entirely on statistical relationships based on a limited number of data points and educated guesses. While the only credible way to verify actual noise emissions is through experiments, a more advanced analytical noise prediction method should be used for a higher-accuracy noise estimate of the X-300.
- Additional effects of the WIT engine (and the aircraft as a whole) on contrail formation and soot emissions have not been analysed. These elements must be considered for a more comprehensive overview of the X-300's environmental impact.
- While material recyclability has been factored into the material selection process, a more complete life cycle appraisal of the selected materials' embodied energy must be finalised.

Bibliography

[1] IATA, "Global Outlook for Air Transport - A local sweet spot," Tech. rep., 2023. URL `https://developer-prod.iata.org/en/iata-repository/publications/economic-reports/global-outlook-for-air-transport---december-2023---report/`.

[2] Bartmański, J., Bootsma, S., Drijfhout, G., Entchev, A., Fulton, M., Karia, J., Martins de Castro, M., Sahakyan, A., Verweij, B., and Wichers, J., "Baseline report: Approach to the development of an environmentally friendly aircraft design," , 2024.

[3] Bartmański, J., Bootsma, S., Drijfhout, G., Entchev, A., Fulton, M., Karia, J., Martins de Castro, M., Sahakyan, A., Verweij, B., and Wichers, J., "Midterm report: Approach to the development of an environmentally friendly aircraft design," , 2024.

[4] Rupcic, L., Pierrat, E., Saavedra-Rubio, K., Thonemann, N., Ogugua, C., and Laurent, A., "Environmental impacts in the civil aviation sector: Current state and guidance," *Transportation Research Part D: Transport and Environment*, Vol. 119, 2023. https://doi.org/10.1016/j.trd.2023.103717.

[5] Grimmea, W., Maertensa, S., and Bingemerb, S., "The role of very large passenger aircraft in global air transport – a review and outlook to the year 2050," *Transportation Research Procedia*, Vol. 59, No. 4, 2021, pp. 76–84. https://doi.org/10.1016/j.trpro.2021.11.099.

[6] Roskam, J., *Airplane Design*, No. pt. 5 in Airplane Design, DARcorporation, 1985. URL https://books.google.nl/books?id=mMU47Ld7yQkC.

[7] Kaiser, S., Schmitz, O., Ziegler, P., and Klingels, H., "The Water-Enhanced Turbofan as Enabler for Climate-Neutral Aviation," *Appl. Sci.*, Vol. 12, No. 23, 2022, p. 12431. https://doi.org/10.3390/app122312431.

[8] C. Stephane, "What does the future hold in store for the Open Rotor?" Safran, 2019. Archived from the original.

[9] Sanford, G., and McBride, B., "Computer Program for Calculation of Complex Chemical Equilibirium Compositions and Applications," *NASA Technical Report*, Vol. NASA-RP-1311, 1994. URL https://ntrs.nasa.gov/citations/19950013764.

[10] Wagnera, W., and Prußb, A., "The IAPWS Formulation 1995 for the Thermodynamic Properties of Ordinary Water Substance for General and Scientific Use," *Journal of Physical and Chemical Reference Data*, Vol. 31, No. 2, 2002, pp. 387–565. https://doi.org/10.1063/1.1461829, URL https://doi.org/10.1063/1.1461829.

[11] Bell, I. H., Wronski, J., Quoilin, S., and Lemort, V., "Pure and Pseudo-pure Fluid Thermophysical Property Evaluation and the Open-Source Thermophysical Property Library CoolProp," *Industrial & Engineering Chemistry Research*, Vol. 53, No. 6, 2014, pp. 2498–2508. https://doi.org/10.1021/ie4033999, URL http://pubs.acs.org/doi/abs/10.1021/ie4033999.

[12] Martin-Candilejo, A., Santillán, D., and Garrote, L., "Pump Efficiency Analysis for Proper Energy Assessment in Optimization of Water Supply Systems," *Water*, Vol. 12, No. 1, 2020. URL https://www.mdpi.com/2073-4441/12/1/132.

[13] Weickgenannt, A., Kantor, I., Maréchal, F., and Schiffmann, J., "On the Application of Small-Scale Turbines in Industrial Steam Networks," *Energies*, Vol. 14, No. 11, 2021. URL https://www.mdpi.com/1996-1073/14/11/3149.

[14] GasTurb GmbH, "GasTurb 14: Design and Off-Design Performance of Gas Turbines," , 2021. Aachen, Germany.

[15] International Civil Aviation Organization, "Emissions Databank (06/2023)," , 2023. URL https://www.easa.europa.eu/en/domains/environment/icao-aircraft-engine-emissions-databank, accessed: 2024-05-01.

[16] American National Standards, "Standard Specification For Aviation Turbine Fuels: D 1655 – 04a," , 2017.

[17] Mattingly, J. D., Boyer, K. M., Haven, B. A., Heiser, W. H., and Pratt, D. T., *Aircraft engine design*, third edition ed., AIAA education series, American Institute of Aeronautics and Astronautics, Inc., Reston, Virginia, 2018.

[18] Kuz'michev, Venedikt, Krupenich, Ilia, Filinov, Evgeny, and Ostapyuk, Yaroslav, "Comparative Analysis of Mathematical Models for Turbofan Engine Weight Estimation," *MATEC Web Conf.*, Vol. 220, 2018, p. 03012. https://doi.org/10.1051/matecconf/201822003012, URL https://doi.org/10.1051/matecconf/201822003012.

[19] Herzog, J., "Electrification of the Environmental Control System," *25th International Congress of the Aeronautical Sciences*, 2006. URL https://www.semanticscholar.org/paper/ELECTRIFICATION-OF-THE-ENVIRONMENTAL-CONTROL-SYSTEM-Herzog-Lindenberg/6b15a29c25cabf3aaeea4aab059fb78a5c23dd4e.

[20] Moir, I., Seabridge, A., and Jukes, M., *"Electrical systems", Civil Avionics Systems*, 2^{nd} ed., John Wiley & Sons Inc., New York, 2013, pp. 235–290.

[21] Seresinhe, R., and Lawson, C., "Electrical load sizing methodology to aid conceptual and preliminary design of large commercial aircraft," *Journal of Aerospace Engineering*, Vol. 229, No. 3, 2015, pp. 445–466. https://doi.org/10.1177/0954410014534638.

[22] Langton, R., Clark, C., Hewitt, M., Richards, L., Moir, I., and Seabridge, A., *Aircraft fuel systems*, John Wiley & Sons, 2009.

[23] Vratny, P., and Kling, U., "Impact of Electric Taxiing on Hybrid-Electric Aircraft Sizing," *Deutscher Luft- und Raumfahrtkongress*, 2018. https://doi.org/10.25967/480115.

[24] Roling, P. C., and Groot, M. G. W., "The Potential Impact of Electric Aircraft Taxiing A Probabilistic Analysis and Fleet Assignment Optimization," *AIAA AVIATION 2022 Forum*, 2022. https://doi.org/10.2514/6.2022-3919.

[25] Schmollgruber, P., Döll, C., Hermetz, J., Liaboeuf, R., and Ridel, M., "Multidisciplinary exploration of DRAGON: an ONERA Hybrid Electric Distributed Propulsion Concept," , 2019. URL https://hal.science/hal-02068597/file/DTIS19036.1552317536_preprint.pdf.

[26] Planès, T., Delbecq, S., Pommier-Budinger, V., and Bénard, E., "Modeling and Design Optimization of an Electric Environmental Control System for Commercial Passenger Aircraft," *Aerospace*, Vol. 10, No. 3, 2023. https://doi.org/10.3390/aerospace10030260.

[27] Sinnett, M., "787 No-Bleed Systems: Saving Fuel and Enhancing Operational Efficiencies," *Boeing*, 2007. URL http://www.boeing.ch/commercial/aeromagazine/articles/qtr_4_07/article_02_2.html.

[28] Holmgren, E., Haldar, D., Tjernberg, L. B., and Johansson, A., "More Electric Aircraft (MEA) Scaling Aspects and Weight Impacts," *33rd International Congress of the Aeronautical Sciences*, 2022. URL https://www.google.com/url?sa=t&source=web&rct=j&opi=89978449&url=http://icas.org/ICAS_ARCHIVE/ICAS2022/data/papers/ICAS2022_0369_paper.pdf.

[29] Ercan, H., Akın, M., and Öztürk, C., "Performance analysis of electrical flight control actuation system in a commercial transport aircraft," *Aircraft Engineering and Aerospace Technology*, Vol. 96, No. 2, 2022, pp. 193–204. https://doi.org/10.1108/AEAT-01-2023-0019.

[30] Inagaki, I., Takechi, T., Shirai, Y., and Ariyasu, N., "Application and Features of Titanium for the Aerospace Industry," *Nippon Steel & Sumitomo Metal Technical Report*, , No. 106, 2014. UDC 669.295:629.735.3.

[31] Dunand, L., "End-of-life Reusing, recycling, rethinking," , 2022. URL https://aircraft.airbus.com/en/newsroom/news/2022-11-end-of-life-reusing-recycling-rethinking.

[32] European Union Aviation Safety Agency, “Certification Specifications for Large Aeroplanes CS-25,” Tech. rep., EASA, Cologne, Germany, 2023. URL https://www.easa.europa.eu/en/document-library/certification-specifications/group/cs-25-large-aeroplanes#cs-25-large-aeroplanes.

[33] Smiths Metal Centres, “8090 Technical Datasheet,” Smiths Metal Centres Ltd., 2023. URL https://www.smithmetal.com/8090-aluminium-lithium-alloy.htm, service. Quality. Value.

[34] Hibbeler, R. C., *Mechanics of materials*, 5th ed., Pearson, Upper Saddle River, NJ, 2002.

[35] Vandam, C. P., “Natural laminar flow airfoil design considerations for winglets on low-speed airplanes,” Tech. rep., Washington, 1984.

[36] Roskam, J., *”Lift and Pitch Moment Prediciton Methods”, Airplane Design Part VI: Preliminary Calculation of Aerodynamic, Thrust and Power Characteristics*, DARcorporation, Lawrence (KS), 1985, pp. 213–354.

[37] Seetharam, H., Rodgers, E., and Wentz Jr, W., “Experimental studies of flow separation of the NACA 2412 airfoil at low speeds,” Tech. Rep. NASA-CR-197497, NASA, 1997.

[38] Samuel, M. S. G., and Rajendran, P., “CFD Validation of NACA 2412 Airfoil,” 2019. https://doi.org/10.13140/RG.2.2.16245.42723.

[39] Jenkinson, L., Simpkin, P., and Rhodes, D., “Civil Jet Aircraft Design,” , 2001. URL https://booksite.elsevier.com/9780340741528/appendices/data-a/default.htm.

[40] Hamburg, H., “Empennage General Design,” , 2019.

[41] Losa, E. T., Arjomandi, A., Hervé Dakpo, K., and Bloomfield, J., “Efficiency comparison of airline groups in Annex 1 and non-Annex 1 countries: A dynamic network DEA approach,” *Transport Policy*, Vol. 99, 2020, pp. 163–174. https://doi.org/https://doi.org/10.1016/j.tranpol.2020.08.013, URL https://www.sciencedirect.com/science/article/pii/S0967070X19309187.

[42] Jenkinson, L., Simpkin, P., and Rhodes, D., *”Aircraft Performance”, Civil Jet Aircraft Design*, American Insitute of Aeronautics and Astronautics, 1999, pp. 223–265.

[43] Noel, G. J., and Boeker, E., “Thrust Reverser Analysis for Implementation in the Aviation Environmental Design Tool,” Tech. Rep. RTV-4F-FA4T-LR1, Volpe National Transportation Systems Center (U.S.), 2007.

[44] Ruijgrok, G., *”Performance in Steady Symmetric Flight”, Elements of airplane performance*, 2nd ed., Delft Academic Press, Delft, 2009, pp. 175–199.

[45] Teoh, R., Schumann, U., Majumdar, A., and Stettler, M. E. J., “Mitigating the Climate Forcing of Aircraft Contrails by Small-Scale Diversions and Technology Adoption,” *Environmental Science & Technology*, Vol. 54, No. 5, 2020, pp. 2941–2950. https://doi.org/10.1021/acs.est.9b05608, URL https://doi.org/10.1021/acs.est.9b05608, pMID: 32048502.

[46] Simons, D., *Introduction to Aircraft Noise*, TU Delft, 2019.

[47] Greco, G. F., Bertsch, L., Ring, T. P., and Langer, S. C., “Sound quality assessment of a medium□range aircraft with enhanced fan□noise shielding design,” *CEAS Aeronautical Journal*, Vol. 12, 2021, pp. 481–493. https://doi.org/10.1007/s13272-021-00515-9.

[48] Bertsch, L., Simons, D. G., and Snellen, M., “Aircraft Noise: The major sources, modelling sources, and reduction possibilities,” Tech. Rep. IB 224-2015 A 110, DRL, 2015.

[49] Bertsch, L., Wolters, F., Heinze, W., Pott-Pollenske, M., and Blinstrub, J., “System Noise Assessment of a Tube-and-Wing Aircraft with Geared Turbofan Engines,” *Journal of Aircraft*, Vol. 56, No. 4, 2019, pp. 1557–1596. https://doi.org/10.2514/1.C034935.

[50] Nöding, M., and Bertsch, L., “Application of Noise Certification Regulations within Conceptual Aircraft Design,” *Aerospace*, Vol. 8, No. 8, 2021. https://doi.org/10.3390/aerospace8080210.

[51] Guynn, M. D., and Olson, E. D., “Evaluation of an Aircraft Concept With Over-Wing, Hydrogen-Fueled Engines for Reduced Noise and Emissions,” Tech. Rep. TM-2002-211926, NASA, 2002.

[52] Lammel, G., and Graßl, H., "Greenhouse effect of NOX," *Environmental Science and Pollution Research*, Vol. 2, 1995, pp. 40 – 45. https://doi.org/https://doi.org/10.1007/BF02987512.

[53] Minnis, P., "CLOUDS AND FOG | Contrails," *Encyclopedia of Atmospheric Sciences (Second Edition)*, edited by G. R. North, J. Pyle, and F. Zhang, Academic Press, Oxford, 2015, second edition ed., pp. 121–132.

[54] Friedl, R., "AIRCRAFT EMISSIONS," *Encyclopedia of Atmospheric Sciences*, edited by J. R. Holton, Academic Press, Oxford, 2003, pp. 60–68. https://doi.org/https://doi.org/10.1016/B0-12-227090-8/00061-0.

[55] Watson, M., Machado, P., da Silva, A., Saltar, Y., Ribeiro, C., Nascimento, C., and Dowling, A., "Sustainable aviation fuel technologies, costs, emissions, policies, and markets: A critical review," *Journal of Cleaner Production*, Vol. 449, 2024, p. 141472. https://doi.org/https://doi.org/10.1016/j.jclepro.2024.141472, URL https://www.sciencedirect.com/science/article/pii/S095965262400920X.

[56] Eswaran, S., Subramaniam, S., Geleynse, S., Brandt, K., Wolcott, M., and Zhang, X., "Techno-economic analysis of catalytic hydrothermolysis pathway for jet fuel production," *Renewable and Sustainable Energy Reviews*, Vol. 151, 2021, p. 111516. https://doi.org/https://doi.org/10.1016/j.rser.2021.111516, URL https://www.sciencedirect.com/science/article/pii/S1364032121007954.

[57] Mankins, J. C., "Technology readiness assessments: Aretrospective," *Acta Astronautica*, Vol. 65, No. 9-10, 2009, p. 1216–1223. https://doi.org/10.1016/j.actaastro.2009.03.058.

[58] van der Weide, T., Deng, Q., and Santos, B. F., "Robust Long-Term Aircraft Heavy Maintenance Check Scheduling Optimization under Uncertainty," *Computers & Operations Research*, Vol. 141, 2021, p. Article 105667. https://doi.org/10.1016/j.cor.2021.105667.

[59] Kinnison, H. A., and Siddiqui, T., *Aviation Maintenance Management, Second Edition*, 2^{nd} ed., McGraw-Hill Professional, New York, NY, 2012.

[60] Fuchte, J. C., "Enhancement of aircraft cabin design guidelines with special consideration of aircraft turnaround and short range operations," Ph.D. thesis, DLR eV, 2014.

[61] Airports Council International, Aerospace Technology Institute, "Integration of Hydrogen Aircraft into the Air Transport System: An Airport Operations and Infrastructure Review," , 2021. URL https://www.ati.org.uk/.

[62] Leipold, A., Aptsiauri, G., Ayazkhani, A., Bauder, U., Becker, R.-G., Berghof, R., Claßen, A., Dadashi, A., Dahlmann, K., Dzikus, N., Flüthmann, N., Grewe, V., Göhlich, L., Grimme, W., Günther, Yves, Jaksche, R., Jung, M., Knabe, F., Kutne, P., Le Clercq, P., Pabst, H., Poggel, S., Staggat, M., Wicke, K., Wolters, F., Zanger, J., and Zill, T., "Development Pathways for Aviation up to 2050 – Study Report," Tech. Rep. 2, German Aerospace Center, 2019.

[63] Grewe, V., Gangoli Rao, A., Grönstedt, T., Xisto, C., Linke, F., Melkert, J., Middel, J., Ohlenforst, B., Blakey, S., Christie, S., et al., "Evaluating the climate impact of aviation emission scenarios towards the Paris agreement including COVID-19 effects," *Nature Communications*, Vol. 12, No. 1, 2021, p. 3841.

[64] Hoelzen, J., Silberhorn, D., Zill, T., Bensmann, B., and Hanke-Rauschenbach, R., "Hydrogen-powered aviation and its reliance on green hydrogen infrastructure–Review and research gaps," *International Journal of Hydrogen Energy*, Vol. 47, No. 5, 2022, pp. 3108–3130.

[65] Cole, J., McClintock, W., and Powis, L., "Market Forecasts Strategy," Tech. rep., Aerospace Technology Institute, 2022.

[66] Raymer, D., *Aircraft Design: A Conceptual Approach, third edition*, AIAA Education Series, J.S. Przemieniecki, 1999, pp. 579–593.

[67] Roskam, J., *Airplane Design Part VIII: Airplane Cost Estimation: Design, Development, Manufacturing and Operating*, DARcorporation, Lawrence (KS), 2006, pp. 3–109.

A

Data for Noise Analysis

Aircraft Model	Engine	BR	N_blades	N1 [rpm]	N2 [rpm]	D_fan [cm]	SLST [kN]	MTOM [t]	MLM [t]	S [m^2]	AR	d_S [deg]	d_F [deg]	D_wheel [in]	N_wheel	Lateral [EPNdB]	Approach [EPNdB]	Flyover [EPNdB]	Cumulative [EPNdB]	Record number (ICAO data base)
GVII (G500)	PW800-GA8	5.9	24	6315	24043	125.5	137.2	36.105	29.188	N/A	N/A	0	39	34	4	87.4	91	75.5	253.9	GULFSTREAM_10084
E190-E2	PW1919G	12	18	10600	24470	185	179.2	56.400	49.050	103	11.04	25	26.9	42	4	85.4	91.4	78.7	255.5	EMBRAER_10591
E195-E2	PW1293G-A	12	18	10600	24470	185	211	55.200	54.000	103	11.97	25	26.9	42	4	86.7	91.7	76.7	255.1	EMBRAER_10660
E195-E2	PW1293G-A	12	18	10600	24470	185	211	58.700	54.000	103	11.97	25	26.9	42	4	86.6	91.7	78.1	256.4	EMBRAER_10653
E195-E2	PW1293G-A	12	18	10600	24470	185	211	61.500	54.000	103	11.97	25	26.9	42	4	86.4	91.7	79.2	257.3	EMBRAER_10647
A220-100	PW1524G	12	18	10600	24470	185	207.4	57.000	52.390	112.3	10.97	N/A	37	42	4	88.2	91.5	77.4	257.1	AIRBUS_CANADA_1
A220-100	PW1524G	12	18	10600	24470	185	207.4	60.781	52.390	112.3	10.97	N/A	37	42	4	88	91.5	78.8	258.3	AIRBUS_CANADA_4
A220-300	PW1521G-3	12	18	10600	24470	185	186.6	64.000	58.740	112.3	10.97	N/A	37	42	4	86.6	92.4	81.5	260.5	AIRBUS_CANADA_11
A319-151N	LEAP-1A24	10.9	18	3894	19391	198	213.6	75.500	63.900	122.4	10.47	27	40	46	4	85.2	91.8	80.8	257.8	AIRBUS_28742
A320-251N	LEAP-1A26	10.9	18	3894	19391	198	260.6	70.000	66.300	122.4	10.47	27	40	46	4	86.5	92.2	78	256.7	AIRBUS_28816
A320-271N	PW1127G-JM	12.2	20	10047	22300	206	240.8	70.000	67.400	122.4	10.47	27	40	46	4	86.5	92.3	78.3	257.1	AIRBUS_28784
A320-271N	PW1127G-JM	12.2	20	10047	22300	206	240.8	79.000	66.300	122.4	10.47	27	40	46	4	86.2	92.1	81.8	260.1	AIRBUS_28783
A320-272N	PW1124G1-JM	12.2	20	10047	22300	206	215.6	70.000	66.300	122.4	10.47	27	40	46	4	85.5	92.1	79.8	257.4	AIRBUS_28786
A320-273N	PW1129G-JM	12.2	20	10047	22300	206	260.2	70.000	66.300	122.4	10.47	27	40	46	4	87.3	92.1	77.4	256.8	AIRBUS_28788
A320-273N	PW1129G-JM	12.2	20	10047	22300	206	260.2	79.000	67.400	122.4	10.47	27	40	46	4	87	92.3	80.7	260	AIRBUS_28787
A321-271NX	PW1133G-JM	11.4	20	10047	22300	206	294.6	80.000	71.500	122.4	10.47	22	21	46	4	88.1	94.8	80.4	263.3	AIRBUS_28789
A330-941	Trent 7000-72	9.4	20	2683	13391	285	648	205.000	191.000	372	11.00	23	32	55	8	92.3	97.6	83.1	273	AIRBUS_28834
A350-941	Trent XWB-75	9.1	22	2649	12424	300	660	280.000	207.000	442	9.49	24	37	55	8	89.9	96.5	88.5	274.9	AIRBUS_25681
A350-941	Trent XWB-84	9.1	22	2649	12424	300	749	210.000	205.000	442	9.49	24	37	55	8	92.3	96.4	78.9	267.6	AIRBUS_28828
A350-1041	Trent XWB-97	9.1	22	2816	12575	300	749	270.000	236.000	464.3	9.03	24	37	55	12	95.3	97	84.3	276.6	AIRBUS_28804
A350-1041	Trent XWB-97	9.1	22	2816	12575	300	749	316.000	233.000	464.3	9.03	24	37	55	12	94.8	97	89.2	281	AIRBUS_28803
A380-842	Trent 972E-84	8.8	24	2900	12200	295	1366	480.000	386.000	845	7.53	33	23	56	20	95.1	97.9	89.8	282.8	AIRBUS_28728
A380-861	GP7270	8.9	24	2738	12200	295	1330	575.000	394.000	845	7.53	33	23	56	20	94.4	97.3	95.9	287.6	AIRBUS_28729
737 MAX 8	LEAP-1B28/B28B1	9	18	4586	19828	176	260.8	68.038	61.234	127	10.16	N/A	40	44	4	89	93.5	77.8	260.3	BOEING_15781
737 MAX 9	LEAP-1B28/B28B1	9	18	4586	19828	176	260.8	74.570	69.308	127	10.16	N/A	40	44	4	88.6	94.1	80.3	263	BOEING_15823
787-8	GEnx-1B70/P2	9.5	18	2778	13368	282	643.2	177.989	156.489	377	9.59	N/A	30	50	8	92.2	93.8	80.4	266.4	BOEING_15444
787-8	Trent 1000-TEN-H	10.5	20	2683	13391	285	568.4	213.188	172.365	377	9.59	N/A	30	50	8	88.4	95.6	87.8	271.8	BOEING_15841
787-8	Trent 1000-TEN-CE	10.5	20	2683	13391	285	662.8	227.930	172.365	377	9.59	N/A	30	50	8	91.3	95.3	86.4	273	BOEING_15876
787-9	GEnx-1B74/75	9.5	18	2726	13425	282	682.4	181.440	174.630	377	9.59	N/A	30	50	8	93.1	94.6	80.1	267.8	BOEING_15480
787-9	Trent 1000-AE	10.5	20	2683	13391	285	615.6	231.900	192.800	377	9.59	N/A	30	50	8	88.9	95.7	87.9	272.5	BOEING_15717
787-10	GEnx-1B76/P2	9.5	18	2778	13368	282	698.4	199.580	156.489	377	9.59	N/A	30	50	8	93.3	93.8	82.1	269.2	BOEING_15539
787-10	Trent 1000-TEN-J	10.5	20	2683	13391	285	695	254.011	201.848	377	9.59	N/A	30	50	8	91.8	96.3	88.7	276.8	BOEING_15755

B
Task Division

Table B.1: Distribution of the workload.

Report Chapter	Related Task(s)	Student Name(s)
Executive Summary		Gerben, Alexander, Miguel, Jochem
Introduction		Alexander
Stakeholder Requirements		Alexander
Aircraft Concept Development		Gerben
Functional Analysis		Alexander
Detailed System Design	Propulsion System	Gerben, Jochem
	Electrical System Power Budget	Alexander
	Fuel System	Ararat
	IWETS	Alexander
	ECS	Alexander
	Airframe - Materials	Matthew, Jakub, Bram
	Airframe - Structures	Jakub, Ararat, Bram
	Airframe - Aerodynamics	Miguel, Matthew, Jay
	Airframe - Stability and Control	Matthew, Jakub
Performance Analysis	Flight Performance	Jay
	CO2 Emissions	Jochem
	NOx Emissions	Jochem
	Noise Emissions	Alexander
	Sensitivity Analysis	Jay, Miguel
Final Design Specification		Bram, Sjoerd
MAI Plan		Jakub, Matthew
Sustainable Development Strategy		Jochem
Operations and Logistics	RAMS Characteristics	Matthew, Jakub
	Concept Description	Ararat, Sjoerd
Business Case		Ararat, Sjoerd
Resource and Budget		Ararat, Miguel
Technical Risks Assessment		Jay
Compliance Matrix		Jay, Miguel
Post-DSE Development Logic		Gerben
Conclusion		Alexander
	Proof reading	All
	CAD-generated figures	Bram
	Document layout	Alexander